LIÈGE université Sciences

FACULTE DES SCIENCES

Freshwater and OCeanic Science Unit of Research (FOCUS)

GREENHOUSE GAS (CO_2, CH_4, N_2O) EMISSIONS FROM ECUADORIAN MOUNTAINOUS STREAMS AND HIGH ELEVATION LAKES

Lake Santa Lucia in the front and in the background the Antisana Volcano - Pichincha Ecuador

Année académique 2022-2023

Dissertation présentée par
Gonzalo CHIRIBOGA G.
Supervisé par:
Alberto BORGES V.
en vue de l'obtention du grade de
Doctorat en Sciences

GREENHOUSE GAS (CO_2, CH_4, N_2O) EMISSIONS FROM ECUADORIAN MOUNTAINOUS STREAMS AND HIGH ELEVATION LAKES

Thesis Jury

Position	Person	Institution
Supervisor	BORGES Alberto	University of Liège
President	GRÉGOIRE Marilaure	University of Liège.
Secretary	LEPOINT Gilles	University of Liège
Member	ABRIL Gwenaël	Muséum National d'Histoire Naturelle
Member	BOUILLON Steven	KU Leuven

ACKNOWLEDGMENTS

Chemistry is the melody you can play on vibrating strings (*Michio Kaku*). Since a teenager, I knew that my destiny would be linked to chemistry; however, I never imagined that one day I would present my doctoral defense at a Chemical Oceanography Unit.

Many people and institutions made it possible. But, first, I have been very lucky to meet Professor Alberto Borges and have him as a tutor, guide, and mentor. Alberto welcomed me four years ago in Belgium. He showed me how to prepare a mission, process samples, analyse data and write an article. He is an endless source of inspiration and an example to follow.

I want to express my gratitude to Steven Bouillon, who kindly opened the doors of his laboratory at KU LEUVEN for me to process POC, DOC, Isotopes, major elements, and plant samples, and eventually accepted to be part of the follow-up committee and the Jury. I am also grateful to the other members of the follow-up committee, Gilles Lepoint and Cedric Morana, who accompanied me for four years and advised how to put together my ideas during presentations; their contributions were fundamental in improving this study.

I would also like to thank the jury members, Marilaure Grégoire, Gilles Lepoint, Gwenaël Abril, and Steven Bouillon for taking time to read and comment on this work and for allowing me to share the most important results of the investigation. Thank you also to Bruno Delille for being a great friend and support. He always made my stay in Liége much easier to achieve. Loris Deirmendjian, a friend from the first moment in Liége, thank you for sharing stories and hosting me. A special thanks to Thibault Lambert for his great help processing the CDOM samples. I am indebted to my colleagues from the laboratory, Fleur Roland, Marc-Vincent Commarieu, Thomas Bousmanne in Liège, and Yannick Stroobandt and Zita Kelemen in Leuven, for supporting me in the sample analysis and for answering my frequently asked questions with the best possible disposition.

Infinitas gracias para mi familia y amigos en Ecuador. Carolina, Ghem y Roberto amigos y maestros. A Isaac, mi hijo, que me enseñó a decir te amo sin hablar.

I am grateful to the University of Liége (ULiége) for accepting me as a doctoral student, to the Académie de recherche et d'enseignement supérieur (ARES) and the Central University of Ecuador (UCE) for funding my research and my stays in Liége, and to the Freshwater and OCeanic science Unit of research (FOCUS) for their scientific support and funding the publication costs of my first publication.

ABSTRACT

Rivers and streams contribute substantially to global emissions of carbon dioxide (CO_2) and methane (CH_4). Most riverine GHG emissions are from the tropics, ~60-80% for CO_2, ~70% for CH_4, and ~79% for nitrous oxide (N_2O). Nevertheless, the total stream surface area (SSA) in the tropics (24°N-24°S) corresponds to ~44% of the total SSA globally, implying that riverine areal emissions of GHGs (per m^2) are higher than in other climatic zones. Ecuador localizes on the tropics, and it is the smallest of the 17 megadiverse countries in the world harboring an astounding number of ecosystems, which offers the conditions to study in a relatively short space the GHG evasions of both, an important river tributary to the Amazon, as well as a diverse lacustrine system. The present thesis is divided into two sections. Firstly, we report for the first time the dissolved concentrations CO_2, CH_4, and N_2O in Andean headwater and piedmont streams in the Napo River basin in Ecuador, part of the Amazon River catchment. We found that concentrations increased exponentially with elevation decrease, i.e., between 3,990 and 175 m above sea level. Conversely, Andean mountainous headwater and piedmont streams are hotspots of CO_2 and CH_4 emissions; the respective areal fluxes are 1.7 and 4.5 higher in headwater streams and 1.2 and 6.6 higher in piedmont streams than in lowland streams.

Secondly, report the dissolved GHGs of 15 lakes along an elevational gradient ranging from 2,213 to 4,361 m. Lakes were grouped into three clusters as a function of their characteristics and obtained outcomes. Most lakes showed lower values of the partial pressure of CO_2 (pCO_2) (644-2,152 ppm) than usually attributed to tropical lakes (~1,900 ppm). Three lakes, influenced by volcanic inputs, denoted higher pCO_2 values (3,269-10,069 ppm), while two lakes bordered by large cities showed the lowest pCO_2 values (208-254 ppm), the remaining ten lakes had moderated pCO_2 and the highest dissolved organic carbon concentrations (8.3 to 12.8 mg L^{-1}) that is characteristic of páramo lakes (644-2,152 ppm). Dissolved CH_4 concentrations ranged between 170 and 24,908 nmol L^{-1} and were negatively correlated to lake area and depth. N_2O saturation levels ranged between 64 % and 101 %. The surface waters were under-saturated in N_2O regarding atmospheric equilibrium, probably due to soil-water inputs with low N_2O levels due to soil denitrification. By upscaling to lakes in the whole Amazon basin, we found that the average areal FCH_4 (per m^2) was 1.3 times higher in highland lakes (0.75 gC m^{-2} yr^{-1}) than in lowland lakes (0.58 gC m^{-2} yr^{-1}) owing to the combination of higher dissolved CH_4 concentration (265 nmol L^{-1} versus 179 nmol L^{-1}) and higher gas transport velocity (k) values (3.5 cm h^{-1} versus 2.5 cm h^{-1}). Meanwhile, the average areal FCO_2 was 11 times lower in

the highlands (23 gC m^{-2} yr^{-1}) than in the lowlands (255 gC m^{-2} yr^{-1}) owing to the lower pCO_2 values (530 ppm versus 2,909 ppm).

RÉSUMÉ

Les rivières et fleuves contribuent de manière substantielle aux émissions globales de dioxyde de carbone (CO_2) et de méthane (CH_4). La plupart des émissions de GES par les rivières proviennent des tropiques, ~60-80% pour le CO_2, ~70% pour le CH_4, et ~79% pour l'oxyde nitreux (N_2O). Néanmoins, la surface totale des cours d'eau situés dans les tropiques (24°N-24°S) correspond à ~44% de la surface totale des cours d'eau dans le monde, ce qui implique que les émissions fluviales de GES par unité de surface (m^2) sont plus élevées que dans d'autres zones climatiques. L'Équateur se situe sous les tropiques et est le plus petit des 17 pays megadivers du monde, abritant un nombre élevé d'écosystèmes différents, ce qui permet d'étudier dans un espace relativement petit, les rejets vers l'atmosphère de GES d'un important affluent de l'Amazone, ainsi que d'un système lacustre diversifié. La recherche s'est réalisée en deux étapes. Dans un premier temps, nous avons documenté pour la première fois les concentrations de CO_2, CH_4 et N_2O dissous dans les cours d'eau andins en amont et en aval du bassin de la rivière Napo en Équateur, qui fait partie du bassin versant de l'Amazone. Nous avons observé que les concentrations augmentaient de manière exponentielle avec la diminution de l'altitude, c'est-à-dire entre 3 990 et 175 m au-dessus du niveau de la mer. Inversement, les cours d'eau en amont et en aval des montagnes andines sont des hotspots d'émission de CO_2 et de CH_4 ; les flux respectifs sont 1,7 et 4,5 fois plus élevés dans les cours d'eau en amont et 1,2 et 6,6 fois plus élevés dans les cours d'eau en aval que dans les cours d'eau en plaine.

Le second volet de notre étude a consisté à échantillonner les concentrations de GES dissous de 15 lacs le long d'un gradient d'altitude allant de 2 213 à 4 361 m. Les lacs ont été regroupés en trois groupes en fonction de leurs caractéristiques et de nos observations. La plupart des lacs présentaient des valeurs de pression partielle en CO_2(pCO_2) (644-2152 ppm) inférieures à celles généralement attribuées aux lacs tropicaux (~1900 ppm). Trois lacs, influencés par des apports volcaniques, présentaient des valeurs de pCO_2 plus élevées (3 269 -10 069 ppm), tandis que deux lacs bordés par de grandes villes présentaient les valeurs de pCO_2 les plus basses (208-254 ppm). Les dix lacs restants présentaient des valeurs de pCO_2 modérées et les concentrations de carbone organique dissous les plus élevées (8.3 à 12.8 mg L^{-1}), caractéristiques des lacs de páramo (644-2152 ppm). Les concentrations de CH_4 dissous variaient entre 170 et 24 908 nmol L^{-1} et étaient négativement corrélées à la superficie et à la profondeur des lacs. Les niveaux de saturation en N_2O étaient compris entre 64 % et 101 %. Les eaux de surface étaient sous-saturées en N_2O par rapport à la

concentration atmosphérique, probablement en raison des apports d'eau provenant des sols avec de faibles niveaux de N_2O dus à la dénitrification des sols. En comparant les résultats avec ceux du bassin de l'Amazone, nous avons constaté que le flux moyen FCH_4 (par m2) était 1,3 fois plus élevé dans les lacs d'altitude (0,75 gC m^{-2} an^{-1}) que dans les lacs de plaine (0,58 gC m^{-2} an^{-1}) en raison de la combinaison d'une concentration plus élevée de CH_4 dissous (265 nmol L^{-1} contre 179 nmol L^{-1}) et de valeurs de coefficient d'échange (k) plus élevées (3.5 cm h^{-1} contre 2.5 cm h^{-1}). Parallèlement, le flux de CO_2 moyen était 11 fois plus faible dans les hautes terres (23 gC m^{-2} an^{-1}) que dans les basses terres (255 gC m^{-2} an^{-1}) en raison des valeurs plus faibles de pCO_2 (530 ppm contre 2 909 ppm

RESUMEN

Los ríos y arroyos contribuyen sustancialmente a las emisiones globales de dióxido de carbono (CO_2) y metano (CH_4). La mayoría de las emisiones de GEI fluviales provienen de los trópicos, ~60-80% de CO_2, ~70% de CH_4 y ~79% de óxido nitroso (N_2O). Sin embargo, el área superficial total de las corrientes fluviales (SSA) en los trópicos (24°N-24°S) corresponde a ~44% del SSA total a nivel mundial, lo que implica que las emisiones de GEI por área (por m^2) son más altas que en otras zonas climáticas. Ecuador se localiza en los trópicos, y es el más pequeño de los 17 países megadiversos en el mundo, por lo que alberga una asombrosa cantidad de ecosistemas, lo que ofrece las condiciones para estudiar, en un espacio relativamente corto, las evasiones de GEI de un importante río afluente del Amazonas, así como un sistema lacustre diverso. La presente tesis se divide en dos secciones. En primer lugar, reportamos por primera vez las concentraciones disueltas de CO_2, CH_4 y N_2O en los arroyos de cabecera y piedemonte andinos en la cuenca del río Napo en Ecuador, parte de la cuenca del río Amazonas. Encontramos que las concentraciones aumentaron exponencialmente con la disminución de la elevación, es decir, entre 3990 y 175 m sobre el nivel del mar. Asimismo, las cabeceras montañosas de los Andes y los arroyos de piedemonte son puntos críticos de emisiones de CO_2 y CH_4. Los flujos respectivos son 1,7 y 4,5 más altos en los arroyos de cabecera y 1,2 y 6,6 más altos en los arroyos de piedemonte que en los de tierras bajas.

En segundo lugar, reportar los GEI disueltos de 15 lagos a lo largo de un gradiente altitudinal que va de 2213 a 4361 m. Los lagos se agruparon en tres tipos; en función de sus características y resultados obtenidos. La mayoría de los lagos mostraron valores más bajos de la presión parcial de CO_2 (pCO_2) (644-2,152 ppm) de lo que se suele atribuir a los lagos tropicales (~1,900 ppm). Tres lagos, influenciados por aportes volcánicos, denotaron valores de pCO_2 más altos (3,269 -10,069 ppm), mientras que dos lagos bordeados por centros urbanos mostraron los valores de pCO_2 más bajos (208-254 ppm). Los diez lagos restantes tenían pCO_2 moderado (644-2,152 ppm) y los valores más altos de carbón orgánico disuelto (8.3 a 12.8 mg L^{-1}), lo cual es característico de los lagos de páramo. Las concentraciones de CH_4 disuelto oscilaron entre 170 y 24,908 nmol L^{-1} y se correlacionaron negativamente con el área y la profundidad del lago. Los niveles de saturación de N_2O oscilaron entre el 64 % y el 101 %. Las aguas superficiales estaban subsaturadas en N_2O con respecto al equilibrio atmosférico, probablemente debido a aportes de agua al suelo con bajos niveles de N_2O debido a la desnitrificación del suelo. Al escalar a los lagos en toda la cuenca del Amazonas, encontramos que el flujo promedio de FCH_4 (por m^2) era

1,3 veces mayor en los lagos de las tierras altas (0,75 gC m^{-2} $año^{-1}$) que en los lagos de las tierras bajas (0,58 gC $m^{-2}año^{-1}$) debido a la combinación de una mayor concentración de CH_4 disuelto (265 nmol L^{-1} versus 179 nmol L^{-1}) y mayores valores de velocidad de transporte de gas (k) (3,5 cm h^{-1} versus 2,5 cm h^{-1}). Mientras tanto, el FCO_2 promedio por área fue 11 veces menor en las tierras altas (23 gC m^{-2} $año^{-1}$) que en las tierras bajas (255 gC m^{-2} $año^{-1}$) debido a los valores más bajos de pCO_2 (530 ppm versus 2,909 ppm)

List of Figures

Chapter 1

Chapter 2

Chapter 3

Chapter 4

List of Tables

Chapter 1

Chapter 2

Chapter 4

CHAPTER 1
INTRODUCTION

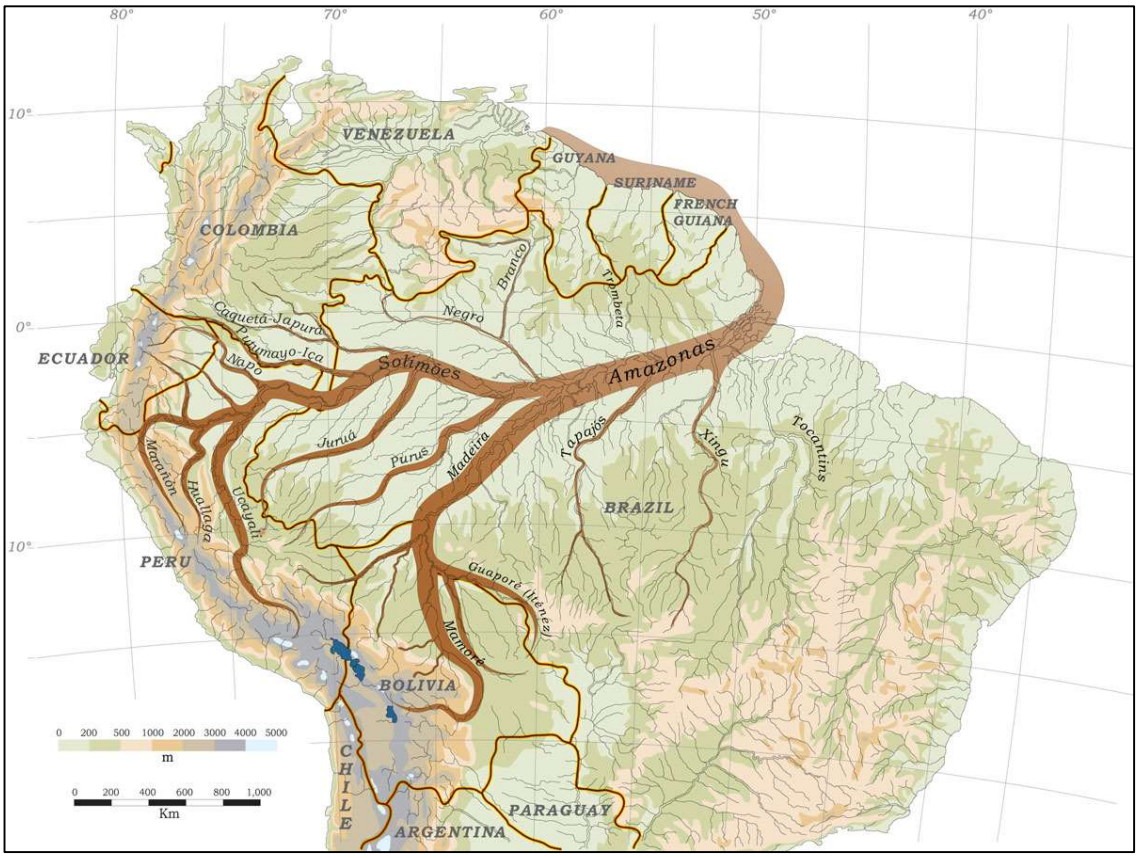

FIGURE 1.1 Amazon Basin - Fluvial Systems Source: (Amazon Waters, 2020)

Climate is physics!

The Nobel Committee 2022 awarded the physics prize for the "Physical modeling of Earth's climate, quantifying variability and reliably predicting global warming." Two of the three laureates —Klaus Hasselmann and Syukuro Manabe— pioneered climate modeling and conceptualized elegant explanations of observed climate properties to the comprehensive analysis based on numerical fluid dynamics used today (Hegerl, 2022). The Nobel prize award highlights that Climate is physics, rendering the question "do you believe in global warming" meaningless and inferring that modeling is a crucial element of understanding and mitigating climate change.

The Climate is a forced, dissipative, chaotic system that is out of equilibrium and whose complex natural variability arises from the interplay of positive and negative feedback, instabilities, and saturation mechanisms (Ghil and Lucarini, 2020). Those factors include many chemical species and all physical phases. The system's heterogeneous phenomenology includes the microphysics of clouds, cloud-radiation interactions, atmospheric and oceanic boundary layers, land and inland waters interactions, and several scales of turbulence (Ghil, 2019). On different time scales, the climate systems' equilibrium has been strongly affected by relatively small changes in the forcing for anthropogenic and natural disturbances (Lucarini et al., 2014). On the macroscopic level, the differences in the absorption of solar radiation throughout the atmosphere drive the Climate, as well as in a thin surface layer of the ocean, continental waters, and soil. Earth's natural greenhouse effect makes life as we know it. By far, the most important GHG is water vapor. However, there is a substantial contribution from carbon dioxide (CO_2), ozone (O_3), methane (CH_4), and nitrous oxide (N_2O) in providing for the relatively mild temperature on Earth (Mitchell, 2009).

FIGURE 1.2 Greenhouse gas effect. Sun acts as perfect blackbody that emits radiation. The balanced composition of the atmosphere sustains life and geochemical processes (World 101, 2022).

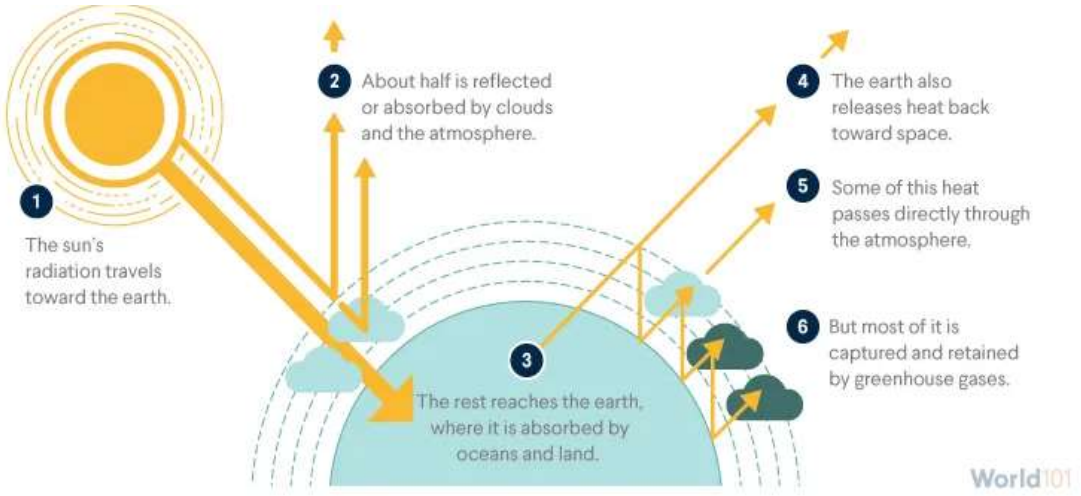

A perfect emitter or blackbody emits radiation over a range of wavelengths. The distribution of energy emitted with wavelength is a function of the temperature of this emitter: the hotter the emitter, the shorter the wavelength of peak emission (Gao et al., 2019). Thus, the Sun, which has a surface temperature of ~ 6000 K, emits most radiation in the range of 0.2 - 4 μm (including ultraviolet, visible, and near-infrared wavelength), whereas the Earth at 255 K emits mainly in the range of 4 - 100 μm.

Although water vapor is such a potent greenhouse molecule, human activities do not substantially influence its dynamics, and it has a short atmospheric life of some days in contrast to CO_2 (Inglezakis, 2016). CO_2 and other greenhouse gases absorb the long-wave radiation emitted from the surface and reradiate it to the surface and space, producing additional warming and maintaining the balance with incoming solar radiation Fig 1.2. As a result, the current global mean surface temperature is substantially warmer than the effective radiating temperature. This increase in surface temperature is known as the "greenhouse effect." The term applies to atmospheric gases, which are relatively transparent to solar radiation but absorb long-wave radiation like glass in a greenhouse. Thus, the term "greenhouse" is misleading, as the atmospheric greenhouse effect is solely due to radiative processes. Nevertheless, the term is universally accepted (Mitchell, 1989).

Consider the following analogy to understand the greenhouse effect. Although the surface of Venus is high enough to melt lead and the temperature on Mars is so low that almost all its relatively small amount of water is frozen, the Earth, orbiting between these two inhospitable neighbors, enjoys a climate that has evolved a vast variety of complex life (American Chemical Society, 2022). Their respective atmospheres have made Venus a furnace and have locked Mars in a deep freeze. Venus's atmosphere is composed of CO_2; however, it started with roughly the same amount of CO_2 as the Earth. Nonetheless, the surface of Venus was so hot and dry that carbon-bearing compounds evaporated rather than remaining in the rocks accumulating a massive greenhouse gas in the atmosphere (Spencer, 2022).

Essentially 100% of the energy that fuels the Earth comes from the Sun, whose temperature in the central interior regions is around 8×10^6 K (Duffie and Beckman, 2013). The solar constant S_o is the energy from the Sun per unit time received on a unit area of the surface perpendicular to the direction of propagation of the radiation at mean Earth-Sun distance outside the atmosphere. The World Radiation Center (WRC) has adopted a value of S_o = 1,367 W m^{-2}, with an uncertainty of the order of ± 1% (Widén and Munkhammar, 2019). This sunlight is in the visible region, where the Earth's atmosphere is almost transparent. According to the Wien Displacement Law, the wavelength of maximum emission for the Sun is 0.5 μm (Pidwirny, 2006). Therefore, almost 99 % of this Sun's radiation is in short wavelengths from 0.15 to 4.0 μm. Of this, 9 % is in the ultraviolet (A < 0.4 μm), 45 % is in the visible (0.4 < A < 0.74 μm), and 46 % is in the near-infrared A > 0.74 μm. Of the total amount of incoming radiation, the Earth's surface (land and oceans) absorbs around ~50 %; the atmosphere absorbs ~20 %; and the clouds, the Earth's surface, and different gases and particles (the Earth's albedo is 0.3 on average) reflect the remaining ~30 % to space Fig 1.3. Therefore, 70% of the Sun's energy causes Earth's surface, clouds, and atmosphere to warm (North Caroline Climate Office, 2016). Since that portion of energy makes its way back out to space the energy balance is well maintained. This cycle occurs 24 hours a day, and the energy emitted by Earth is in the longwave radiation due to the characteristic temperatures of the Planet (US National Weather Service, 2019).

The stratosphere is heated directly by O_3's absorption of solar radiation and is approximately in radiative equilibrium. All molecules with three or more atoms meet this criterion of IR absorbers. While the Earth's (dry) atmosphere is predominantly composed of non-IR absorbers, N_2 (78 %), O_2 (21 %), and Ar (~0.9 %), the 0.1 % of remaining trace gases contain CO_2, CH_4, N_2O, and O_3 that absorb IR. Collisions between these energized molecules and others transfer energy through the atmosphere, increasing the average thermal energy and raising the temperature. As a result, heat distributes through the troposphere by convective (vertical) mixing (Mitchell, 2009). In the presence of an atmosphere, much of the longwave emission to space emanates from atmospheric gases rather than the surface. Thus, the level at which the mean radiating height occurs varies principally with the infrared opacity. Gases such as CH_4, N_2O, O_3, CO_2, and water vapor (IPCC, 2021) tend to be sensitive to infrared opacity (Smirnov, 2016). Regaining our planetary analogy, Mars, with a relatively thin atmosphere, has a small mean radiating height and a weak greenhouse effect. In contrast, Venus, with its dense, highly

absorbing CO_2 atmosphere, has a considerable mean radiating height and a potent greenhouse effect (Mitchell, 2009). Manabe and Wetherald (1967) postulated that an increase of 2.3°C for a doubling of atmospheric CO_2.

FIGURE 1.3 Earth's atmospheric opacity to various wavelengths of electromagnetic radiation. The wavelength range of interest for climate science and atmospheric warming is from about 0.1 to 100 µm. (NASA, 2008).

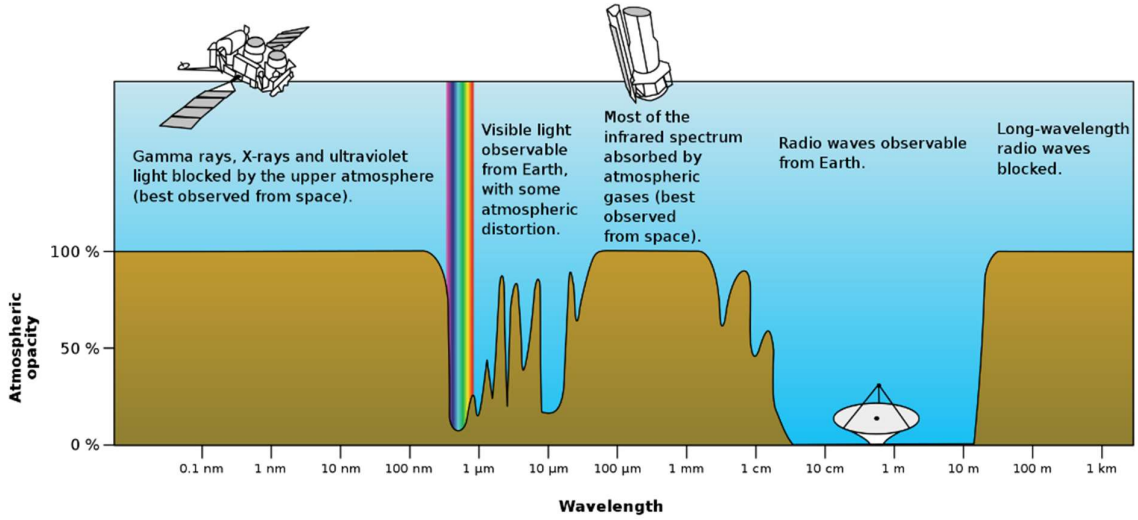

The energy balance in the atmosphere comprehends mainly the estimates of incoming radiation 342 W m^{-2}(I) Fig 1.4, the outgoing longwave radiation provided by satellite data (F) at the top of the atmosphere 235 W m^{-2}, and the reflected 107 W m^{-2} (E) solar radiation. The Earth has a mean radiating height of 5.5 km and a global mean lapse rate of 6 K km^{-1}, giving a current greenhouse warming of 33 K (Berger and Tricot, 1992).

FIGURE 1. 4 Global energy balance based on an input of 342 Wm^{-2} of solar radiation (NASA, 2022).

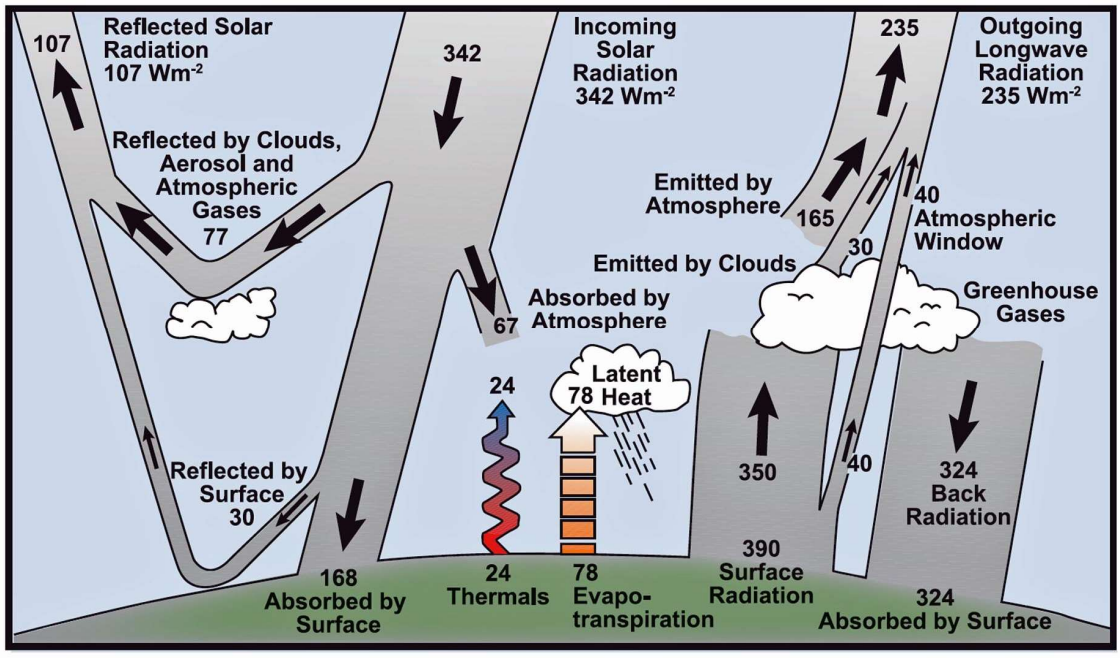

Any change in E or F, like that due to the increase in the atmospheric concentration of the GHGs, leads to a perturbation of the greenhouse effect (American Chemical Society, 2022; Pidwirny, 2006; Wei et al., 2018).

Greenhouse recognition and role of inland waters

GHGs keep the Earth heartfelt and necessary for naturally happening atmospheric functions. In fact, without their presence, the expected effective temperature just with the Sun's radiation would be $^{-1}9$ °C (Kweku et al., 2018). However, it was not until the mid-^{1}950s that the term greenhouse effect was attached to climate alteration concerns (Mitchell, 1989). 20 years later with computing modelling came along, Manabe and his colleagues laid the foundations for predicting the climate response to GHGs emissions. At present, global average temperature has reached 1.1 °C above pre-industrial levels (European Commission, 2020) —anthropogenic activities mainly cause this. According to their contribution to the warming effect, we highlight the CO_2 (74,4 %) that enters the atmosphere through the burning of fossil fuels, solid waste, wood, and other biological materials and because of specific chemical reactions such as respiration or cement production (Friedlingstein et al., 2022). CO_2 is removed from the atmosphere by plants as part of the biological carbon cycle.

FIGURE 1.5 Global Carbon Dioxide Balance (Global Carbon Project, 2022).

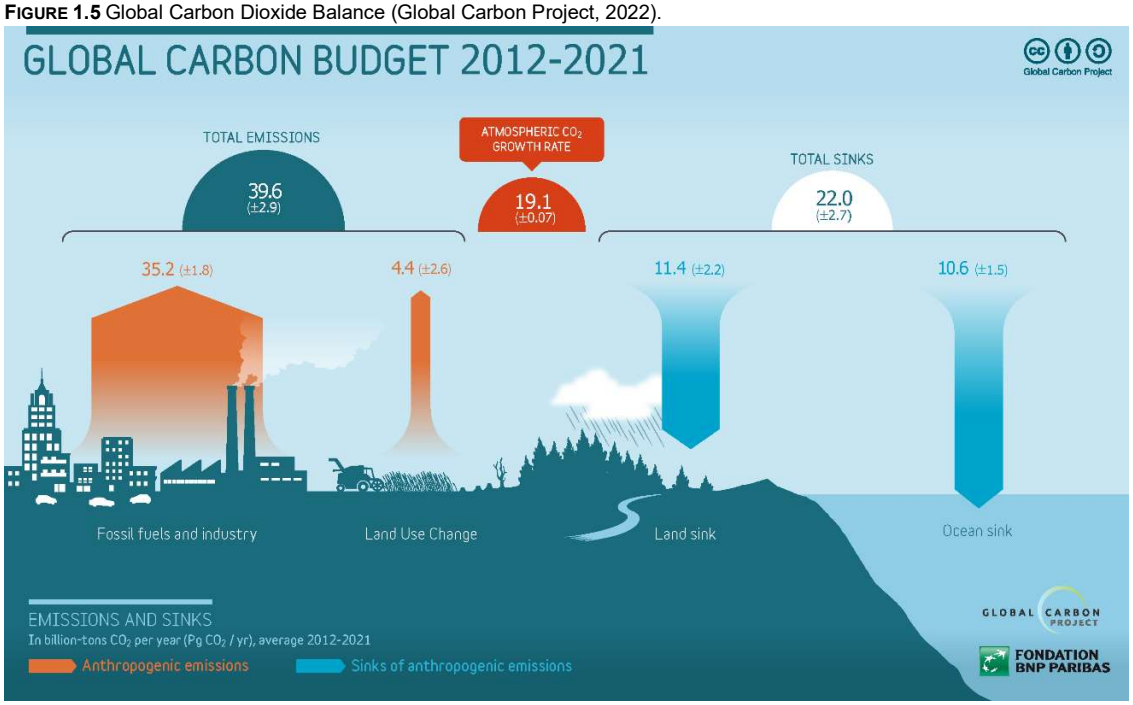

Then, we have the CH_4 (17.3 %) emitted during coal, natural gas, and oil production and transport. CH_4 emissions also result from livestock and other agricultural practices, land use, and the decay of organic matter in natural ways or landfills (Van Amstel, 2012; Kweku et al., 2018)

FIGURE 1. 6 Global Methane Balance (Global Carbon Project, 2018)

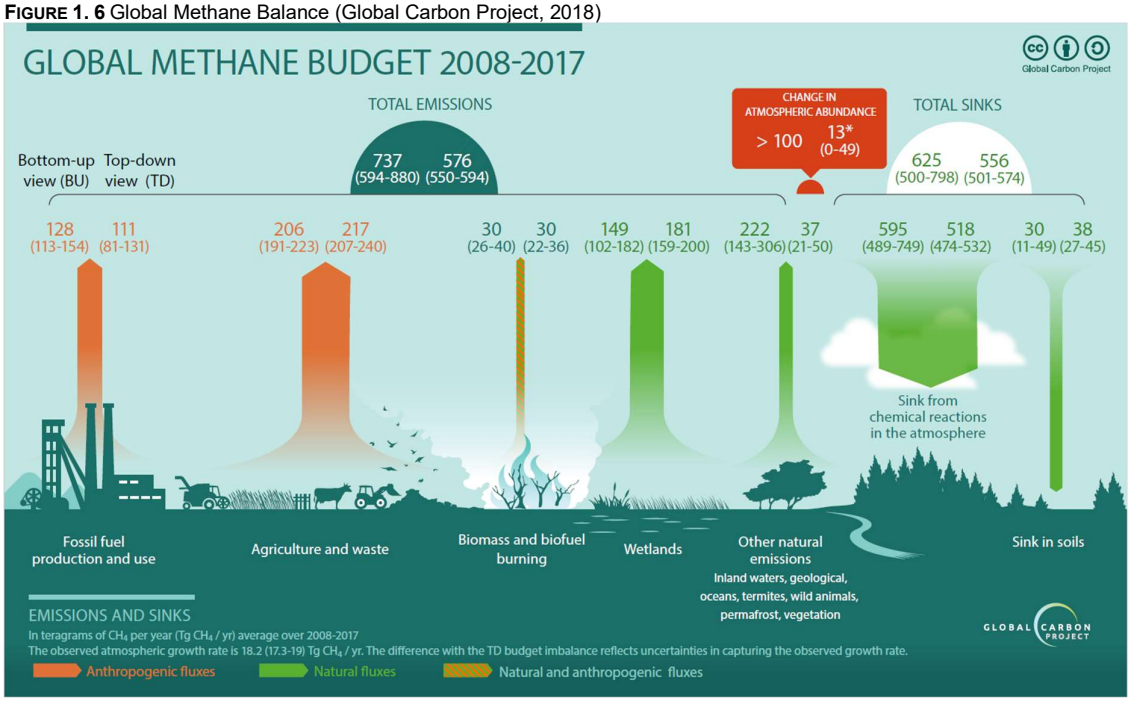

Finally, the N_2O (6,7 %) is emitted during agricultural, land use, and industrial activities; combustion of fossil fuels and solid waste; as well as during treatment of wastewater. Together, the three account for ~98,4 % of global greenhouse gases (IPCC, 2021; EPA, 2020).

FIGURE 1. 7 Global Nitrous Oxide Balance (Global Carbon Project, 2021).

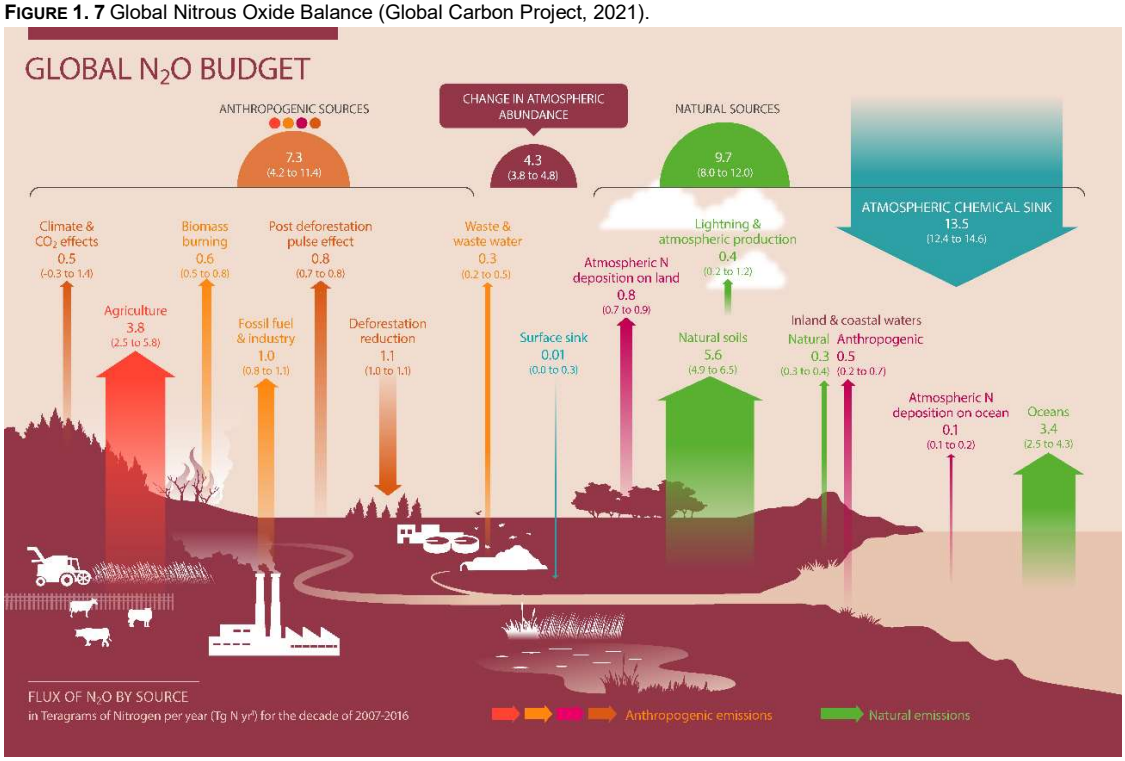

Total net anthropogenic GHG emissions have continued to rise from 2010–2019 up to 59 ± 6.6 Gt CO_2-eq, about 12% higher than in 2010 and 54 % higher than in 1990. Nevertheless, the average annual growth rate slowed from 2.1% yr^{-1} between 2000 and 2009 to 1.3% yr^{-1} between 2010 and 2019 (IPCC, 2022).

The ways how carbon (C) and nitrogen (N) interact between land, atmosphere, and oceans obey the pathways determined by their biogeochemical cycles, which correlate mutually since the productivity of plants and soil organisms strongly depends on N availability (Zaehle and Dalmonech, 2011; Schimel et al., 1997). The carbon cycle is a biogeochemical process by which C exchanges among the lithosphere, biosphere, hydrosphere, and atmosphere. The main C form exchanged with the atmosphere is CO_2, whose concentration has increased from 227 ppm in 1750 to ~ 410 ppm in 2020. Initially, this increment was due to deforestation and other land-use change activities(Friedlingstein et al., 2022; House et al., 2002). Nevertheless, after the industrial revolution (Pongratz and Caldeira, 2012)fossil fuel burning became the primary anthropogenic C source.

The recognition of GHGs and climate change began in 1861 when physicist John Tyndall noted the influence of atmospheric absorption on the Climate (Tyndall, 1861). In 1896, Arrhenius highlighted that the selective absorption of the aqueous vapor and carbonic could substantially alter the surface temperature through the greenhouse effect (Arrhenius, 1896). On his part, Guy Callendar calculated that from ~1870 to ~1940, anthropogenic fuel combustion added about 150,000 million tons of CO_2 to the air and connected it to global warming (Callendar, 1938). In 1941,(Maslin, 2016) explained the fundamental causes of the ice ages and how humanity has disrupted the natural cycles. By 1956 Plass formulated the Carbon Dioxide Theory of Climate Change, predicting that the warming trend would continue, at least for several centuries (PLASS, 1956), and introduced the influence of temperature on the CO_2 equilibrium between oceans and atmosphere. By 1979, oceanographers consented that biota in oceans could be a sink (Broecker et al., 1979) and a CO_2 source for the atmosphere. Shortly after, limnologists came into play (Schlesinger and Melack, 1981) estimating the transport of dissolved and particulate organic carbon (DOC and POC) to the world's oceans by river flow. They emphasized the importance of these significant amounts of C stored in deep ocean sediments or released to the atmosphere for the global C cycle. Until then, studies revealed the importance of rivers in the C cycle because they enabled the transport of C (organic and inorganic) as a pipeline connection between land and ocean. This delivery of terrestrial C is partly the result of several transformations and losses in aquatic systems.

Nevertheless, they did not directly include the aquatic systems as a source of CO_2. Instead, these approaches resulted in simplified depictions of the global C cycle that considered ocean and land connected through gas exchanges with the atmosphere (Siegenthaler and Sarmiento, 1993), i.e., the biota, photosynthesis, and respiration. However, they still overlooked the role of inland waters -as reactors- in addressing the global budget. By the 1990s, the modeling underwent significant improvements; for instance, (Schimel et al., 1997; Canadell et al., 2000) showed a strong correlation between C, N, and terrestrial water fluxes. A disruptive study (Cole et al., 2007) formulated a simplified mass balance to track the fate of C in an integrated freshwater and terrestrial budget. They hypothesized that the C imported annually to the global aquatic ecosystems (1,9 Pg C yr^{-1}) could have three fates, i.e., CO_2 evasions to the atmosphere (0.75 Pg C yr^{-1}), sediment storage in the river (0.23 Pg C yr^{-1}), and transport to the oceans (0.9 Pg C yr^{-1}). To explain this foretaste, they brought up the global role of inland aquatic systems in the C cycle pathways. They began implying that if the inland freshwaters were important CO_2 sources, the C should have been an active input from soil respiratory products or the oxidation of terrestrially derived organic carbon (OC) within the aquatic system (Cole et al., 2007). If this hypothesis was true, it was essential to differentiate between the inland water systems and their characteristics. For example, the type (rivers, lakes, reservoirs, and wetlands), the presence (permanent, seasonal covered), the latitude (tropical, temperate, and frozen), and the origin (raining, melting,

groundwater, headwaters), since different drivers can modify the mechanisms, velocity, and reaction yields within the processes of storage, evasion, and transport of C.

CH_4 is also critical for assessing realistic climate change pathways, given that it is the second most important GHG in terms of climate forcing. Its concentration is higher than ever, as observed in the ice-core record over the past 800,000 years (Van Amstel, 2012). Although global anthropogenic emissions of CH_4 are around 366 $TgCH_4\ yr^{-1}$ (3% of the global CO_2 anthropogenic), it contributed ~ 25% (~0.62W m^{-2}) to the radiative forcing accumulated in the lower atmosphere since 1750 (Friedlingstein et al., 2022). Agriculture and fossil fuels account for ~70 % of the anthropogenic CH_4. Natural sources include wetlands, termites, oceans, hydrates, geological sources, wild animals, and wildfires. The first estimations of CH_4 emissions relied on 3D models, (Bergamaschi et al., 2007, 2005; Hein and Heimann, 1994; Houweling et al., 2000, 1999; Lelieveld et al., 1998; Tans et al., 1990) have all published analyses of the CH_4 budget based on measurements and model calculations. IPCC has summarized them in the Second, Third, and Fourth Assessment Reports. The bottom-up estimates issued by the Emissions Database for Global Atmospheric Research EDGAR (Wunch et al., 2009) and summarized by (Van Amstel, 2012) have contributed to the scientific literature since 1970. From 2012 onwards, bottom-up global anthropogenic inventories were available in a systematic record, which permitted (Friedlingstein et al., 2022) to elaborate on the Global Methane Budget 2000–2017, whose results are sorted by decades (2000 – 2009) 547 $TgCH_4\ yr^{-1}$ and (2008 – 2017) 576 $TgCH_4\ yr^{-1}$.

Inland waters (lakes, ponds, reservoirs, streams, rivers) are natural sources of CH_4 (Wunch et al., 2009; Van Amstel, 2012; Bastviken et al., 2011; Borges et al., 2015c), through several pathways, such as ebullition from sediments, diffusive flux, and plant-mediated transport through emergent aquatic plants (Bastviken et al., 2011). Most fluvial systems show oversaturation of CH_4 with global emissions of 26.8 Tg $CH_4\ yr^{-1}$, equivalent to ~15-40% of wetland and lake effluxes, respectively (Stanley et al., 2015). Lakes and ponds prefer (3:1) ebullition rather than diffusive mechanisms to release CH_4 (Bastviken et al., 2011), mainly smaller and shallower lakes. Prevailing studies (Saunois et al., 2020) lead to a mean estimate of all inland freshwaters at 159 Tg $CH_4\ yr^{-1}$ ranging from 117 to 212 Tg $CH_4\ yr^{-1}$, which suggests that lakes or natural ponds, flooded land–reservoirs, and streams–rivers account for 70 %, 13 %, and 17 % of the average inland water fluxes, respectively (Bastviken, 2022; Canning et al., 2021).

FIGURE 1. 8 Nitrification and denitrification cycles (Thakur et al., 2019).

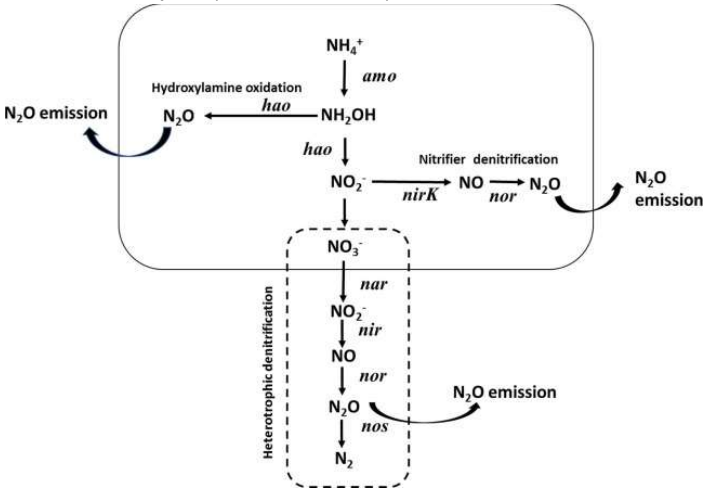

N_2O, like CO_2 and CH_4, is a long-lived greenhouse gas accumulating in the atmosphere. The concentration of atmospheric N_2O has increased by more than 20 % from 270 parts per billion (ppb) in 1,750 to 331 ppb in 2018 (Akshit, 2020). Two key biochemical processes—nitrification and denitrification—control N_2O production in terrestrial and aquatic ecosystems and are regulated by multiple environmental and biological factors, including temperature, water and oxygen levels, acidity, and substrate availability (Butterbach-Bahl et al., 2013) Fig 1.8. Like CO_2 and CH_4, the N_2O emissions have been reported annually by IPCC. However, these inventories do not provide a complete picture of N_2O emissions owing to their omission of natural sources, the limitations in methodology for attributing anthropogenic sources, and missing data on key regions like Africa or South America. Nevertheless, bottom-up and top-down approaches have improved to give consistent estimates for the decade between 2007 and 2016 ~ 17 Tg N yr^{-1}. 23% of this value is not absorbed in natural sinks. Therefore, there is an accumulation of ~4 Tg N yr^{-1}. Anthropogenic sources contributed, on average, 43 % of the total N_2O evasions to the atmosphere (Butterbach-Bahl et al., 2013). Agricultural soil management is the largest source accounting for about 74 %.

When comparing the global annual GHG emissions from natural systems with those generated by human activity, results indicate that the global annual evasions range between 54.33 and 75.50 Gt CO_2-eq, of which natural emissions account for 18.13–39.30 Gt CO_2-eq, with the most likely value being approximately 29.07 Gt CO_2-eq (Yue and Gao, 2018; Friedlingstein et al., 2022). The natural to anthropogenic-emissions ratio is approximately 0.8 (Yue and Gao, 2018); for both, interactions between the terrestrial C and N cycles shape the response of ecosystems to global change. Therefore, their accurate assessment of the pathways and dynamics among the atmosphere, ocean, and terrestrial biosphere is critical to developing policies and projecting future climate change (Friedlingstein et al., 2022).

Sinks and sources

As the Earth's system has evolved, the global Climate has continuously changed. In recent decades, the issue of climate change, especially the relationship between human activities and global warming, has drawn widespread attention (Stocker et al., 2013; Yue and Gao, 2018). However, some different voices have questioned these conclusions. For example, (Barnett et al., 1999) suggested that changes in global Climate inferred from surface air temperature are likely, not due solely to anthropogenic causes. Instead, the atmospheric system must combine natural and human dynamics (sinks and sources) to explain the problem better. All these drivers were inputs to develop several modelings that simulate, every time more trustful, the evolution of the global average temperature in the 20th century (Baede et al., 2016). The natural inputs include solar variability, volcanic eruptions, and interactions within the Climate system.

Conversely, human inputs embrace the atmosphere's composition (including increases in the concentrations of greenhouse gases and aerosols) caused by industrial and social activities and changes in land use and coverage. It is worth nothing that sinks, and sources could change their storage and emission capacity according to the driving forces that control them. For instance, although emissions from fossil fuels started before the Industrial Era, they became the dominant source of anthropogenic emissions to the atmosphere from around 1950 (Friedlingstein et al., 2022; Pittock, 2013).

Natural sources

Forest fires

Forest fires are a significant source of GHG emissions, and their natural causes include drought, heat, and lightning. Approximately 90% of the gases emitted from forest fires are CO_2 (van der Werf et al., 2009). At the regional scale, boreal forest fires have received widespread attention (Ribeiro-Kumara et al., 2020). A comprehensive study based on a biogeochemical model and improved satellite-derived estimates of area burned, fire activity, and plant productivity to calculate fire emissions for 1997–2009. The study showed that most carbon emissions were from fires in grasslands and savannas (44 %), with smaller contributions from tropical deforestation and degradation fires (20 %), woodland fires (mostly confined to the tropics, 16 %), forest fires (mainly in the extratropic, 15 %), agricultural waste burning (3%), and tropical peat fires (3 %). The annual global GHG emissions from forest fires range between 1.9 to 4.3 GtC, with a most likely value of 3.0 GtC (van der Werf et al., 2010).

Wetlands

Wetland soils contain some of the highest soil C stores in the biosphere. However, there needs to be more understanding of the quantity and distribution of C stored in the remaining wetlands or the potential effects of human disturbance on these stocks (Nahlik and Fennessy, 2016). Their C stocks account for approximately 15% of land surface carbon. Wetland CH_4 emissions are the most significant natural source in the global CH_4 budget, contributing to roughly one-third of natural and anthropogenic emissions (Zhang et al., 2017). Existing studies indicate that they range from 0.65 to 2.04 Gt C, with the most likely value being approximately 1.36 GtC (Friedlingstein et al., 2022; Saunois et al., 2020).

Permafrost

Carbon stored in permafrost regions is one of the least understood and potentially most significant carbon-climate feedbacks because of the size of the carbon pools and the intensity of Climate forcing at high latitudes. Permafrost distributes mainly in Siberia, Canada, and Alaska, with the global permafrost area totaling approximately 18,782 x 10^6 km^2 (Tarnocai et al., 2009). Methane hydrates have been found in continental shelves and below sub-sea and land permafrost. This CH_4 can be either biogenic or thermogenic (Saunois et al., 2020). Research on GHG emissions from permafrost has focused on C, CO_2, CH_4, and N_2O, many of which were flux observations. For example, (Koven et al., 2011) simulated CH_4 emissions under different scenarios for 1860 to 2100 in high latitudes for the three major frozen regions. They found that from the end of the 19th century to the beginning of the 21st century, annual CH_4 emissions at high latitudes remained at 30 to 40 TgC, but this value could triplicate by 2080. The mode values for the annual GHG emissions from permafrost range between 0.6 and 2.1 GtC, with the most likely value being approximately 1.6 GtC per year (Yue and Gao, 2018).

Volcanoes

Volcanic eruptions can release many volcanic gases into the atmosphere, including CH_4 and CO_2. The CO_2 released directly from active volcanoes has three primary sources, dissolved in the mantle, recycled from subducted crustal material, and decarbonation of shallow crustal material (Burton et al., 2013). The level of GHG emissions from volcanic eruptions could be very high. For example, the eruption of the Pinatubo volcano in the Philippines in June 1991 released more than 20 Mt SO_2 and 200 Mt CO_2 into the atmosphere. It formed the largest volcanic cloud event of the 20th century. McCartney et al. (1990) estimated the CO_2 emissions from the Tegan basalt at the peak of eruption (1.36 Ma) to be 13,000 Gt. Intermittent volcanoes release gas much more slowly but last longer, so the total amount of GHGs released by intermittent volcanoes could be more significant than those from eruptions (Burton et al., 2013; Zhang et al., 2019). The GHG

emissions from global volcanic eruptions are estimated to range between 5.45 and 30 Mt per year, with an interphase of approximately 4.5. Hence, the annual total GHG emissions from volcanoes range between 187 and 277 Mt CO_2-eq (Mccartney et al., 1990).

Mud volcanoes

They are the eruption of mud, and the mechanisms and drivers that govern eruptions still need to be better understood. During their formation and subsequent activity, they can also produce large amounts of hydrocarbon gas (Huff and Owen, 2015). GHG mud volcanoes primarily emit CH_4, which accounts for 95 % of the total hydrocarbon gas and small amounts of CO_2. GHGs released during a mud volcano eruption are estimated to be approximately 60% to 80% of the total gas content. Large amounts of gas can also be released during periods of dormancy. Based on the mode values, the global annual CH_4 emissions from mud volcanoes are estimated to range between 0.5 and 6.15 Mt, equivalent to 0.03 to 0.43 MtC. The total GHG emission from mud volcanoes is approximately 200 MtC annually (Shi et al., 2016).

Earthquakes

Earthquakes are another source of GHGs, including the immediate release of CO_2 from the Earth and that from the decay of plants and animals buried after earthquake events (YUE and GAO, 2018). (Saito et al., 2015) estimated the total GHGs from the Tohoku earthquake to be 5.1 Pg C. However, researchers have rarely approximated earthquake GHG.

In summary, global GHG emissions from natural systems range from 18.13 to 39.30 Gt CO_2-eq per year, with a most likely value of 29.07 Gt CO_2-eq. Forest fires account for the most significant component of total emissions at 37.8%, followed by oceans, permafrost, and wetlands at 21.05 %, 20.64 %, and 17.20 %, respectively. Volcanoes and mud volcanoes contribute relatively low GHG emissions, i.e., approximately 1 to 3 % of the total.

Anthropogenic sources

According to the GHG inventory data for global human activity compiled by the UN, CO_2 emissions from global fossil fuel usage and cement production rose from 22.3 Gt in 1990 to 36.2 Gt in 2016, representing a growth rate of approximately 70%. The estimates of global and national fossil CO_2 emissions include the oxidation of fossil fuels through both combustion (e.g., transport, heating) and chemical oxidation (e.g., carbon anode decomposition in aluminum refining) activities, and the decomposition of carbonates in industrial processes (e.g., the production of cement) (Friedlingstein et al., 2022; Saunois et al., 2020).

Fossil CO_2 emissions

Cumulative fossil CO_2 emissions for 1850–2021 were 465 GtC, including the cement carbonation sink. In this period, 46 % of fossil CO_2 emissions came from coal, 35 % from oil, 15 % from natural gas, 3% from the decomposition of carbonates, and 1 % from flaring. Global fossil CO_2 emissions were 5.1 % higher in 2021 than in 2020 because of the global rebound from the worst COVID-19 pandemic, with an increase of 0.5 GtC to 9.9 GtC (including the cement carbonation sink) in 2021 (Friedlingstein et al., 2022). Since the 1960s, there has been a noticeable increase in GHG emissions from coal, oil, and gas combustion, which have increased from 5 Gt to 14.5 Gt, from 3 Gt to 12.5 Gt, and from 0.8 Gt to 7.0 Gt, respectively. Meanwhile, GHG emissions from oil increased significantly from 1960 to 1980, and GHG emissions from coal combustion showed significant growth at the beginning of the 21st century but have decreased slightly since 2014. In 2021, the most considerable absolute contributions to global fossil CO_2 emissions were from China (31 %), the USA (14 %), the EU27 (8 %), and India (7 %). These four regions account for 59% of global CO_2 emissions, including international aviation and marine bunker fuels (2.8 % of the total) (Jiang and Green, 2017; Massetti, 2011).

Land use changes

Cumulative CO_2 emissions from land-use changes (ELUC) for 1850–2021 were 205 GtC (Friedlingstein et al., 2022). The cumulative emissions from ELUC show a large spread among individual estimates of 140 GtC (updated in 2017), 280 GtC (BLUE), and 190 GtC (OSCAR) for the three bookkeeping models and a similar comprehensive estimate of 185 GtC for the Dynamic Global Vegetation Model (DGVM) (all cumulative numbers rounded the 5 GtC) (Friedlingstein et al., 2022). These estimates are broadly consistent with indirect constraints from vegetation biomass observations, giving a cumulative source of 155 GtC over the 1901–2012 period (Li et al., 2017). However, given the large spread, the best estimate is difficult to ascertain. In contrast to growing fossil emissions, CO_2 emissions from land use, land-use change, and forestry have remained relatively constant over the 1960–1999 period but show a slight decrease of about 0.1 GtC per decade since the 1990s, reaching 1.2 to 0.7 GtC yr^{-1} for 2012–2021 (Hong et al., 2021).

Total anthropogenic emissions

Cumulative anthropogenic CO_2 emissions for 1850–2021 totaled 670 GtC, of which 70 % (470 GtC) occurred since 1960 and 33 % (220 GtC) since 2000. Total anthropogenic emissions more than doubled over the last 60 years, from 4.5 ± 0.7 GtC yr^{-1} for the decade of the 1960s to an average of 10.8 ± 0.8 GtC yr^{-1} during 2012–2021 and reaching 10.9 ± 0.9 GtC in 2021. During 1850–2021, 30 % of historical emissions were from land-use change and 70 % from fossil emissions. However, fossil emissions have grown significantly since 1960, while land-use changes have not. Consequently, the contributions of land-use change to total anthropogenic emissions were smaller during recent periods, 11 % during 2012– 2021 (Hong et al., 2021) .

Natural sinks

Atmosphere

The mass of carbon in the atmosphere increased by 48% from 1750 to 2021. Current CO_2 concentrations in the atmosphere are unprecedented in the last 2 million years, and the current rate of atmospheric CO_2 increase is at least 10 times faster than at any other time during the last 800,000 years (Van Amstel, 2012). In fact, concentrations of CO_2, CH_4, and N_2O increased from 1750 to 2019 by 131.6 ± 2.9 ppm (47.3%), 1137 ± 10 ppb (156%), and 62 ± 6 ppb (23.0%) respectively (Friedlingstein et al., 2022). The growth rate in atmospheric CO_2 level increased from 1.7 ± 0.07 GtC yr^{-1} in the 1960s to 5.2 ± 0.02 GtC yr^{-1} during 2012–2022 with important decadal variations.

Ocean

The carbon content of the oceans is 50 times that of the atmosphere and 20 times that of the biosphere. Global oceans serve simultaneously as a C source and sink, and their substantial thermal mass partially delays the global response to forcings (Ribeiro-Kumara et al., 2020). Since 1850, the ocean sink has added up to 175 ± 35 GtC; more than two-thirds of this amount (120 GtC) has accumulated since 1960 (Kenneth L & Guy, 2016). Anthropogenic emissions represented close to 26% of this total. Besides the concentrations, the growth rate also increased; for example, by the decade 1960s, the average rate was 1.1 ± 0.4 GtC yr^{-1}. Conversely, during 2012-2021, it increased to 2.9±0.4 GtC yr^{-1} with interannual variations of a few tenths of a GtC yr^{-1}. The increased atmospheric CO_2 concentration primarily drives the increase in the ocean sink; nevertheless, other drivers, such as La Niña conditions, expect to weak the sink capacity (McKinley et al., 2017).

Land

Since 1850, the terrestrial CO_2 sink has amounted to 31% of total anthropogenic emissions. Over the historical period, the sink increased with the exponential anthropogenic emissions increase. Over the period from 1960 to the present, the increase in the global terrestrial CO_2 sink is mainly due to the CO_2 fertilization effect. The terrestrial CO_2 sink from the DGVMs ensemble was 3.5 ± 0.9 GtC in 2021, slightly above the decadal average of 3.1±0.6 GtC yr^{-1} (Friedlingstein et al., 2022)

Exchanges between reservoirs

Exchanges are movements called a flux or flow. Sources of carbon are releases from a particular reservoir to the atmosphere, and sinks are places where carbon is removed (taken up) from the atmosphere to another reservoir (Keller et al., 2018).

The atmosphere and the terrestrial biosphere

When carbon that is already in the short-term carbon cycle changes form or flows to a different reservoir (for example, moving from the land to the atmosphere when organic matter is burned), the total amount of carbon in the cycle remains the same. The short-term carbon cycle is roughly balanced, and the amount of carbon-containing greenhouse gases is steady. Fossil fuels, on the other hand, are extracted from underground, so they are not a natural part of the short-term cycle. Thus, when fossil fuels are burned, carbon from long-term storage is added to the short-term cycle. When this happens, not only does the greenhouse effect increase because there are more carbon-containing greenhouse gases in the atmosphere, but the balance of the cycle is disrupted. Until about 150 years ago, fossil fuels were not an important part of the short-term cycle. Now, they must be included in any consideration of this cycle. The fossil-fuel reservoir is estimated at 5,000 Gt C—almost eight times the amount that is currently in the atmosphere. Current fossil-fuel emissions are about 6.7 Gt C per year (Keller et al., 2018).

How do we know that the increased CO_2 in the atmosphere comes from fossil-fuel burning and other human actions rather than from natural processes? An important indicator is provided by the isotopes (different chemical forms) of carbon. Compared to atmospheric carbon, carbon originating in the terrestrial biosphere—including fossil-fuel carbon, which started life as plant material—is also low in the isotope $\delta^{13}C$ relative to $\delta^{12}C$. Measurements from ice cores show a general decrease over the last century in atmospheric levels of $\delta^{13}C$ relative to $\delta^{12}C$, indicating that the increased carbon comes from either fossil-fuel burning, biomass burning, or both (Ferrio et al., 2003; Staddon, 2004).

Oceans and the atmosphere

The role of the oceans in the global carbon cycle is twofold. First, they absorb excess atmospheric CO_2, and second, changes in the physical, chemical, and biological state of the oceans may affect future atmospheric CO_2. The ocean absorbs excess CO_2 in a three-step process: the CO_2 gas passes through the air-sea interface, it reacts chemically with dissolved inorganic carbon in the ocean's surface waters, and then it is transported into the deeper waters (Siegenthaler and Sarmiento, 1993; Lars J. Tranvik et al., 2009) Oceanic circulation is important in the carbon cycle because it affects carbon storage in the ocean. The ocean waters circulate mainly because of three factors: winds, which create surface currents; differences in saltiness throughout the oceans (caused by differences between evaporation and precipitation as well as by freezing and thawing); and differences in water temperature. CO_2 is more soluble in cold water than in warmer water, so surface water from the tropics continues to absorb additional CO_2 as it moves toward higher latitudes and colder temperatures (Sulzman, 2000). In the rainy North Atlantic, the addition of fresh water—which weighs less than saltwater—pushes the more saline

water (and the extra CO_2) toward the ocean floor. Only the movement of carbon from shallow to deeper waters in the conveyor- belt circulation allows large amounts of CO_2 to be stored in the oceans. The surface water has a limited capacity to absorb CO_2. It will even emit CO_2 to the atmosphere if the local atmospheric concentration is lower than the concentration in the surface water.

Chemical processes in the ocean also affect carbon storage. When CO_2 enters the ocean, it reacts chemically with the water to form carbonate and bicarbonate ions. (Ions are chemical compounds of atoms that have gained or lost electrons, leaving them with a positive or negative charge.) As more of these ions are formed, more atmospheric CO_2 can enter the ocean. This reaction depends on temperature, the amount of dissolved inorganic carbon already in the surface water, and, to a lesser extent, the water's salinity and alkalinity (opposite of acidity) (Sulzman, 2000; Farquhar et al., 2001).

Biological processes in the oceans are driven by the marine biota (oceanic plants and animals). The marine biota is believed to play a minor role, if any at all, in the oceans' ability to absorb the CO_2 added to the carbon cycle by humans. In fact, marine biota contributes only about 3 Gt C to the world's total carbon balance. The marine biota plays a crucial role, however, in keeping the level of atmospheric CO_2 steady. Phytoplankton (microscopic ocean plants) take up dissolved inorganic carbon through photosynthesis, just as terrestrial plants take up atmospheric CO_2 during photosynthesis. If that dissolved inorganic carbon remained in the ocean waters, the oceans could not absorb as much CO_2 from the atmosphere as they do. In fact, if there were no oceanic photosynthesis, the atmospheric concentration of CO_2 would be approximately 520 pm—much higher than nowadays level of 400 ppm. In the open ocean, there is more carbon available than the marine biota use for photosynthesis. Scientists think that phytoplankton populations do not use this extra carbon to grow and multiply either because they don't have enough other nutrients and/or light or because zooplankton (minute ocean animals) graze on them and keep their numbers down (Sarmiento and Gruber, 2002). If the nutrients in the ocean were evenly distributed in areas suitable for phytoplankton to live, the increase in photosynthesis would cause today's atmospheric CO_2 concentration to drop to only 230 ppm. Besides using dissolved inorganic carbon for photosynthesis, the marine biota uses it to manufacture both inorganic compounds (e.g., shells) and organic matter, such as cell tissue. As the organisms die and sink, the organic material falls into the deeper ocean, where it is decomposed and converted back to dissolved inorganic carbon. This mechanism of carbon transport to the deep ocean is called the biological pump If the ocean takes up more atmospheric CO_2, thus increasing the amount of dissolved inorganic (Sulzman, 2000).

Terrestrial biosphere and oceans

Carbon moves from the terrestrial biosphere to the oceans indirectly via the global hydrologic cycle (through evaporation from land and rain over the oceans) (Sulzman, 2000), and directly via rivers. This riverine delivery is, in fact, the result of several transformations and losses in aquatic systems en route. River export of organic carbon to the sea ranges from 0.38 to 0.53 Pg C yr^{-1}, whereas export of dissolved inorganic carbon resulting from the fixation of atmospheric carbon through rock weathering is likely to be between 0.21 and 0.3 Pg C yr^{-1}. Collectively, using mid-range values for the river and groundwater components inland waters thus deliver about 0.9 Pg C yr^{-1} to the oceans (Cole et al., 2007).

The role of inland waters in the global and regional carbon balance

The C budget is simply one of the reallocations of C among pools. The only input to the organic pool is from Gross Primary Production (GPP); the return to CO_2 comes from respiration

(R) and abiotic oxidations. Storage (S) is simply the balance between GPP and oxidations. Imports (I) and exports (E) are irrelevant at this scale; the mass balance of C occurs entirely within the boundaries of the global ecosystem. Any change in S has a concomitant change in CO_2 (Cole, 2013).

Net ecosystem production (NEP) can be determined by:

$$NEP = GPP - R = E + \Delta s - I$$

Eq. 1

Also important is the Net primary production (NPP), equal to GPP − Ra and is the fraction of primary production potentially available to consumers. Finally, Rh is the respiration of heterotrophs, including all consumers and microorganisms.

$$R = R_h + R_a$$

Eq. 2

For inland waters, the interaction between CO_2, CH_4, and O_2 is essential to track, and there are five pathways shown in **Fig 1.9** with significant fluxes to consider.

FIGURE 1.9 Carbon pathways at inland waters. About 70% of the C introduced in the water body is emitted GHG. Adapted from (Oak Ridge, 2020)

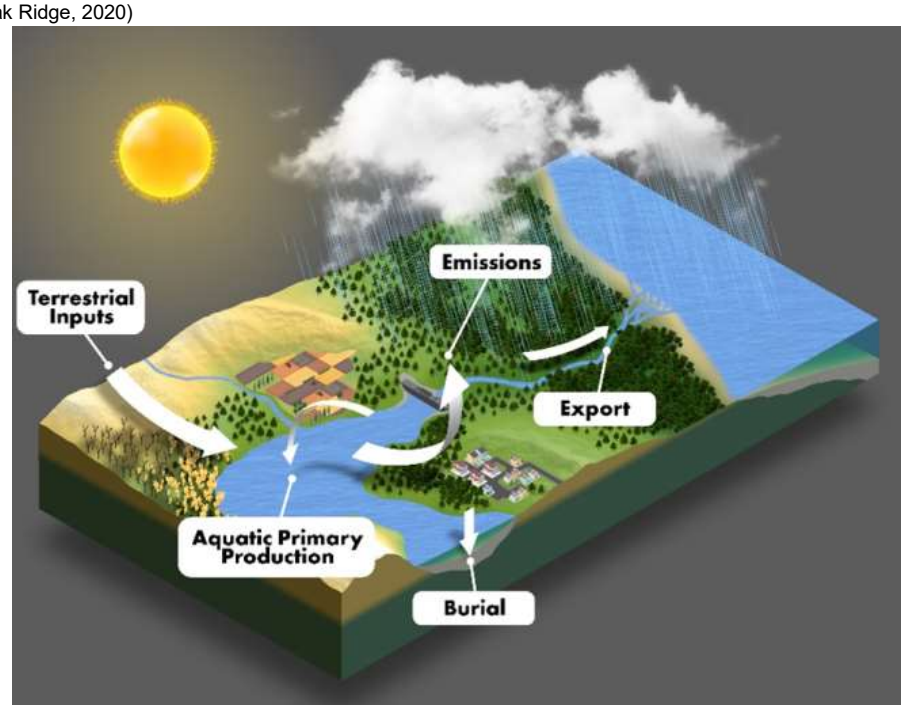

The export of dissolved bicarbonate from land to water represents 'hidden' terrestrial respiration (Cole, 2013). The HCO3 − ion dominates the dissolved inorganic C (DIC) that enters a water body rather than free CO_2. Dissolved bicarbonates are formed principally by dissolving carbonate and aluminosilicate minerals with CO_2 and water. The CO_2 involved in these reactions comes mainly from the respiration of the terrestrial biosphere.

Carbonate weathering

$$CaMg(CO_3)_2 = Ca^{++} + Mg^{++} + 4HCO_3^-$$

Eq. 3

Silicate weathering

$$2\,CO_2 + 3H_2O + MgSiO_3 = Mg^{++} + 2HCO_3^- + H_4SiO_4$$

Eq. 4

Large CO_2 fluxes from inland waters significantly impact our understanding of overall C fluxes and cycling at the landscape or catchment scale. The respiration of upland and wetland vegetation is part of the CO_2 emitted to the atmosphere from inland waters. Whether it is related to lateral transport of soil/wetland CO_2 (that is, respiration taking place in terrestrial or wetland habitats) or lateral transport of soil or wetland DOC and POC mineralized to CO_2 within the aquatic domain. Hence, the lateral transport of C from the upland terrestrial biosphere and wetlands to inland waters and its subsequent emission to the atmosphere offsets the estimates of terrestrial NEP. Furthermore, the lateral transport of soil DOC leads to an underestimation of NEP based on biomass accumulation techniques. In contrast, the lateral transport of soil CO_2 leads to an overestimation of NEP derived from atmospheric measurements (eddy-covariance or flux towers) (Cole, 2013).

Terrestrial net ecosystem production (NEP) can enter aquatic ecosystems as DOC and POC. Both phases form a continuum along physical, chemical, and biological properties with continuous interactions. Revised carbon fluxes of the major world rivers identify the flux of terrestrial DOC (0.25 Pg C yr^{-1}) as the most significant transfer of reduced carbon from the land to the ocean, with POC export estimated at 0.18 Pg C yr^{-1} (J. A. Downing et al., 2008). Nevertheless, carbon fluxes into and out of inland waters have received little attention in global-scale analyses, and their presence is not totally integrated into traditional carbon budgets. Their quantification could prove critical for constraining estimates of terrestrial ecosystem fluxes, adequately integrating all vertical and lateral carbon fluxes over regional and global scales and predicting feedback to climate change (Ciais et al., 2008). For example, (Battin et al., 2009) highlighted that the 'conventional carbon cycle' pool together outgassing from inland waters with fluxes of terrestrial ecosystem respiration and underestimates the potential for lateral transport.

Nevertheless, terrestrially sourced OC can also fuel secondary production by heterotrophic biota in inland waters. Globally, that biota respires 1.2 Pg of terrestrial C each year and releases it to the atmosphere (Battin et al., 2009). In contradiction to the conventional belief that terrestrial OC is recalcitrant and contributes little to the support of aquatic metabolism, (J. A. Downing et al., 2008) suggest that the metabolism of terrestrial OC in freshwater ecosystems is responsible for a large amount of CO_2 outgassing to the atmosphere. Inland waters — ponds, lakes, wetlands, streams, rivers, and reservoirs — permeate terrestrial ecosystems and often shape the Earth's landscapes. Although only about 1% of the Earth's surface is assumed to be covered by inland waters, their collective contribution to global carbon fluxes is substantial compared with terrestrial and marine ecosystems (Battin et al., 2009).

Natural ecosystems must account for the Earth's energy budget because they exchange large amounts of CO_2 with the atmosphere and currently offset ˜ 4Pg Cyr^{-1} of anthropogenic emissions (Raymond et al., 2013). CO_2, CH_4, and N_2O transfer from inland waters to the atmosphere, known as GHG evasions, are components of the global carbon and N cycles. (Kempe, 1984) showed that CO_2 in inland waters calculated from alkalinity and pH were substantially higher than atmospheric values. Anthropogenic driving forces can seriously alter this natural pattern. For instance, the increase of erosion following deforestation and agriculture removes C from the biosphere into inland waters deposition centers, lakes, and reservoirs and causes the OC load of rivers to increase; organic sewage and eroded soil carbon fuel respiration in inland waters; and nutrient release provokes eutrophication mainly in lakes and coastal estuaries, resulting in enhanced primary productivity and CO_2 sequestration. (Raymond et al., 1997) have directly measured the partial pressure of CO_2 in the tidal-freshwater portion of the Hudson River Estuary over 3.5 years. At all times, the Hudson was supersaturated in CO_2 (1125 ± 403 SD) concerning the atmosphere averaged (416 ± 68) µatm. By 2007 this study (Cole et al., 2007) recognizes that inland waters are active components of the global C cycle that store

terrestrially derived carbon in sediments and lose CO_2 as emissions to the atmosphere. A conservative analysis suggests that inland waters annually receive ~ 1.9 Pg C yr^{-1} from the terrestrial landscape, of which about 0.2 ends in aquatic sediments, 0.8 returns to the atmosphere as gas exchange, and finally, The remaining 0.9 Pg yr^{-1} reaches the oceans. The global estimates of CO_2 outgassing fluxes rely on pCO_2 concentrations, k (a parameter related to the physics that determines the rate of gas exchange), and areal extent of inundation per unit area of surface water – along with a more balanced consideration of the tropics and wetlands. (Aufdenkampe et al., 2011) compiled estimates of the global flux of CO_2 outgassing from inland surface waters that range from 0.75 to 1.4 PtC yr^{-1} globally. These values are essential when compared with estimates of net C accumulation on continents (2.2 Pg C y−1) or in the oceans (Cole et al., 2007; Battin et al., 2009).

By the 2010s' the CO_2 data distribution was skewed towards temperate and boreal systems in the Northern Hemisphere. Data in several tropical basins (including Africa and Amazon) were derived from interpolation from adjacent basins rather than actual measurements. In this context, (Borges et al., 2015) brought out the role of tropics in the global C cycle, indicating that global CO_2 emission from rivers and streams of 1.8 PgC y−1 is related chiefly to tropical areas that account for 1.4 PgC y−1 (78%). Similarly, about 49% of the CH_4 emission to the atmosphere from freshwater ecosystems occurs in the tropics. However, there is equally a substantial under-representation since most global syntheses resorted to extrapolating CH_4 fluxes from temperate rivers. Besides the under-representation of tropical waters, the prevailing significant uncertainty involved in GHG flux estimates for inland waters, essentially due to the paucity of available data, is coupled with a poor understanding of underlying processes (Borges et al., 2015), both of which preclude gauging of future fluxes in response to human pressures. There is a need to understand further the link between inland water GHG fluxes and catchment characteristics, regarding their connectivity with upland terrestrial, wetland C production and stocks (Borges et al., 2015c), gas transfer velocity (k), and high-quality direct CO_2 measurements.

GHG drivers

Studies in rivers and streams have also progressed. Regional studies have attempted a more systematic evasion estimation thanks to developing high-resolution remote sensing, scaling computational tools, partial pressure direct measures, and water surface satellite mapping. A strong positive correlation exists between stream and river surface area and precipitation; conversely, there is a weaker negative relationship between surface area and temperature. The former is driven mainly by a strong positive correlation between stream width per Strahler stream order and precipitation. (Raymond et al., 2013) calculated the global CO_2 emissions from inland waters. They found that globally, a 0.07 % increase in the fraction of stream area for a 10-cm increase in precipitation and a 0.02 % decrease with an increase in temperature by 1 ^oC. Combining lakes and reservoirs with streams and rivers provides a total surface area of inland waters of 3 620,000 km^2. The estimate of the surface area does not include wetlands.

The gas exchange velocity between water and atmosphere depends on the gradient concentration of air/water and the physical processes at the interface, usually parameterized as a gas transfer velocity (k) (Melack, 2017), also called a piston velocity or gas exchange coefficient. Gas transfer velocities are a function of turbulence, the water's kinematic viscosity, and the gas's molecular diffusion coefficient; the Schmidt number is the ratio of the latter two terms and is gas specific. Despite numerous studies on the subject, significant uncertainty remains regarding the parameterization of k600 in lakes. The widely used parameterizations based on wind speed do not account for other drivers (or inhibitors) of turbulence at the interface, such as the friction of the current on the bottom evaporative heat gain and loss and the associated buoyancy fluxes, or the release of organic molecules that might behave as surfactants by the vegetation (Abril et al., 2014; MacIntyre et al., 2010). With increasing stream order, the global average gas transfer velocity of 5.7m d^{-1} for streams and rivers increases. In a new metadata analysis of whole-stream tracer releases in streams and small rivers, the average value was 4.7md^{-1}. The wind speed and

lake size models provided global average estimates of 0.74 and 1.33md^{-1}, respectively. Thus, the global average gas transfer velocity for lakes and reservoirs is approximately 1.0md^{-1}, much lower than the global average for streams and rivers but is consistent with regional studies (McDonald et al., 2013; Raymond et al., 2013).

Global GHGs evasions from inland waters.

Climate predictions necessitate a complete and robust account of natural and anthropogenic greenhouse gas (GHG) fluxes, especially for CO_2, CH_4, and N_2O. (Borges et al., 2015c). (Raymond et al., 2013) calculated the global carbon emissions by compiling the 6 708 stream and river sampling location results. The average of these median values was 2,300 µatm, which increases to an average pCO_2 of 3,100 µatm after discounting for potential biases in the calculation and normalizing interpolated pCO_2 from each region to stream. Similarly, they assembled 20,632 pCO_2 observations from 7,939 lakes and reservoirs. They found that Inland waters present supersaturation of CO_2 concerning equilibrium with the atmosphere. At the same time, the concentration of CO_2 in water did not strongly relate to climatic or landscape variables for rivers and streams. Based on pCO_2, three groups of lakes distinguish non-tropical freshwater, tropical, and saline lakes.

The study conducted by (Raymond et al., 2013) used two methods to estimate the gas transfer velocity for lakes and reservoirs. The first uses globally gridded wind speed and an empirical relationship between k600. The second employs new estimates of the gas transfer velocity for lakes of different sizes, which assumes a primary role of fetch, the distance traveled by the wind over the water, in regulating k in these systems. The wind speed and lake size models provided global average estimates of 0.74 and 1.33md^{-1}, respectively.

Global CO_2 and CH_4 emissions were estimated at 2.1 PgC yr^{-1} (Raymond et al., 2013) and 0.7 PgC yr^{-1} (Bastviken et al., 2011) (CO_2-equivalents; CO_2e), respectively. The global C budget's GHG flux from inland waters is significant, considering that the oceanic and land C sinks correspond to ~1.5 and ~2.0 PgC yr^{-1}. Over the past half-century, human activities have doubled the reactive N addition on Earth, resulting in saturation of the N assimilative capacity of some terrestrial ecosystems. This fact has led to a corresponding approximate doubling of riverine N loads. As a result, N_2O emission rates from rivers have increased, with an estimated 0.3 – 2.1 Tg N_2O–N yr^{-1} or 6–30% of global anthropogenic N_2O emissions. N_2O emissions from rivers have been dramatically revised downwards from early estimates of 2,100 GgN_2O-N yr^{-1} to 32 GgN_2O-N yr^{-1} (Kroeze et al., 2010; Hu et al., 2016).

Approximately 70% of the stream CO_2 evasion originates from waters on only 20% of the total stream surface area, whereas 50% of the emissions are from the world's largest lakes, owing to their large surface area and gas transfer velocity. However, large lakes must be more adequately surveyed for concentration and k. The role of wetlands could be significant in hotspots such as Amazonia and Southeast Asia. Systematic campaigns are needed to evaluate further the relative importance of different sources (Abril et al., 2014; Raymond et al., 2013). CH_4, expressed as CO_2 equivalents, corresponds to at least 25% of the estimated terrestrial GHG sink (2.6 ± 1.7 Pg of C yr^{-1}). Finally, N_2O, responsible for ~9% of global Climate radiative forcing, has a global warming potential of ~310 times that of CO_2.

Unlike CO_2 and CH_4, N_2O has a more significant anthropogenic origin (Hu et al., 2016). Riverine N_2O fluxes varied by dominant land-use type with higher fluxes (µg N_2O–N m^{-2} h^{-1}) observed in agricultural (25.1 ± 80.6, n = 97) and residential rivers (23.3 ± 9.6, n = 31) and lower values observed in forest rivers (6.7± 17.9, n = 41), which is consistent with (Borges et al., 2018), suggesting that the available N level mainly determines the magnitude of N_2O emission fluxes in river systems. The high dependence of N_2O flux on both NH_4^+ and NO_3 levels further implies that N_2O emission from rivers derives from nitrification and denitrification processes. Due to the role of both nitrification and denitrification, N_2O emission fluxes demonstrated a higher correlation with

DIN concentrations than with either NH_4^+ or NO_3 concentrations alone. All those mechanisms intensify in small rivers due to the proximity of N sources (Hu et al., 2016; Maavara et al., 2019).

The Amazon's role in GHG emissions from inland waters

Most riverine GHG emissions are from the tropics, ~60-80 % for $_{CO2}$, ~70 % for CH_4, and ~79 % for N_2O. However, the total stream surface area (SSA) in the tropics (24°N-24°S) corresponds to ~44 % of the total SSA globally, implying that riverine areal emissions of GHGs (per m^2) are higher than in other climatic zones. However, the CO_2 data distribution is skewed towards temperate and boreal systems in the Northern Hemisphere. Data in several tropical basins (including the Congo and Amazon) originated from interpolation from adjacent basins rather than actual measurements.

Although the magnitude and variability of these fluxes remain uncertain, especially in tropical regions, recent studies are improving our understanding of C dynamics in the streams, rivers, lakes, reservoirs, and wetlands of the Amazon basin (Abril et al., 2014; Borges et al., 2015a; Melack, 2017). The Amazon basin lay on the equator within the circumglobally belt of evergreen tropical rainforest. Approximately 68 % of the basin corresponds to Brazil, and the remainder splits between Bolivia, Colombia, Ecuador, French Guiana, Peru, Suriname, and Guyana (Melack, 2017) suggested that the evasion of CO_2 from Amazonian rivers, lakes, and temporally inundated aquatic habitats is similar to net ecosystem exchanges in non-inundated upland forests. In addition, Amazonian aquatic ecosystems account for a significant proportion of the global methane flux from natural wetlands. The whole Amazon basin (regions <500 m) corresponds to ~ seven million square kilometers, from which about 30% comply with international criteria for wetland definition (Junk et al., 2011). To determine the role of the Amazon basin in the global scenario of the carbon budget is necessary to characterize the aquatic systems. In this context, several studies have emerged to gather valuable information to estimate the carbon dynamics, for instance, floodable area, inundated area, and areal extent of significant habitats permanently or periodically inundated. High-resolution, remotely sensed products are available for specific locations in the Amazon and provide information appropriate for the validation of basin-scale products. Geomorphological approaches are applied to determine the river areas. (Beighley and Gummadi, 2011) present a methodology for estimating full bank discharge and a station's hydraulic geometry coefficients and exponents using limited data, only stage-discharge and Landsat imagery. The approach utilizes 82 streamflow gauging locations in the Amazon Basin. They conclude that the Amazon Basin contains approximately 4.4 million kilometers of channels with a combined surface area of 59,700 km^2. Other studies focus on the Modelling of Inundation (De Paiva et al., 2013) developed hydrologic/hydrodynamic modeling of the Amazon River basin. They showed that Amazon hydrological processes govern most of the Amazon terrestrial water storage changes (56 %), followed by soil water (27 %) and groundwater (8 %).

Moreover, floodplains play a significant role in stream flow routing, although backwater effects are also essential to delay and attenuate flood waves. Atmospheric stability influences gas transfer velocities (Harrison et al., 2012). Latent heat fluxes are critical in warm tropical waters like the Amazon basin, leading to convective mixing and enhanced k values. Conversely, diurnal heating under intense insolation can cause stable water column stratification that may lead to low or high k values. Hence, given the pronounced diel cycle of heating and cooling often observed in shallow tropical lakes, measuring stratification, mixing, and gas exchanges over these diel cycles are essential. However, such measurements are unusual. The lack of studies of k values and gas concentrations in vegetated habitats adds further uncertainty, mainly because of the large areas of flooded forests and floating macrophytes throughout the Amazon basin (Melack

and Hess, 2010) It is also essential to investigate the variation of k for the change in altitude above 500 m, where the mountains that feed sediments and organic matter to the Amazon basin come together. In these areas, the turbulence and speed of discharge would increase the degassing of rivers and streams. Flux and concentrations measurements intend to provide the basis for the entire basin-wide estimates. However, they need to look at the Andean component.

According to Johnson et al (2008), 77 % of carbon transported by water from the landscape was as terrestrially respired CO_2 dissolved within soils, over 90% of which evaded to the atmosphere within headwater reaches of streams. Evasion of CO_2 from headwater streams in the Amazon decouples from those larger rivers and wetlands. In larger lotic systems, instream processing of allochthonous organic C is the primary driver of the CO_2 supersaturation typical of tropical rivers. In headwater streams, however, CO_2 supersaturation results primarily from groundwater discharge of terrestrially respired CO_2 dissolved within deep soils. (Neu et al., 2011) measured C losses as soil respiration, direct CO_2 and CH_4 fluxes from the stream surface, and fluvial export of DIC and DOC over an annual hydrologic cycle from forested Amazon perennial first-order headwater watershed at Tanguro. They reported pCO_2 concentrations from 6,490 to 14,980 µatm and evasion rates from the stream surface of 6490 ± 680 gCm^{-2} yr^{-1}; methane concentrations in the stream ranged from about 290–440 µatm and evasion averaged 990 ± 220 gCm^{-2} yr^{-1}. (Borges et al., 2015) sampled along the mainstem Solimoes and Amazon rivers and at the mouths of major tributaries and reported a range in pCO_2 concentrations from 70 to 16,880 ppm. (Abril et al., 2014) conducted eight 800-km cruises along the main channel of the Solimoes-Amazon River and portions of its major tributaries in the central basin and measured pCO_2 every minute while underway. Values of pCO_2 were similar to previous studies and varied from 1,000 to 10,000 ppmv. (Raymond et al., 2013) included regional information in their global estimates of CO_2 emissions from streams and rivers. CO_2 concentrations in streams and rivers of the Amazon basin (including the Andes) averaged about 6,890 µatm. The k600 value used is at the high end of those reported by others for the rivers of the lowland Amazon as it includes streams and rivers in highland portions of the basin. Hence, the areal efflux is probably too high as a basin-wide average. (Sawakuchi et al., 2014) assessed the spatial-temporal variability of CH_4 fluxes from the Amazon and its main tributaries, the Negro, Solimoes, Madeira, Tapajos, Xingu, and Para Rivers, based on direct measurements using floating chambers. Considering only river channels, the Amazon Basin release between 0.40 and 0.58 Tg CH_4 yr^{-1}. Meanwhile, the estimates of CH_4 flux from all tropical rivers and rivers globally were 19–51% to 31–84 % higher than previous estimates, with large rivers of the Amazon accounting for 22–28 % of global river CH_4 emissions.

Regarding N_2O, the Bottom-up, and top-down approaches indicate that Africa was the largest source of N_2O in the last decade, followed by South America (Tian et al., 2020). Guilhen et al., (2020) quantify the average yearly denitrification and associated N_2O emissions over the entire watershed at 17.8 $kgN\ ha^{-1}\ yr^{-1}$, and 0.18 $gN\text{-}N_2Om^{-2}\ yr^{-1}$ respectively for the period 2011–2015. They found that the Amazonian wetlands have similar emissions of N_2O with the Congo tropical wetlands and lower emissions than the temperate and tropical anthropogenic wetlands of the Garonne (France), the Rhine (Europe), and south-eastern Asia rice paddies. Nitrification fluxes exceed inland waters' denitrification fluxes by 5-20 %, depending on the system. (Maavara et al., 2019) estimate global inland water N_2O emissions of 0.148–0.277 Tg N y^{-1}, considerably lower than those of Tian et al., (2020), corresponding to ~ 17.0 Tg N y^{-1} between 2007 and 2016. Notably, most riverine GHG emissions are from the tropics, with ~79 % for N_2O (Hu et al., 2016). Regarding to lakes, (Raymond et al., 2013) calculated CO_2 concentrations in lakes of the whole Amazon basin (including the Andes) as averaging about 1,906 µatm and an efflux, using a k600 of 5.8 cm h^{-1}, of 1230 kg C km^{-2} d^{-1}. They expressed the results to the surface area of rivers and streams, not land area. Large savanna floodplains occur in the Llanos de Moxos (Bolivia) and in Roraima (Brazil) (Melack et al., 2004) approximated mean annual methane emission from these two areas as 70 Mg C km^{-2} yr^{-1}. Jati (2013) made monthly measurements of carbon dioxide and methane flux with floating chambers in 80 wetlands near Boa Vista (Roraima); mean values from

his results were about 9,670 kg C km $^{-2}$ d^{-1} and 9.6 kg C km $^{-2}$ d^{-1} for CO_2 and CH_4, respectively. (Melack et al., 2022) proposed a comprehensive study for methane emissions for the Amazon basin and summarized published fluxes and regional levels extracted from the WetCharts ensemble of wetland models corresponding to 39.4 ± 10.3 Tg CH_4 y^{-1}. Conversely, Gedney et al. (2019) provided CH_4 flux estimates for the Amazon basin using the Joint UK Land Environment Simulator (JULES) model ranging from ~24 to ~58 Tg CH_4 y^{-1}.

Andean influences on the biogeochemistry of the Amazon River

The Amazon River exits the Andes mountains more than 4,000 kilometers (km) from its estuary. Alfred Russel Wallace (1853) was the first naturalist to write about the white-water, clear-water, and black-water river types of the Amazon basin and to relate the color of tributaries to the nature of their drainage basins. He linked the sediment load of white-water tributaries to erosion in their steep Andean headwaters and identified clear-water rivers with the crystalline mountains of Brazil. Furthermore, he linked the black-water rivers emerging from lowland sources and correctly attributed their dark coloring to the leaching of "decaying leaves, roots, and other vegetable matter" (Wallace, 1853). Similarly, Henry Bates (1963) highlighted the transport of volcanic pumice in the main-stem Amazon River and assigned its origin to volcanic ranges thousands of kilometers away in the Ecuadorian Andes. Steep terrain and young lithologies make the Andes a vital source of sediments and solutes to the lower reaches of the Amazon River. The most visible characteristics of the main-stem Amazon and its Andean tributaries are high discharge and heavy loads of suspended and bedload sediments, nutrients, and organic matter. The dominant downstream trend in biogeochemical and trophic characteristics of the main-stem Amazon and its large Andean tributaries is the progressive dilution of Andean contributions by lowland inputs of tributaries (Devol and Hedges, 2001).

The Andes mountains rise steeply along the western margin of the Amazon basin. Approximately half of the Andean Amazon lies at elevations between 500 and 2,000 m, while most of the remainder is between 2,000 and 4,000 m; about 16 % is above 4,000 m. Active volcanoes are prominent features of the Ecuadorian and Bolivian Andes. The primary vegetative cover types in the Andean Amazon are submontane (700 to 2,000 m) and montane (to 3,700 m) forests, which together constitute approximately 42 % of the region. The entire north-south length of the Andean Amazon basin is drained by eight important rivers—the Caquetá, Putumayo, Napo, Marañon, Ucayali, Madre de Dios, Beni, and Mamoré (McClain and Naiman, 2008).

The Andes cover only about 13 % of the Amazon basin. The combined flow of the Andean tributaries amounts to approximately half of the mainstem flow. Nevertheless, while Andean water contributions to the main-stem Amazon may be proportional to area, contributions of sediments and solutes are disproportionately greater (GHGs drivers). Moreover, the river's energy and nutrients from the Andes drive direct and indirect main-stem productivity through biophysical feedback with the massive lowland floodplain. Gibbs (1967) estimated that 86 percent of the total dissolved salts and 82 percent of suspended solids discharged by the Amazon were supplied from ~ 13 percent of the mountainous-environment type's total area. This statement is consistent with (Meade, 1994). Most of the suspended matter sediments at the base of the Andes, measured along the entire length of the Madeira River from its Andean headwaters, show a sharp decrease in sediment load (as much as 60%) and diameter at the piedmont base of the Andes (Guyot et al., 1999) . In Ecuador, the sediment discharge in the Amazon basin (Napo, Pastaza, and Santiago) corresponds to 47 × 10^6 t yr^{-1}, whereas the suspended sediment load in the Pacific basin was 6 × 10^6 t yr^{-1}. The difference between these contributions is likely due to the tectonic

uplift and the seismic and volcanic dynamics on the Amazon side (Armijos et al., 2013). Conclusive evidence from an Andean source depicts the mineralogical and isotopic composition of the suspended sediments (Bouchez et al., 2014) reported that 15% of fine particulate OC (FPOC) originates from rocks in the Andean part of the Madeira Basin. Andean tributaries deliver an order of magnitude more particulate nitrogen (1,170 megagrams [Mg] per year) and phosphorus (806 Mg per year) to the main stem than their lowland counterparts 119 and 43 Mg per year, respectively (McClain et al., 2008). Most particulate nitrogen is likely organic, whereas phosphorus is mainly phosphate strongly adsorbed to iron and aluminum oxide surfaces. Andes contain the only significant evaporite and carbonate deposits in the Amazon basin (Stallard and Edmond 1983). High fluxes of Ca^{2+} (calcium), Mg^{2+} (magnesium), HCO^{3-} (bicarbonate), and SO_4^{2-} (sulfate) ions occur in rivers draining carbonate deposits, and high fluxes of Na^{+} (sodium) and Cl^{-} (chloride) ions occur in rivers draining evaporite deposits. Also, Among the Amazon tributaries that drain basins dominated by less-weatherable silicate rocks, Andean rivers have consistently higher total cation concentrations (Mortatti and Probst, 2003)

Organic matter

Mountain rivers play a key role in the delivery of POC to large river systems and the ocean. Andean-derived suspended sediments carry a significant amount of organic matter, 90% of which is made up of particles less than 63 micrometers (μm) in diameter FPOC (Mortatti et al., 2003; McClain et al., 2008) (. Total organic carbon is approximately 1%, by mass, of suspended sediment in the main stem, constituting a flux of 5 to 14 TgC yr^{-1} to the Atlantic Ocean. Measurements show that more than 90% of particulate organic carbon (POC; > 0.5 μm) in the main-stem Amazon River comes from Andean tributaries (Richey et al., 2002). Few FPOC is transported directly from the Andes; most is stored for varying periods of time in point-bar and floodplain sediments. The actual proportion of FPOC of Andean origin has been approximated using ($\delta^{13}C$) stable isotopic ratios as a “fingerprint” of its origin. There is a clear separation of FPOC $\delta^{13}C$ between Andean and lowland rivers, and this separation can be used to estimate the relative proportion of each in the main stem. For example, since FPOC in purely lowland rivers has $\delta^{13}C$ values near to –28.5‰ (McClain and Naiman, 2008) and –26.5‰ corresponds to the discharge of FPOC of the exiting Andean Peruvian, a discharge in the main-stem Amazon River at Óbidos of –27.4‰ would suggest a mixture of 50% Andean FPOC and 50% lowland FPOC (Quay et al., 1992). Unlike particulate organic matter, this DOM appears to derive largely from lowland sources mainly. Andes largely regulate the particulate load to the main-stem Amazon River, not simply with respect to its particulate mineral load but also with respect to associated nutrients and organic matter.

Feedback between land C pools and Climate provides one of the largest sources of uncertainty in our global climate predictions. The magnitude and timing of these fluxes depend on the hydrological regime(Borges et al., 2015) of C and have two significant pools the Above/Below-ground biomass (AGB/BGB) and the soil. The Amazon basin and Andean store a vast amount of C(Raymond et al., 2013). Overall estimations of the total AGB of intact Amazonian rainforests (~5.76 × 106 km^2) result in 93 ± 2 PgC, considering lianas and small trees. Including dead biomass and BGB the value would increase to 111,6 PgC(Saunois et al., 2020). Riverine systems transport C (Tian et al., 2020) mainly in the form of dissolved organic DOC, POC, and dissolved inorganic (DIC); globally, rivers export approximately 0.89 Pg C to oceans every year, including 0.24 Pg DOC, 0.24 Pg POC and 0.41 Pg DIC. DOC, POC, and DIC are associated with soil organic C amount, amount of soil erosion, and CO_2 consumption by rock weathering, respectively. However, external drivers like catchment slopes, vegetation, geology, Climate, and size can also play a significant role (Tamooh et al., 2012).

Riverine POC derives from soil litterfall and autochthonous production and is a function of the total solid matter (TSM), which in turn depends on the rainfall intensity, drainage intensity, and basin slope. Usually, there is a positive correlation between elevation (basin slope) and biomass density (cultivation areas); nevertheless, the most significant driver is the TSM flux, showing that

the %POC in suspended solids decreases when increases the concentration of TSM(van der Werf et al., 2009). Regarding DOC, drainage intensity would control the DOC mainly, followed by morphology flatness and the C soil availability. DOC has two origins autochthonous (C produced by phytoplankton) and allochthonous (C produced by terrestrial biosphere) (van der Werf et al., 2009). The former is important in downstream rivers where the size, the interface area soil/water, and residence time increase, enabling leaching processes to be more intense. Conversely, steep basins result in a higher share of surface runoff concerning total runoff. This restricted contact between soil and water makes rivers less DOC concentrated (Tamooh et al., 2012).

The Amazon drainage basin comprehends the Andean Cordillera, the lowland Amazon basin, Precambrian shields, and a large floodplain (i.e., Varze) that covers - 100,000 km^2. This geomorphological diversity of drainage regions results in rivers that have a large range of chemical characteristics (Quay et al., 1992). Rivers within the Amazon drainage basin have been classified previously by color. For example, whitewater rivers have high suspended and dissolved loads; clearwater rivers with depletion of suspended and dissolved material; blackwater rivers have low-suspended sediments and dissolved inorganic material but high concentrations of dissolved organic materials. The Andes are a crucial source of water and sediments to the Amazon River, the largest single source of fresh water and OC to the oceans (Gibbs, 1967). In the Amazon basin, the average export of total OC was 36.1 Tg yr^{-1} (8.5 g m^{-2} yr^{-1}), of which 62% was DOC and 38% POC(Richey et al., 1990). the isotopic data (+19 $\Delta^{14}C$ ‰) provide information that POC in the main stem have a trustworthy Andean source, much of it would have to be hundreds to thousands of years old (McClain and Naiman, 2008). Since stable isotopic $\delta^{13}C$ ratios of plant leaves are positively correlated with elevation (-30‰ at 1000 - 2000 m to –26‰ at 4000 m)(Townsend-Small et al., 2007), they permit identifying the proportion of POC of Andean origin. Unlike POC, DOM appears to derive mainly from lowland sources.

Although scientific information asserts that Andean Cordillera significantly influences the overall biogeochemistry of the Amazon, there needs to be more research considering the integrated Andean-Amazon-fluvial system. We describe gradients of TSM, POC, DOC, δ13C-DOC, $\delta^{13}C$-POC in function of altitude, morphology patterns, and biomass covertures. The outcomes report a comprehensive data set of DOC, POC, and TSM of inland waters of three ecosystems in Ecuador: paramo (>3000 m), highland (500-3000 m), and lowland (<500 m). This variation in the altitude allows testing the response of the ecosystem to different drivers, for instance, at the highest altitude, significant erosion, and low organic matter inputs, except in paramo where soil characterizes for storage high levels of organic matter. In the middle altitudes, an increase in organic matter availability and moderate erosion rates. Finally, significant amounts of organic matter and minimal erosion rates at lowlands.

Productivity

The Amazon floodplain is a highly productive regional system, with a net production of 11.9–16.8 Mg C ha−1 (Clark et al., 2013) that occurs over an area of 67,900 km2. Annual floodplain deposition at any given place depends mostly on river-level fluctuation and duration of flooding. This process builds the fertile floodplain soils along Andean tributaries and the main stem. The sediments of the lateral flux between the channel floodplains in the main stem (2,100 km) range from 1,570 to 2,070 Tg yr^{-1} and exceed the downstream flux of 1,200 Tg yr^{-1}. Approximately 500 Tg yr^{-1} of upstream-derived sediment and nutrients accumulate on the floodplain and the river floor (McClain and Naiman, 2008a; Amazon Waters, 2022). Most primary productivity derives from macrophyte (65%) and floodplain forest (28%) communities. Floodplains of the mainstem Solimoes emitted CH_4 at an annual rate of 1.3 TgC yr^{-1}. CH_4 emission from a 1.77 million km^2 area in the central basin had a mean of 6.8 TgC yr^{-1}, a greenhouse flux of about 0.5 PgC as CO_2 equivalent (Melack et al., 2004).

Lakes

The global importance of any ecosystem type in a process or cycle is the product of the areal extent and the intensity of the process in those ecosystems. In this sense, lakes play a much

more significant role in global carbon cycling than their area would otherwise predict (Downing, 2010) While lakes make up less than 2% of Earth's surface area, they bury over three times more carbon in their sediments than all of the world's oceans combined. This statement means lakes bury over 100 times more carbon than the oceans per area (Downing et al., 2008). Lakes storage of 0.07 to 0.14 Pg of organic C y−1 is co-equal with long-term sediment accumulation of organic C in the ocean 0.1 Pg C y^{-1} (LaRowe et al., 2020). Although lakes bury vast amounts of carbon, they also tend to release more CO_2 to the atmosphere than they absorb, making them net sources of greenhouse gases. Most of the world's lakes are supersaturated in CO2, releasing some into the atmosphere. Several internal processes involve GHGs in lakes; for instance, GHGs are transported from surrounding systems, originate within sediments or in the water column, and are emitted to the atmosphere for different reasons. Any fate follows complex chemical and biological pathways that have not been fully understood. The advent in the early 1980s of techniques that could measure the rate at which bacteria synthesize new biomass revealed that pelagic bacterial production was co-equal or even more significant than primary production. Therefore, one could infer that bacterial respiration in many freshwater and marine systems is too high to explain if the only source of labile organic C is autochthonous primary production (Pradeep Ram et al., 2007; Roland et al., 1999). Actually, Cole et al., (2000) note that this pattern repeats in whole systems of fresh waters; namely, respiration (R) often exceeds GPP, and the only way to explain this excess is to have some of the external terrestrial supply of organic matter actively respired within the water body.

Most of the lakes sampled show supersaturation in CO_2 and CH_4; therefore, they are sources of GHGs in the atmosphere (Borges et al., 2022). However, direct sampling is geographically skewed, with an overrepresentation in North America and Scandinavia global datasets. At the same time, tropical regions are much less covered, which can provoke misleadings in global estimations. For example, Tropical lakes accounted for 34% of the global lake CO_2 emission, although they represented only 1.5% of the CO_2 dataset used in the global estimations (Raymond et al., 2013). The content of CO_2, CH_4, and N2O in lakes' surface waters results from the balance of C sources and sinks, which are specific to each gas (Borges et al., 2022). The main drivers are allochthonous organic matter, nutrients, internal organic matter production, and degradation. Also, the characteristics of the surrounding ecosystems play a significant role, such as catchment and land cover, size, depth, shape, and weather conditions. The interaction of these variables makes global-scale emissions predictions challenging to dimension. For example, (Borges et al., 2022) carried out several 24-lake missions that accounted for 49% of the total lacustrine surface area of the African continent to evaluate the CO_2, CH_4, and N_2O content. They found that the concentrations of dissolved CO_2 were much lower than values attributed in literature to tropical lakes and lower than in boreal systems because of higher productivity (triple that of boreal systems). In contrast, surface CH_4 concentrations were generally higher than in boreal systems. The main drivers that make the difference between the dynamics of boreal and tropical lakes were phytoplankton biomass, temperature, sunlight (restricted to the time of year), and low DOC enrichment.

Accurate estimates GHG fluxes to and from the atmosphere are essential to understanding the global carbon (C) budget and making projections of the trajectory of climate change. Several approaches have tried to calculate GHG fluxes, for example, by multiplying the average rate of CO_2 emission from lakes, determined from a literature review, by their total area to calculate a global emission rate of 0.81 Pg C yr^{-1} (Lars J. Tranvik et al., 2009) the same was developed by (Bastviken et al., 2011) for CH_4; resulting in 69 Tg C y^{-1} or about 0.85 Pg C as CO_2 emission equivalents. Regarding N_2O, (Soued et al., 2016) published a first-order approximation of the global emissions for lakes and reservoirs. They determined approximately 0.08 Pg of C equivalent (0.627 ± 0.296 Tg of N_2O-N yr^{-1}). (DelSontro et al., 2018) improve the estimations by applying the following considerations to the approach by linking the data on the global distribution of lake size and productivity with current empirical models of GHG emissions, including the three

GHGs in one study; and assessing the sensitivity of lentic GHG emission to expected future changes in lake and impoundment productivity. This analysis indicates that lentic systems are essential sources of GHGs driving climate change. Also, CH_4 emissions may be of disproportionate importance due to their link with lake productivity and the high potency of CH_4 as a GHG. Global emissions from lakes and impoundments are equivalent to 20% of global fossil fuel CO_2 emissions (9.5 ± 0.5 Pg C-CO_2 yr^{-1}) (Friedlingstein et al., 2022).

Project description

The project is carried out within the cooperation program of the Central University of Ecuador and the University of Liège under the sponsorship of ARES. Given the importance of continental waters in climate change and the understanding of geochemical processes and cycles, this Ph.D. project focuses on two aspects with current gaps in the literature. The first part corresponds to the sampling and estimation of GHGs flow from the Napo River Basin (a tributary of the Amazon). The second part focuses on studying GHGs in 15 lakes in the Andean moorlands and Ecuador's highlands. In this way, we reported data from two ecosystems and their respective continental waters.

Napo Basin

The Republic of the Equator is a country in northwestern South America, bordered by Colombia on the north, Peru on the east and south, and the Pacific Ocean on the west. Four natural regions and ten hydrographic basins split according to their stream's direction. East's basins flow into the Amazon, and west's basins into the Pacific Ocean Fig 1.10. The Napo basin covers approximately 110,000 km2 and represents 1,6 % of the Amazon basin. Approximately 60 % of the Napo basin is in Ecuador, while the other 40 % is in Peru.

The studies conducted to explain the GHGs in the Amazon basin focused on altitudes under 500 m. However, the degassing magnitude, lateral transportation, and the chemical dynamics occurring in low-order streams at highlands are still uncertain (Marx et al., 2017). Several aspects driving the biogeochemistry of the Amazon main stem link to the magnitude and variability of water and materials supplied from the Andes (McClain and Naiman, 2008). Here, we studied those aspects harnessing the geographical features of Ecuador, where Andean mountains and Amazon basins occur along relatively short distances.

FIGURE 1.10 Project localization. Napo Basin is in the Ecuadorian Amazon Region.

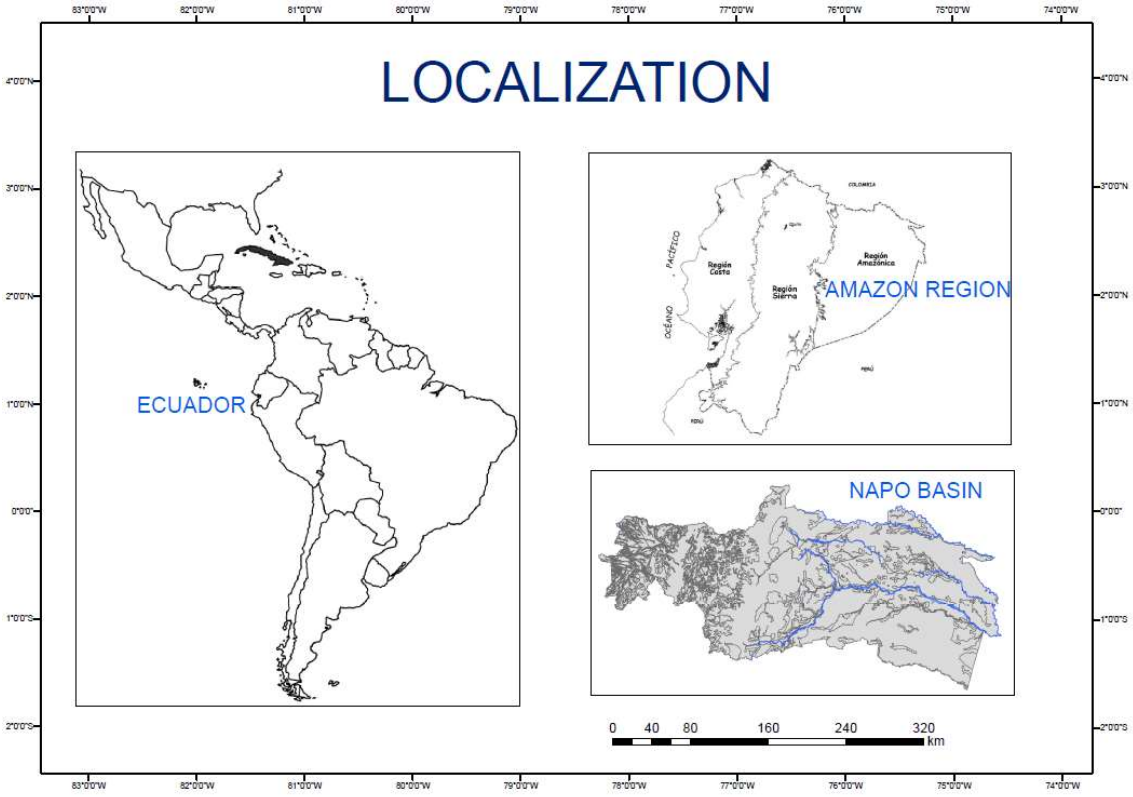

The sampling area covers the largest hydrological basin of Ecuador called Napo, which consists of about 60,000 km2, with an average discharge of 2,889 m3 s^{-1} ranging from 642 to 4,122 m3 s^{-1} for June and September, respectively (National Institute of Meteorology and Hydrology, 2021). The vegetal coverage consists mainly of forests 62 %, crops 15 %, grasslands 15 %, and others uses 7% (Technical Secretary of Planning, 2021). Therefore, we cover the basin's two longest possible routes into three sampling sections. The first one (El Coca) starts in the moorland of Salve Faccha at the Cayambe-Coca Reserve, the second starts in Puerto Napo (Napo upstream) at the piedmont of Antisana and Cotopaxi, and they both confluence at Francisco de Orellana, where starts the third section until the Yasuní National Park.

Due to the country's diversity along the sampling route, we found five climatic floors, sorted by altitude, i.e., the warm from 0 to 1,000 m, the temperate from 1,000 to 2,000 m, the cold from 2,000 to 3,000 m, and the moorland above 3,000 m (Farfan Portilla, 2018). The above-ground biomass varies along a small-scale elevation gradient from an Evergreen Amazon Forest < 500 m to the páramo grasslands > 3,000 m and their implications in terms of carbon storage (Torres et al., 2020). For instance, below 500 m values of 39.2 kgdb m^{-2} have been reported. However, between 600 to 1,000 m, the average value decreases to 29.1 kgdb m^{-2} (Farfan Portilla, 2018). And in the highlands above 2,700 m we find values of 19.6 kgdb m^{-2}.

The first route is El Coca. It comprehends 241 k(Lauerwald et al., 2015)m of sampling road and starts on the upper area of Salve Faccha páramo reserve at 4,200 m. This ecosystem is called the Andean moorland, with low temperatures throughout the year 5 ± 4 °C, precipitations 1,953 ± 134 mm yr^{-1}, and relative humidity around 85 %. The second route is the Napo upstream, sampled entirely by boat over 146,5 km. It begins in Puerto Misahuallí, located at 408 m. The Climate is tropical, and there is rainfall throughout the year, even during the driest months. The average

annual temperature is 22 ± 1.5 °C, precipitation is 3,832 ± 187 mm yr^{-1}, and humidity is about 87 %. The third route is Napo downstream, from the confluence of the Coca and Napo rivers until the Yasuní National Park at the border with Peru; the altitude corresponds to 175 m and is in a tropical forest. The average temperature is 23 ± 1.5 C, and the precipitation level is around 2,832 mm yr^{-1}.

FIGURE 1.11 Stations and river pathway.

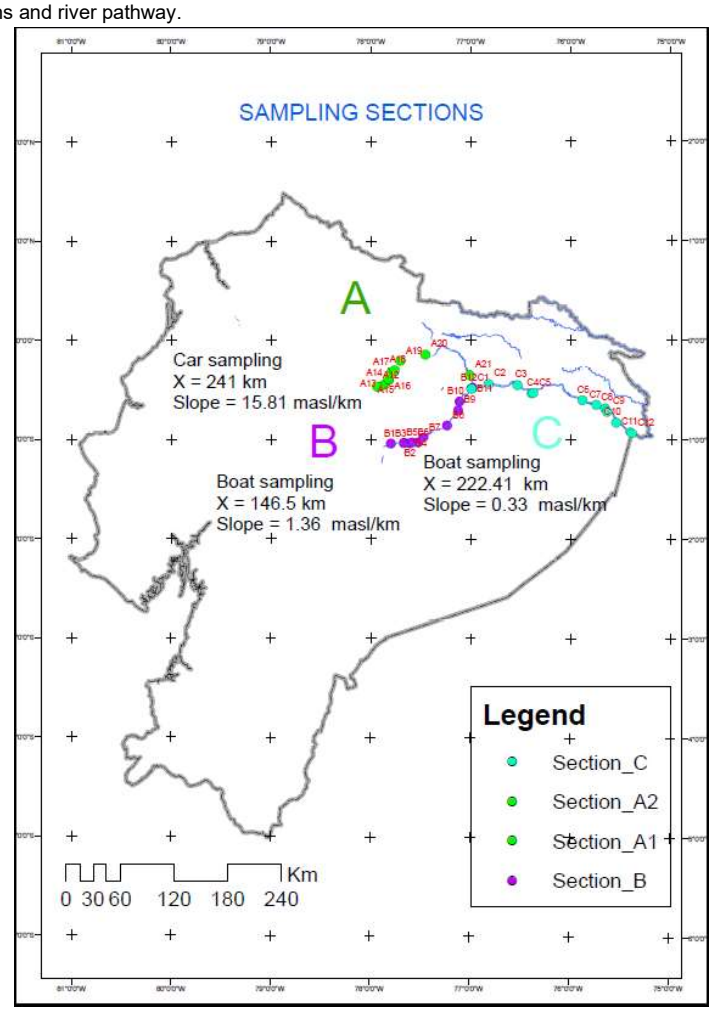

There are two small cities in the sampling area. First, El Tena, with 23,000 inhabitants and a population density of 90 persons per km2, is located near Puerto Napo (station B1). The second is El Coca (Puerto Francisco Orellana), with 40,700 inhabitants and a density of 278 persons per km2, located at the confluence of the Coca and Napo rivers near stations B12 and C1 (Fig. 1.11). El Tena is a settlement dedicated to tourism and poorly industrialized agriculture without much use of fertilizers. In the same way, El Coca devotes to tourism development, but to a minor degree, its primary income source is the exploitation and provision of oil services. Besides these two settlements, several small towns are distributed along the river, both in the Napo and Coca. Usually, the sewage of these towns is not treated, just disposed directly into the river or indirectly through latrine systems and soil leaching.

TABLE 1.1 Sampling dates, the missions were carried out quarterly from October 2018 to March 2021.

Month	Missions	2018	2019	2020	2021
January February March	M2		Accomplished	Accomplished	Accomplished
April May June	M3		Accomplished	Re-programmed	
July August September	M4		Accomplished	Accomplished	
October November December	M1	Accomplished	Accomplished		

The second mission of 2020 was rescheduled due to mobility restrictions caused by COVID-19

FIGURE 1.12 Seasonal variation discharge and sampling planning, from April to July we have the season with the highest discharges values.

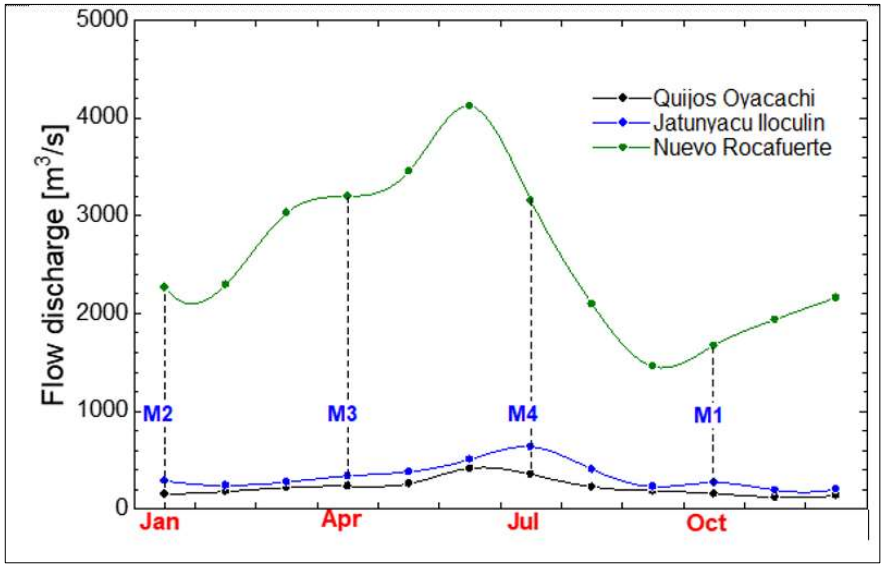

We took the series of flow discharge data from the Institute of Hydrology and Meteorology (INHAMI Table 1.2) to study the temporality's effect. We processed the available average flows from the last three years. Unfortunately, the mission planned for April 2020 was postponed due to the restrictive mobility measures (COVID 19) to next year in March 2021. Missions M1 and M2 correspond to the low-level season, typically from September to February, whereas missions M3 and M4 correspond to the high-level discharge season from March to August (Fig. 1.12). We selected one gauge station per route at 1,644, 570, and 180 m; the lower the altitude, the higher the catchment area.

TABLE 1.2 Stations, location, and length of the rivers.

Section	Length (km)	Altitude (m)	Estations	Main stem	Tributaries
Coca	241,0	4,209 – 388	21	12	9
Napo upstream	146,5	444 – 245	12	6	6
Napo downstream	222,4	244 – 175	12	6	6

The route is 610 km per campaign, from which 39 % is sampled by car and 61 % by boat. The schedule is repeated for two years, fulfilling eight quarterly campaigns. In the lab, the sampling stations were georeferenced using ArcGIS 10.8.1. The total number of stations was 45, divided between the main river and tributaries. In situ measurements of pCO_2 are performed with the Li-Cor 820 equipment and its software employing the headspace technique for four syringes. In the same way, we directly measured the pH, conductivity, dissolved oxygen, and temperature with the YSI ProPlus probe.

Moorland`s lakes

Paramos or moorlands are Andean Mountain ecosystems belonging to the Amazonian basin domain; they are located discontinuously in the neotropics, at altitudes between 3,000 and 4,300 m (Santander, 2015) mainly from Venezuela to northern Peru. The paramo occupies more than 30,000 km² in South America. Ecuador has the highest proportion of its territory covered by moors, with 7%. They constitute a primary source of drinking water for large populations in Ecuador, Colombia, and Venezuela. In Ecuador, the temperature is relatively constant, the average annual rainfall is 1 345 mm, and it occurs throughout most of the year (Santander, 2015). Only ~12 % of the days are dry. These conditions have favored the formation of peat and a large number of wetlands and lakes. The paramo usually presents deep organic-rich soils (30 % by volume), and grasslands dominate the vegetation (Zapata et al., 2021).

The Andean Moorland ecosystem contains the richest high-mountain flora in the world and is high in endemism. The grasslands contain many rare or endangered species, some of them restricted to just one mountain or valley. The headwaters are highly active sites for transporting, transforming, and storing considerable amounts of carbon from the terrestrial environment. Therefore, considering their spatial extent, they may have a disproportional effect in terms of GHGs emissions (Lars J Tranvik et al., 2009).

This study seeks to determine the GHG emissions, drivers, and carbon dynamics from 15 lakes in the northern Ecuadorian Andes region, which is rich in number and size. Twelve stations are in the paramos of Salve Faccha, Antisana y Mojanda above 3000 m (Fig 1.13). Three stations correspond to lower altitudes (between 2200 and 2800 m) with more anthropic influence and higher average temperatures. Given the area's diversity, we could select lakes with different characteristics such as depth, area, surrounding ecosystem, and formation. The study extends to 3 provinces Pichincha, Imbabura, and Napo.

FIGURE 1.13 Lake locations and georeferencing.

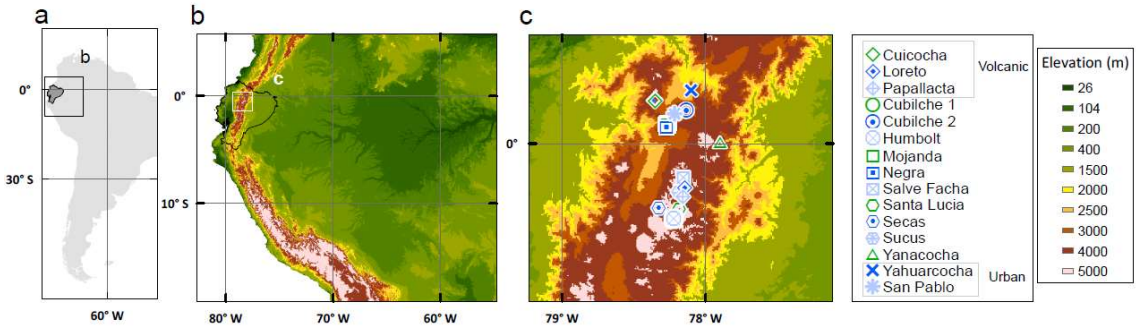

Moorland spreads out from Venezuela to Perú. In Ecuador, the soils have developed on the pyroclastic deposits resulting from volcanic eruptions. They generally have high water retention capacities (from 60 to 200%) and often significant accumulations of organic matter. The vegetation cover consists mainly of native forest, grassland, grassland, paramo, crops, humid forest, and populated areas. We sampled 54 points, performing in situ measurements of pCO_2 with the Li-Cor 820 through the headspace technique for four syringes. Sampling was carried out approximately in the center of the lakes, and we directly measured pH, conductivity, dissolved oxygen, and temperature with the YSI ProPlus probe and the lake depth.

OBJECTIVES

General objective

We aim to determine the greenhouse gas emissions (CO_2, CH_4, N_2O) in mountainous streams and lakes of the Andes Cordillera in Ecuador and their relative contribution at the scale of the whole Amazon basin.

Specific objectives

To achieve this overarching objective, our more specific objectives were to:

Collect data along a 600 km-length river stretch in the Napo River basin, mountain streams, the foothills of the cordillera, and lowland rivers of CO_2, CH_4, and N_2O concentrations, as well as ancillary variables such as organic matter concentration and inorganic nutrients.

Analyze the patterns of variations of CO_2, CH_4, and N_2O concentrations in streams as a function of catchment morphology (slope) and land cover (grassland, forest, and wetland coverage) basin.

Collect data of CO_2, CH_4, and N_2O concentrations, as well as ancillary variables such as organic matter concentration and inorganic nutrients in 15 lakes in the Andean páramos of Salve Faccha, Mojanda, and Antisana, covering three main groups: volcanic, urban and páramo lakes.

Analyze the patterns of variations of CO_2, CH_4, and N_2O concentrations in lakes as a function of morphology (surface area and depth) and organic carbon content and dissolved inorganic nitrogen.

Estimate CO_2, CH_4, and N_2O emissions from rivers and lakes scale them to the entire Amazon basin and determine the relative contribution of Andean rivers and lakes in the overall basin GHG emissions.

METHODS

In situ sampling

As mentioned in the previous section, the study consists of two sampling areas the Napo Basin and the lakes in the Ecuadorian mountains. In the former, the total number of stations was 45, divided between the main river and tributaries and sampled quarterly. The second stage consists of 15 Andean Páramo and Ecuadorian highlands lakes. here, we sampled 54 points using an inflatable boat and procuring to reach the lake's center.

we performed in situ measurements of pCO_2 with a Li-Cor Li-820 infrared gas analyser based on the headspace technique with 4 polypropylene syringes that were filled directly with river water. The pCO_2 in the atmosphere was measured by injecting ambient air sampled with an additional polypropylene syringe. Water temperature, specific conductivity, pH, and %O2 were measured in-situ with a YSI multi-parameter probe (ProPlus). Water for CH_4 and N_2O samples was collected with a sampling devise consisting of a 2L polyethylene bottle with the bottom cut and fitted with a silicone tubing at the stopper. The equipment's calibration was as follows (1) YSI ProPlus Probe, oxygen in the air, and pH with the 4,0 and 7,0 buffer solutions (2) the Li-Cor 820 equipment was calibrated annually in the laboratory using standards of 388, 813, 3,788, and 8,300 ppm of CO_2 (Air Liquide Belgium).

Additionally, two borosilicate serum bottles (Weathon) with a volume of 40 ml were filled with the silicone tubing, poisoned with 100 µl of a saturated solution of $HgCl_2$ and sealed with a butyl stopper and crimped with an aluminium cap. Finally, we collected a sample of 12 ml (exetainer) poisoned with 50 µL $HgCl_2$ for δ^{13}C-DIC.

Laboratory analyses

The samples for CH_4 and N_2O are processed in duplicate using the nitrogen headspace technique, then injected into a gas chromatography equipment with a flame ionization detector for CH_4 and an electron capture detector for N_2O. For the δ^{13}C-DIC, we used the headspace technique with helium and added 100 µL of 99 % H_3PO_4 to convert all the inorganic carbon into CO_2 (HCO_3^{1-}, CO_3^{2-}). The headspace formed was analyzed by an elemental IRMS analyzer.

The TSM (total solid matter) is carried out by gravimetry. First, we made pass about 400 mL of water through a 47 mm filter, previously weighed. For the POC, we filter an approximate amount of 100 mL, decarbonize in an atmosphere rich in HCl so that the inorganic carbon becomes CO_2, and keep only the organic one. Finally, we dried the filters and encapsulated them in metallic paper to be fed to EA-IRMS equipment to identify the concentration of POC, PN, and the composition of δ^{13}C-POC. The POP samples are previously treated to mineralize organic phosphorus, which means orthophosphate (SRP) by hydrolysis and Plon's reagent in an autoclave. Then, in an acid medium and the presence of ammonium molybdate, the SRP forms

the phosphomolybdic complex with a blue coloration, whose concentration can be quantified in a spectrophotometer wavelength of 880 nm.

Total alkalinity is determined by automatic titration with 0.1N HCl. Measurements are verified using reference material for oceanic CO_2 measurements. CDOM and FDOM analysis is carried out by fluorescence and UV / VIS spectrometry, respectively, in high precision 10 mL cells. The major elements are analyzed by inductively coupled plasma MS (ICP-MS), including K, Ca, Cr, Mn, Fe, Co, Ni, Cu, Zn, As, Sr, Mo, Cd, Ba, and Ba Pb. For DOC, we use amber bottles acidified with 50 µL of H_3PO_4 then they are analyzed through wet oxidation. In addition, we processed nutrients (NO_3^-, NO_2^-, NH^{4+}, PO_4^-) from a 50 mL sample by photometry. Nitrates and nitrites colored with sulfanilamide at 540 nm, Ammonium with dichloro isocyanurate-salicylate-nitroprusside at 655 nm, and Phosphates followed the technique described previously for POC.

CHAPTER 2.

ANDEAN HEADWATER AND PIEDMONT STREAMS ARE HOT SPOTS OF CARBON DIOXIDE AND METHANE EMISSIONS IN THE AMAZON BASIN.

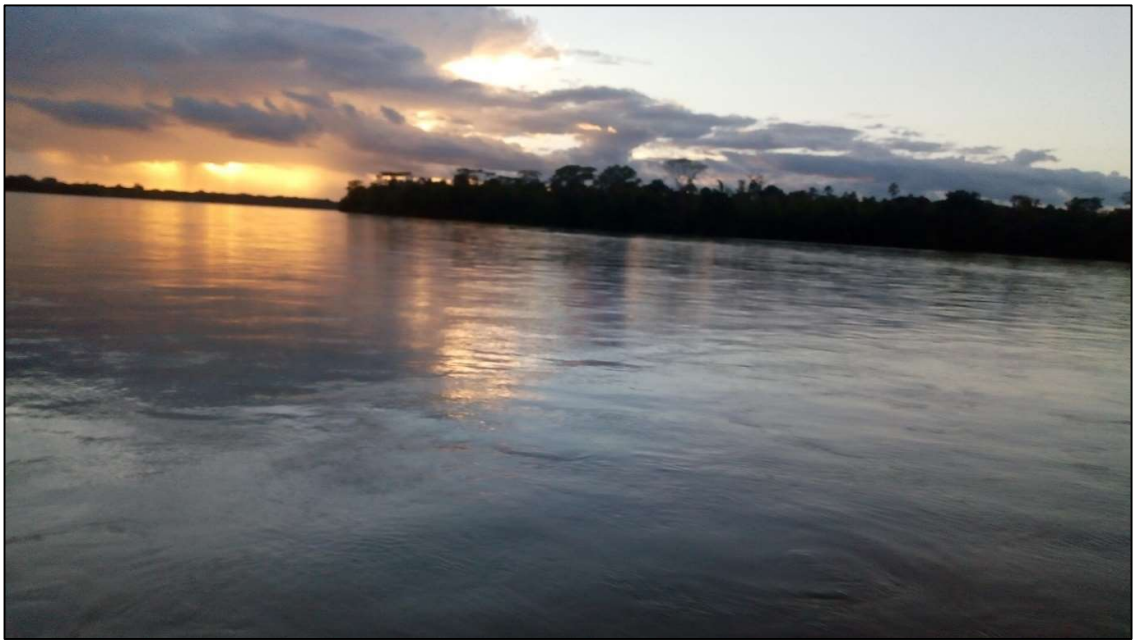

Sunset in the Napo River

Andean headwater and piedmont streams are hot spots of carbon dioxide and methane emissions in the Amazon basin.

This chapter is a published article in Communications Earth & Environment available at: https://www.nature.com/articles/s43247-023-00745-1

Reference: Chiriboga, G., Borges, A.V. Andean headwater and piedmont streams are hot spots of carbon dioxide and methane emissions in the Amazon basin. Commun Earth Environ 4, 76 (2023). https://doi.org/10.1038/s43247-023-00745-1

Gonzalo Chiriboga1,2, Alberto V. Borges1,*

1 Chemical Oceanography Unit, University of Liège, Liège, Belgium
2 Facultad de Ingeniería Química, Universidad Central del Ecuador; Ritter s/n y Bolivia, Quito, Ecuador

* alberto.borges@uliege.be

Abstract

Rivers substantially contribute to global greenhouse gas emissions, yet emissions from headwater streams are poorly constrained. Here, we report dissolved concentrations of carbon dioxide (CO_2), methane (CH_4) and nitrous oxide (N_2O) in Andean headwater and piedmont streams in the Napo River basin in Ecuador, part of the Amazon River catchment. Concentrations increased exponentially with elevation decrease between 3990 and 175 m above sea level. Concentration changes scaled with catchment slope, and were attributed to variations in gas transfer velocity, forest cover, inundation extent, and water temperature. We estimate river emissions across the whole Amazon basin using existing data for the lowland Central Amazon. We find that Andean mountainous headwater and piedmont streams are hotspots of CO_2 and CH_4 emission, with respective areal fluxes being 1.7 and 4.5 higher in headwater streams, and 1.2 and 6.6 higher in piedmont streams than in lowland streams. Together, Andean mountainous headwater and piedmont streams and rivers represented 35% CO_2 and 72% CH_4 of basin scale integrated fluvial diffusive emissions. Conversely, N_2O emissions from headwater and piedmont streams were low compared to lowland streams.

Introduction

Rivers and streams contribute substantially to global natural and anthropogenic emissions of CO_2, CH_4, and N_2O (Maavara et al., 2019a; Raymond et al., 2013; Stanley et al., 2015). Estimates of CO_2 emissions from rivers range between 0.7 and 2.9 PgC (10^{15} gC) yr^{-1} (Lauerwald et al., 2015; Raymond et al., 2013; Sawakuchi et al., 2014) and are comparable to the land net CO_2 sink of ~2 PgC yr^{-1} (Friedlingstein et al., 2022). Estimates of CH_4 emissions from rivers range between 7 and 27 $TgCH_4$ (10^{12} gCH_4) yr^{-1} (Rosentreter et al., 2021; Stanley et al., 2015), which is lower than the source of CH_4 from freshwater wetlands of ~150 $TgCH_4$ yr^{-1}. Collectively, aquatic ecosystems (freshwater wetlands, rivers, streams, lakes, ponds, reservoirs, rice paddies, aquaculture ponds, coastal vegetated habitats, estuaries and ocean) contribute 41% of total global CH_4 emissions from natural and anthropogenic sources (Rosentreter et al., 2021). Estimates of N_2O emissions from rivers have been dramatically revised downwards from early estimates of 2,100 GgN_2O-N (10^9 gN_2O-N) yr^{-1} (Kroeze et al., 2010) to 32 GgN_2O-N yr^{-1} (Hu et al., 2016). This large difference is attributable to N_2O riverine emissions being computed from nitrogen (N) deposition and emissions factors that are uncertain (Clough et al., 2006) and have been revised downwards(Webb et al., 2021).

The majority of riverine GHG emissions are from the tropics, ~60-80% for CO_2 (Borges, et al., 2015; Borges, Darchambea et al., 2015a; Lauerwald et al., 2015; Raymond et al., 2013; Rosentreter et al., 2021; Sawakuchi et al., 2014), ~70% for CH_4 (Sawakuchi et al., 2014), and ~79% for N_2O (Hu et al., 2016). Yet, the total stream surface area (SSA) in the tropics (24°N-24°S) corresponds to ~44% of the total SSA globally, implying that riverine areal emissions of GHGs (per m^2) are higher than in other climatic zones. The higher areal GHG emission rates in the tropics compared to other climate zones is partly related to year-round high temperature that sustains high microbial activity leading to GHG production in soils and in-stream. Additionally, tropical forests with high organic carbon biomass (55% of total) (Pan et al., 2011) and extensive wetlands(Fluet-Chouinard et al., 2015) sustain an important supply of organic carbon to rivers that fuel in-stream microbial production of GHGs.

Yet, the estimates of GHG emissions from tropical rivers and streams remain highly uncertain for several reasons. One being the scarcity of data to characterize the variability within river basins, related for example to differences in river size and land cover on the catchment, but also among river basins, related for example to differences in climatic zones and concomitant differences in land cover. Additionally, emissions of GHGs are disproportionately higher in headwaters and low order streams (Marx et al., 2017), including mountainous reaches (Horgby et al., 2019). For example, in the Congo River, streams with a Strahler order 1 alone accounted for 62%, 59%, and 45% of basin wide total CO_2, CH_4 and, N_2O emissions, respectively (Borges et al., 2019). Streams with Strahler order 1 and 2 accounted, together, for even more, 79%, 77% and, 59% of basin wide total CO_2, CH_4, and N_2O emissions, respectively (Borges et al., 2019).. Higher CO_2, CH_4 and N_2O emissions from low order streams result from a higher input of GHGs from soil-water and ground-water in low order streams, although highly variable in space and seasonally because soil-water inputs occur during short-lived high-flow events that promote shallow flow paths (Duvert et al., 2018). Additionally, low order streams and in particular mountainous ones are characterized by high values of gas transfer velocity (k) (Ulseth et al., 2019). The strong degassing to the atmosphere due to high k values results in concentrations of CO_2 and CH_4 close to equilibrium with the atmosphere in mountainous streams (Crawford et al., 2015) Conversely, in lowland river reaches, the presence of wetlands strongly enhances the fluvial riverine CO_2 and CH_4 emissions (Abril et al., 2014; Abril & Borges, 2019; Borges, Abril, et al., 2015b; Borges, Darchambeau, et al., 2015a; Borges et al., 2019). There is then a need to describe the spatial variations of GHG fluxes from headwaters to lowlands and understand the underlying drivers. This knowledge should allow choosing the appropriate landscape metrics (catchment slope, land vegetation cover, inundation cover, precipitation, among others) and/or stream attributes (river size, stream gradient, discharge, among others) to statistically model and

upscale GHG concentrations and *k* and compute and integrate riverine GHG fluxes, either at local scale (Borges et al., 2019) or globally (Lauerwald et al., 2015; Liu et al., 2022).

The Amazon is the largest river on the Earth in terms of freshwater discharge and watershed surface area; its basin covers a large portion of the humid Neotropics. The lowland Amazon rivers and streams (channels only at an elevation < 500 m) were reported to emit CO_2 at a rate ranging between 0.09 (Liu et al., 2022) and 0.14 (Melack, 2017) PgC yr^{-1}. Additionally, headwater Amazonian streams emit CO_2 at a rate ranging between 0.09 (Johnson et al., 2008) and 0.17 (Liu et al., 2022) PgC yr^{-1}. The total CO_2 emission from the Amazon running waters (rivers and floodplains) range between 0.5 (Richey et al., 2002) and 1.4 PgC yr^{-1} (Sawakuchi et al., 2017). Rivers and floodplains of the Amazon River entire basin emit CH_4 rate of ~22 $TgCH_4$ yr^{-1}, but rivers represented about ~0.6% of the total flux, although only integrated for the Solimões-Amazon mainstem (Melack et al., 2004). The CH_4 emissions from large rivers of the Amazon River have been evaluated to 0.5 $TgCH_4$ yr^{-1} (Sawakuchi et al., 2014), and CH_4 emissions for the whole lowland Amazon basin (elevation < 500m) to 0.3 $TgCH_4$ yr^{-1} (Barbosa et al., 2016). The total emission of CH_4 from Amazonia (including all terrestrial and aquatic compartments) converge to ~40 $TgCH_4$ yr^{-1} and have been evaluated with a variety of methods (Basso et al., 2021; Pangala et al., 2017), either based on atmospheric observations ("top down" approach) or upscaling of flux measurements in various relevant components ("bottom up" approach).
Research on GHGs in rivers and streams has mainly focussed on the Central Amazon (Abril et al., 2014; Alin et al., 2011; Barbosa et al., 2016; Borges et al., 2015a; Call et al., 2018; de Fátima F. L. Rasera et al., 2008; Johnson et al., 2008; Melack et al., 2004; Richey et al., 2002; Sawakuchi et al., 2017, 2014; Scofield et al., 2016). Most research has focussed on high order streams and rivers, and only occasionally in headwater streams (Johnson et al., 2008a; Schneider et al., 2020). Here, we report data of the dissolved CO_2, CH_4 and N_2O concentration in the Andean headwater mountainous and piedmont rivers and streams of the Napo basin in Ecuador (Fig 2.1 and Supplementary Fig 2.1). We describe gradients of dissolved concentrations of CO_2, CH_4 and N_2O with elevation and their drivers in terms of catchment attributes (slope and land cover), and we model gas emissions at the scale of whole Amazon basin using in addition for lowland rivers a compilation of published data.

FIGURE 2.1 Location of sampling stations in Andean headwater and piedmont streams of the Amazon basin a-c. The outline of the catchment of the Napo River is shown in red, stations in the main-stem are shown by blue circles and in the tributaries by green squares.

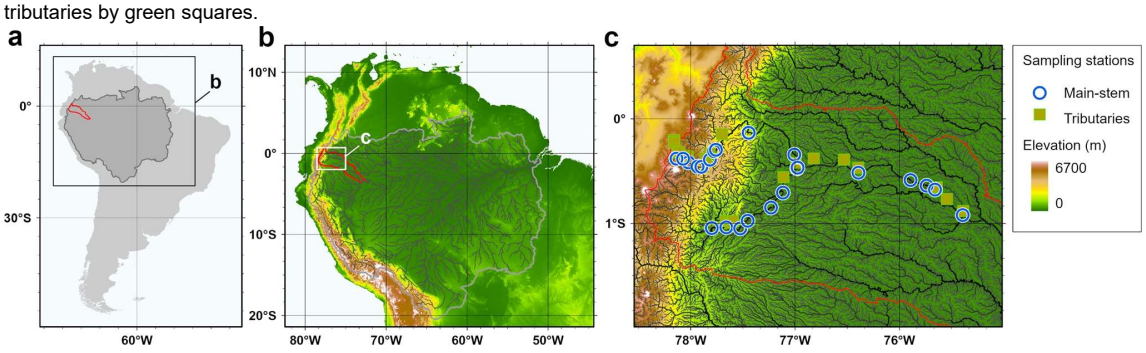

Methods

Site description

The Napo River catchment is ranges from 100 to 6,300 m above sea level, and has a total area of 100,500 km^2, distributed among Ecuador (59%), Peru (40%) and Colombia (1%). The Ecuadorian part of the Andean Cordillera is the narrowest within the Central Andes and is characterized by an important volcanic and seismic activity. Below an elevation of 500 m is located a fairly flat and homogeneous forest, part of the Amazonian plains, that covers 82% of

the total surface of the Napo basin. The rest of the basin (18%) is constituted by the Andean Cordillera with a vegetation cover composed by grasslands (puna and páramo). The drainage basin receives on average 3,200 mm of rainfall per year. At high elevations, rainfall is bimodal and is maximal in April and October and minimal in July-August and in January. In the upper basins, two discharge maxima occur during the two rainfall maxima. In the lowlands, seasonal variability of rainfall and discharge is very weak. The annual discharge of the Napo is 6,300 m3 s^{-1} corresponding to 4% of the Amazon River total discharge at Obidos. The Napo is a 'white water' river type characterized by high levels of total suspended matter, and the sediment transport of the Napo River corresponds to 6% of the sediment flow of the Amazon River at Obidos (Hall et al., 2016).

Sampling and chemical analysis

Sampling was carried out on eight occasions (October 2018 and 2019, January 2019 and 2020, April 2019 and 2021, July 2019 and 2020) (Supplementary Figure 2.1). Stations A1 to A21 were sampled travelling by car, and the others travelling by boat. Sampling was carried out during day-time only (early morning to late afternoon). In some streams, during day-time, oxygen concentrations can strongly increase (Gómez-Gener et al., 2021), and, conversely, CO_2 concentrations can decrease (Descy et al., 2017), in response to aquatic photosynthesis. Fluvial CO_2 emissions can, thus, be under-estimated (Descy et al., 2017) if data are only acquired during day-time, because night-time CO_2 concentrations and fluxes can be higher than during day-time. Note that a day-time decrease of stream CO_2 and increase of O_2 are not necessarily systematic patterns that depend on the level of in-stream productivity. In lowland streams, rich in DOC, such as in the Congo River network, day-night differences of pCO_2 were low (Borges et al., 2019) due to low planktonic primary production and much smaller than the differences among streams (spatial gradients).

Water temperature, specific conductivity, pH, and $\%O_2$ were measured in-situ with a YSI multi-parameter probe (ProPlus). Water for CH_4 and N_2O samples was collected with a sampling devise consisting of a 2L polyethylene bottle with the bottom cut and fitted with a silicone tubing at the stopper . Two borosilicate serum bottles (Weathon) with a volume of 40 ml were filled with the silicone tubing, poisoned with 100 µl of a saturated solution of $HgCl_2$ and sealed with a butyl stopper and crimped with an aluminium cap. Measurements were made, after over-night equilibration, on an headspace (Dickson et al., 2007) (created by injecting 15 ml of high-purity N_2 into the 40 ml sample bottles), with a gas chromatograph (SRI 8610C) with a flame ionisation detector for CH_4 and electron capture detector for N_2O calibrated with $CH4:N_2O:N_2$ gas mixtures (Air Liquide Belgium) with mixing ratios of 1, 10 and 30 ppm for CH4, and 0.2, 2.0 and 6.0 ppm for N_2O. The precision of measurement based on duplicate samples was ±10.9% for CH_4 and ±5.8% for N_2O based on 309 replicates.

pCO_2 was measured in the field with a Li-Cor Li-820 infra-red gas analyser based on the headspace technique with 4 polypropylene syringes that were filled directly with river water. The pCO_2 in the atmosphere was measured by injecting ambient air sampled with an additional polypropylene syringe. The Li-Cor Li-820 was calibrated with pure N_2 and $CO_2:N_2$ gas mixtures (Air Liquide Belgium) of 388, 804, 3707 and 8146 ppm. The final pCO_2 value was computed taking into account the partitioning of CO_2 between water and the headspace, as well as equilibrium with HCO3- 110 using water temperature measured in-stream and after equilibration, and total alkalinity (data not shown). Samples for total alkalinity were conditioned, stored and analysed as reported. The precision of pCO_2 measurement was ±5.2%.

The CO_2 concentration is expressed as partial pressure in parts per million (ppm) and as dissolved concentration for CH_4 (nmol L^{-1}), in accordance with convention in existing topical literature. Variations of N_2O were modest and concentrations fluctuated around atmospheric equilibrium, so data are presented as percent of saturation level ($\%N_2O$, where atmospheric equilibrium corresponds to 100%), computed from the global mean N_2O air mixing ratios given by the Global Monitoring Division (GMD) of the Earth System Research Laboratory (ESRL) of the

National Oceanic and Atmospheric Administration (NOAA) (https://www.esrl.noaa.gov/gmd/hats/combined/N_2O.html), using the Henry's constant (APHA, 1998).

Water was collected in the stream surface with a 2L polyethylene bottle. The water filtered through GF/F Whatman glass fibber filters was collected and further filtered through polyethersulfone syringe encapsulated filters (0.2 µm porosity) for nitrate (NO3-), nitrite (NO_2-) and ammonium (NH4+). Samples were were stored frozen (-20°C) in 50 ml polypropylene vials. NO3- and NO_2- were determined with the sulfanilamide colorimetric with the vanadium reduction method (Standing committee of Analysts., 1981)., and NH4+ with the dichloroisocyanurate-salicylate-nitroprussiate colorimetric method (Abril et al., 2015). Detection limits were 0.3, 0.01, and 0.15 µmol L^{-1} for NH4+, NO_2- and NO3-, respectively. Precisions were ±0.02 µmol L^{-1}, ±0.02 µmol L^{-1}, and ±0.1 µmol L^{-1} for NH4+, NO_2- and NO3-, respectively.

Computation and upscaling of FCO_2, FCH4, FN_2O

The dissolved concentrations of CO_2, CH_4 and N_2O were derived from statistical relations as function of catchment slope for each of the river segments in RiverATLAS(Linke et al., 2019) (n=744,786). The statistical relations we derived from our own data in the Napo and data available from literature in the lowland rivers and streams of the Central Amazon (Figure 2.4).

The pCO_2 (in ppm) was computed according to:

$$\log(pCO_2) = 3.57(\pm 0.02) - 0.0043(\pm 0.0002) \times CS \quad (1)$$

(r^2=0.59, p<0.0001, n=473)

where CS is the catchment slope (x10°).

The CH_4 (in nmol L^{-1}) was computed for an elevation > 180 m according to:

$$\log(CH_4)=3.18(\pm 0.08) - 0.0081(\pm 0.0005) \times CS \quad (2)$$

(r^2=0.42, p<0.0001, n=305)

and for an elevation < 180 m according to:

$$\log(CH_4)=2.60(\pm 0.08) - 0.0178(\pm 0.003) \times CS \quad (3)$$

(r^2=0.21, p<0.0001, n=174)

The $\%N_2O$ (in %) was computed for an elevation > 200 m according to:

$$\%N_2O = 106.9(\pm 2.3) - 0.048(\pm 0.014) \times CS \quad (4)$$

(r^2=0.04, p=0.0011, n=277)

and for an elevation of < 200 m the median of values reported by Richey et al.2016 (205.6%) was applied uniformly.

To avoid the computation of unrealistic values outside the determination bounds of the regressions, for CS > 200 (x10°), a constant value (based on the median of observations within that range of slope values) was applied: 542 ppm for pCO_2 and 96.3 % for %N2O. For CH4, for an elevation > 180 m, a constant value of 18.5 nmol L^{-1} was applied for a CS > 200 (x10°); for an elevation of < 180 m, a constant value of 60.0 nmol L^{-1} was applied for a CS > 50 (x10°).

The water temperature (WT in °C) was computed from the air temperature (AT in x10°C) from RiverATLAS (Linke et al., 2019), according to:

$$WT = 0.00054 \times AT2 - 0.0964 \times AT + 15.2 \quad (5)$$

(r^2=0.93, n=371)

FCO_2, FCH_4, FN_2O between surface waters and the atmosphere was computed according to:

$$F = k \times \Delta G \quad (6)$$

where k is the gas transfer velocity (m d^{-1}) and ΔG is the air-water gradient of a given gas.
The k normalized to a Schmidt number (Sc) of 600 (k600 in m d^{-1}) was derived from the parameterisation as a function slope and stream water velocity (Raymond et al., 2012):

$$k600 = 2.02(\pm 0.21) + 2841(\pm 107) \times V \times S \quad (7)$$

where V is stream velocity (m s^{-1}) and S is stream slope (unitless).
k600 was converted to k for the Sc at in-situ temperature47 according to:

$$k = k600 \times (Sc/600)\text{-}0.5 \quad (8)$$

The values of S are given by RiverATLAS (Linke et al., 2019) and V was computed from discharge (Q in m3 s^{-1}) also given by RiverATLAS (Linke et al., 2019) according to (Liu et al., 2022):

$$\ln(V) = 0.12 \times \ln(Q) - 1.06 \quad (9)$$

A Monte-Carlo error analysis was made by propagating errors (10,000 iterations) on the slope and constant of the equations to compute k600 and the gas concentrations (refer to above equations), and an error of ±1°C for water temperature.

Results and discussion

Altitudinal patterns of stream GHG content

We sampled 25 stations in the mainstem Napo and Coca rivers and 19 stations in the tributaries along an elevation gradient from 3990 m to 175 m above sea level, on 8 occasions from 2018 to 2021 (Figure 2.1 and Supplementary Figure 2.1). In surface waters of the sampled streams, the values of the partial pressure of CO_2 (pCO_2) ranged between 152 and 10,873 ppm, and dissolved CH_4 concentrations between 4 and 38,666 nmol L^{-1} (Figure 2.2a,e). Values of pCO_2 below atmospheric equilibrium (~404 ppm, average of in-situ measurements) were only observed in 22 cases (7% of the total number of observations), while dissolved CH_4 concentration values in surface waters were always above atmospheric equilibrium (~2 nmol L^{-1}, based on the global average CH_4 mixing ratio of 1.9 ppm).

FIGURE 2.2 Strong elevation gradients of pCO_2, CH_4 and $\%N_2O$ in the Andean headwater and piedmont streams. Variations of the partial pressure of CO_2 (pCO_2), CH4 dissolved concentration, N_2O saturation level ($\%N_2O$), and oxygen saturation level ($\%O_2$) in the Napo streams as a function of elevation (a, e, i, m), catchment slope (b, f, j, n), forest cover (c, g, k, o), and water temperature (d, h, l, p). Symbols show the median and error bars the interquartile range, stations in the main-stem are shown by blue circles and in the tributaries by green squares, and black lines indicate linear or exponential fits to the data. Solid lines show fits to the data (Supplementary Table 2.4).

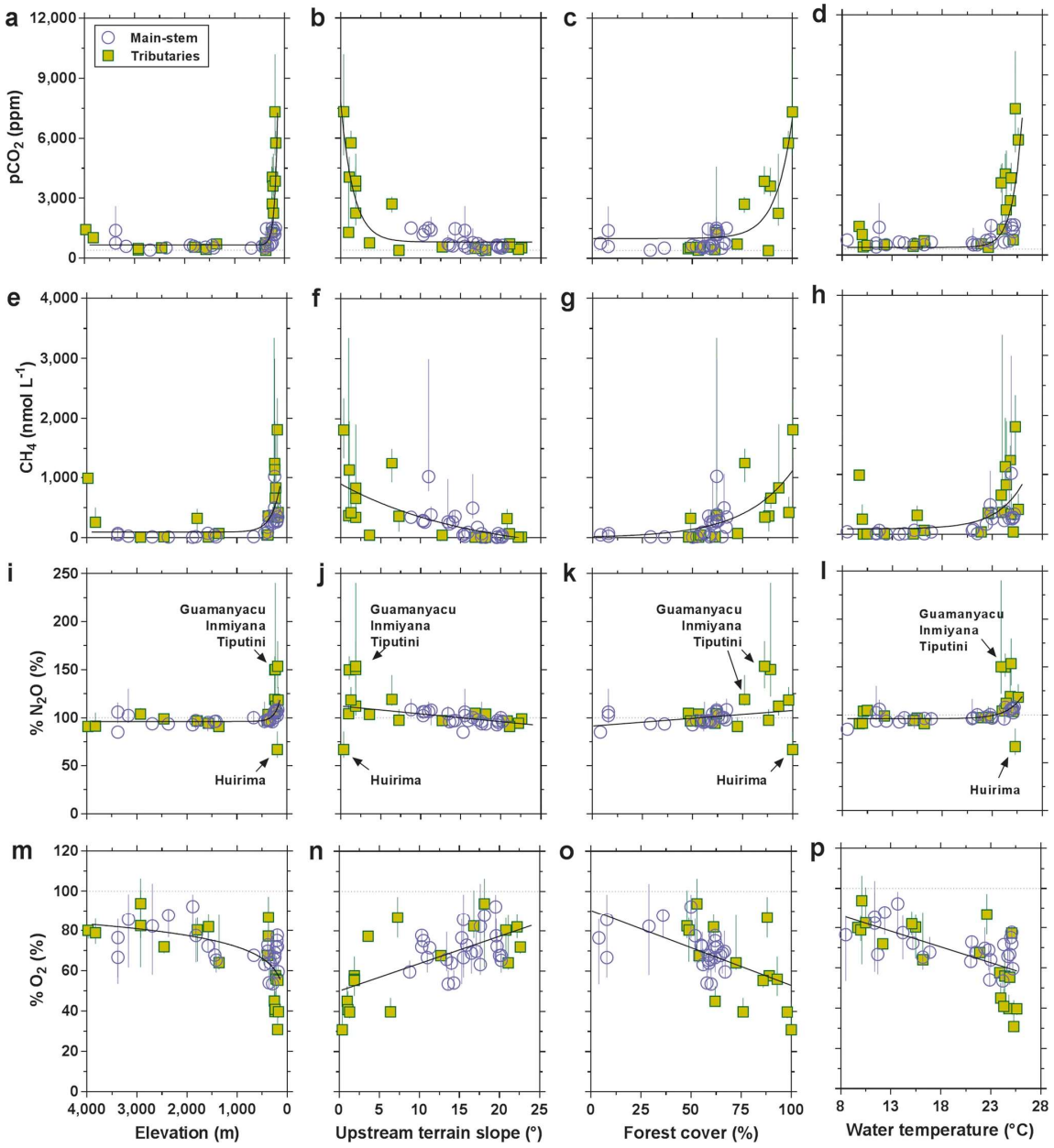

FIGURE 2.3 Strong correlations between pCO_2, CH4, $\%N_2O$ and $\%O_2$ in the Andean headwater and piedmont streams. Variations of the partial pressure of CO_2 (pCO_2), CH_4 dissolved concentration, N_2O saturation level ($\%N_2O$), as a function of oxygen saturation level ($\%O_2$) (a, c, e), CH_4 and $\%N_2O$ as a function of pCO_2 (b, d), and $\%N_2O$ as a function of dissolved inorganic nitrogen (DIN) (f) in the Napo streams. Symbols show the median and error bars the interquartile range, stations in the main-stem are shown by blue circles and in the tributaries by green squares, and black lines indicate linear or exponential fits to the data. Solid lines show fits to the data (Supplementary Table 2.4).

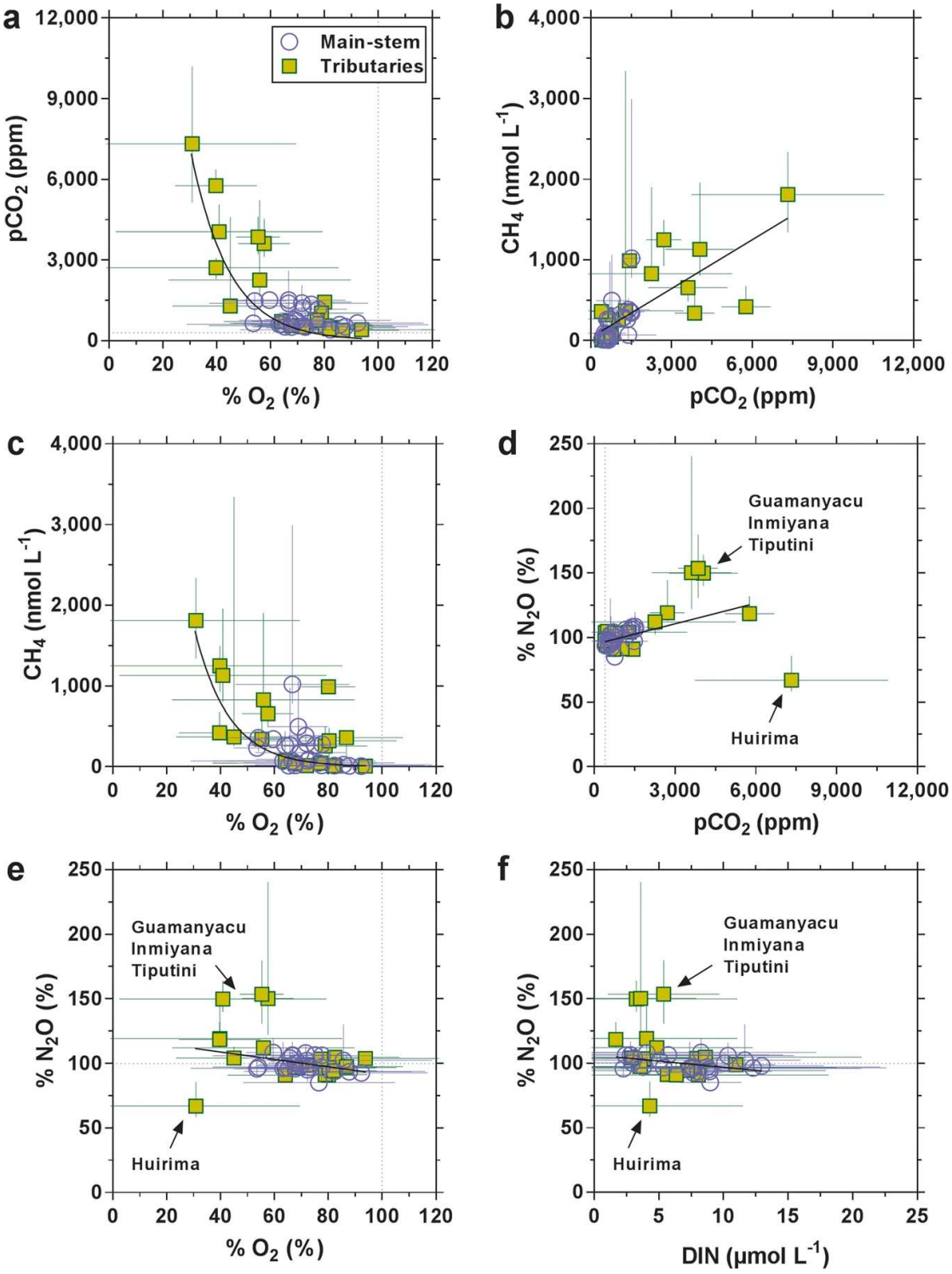

The pCO_2 and dissolved CH_4 concentration values in streams at elevations > 500 m (median 560 ppm and 17 nmol L^{-1}, respectively) were distinctly lower than at elevations < 500 m (median 1,280 ppm and 370 nmol L^{-1}, respectively). The pCO_2 and dissolved CH_4 concentration in streams increased exponentially from highlands to lowlands (Figure 2.2a,e). The patterns of oxygen saturation level ($\%O_2$) in streams generally mirrored those of pCO_2 and dissolved CH_4 concentration. The $\%O_2$ values in streams at elevations > 500 m (median 74.4 %) were higher than at elevations < 500 m (median 63.2 %), and $\%O_2$ decreased exponentially from highlands to lowlands (Figure 2.2m).

The pCO_2 and dissolved CH_4 concentration values were positively correlated (Figure 2.3b), and they were negatively correlated to $\%O_2$ (Figure 2.3a,c), strongly suggesting that pCO_2 and dissolved CH_4 concentration in streams were controlled by the same combination of input and output processes (that also involved opposite changes of O_2). A likely important output process of CO_2 and CH_4 is the loss to the atmosphere that depends on k. The calculated k values increased with increasing elevation (Supplementary Figure 2.2b). Higher k values strongly promoted the emissions of CO_2 and CH_4 to the atmosphere, contributing to drive pCO_2 and dissolved CH_4 concentrations to values close to saturation in the highland streams compared to lowland streams, and could explain in part the decreasing pattern of pCO_2 and dissolved CH_4 concentrations with elevation. A likely important input process of CO_2 and CH_4 is organic matter mineralization in-stream, in fringing wetlands, and in terra firme soils of the watershed. Altitudinal changes of organic matter mineralization might have resulted from changes in temperature, soil organic carbon content and land cover. Water temperature strongly increased from highlands to lowlands, from ~13.5°C > 500 m elevation to ~24.3°C < 500 m (Figure 2.S2a). Rates of respiration (Cardoso et al., 2014; Kirschbaum, 1995) and methanogenesis (Yvon-Durocher et al., 2014) in soils and riverine sediments are positively related to temperature, suggesting the warmer conditions in the lowland rivers contributed to higher pCO_2 and dissolved CH_4 concentration values. Indeed, pCO_2 and dissolved CH_4 concentration values also increased exponentially with water temperature (Figure 2.2d,h). Changes of water temperature could contribute to explain the decreasing pattern of pCO_2 and dissolved CH_4 concentration with elevation.

There were also changes of land cover with elevation with a transition from a dominance of grasslands in uplands (known as páramos) to forests in lowlands (Supplementary Figure 2.3a,b) (McClain et al., 1995). Additionally, the presence of fringing wetlands (indicated by inundation extent) strongly increased in the piedmont streams (Supplementary Figure 2.3c). Stream pCO_2 and dissolved CH_4 concentration values increased exponentially with forest cover (Fig 2c,g), and were generally higher where grassland cover was low to zero (Supplementary Figure 2.4a,c). Fluvial pCO_2 and dissolved CH_4 concentrations values were positively related to inundation extent in the reach with different slopes for tributaries and main-stem (Supplementary Figure 2.4b,d). Fringing wetlands might have a local impact on pCO_2 and dissolved CH_4 concentration in smaller streams (tributaries) in the piedmont region and explain in part the increasing pattern of pCO_2 and dissolved CH_4 concentration with decreasing elevation. Lateral inputs from fringing wetlands strongly influence the fluvial content of dissolved organic carbon (DOC) (McClain et al., 1997) and CO_2 (Abril et al., 2014) in the Central Amazon River. Note that inundation extent was locally high in some of the lowland streams at reach level, but for the whole upstream catchment the inundation extent values were much lower (≤2%). Wetlands have been shown to strongly influence pCO_2 and dissolved CH_4 concentration values in lowland African rivers where the wetland cover was higher for the whole upstream catchment (Borges et al., 2015d).

The k values strongly depend on stream gradient and water flow (Raymond et al., 2012) that both scale with catchment slope, that itself varies with elevation. Vegetation cover (forest and riparian wetlands) and temperature also vary as function of elevation, so, also with catchment slope. Consequently, catchment slope could be used as an integrative metric for processes that affect GHGs. Indeed, pCO_2 and dissolved CH_4 concentration values in the sampled streams were found to be negatively related to catchment slope, while $\%O_2$ was positively related to catchment slope (Figure 2.2b,f,n). The N_2O saturation levels ($\%N_2O$) in streams at an altitude > 500 m

(median 95.4 %) were lower than at elevations < 500 m (median 105.0 %) (Figure 2.2i). The $\%N_2O$ increased exponentially with decreasing elevation, although the exponential increase was less steep than for pCO_2 and dissolved CH_4 concentration (Figure 2.2). Lower N_2O in high elevation streams was consistent with reported elevation gradients of N_2O soil-air fluxes in the Ecuadorian Andes, with a soil N_2O sink at high elevation (2,200-3,010 m) and a N_2O source from soils to the atmosphere at lower elevation (400-1,100 m)48. The low fluvial $\%N_2O$ probably resulted from inputs to river reaches of soil water with low N_2O content. The removal of N_2O in soils was due to complete denitrification (reduction of N_2O to N_2) in highlands related to low soil dissolved inorganic N (DIN) content (Pineda Lampreda et al., 2021). Conversely, the N_2O emissions from soils to the atmosphere from lowland soils to the atmosphere was related to high DIN content in soils combined to higher temperature and higher soil water content (Pineda Lampreda et al., 2021). The DIN in streams (Supplementary Figure 2.5c) was higher in highland streams than in lowland streams, so did not seem to follow the pattern of soil DIN that was higher in lowlands than highlands (Pineda Lampreda et al., 2021). The same elevation pattern of stream DIN was reported in Andean streams in Venezuela (Allan et al., 2006). High DIN levels were reported in 55 streams in montane forests in Central America and the Caribbean (Brookshire et al., 2012). Large loss of inorganic nitrogen by leakage to streams from unpolluted mature tropical forests occurs ubiquitously across a range of soil types. The higher DIN in highland streams could be related to higher transfer of DIN from soils to streams related to a lower retention due to differences in vegetation types (grassland versus forest) (Templer et al., 2012) or higher catchment slopes that promote soil-river transfer of DIN (Becker et al., 2014; Fu et al., 2004). In addition, there could have been a higher DIN uptake in the water column by primary producers (phytoplankton or macrophytes) related to decrease in flow and an increase in water residence. The combination of higher stream DIN and low $\%N_2O$ in highland streams, and the opposite pattern in lowland streams led to a negative relation between $\%N_2O$ and DIN (Figure 2.3f). Such a negative relation is unique compared to patterns previously reported, as N_2O content in rivers is in general positively related to DIN (Herreid et al., 2021; Rosamond et al., 2012; Zhang et al., 2022).

Four streams showed %N2O values diverging from general patterns, the Huirima and a cluster of three streams (Guamanyacu, Inmiyana, Tiputini). The Huirima showed distinctly lower $\%N_2O$ (67%) than the other lowland streams at equivalent elevations (104-119%) but also the lowest $\%O_2$ (30.9%) and highest pCO_2 (7,317 ppm) values (Figure 2.3d,e). The Huirima stream was also characterized by much higher DOC concentrations than all the other streams, suggesting a stronger removal of N2O by denitrification in soils and/or sediments associated to streams with high DOC and low $\%O_2$, as also shown in black-water rivers and streams of the Congo basin (Borges et al., 2019). The Huirima was characterized by the lowest catchment terrain slope (0.4°) among the sampled streams. Aerial view (Supplementary Figure 2.6) showed a dense forest cover and suggested extensive inundation of the Huirima river that probably promoted conditions favorable for complete denitrification and N_2O removal (reducing conditions associated to high DOC and low $\%O_2$).

The Guamanyacu, Inmiyana, and Tiputini streams drain (in part) oil palm plantations (Supplementary Figure 2.7a-c) that could explain the higher stream $\%N_2O$ levels (150-153%) compared to surrounding streams (104^{-1}19%). In the area, artificial fertilizers are not used in the oil palm plantations, and accordingly, the DIN levels in these streams were comparable to the others at same elevation (Figure 2.3f). However, the conversion of natural forest to oil palm plantations itself leads to an increase of N_2O production in soils due to changes in N microbial cycling due to disturbance of the soils(Skiba et al., 2020) . Overall, oil palm plantations did not seem to lose markedly DIN to rivers but there seemed to be intense N_2O production in soils that was transported to streams.

Stream size has been shown to be an important predictor of CO_2 and CH_4 emissions that scale with stream Strahler order in boreal (Wallin et al., 2018), temperate (Borges et al., 2019b; Butman and Raymond, 2011) and tropical river basins. In highland streams (elevation > 500 m), there were no clear patterns with stream size for pCO_2, dissolved CH_4 concentration, $\%N_2O$ and

$\%O_2$ (Supplementary Figure 2.8e-h). In the lowland streams, there was an increasing pattern with stream size of pCO_2 and dissolved CH_4 concentration (mirrored by a decreasing pattern of $\%O_2$) (Supplementary Figure 2.8i-l) as frequently observed in other river networks (Borges et al., 2019a, 2018; Butman and Raymond, 2011; Wallin et al., 2018) . However, when streams were taken together irrespective of altitude, there was no clear relation with streams size for pCO_2, dissolved CH_4 concentrations, $\%N_2O$ and $\%O_2$ (Supplementary Figure 2.8a-d), suggesting that the effect of altitudinal gradient overwhelmed the effect of stream size on the variability of these quantities.

Exchange of CO_2, CH_4 and N_2O with the atmosphere from the Napo river network

The air-water diffusive flux of CO_2 (FCO_2) ranged between -1 and 1,074 mol m^{-2} yr^{-1}, and was higher in tributaries (median 128 mol m^{-2} yr^{-1}) than in the main-stem (median 34 mol m^{-2} yr^{-1}). The air-water diffusive flux of CH_4 (FCH_4) ranged between 45 and 8,985 mmol m^{-2} yr^{-1}, and was generally higher in tributaries (median 999 mmol m^{-2} yr^{-1}) than in the main-stem (332 mmol m^{-2} yr^{-1}). Both FCO_2 and FCH_4 were inversely correlated to elevation and upstream terrain slope (Supplementary Figure 2.9a,b,e,f). The air-water diffusive flux of N_2O (FN_2O) ranged between -23 and 27 mmol m^{-2} yr^{-1} and did not show marked difference between tributaries and main-stem. There was a general tendency towards a sink of N_2O at an elevation > 1,000m with 12 sites showing negative FN_2O values and only 4 showing positive FN_2O values (Supplementary Figure 2.9i,j). At an elevation < 1,000m the FN_2O values were close to zero (-1.3 to 3 mmol m^{-2} yr^{-1}), except for the Guamanyacu, Inmiyana, and Tiputini streams that showed distinctly positive FN_2O values (9.7 to 21.6 mmol m^{-2} yr^{-1}) and the Huirima that showed a distinctly negative FN_2O value (-7.6 mmol m^{-2} yr^{-1}).

In river geomorphology, the concept of sediment transport capacity has been used to determine if bedload transport is primarily constrained by sediment supply (supply-limited rivers) or river flow hydraulics (transport-limited rivers) (Wainwright et al., 2015). This concept has been extended by some authors to fluvial CO_2 and CH_4 fluxes (Crawford et al., 2015; Rocher-Ros et al., 2019; Schneider et al., 2020). The underlying idea being that in highly turbulent systems (high k values) degassing brings gases close to equilibrium with atmosphere and emissions are close to zero, consequently the gaseous emission is assumed limited by gas availability. Transport- or supply-limitation of the gaseous exchange with the atmosphere can be visualized by plots of gas concentration versus k600 (Rocher-Ros et al., 2019) (Supplementary Figure 2.10). At an elevation above 1,500 m, computed k600 values were higher than 25 m d^{-1} while pCO_2 (< 746 ppm) and CH_4 (< 72 nmol L^{-1}) values were low indicating supply-limitation of CO_2 and CH_4 emissions (Supplementary Figure 2.10a,b). Conversely, in some of the lowland tributaries, particularly high pCO_2 (> 1,500 ppm) and CH_4 (> 500 nmol L^{-1}) values indicate transport-limitation of CO_2 and CH_4 emissions. There was an exception for both CO_2 and CH4, corresponding to high concentrations values (pCO_2=1,395 ppm and CH4=320 nmol L^{-1}) in highland streams with high k600 values (74 and 88 m d^{-1}, respectively) (indicated by asterisks in Supplementary Figs. 9 and 10). For N_2O, the interpretation of concentration-k600 plot in terms of transport- or supply-limitation was not as clear as for CO_2 and CH_4 (Supplementary Figure 2.10c). The sampled streams were more or less strongly over-saturated in both CO_2 and CH4, consequently the flux was unidirectional from the water to the atmosphere (emission). In contrast, N_2O oscillated between under- and over-saturation, corresponding to a sink or a source of N_2O the atmosphere, respectively. In the case of a stream acting as a sink of a gas, the supply-limitation is from the atmosphere and not within the stream itself. In this situation, the use of concept of transport capacity as used for sediments(Wainwright et al., 2015) becomes awkward. At an elevation > 1,500 m, N_2O concentrations were close to saturation in conjunction with high k600 values (Supplementary Figure 2.10c). At an elevation below 1,500 m, N_2O concentrations markedly above or below saturation were observed in some streams. In this case, the direction and intensity of the N_2O exchange should be more strongly driven by variations of concentrations rather than by those of k600. FCO_2, FCH_4 and FN_2O strongly correlated with pCO_2, CH4, and $\%N_2O$, respectively, and did not correlate to k600 (Supplementary Figure 2.9c,g,k,d,h,l), showing that for the whole data-set the variations of gaseous exchanges with the atmosphere were strongly driven

by the variations of the concentrations (supply-limitation) rather than by k600 (transport-limitation). In highly turbulent systems with high k600 values, the gaseous exchanges with the atmosphere bring the concentrations close to equilibrium with the atmosphere, strongly decreasing the flux values that converge to zero.

Comparison of stream GHG content with Central Amazon basin

The pCO_2 values in the rivers and streams of the Central Amazon (median 2950 ppm) were higher than piedmont (median 1280 ppm) and highland (median 555 ppm) streams of the Napo and there was a general decreasing pattern with elevation and slope (Figure 2.4a). In contrast, the CH_4 concentrations in the piedmont streams (median 341 nmol L^{-1}) were higher than in the rivers and streams of the Central Amazon (median 120 nmol L^{-1}), that in turn were higher than in the highland streams (median 16 nmol L^{-1}) (Figure 2.4b). There was a general decreasing tendency of CH_4 as function of catchment slope, but at equivalent slope values (at the low end of the range of values), CH_4 concentrations were higher in piedmont streams than lowland stream and rivers. The ratio of CH_4 to CO_2 dissolved concentrations ($CH4:CO_2$ in µmol:µmol) followed the same patterns as dissolved CH_4 concentration (Figure 2.4c), indicating that for a similar input of CO_2 (lateral input from soils or in-stream mineralization) there was a larger input of CH_4 in piedmont streams than in lowland rivers and streams. The forest cover and water temperatures in piedmont streams are equivalent to those in lowland rivers and streams. The higher dissolved CH_4 concentration in piedmont rivers might result from the combination of relatively higher CH_4 production in the piedmont streams and relatively higher losses of dissolved CH_4 in the lowland rivers. The piedmont region is an area of deposition of suspended particles delivered from the highland streams originating from erosion, up to 30% of the total annual load in the Mamoré river (Vauchel et al., 2017), with an annual freshwater discharge equivalent to the one of the Napo. The deposition of sediments combined by presence of forests in the piedmont region are most probably favorable to high in-stream CH_4 production. In larger lowland river channels that are relatively disconnected from floodplains, the deep water column and strong currents do not promote the accumulation of dissolved CH_4 in the water column, but promote the removal of dissolved CH_4 either by emission of CH_4 to the atmosphere or by microbial oxidation (Borges et al., 2015).

The only N_2O data in streams and rivers of the Amazon River network were reported by Richey et al 1998. When plotted against pCO_2, the $\%N_2O$ values were higher in the Central Amazon streams and rivers (median 205.6%) compared to piedmont (median 105.0%) and highland (median 95.7%) streams (Supplementary Figure 2.11a). We do not have a conclusive hypothesis for the higher $\%N_2O$ in lowland streams and rivers, but the general tendency of higher pCO_2 and N_2O in lowland streams and rivers than in piedmont and highland streams (Supplementary Figure 2.11b) suggests more intense mineralization in soils or in-stream leading to higher CO_2 and presumably N_2O levels in rivers in the former systems (Pineda Lampreda et al., 2021). The pattern of higher $\%N_2O$ in Central amazon streams compared to headwater and piedmont streams was also consistent with higher N_2O soil-air fluxes (79 ± 7 µgN m^{-2} h^{-1}) in the central part of the basin from oxisols (Keller et al., 2018) that are dominant in the Amazon forests than in piedmont forests (8 ± 12 µgN m^{-2} h^{-1} at 400 m elevation) (Bernoux,. 1998), Comparatively higher dissolved CH_4 concentrations in piedmont streams than in lowland streams was also evident relative to pCO_2 when compared with the data-set of Richey et al.1998 (Supplementary Figure 2.11a).

Exchange of CO_2, CH_4 and N_2O with the atmosphere from the whole Amazon basin including Andean mountainous and piedmont streams

We used catchment slope as an integrative metric to scale pCO_2, CH_4 and $\%N_2O$ available in the Amazon River network, as detailed in the Methods section. The k values were derived from stream gradient (slope) and flow velocity (Raymond, Hartmann, 2013), itself

computed from discharge (Liu et al., 2022), for all the river segments given by RiverATLAS (Linke et al., 2019). The areal FCO_2, FCH_4 and FN_2O (per m^2) were computed from k and concentrations of CO_2, CH4, N_2O for each river segment of the Amazon catchment given by RiverATLAS (n=744,786) and then integrated with the corresponding SSA.

The piedmont streams accounted for 62% of the total integrated diffusive FCH_4 (0.4±0.1 $TgCH_4$ yr^{-1}), higher than the contribution from lowland rivers (28%), while highland streams accounted for only 10% (Figure 2.5b). The diffusive FCH_4 per m^2 in highland streams (1,077±240 mmol m^{-2} yr^{-1}) was 4.5 times higher than in lowland rivers (237±79 mmol m^{-2} yr^{-1}) despite the fact that dissolved CH_4 concentrations were ~2 times lower (157±35 versus 307±100 nmol L^{-1}), due to much higher k values (148.8±3.2 versus 14.5±0.4 cm h^{-1}, Fig 5e). The diffusive FCH_4 per m^2 in piedmont streams (1,573±350 mmol m^{-2} yr^{-1}) was 6.6 times higher than in lowland rivers (137±79 mmol m^{-2} yr^{-1}) because of much higher dissolved CH_4 concentrations (797±174 versus 307±100 nmol L^{-1}), while k was relatively closer (20.0±0.5 versus 14.5±0.4 cm h^{-1}).

The integrated FCO_2 (64±5 TgC yr^{-1}) was dominated by lowland rivers (65%) (Figure 2.5a). However, FCO_2 per m^2 in highland and piedmont rivers (197±35 and 143±3 mol m^{-2} yr^{-1}) were 1.7 and 1.2 times higher than lowland rivers (115±8 mol m^{-2} yr^{-1}), respectively (Figure 2.5d), due to higher k values, since pCO_2 values were lower in highland streams (1,033±88 ppm), although comparatively similar in piedmont streams (2,599±146 ppm) and lowland rivers and streams (2,735±148 ppm) (Figure 2.5g).

The integrated FN_2O (25±4 GgN_2O-N yr^{-1}) was overwhelmingly dominated by lowland rivers and streams (99% of total), while piedmont streams were an extremely small source of N_2O, and highland streams were a very small sink of N_2O (Figure 2.5c). The computation of FN_2O is comparatively more uncertain than FCH_4 and FCO_2 since we extrapolated to all lowland river segments the median $\%N_2O$ value given by Richey et al.34, unlike for the other two GHGs for which relations with slope were used to compute concentration values for individual river segments. The median $\%N_2O$ value (206%) reported by Richey et al. 1988 for the Central Amazon rivers and streams was higher than the median value of $\%N_2O$ reported in two large African rivers, the Zambezi (Teodoru et al., 2015) and the Congo (Borges et al., 2019) rivers of 116% and 131%, respectively. Another study provided a lower $\%N_2O$ average value (134±25%, n=131) in the Solimões and Negro Rivers (Oliveira, 2006) than the median $\%N_2O$ value (206%) reported by Richey et al. 1988. Using the lower $\%N_2O$ value of 134% for all the lowland rivers provided an integrated FN_2O value for the Amazon River basin of 9±4 GgN_2O-N yr^{-1}, which was close to the range of N_2O emissions for the Amazon River basin of 11 to 16 GgN_2O-N yr^{-1} modelled from N deposition and emission factors (Maavara et al., 2019). The wide range of $\%N_2O$ values reported in literature calls for additional data of N_2O in lowland rivers of the Amazon basin for a more accurate evaluation of FN_2O.

FIGURE 2.4 Strong elevation gradients of pCO_2 and CH_4 in streams and rivers across the whole Amazon basin. Variations of the partial pressure of CO_2 (pCO_2), CH_4 dissolved concentration, and the ratio of CH_4 and CO_2 ($CH4:CO_2$) concentration as function of elevation (a, c, e) and catchment slope (b, d, f). Data in the lowland rivers and streams was compiled from literature for pCO_2 (Abril et l., 2014; Rasera et al., 2008; Rasera et al., 2013; Mitchell et al., 2018) and CH_4 (Borges et al., 2015; Sawakuchi., et al 2014; Barbosa et al., 2016., Mitchell et al., 2018). For consistency, only studies based on direct measurements of pCO_2 were selected, excluding data derived from the computation of pCO_2 from pH and total alkalinity, as this computation can provide erroneous and unrealistically high pCO_2 values (Abril et l., 2015). Data from Scofield et al.2016 was excluded because the pCO2 values reported by these authors in the Negro River (upstream of Manaus) were distinctly lower (710 ppm during low water period and 2608 ppm during higher water period) than other studies in the same system (~2000–3000 ppm during low water period and ~5000-8000 ppm during higher water period). Small symbols show individual measurements, large symbols indicate the median; the blue triangles show the data in the mountainous headwater streams, green triangles show the data in piedmont streams, and the grey circles show the data in the lowland streams and rivers, and black lines indicate linear or polynomial fits to the data. Solid lines show fits to the data (Supplementary Table 4).

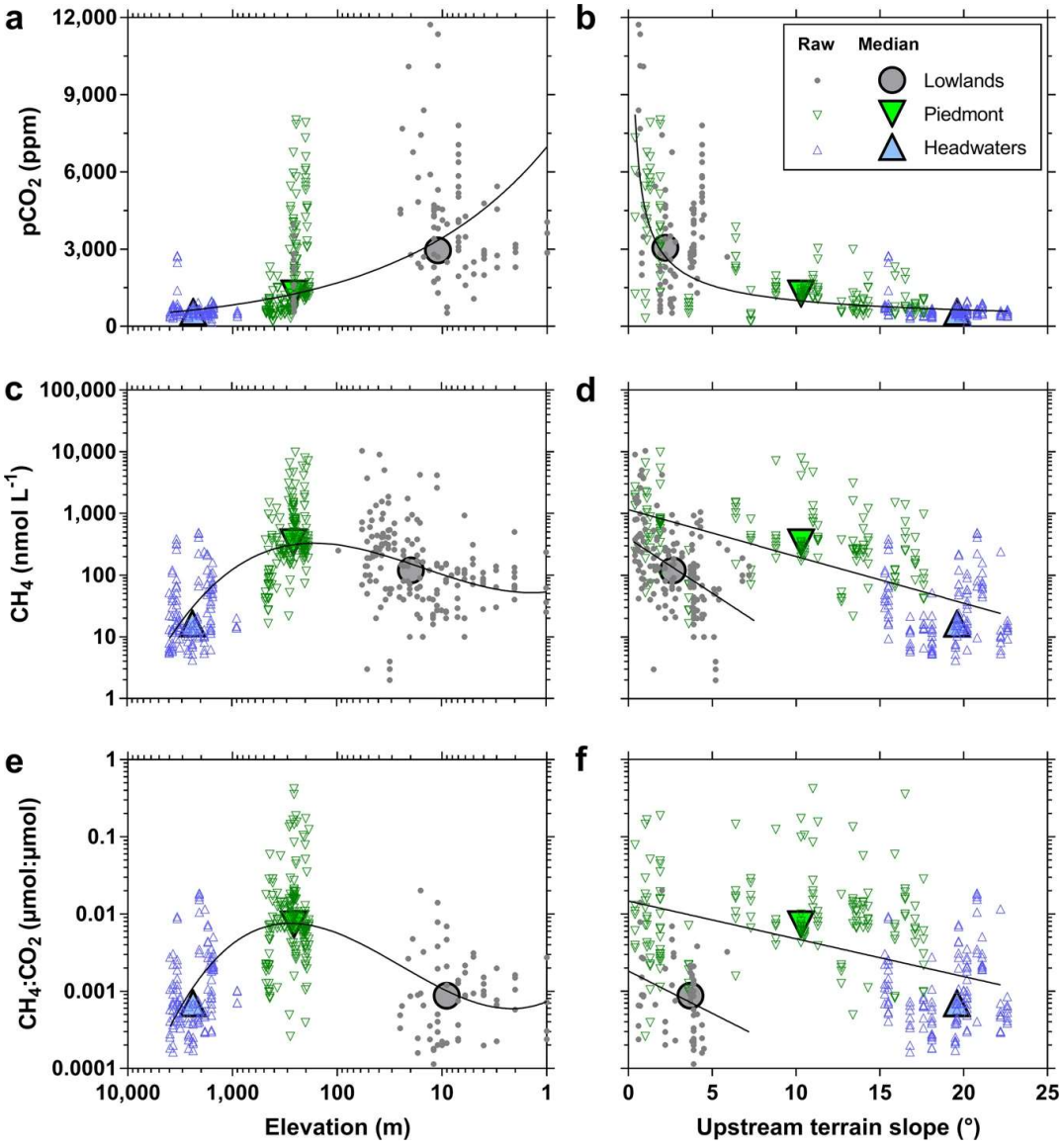

The FCO_2 and FCH_4 estimates per m^2 were consistent (within uncertainties) with those previously reported in the Amazon basin, for lowland basin wide FCO_2 5,27 and FCH_4 (Barbosa et al., 2016), FCH_4 for large lowland rivers (Sawakuchi et al., 2014), and the Amazon/Solimões mainstem FCH_4 (Melack et al., 2004) (Supplementary Table 2. 1). Our lowland basin wide diffusive FCH_4 per m^2 is higher than the one reported by Barbosa et al. 2016 because our estimate includes the piedmont rivers with high diffusive FCH_4 values (Figure 2.5e) while the estimate of Barbosa et al. 2016 is based on data from large lowland rivers (Xingu, Tapajós, Madeira, Purus, Juruá, Japurá, Solimões, Negro).

Uncertainties in scaling the exchange of greenhouse gases with the atmosphere.

The integrated FCO_2, FCH_4 and FN_2O estimates have three sources of uncertainty from each of the terms of the flux computation: the respective modelled dissolved gas concentrations, the k values, and the SSA.

Previous studies that modelled fluvial pCO_2 at continental or global scales either used averaged values per stream order (Butman and Raymond, 2011) or multi-parametric approaches (Lauerwald et al., 2015; Liu et al., 2022) using several catchment proprieties and climate data as predictors. At the continental scale of the USA, Lauerwald et al. 2013 modelled pCO_2 in streams and rivers with multiple linear regressions (MLR) using catchment slope, mean air temperature, and mean precipitation as predictors. At global scale, Lauerwald et al.2015 modelled pCO_2 in streams and rivers with MLR using catchment slope, mean air-temperature, land net primary production, and population density as predictors. Also at global scale, Liu et al. (2022) modelled pCO_2 in streams and rivers with a random forest model that used as primary inputs 15 watershed properties including catchment slope, elevation, soil pH, temperature, soil respiration, watershed area, land gross primary production, base saturation, population density, gravel, soil organic carbon, sand, precipitation, land net primary production, and wetland cover (ranked in order of decreasing importance). Note that some of these 15 watershed properties are intimately linked such as land net primary production, gross primary production and soil respiration (Lauerwald et al., 2013), or geomorphological variables such as slope and catchment area (Flint, 1974), so there could be redundancy in part of the variables used in this random forest model.

FIGURE 2.5 Andean headwater and piedmont streams are hot spots of CO_2 and CH_4 emissions within the Amazon basin. Air-water fluxes of CO_2 (FCO_2), CH_4 (FCH_4) and N_2O (FN_2O) integrated by area (a–c) and per surface area (m^2) (d–f), partial pressure of CO_2 (pCO_2) (g), dissolved CH_4 concentration (h), and N_2O saturation level ($\%N_2O$) (i), gas transfer velocity (k600) (j) and stream surface area (SSA) (k) in the Andean headwater (elevation >500 m), piedmont (elevation 180–500 m) and lowland (elevation <180 m) streams and rivers of the whole Amazon basin. Fluxes were computed from concentrations and k600 modelled from attributes of RiverATLAS68 for 744,786 river segments. Error bars indicate uncertainties derived from error propagation.

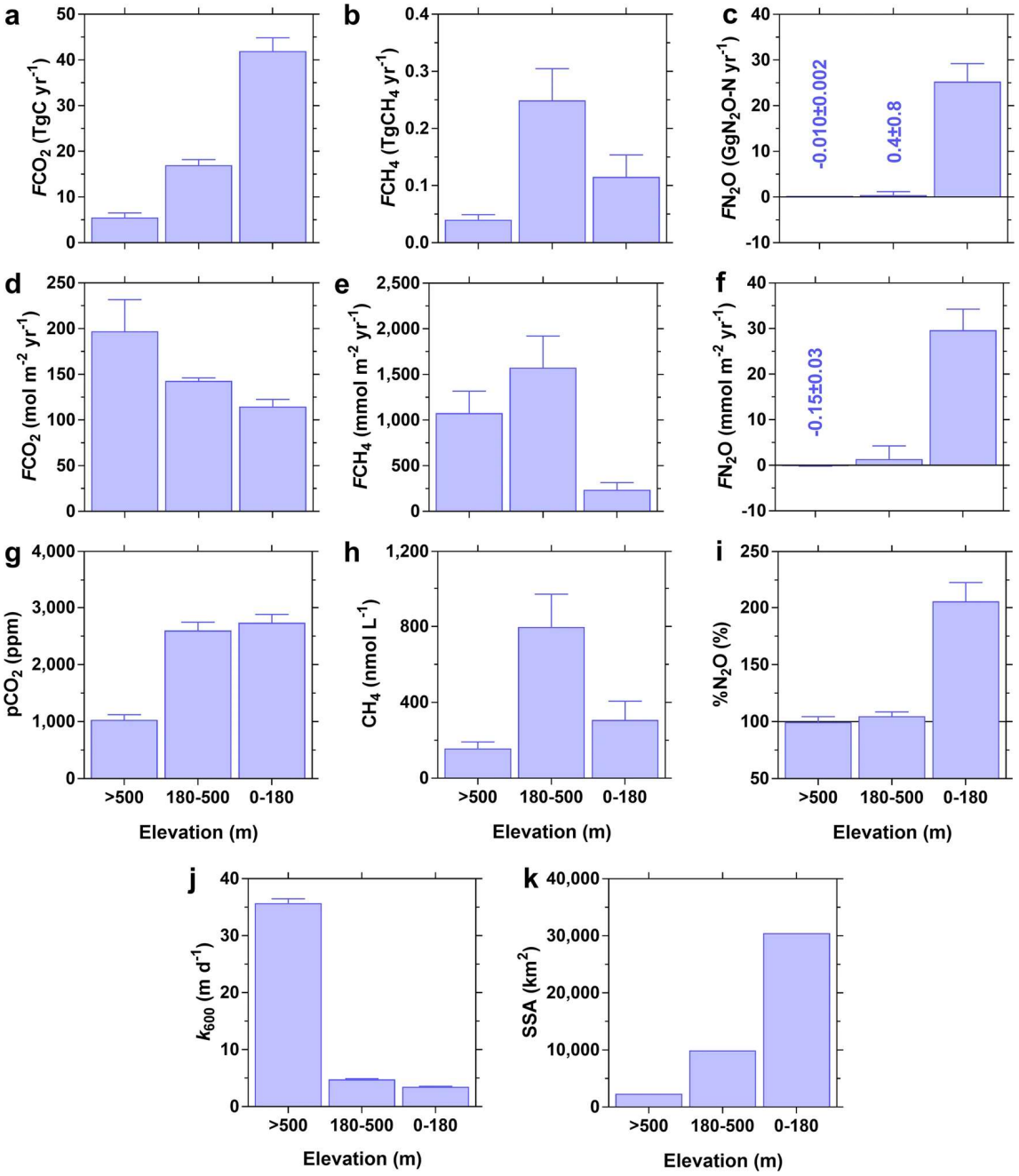

There is no standardized procedure to upscale GHG emissions from inland waters which is challenging given the large inherent variability and the comparatively low data coverage. Some studies have used multi-parametric approaches, while we use a simple relation to a single predictor. Complex mathematical approaches do not necessarily provide more reliable results, and, in fact, potentially produce more uncertain estimates (Puy et al., 2022). Admittedly, it is unrealistic to model fluvial pCO_2 using a single predictor at continental or global scales. Indeed, at very large spatial scales, it is required to account for strong latitudinal variations as in climate (temperature, precipitation, ice cover) and in soil organic carbon (Langeveld et al., 2020) (among others) that are expected to strongly affect fluvial pCO_2, in addition to local topographic effects that might have a more ubiquitous and uniform effect per latitude (such as the effect of stream slope on k). Yet at the scale of a single river basin, it should be possible to reduce the number of variables to model fluvial pCO_2. A simpler model has the advantage to reduce unrealistic results computed outside the bounds of determination of available data, especially from strongly non-linear relationships. We did not find a relation between pCO_2 and dissolved CH_4 concentration and stream order (Supplementary Figure 2.8), as used to scale FCO_2 or FCH_4 in some studies at basin or continental scales(Borges et al., 2019a; Butman and Raymond, 2011; Wallin et al., 2018) 21,60,61, and we modelled fluvial pCO_2 and dissolved CH_4 concentration based on catchment slope. In the above mentioned three models of fluvial pCO_2 at continental or global scales, catchment slope explained the largest fraction of variance in the MRL (Lauerwald et al., 2015) or random forest model(Liu et al., 2022), and as such was the most important predictor. This high predictive power shows that catchment slope strongly controls fluvial CO_2 content directly or indirectly at multiple levels.

It is well established that topography of a catchment strongly influences hydrological, geomorphological and biological processes active in the landscape. Catchment slope determines to a large extent broad patterns in the variation of soil organic carbon content (de Brogniez et al., 2015; Connolly et al., 2018; Thompson and Kolka, 2005), ground water discharge (Leach et al., 2017), stream water residence time, and wetland abundance (Merot et al., 2003; Rodhe and Seibert, 1999), that, combined, have a major impact on fluvial carbon cycling, including CO_2 and CH_4 dynamics. These processes also determine the inputs to streams and the fluvial content of DOC. Highland steep streams with poorly developed soils and substantial exposed bedrock are characterized by lower fluvial DOC than lowland low-relief streams, and fluvial DOC content correlates to catchment slope(Harms et al., 2016; Mulholland, 2007; Ran et al., 2017). Since catchment slope strongly determines fluvial DOC (Harms et al., 2016; Mulholland, 2007; Ran et al., 2017) and wetland coverage (Merot et al., 2003; Rodhe and Seibert, 1999), it is also expected to strongly influence fluvial pCO_2 that has been shown to strongly correlate with DOC (Borges et al., 2015c; Liu et al., 2021; Rasilo et al., 2017; Willgoose, 1994) and wetland coverage (Abril et al., 2014; Borges et al., 2015c, 2015) at river basin and continental scales. Wetland coverage can also explain in part the spatial variations of fluvial dissolved CH_4 concentration(Horgby et al., 2019; Borges et al., 2015). Additionally, the k values strongly increase with increasing stream slope (Horgby et al., 2019; Raymond et al., 2012) that scales with catchment slope(Hua et al., 2018) and catchment area(Flint, 1974). High k values in steeper terrains will promote degassing and equilibration with the atmosphere, while lower k values will allow an accumulation of gases in the water. An additional reason to use catchment slope as a predictor is that this variable can be determined with very high confidence based on detailed and precise digital elevation models. Other variables such as land vegetation cover (Gao et al., 2020; Liu et al., 2018) or terrestrial productivity (Huotari et al., 2013; Zhang and Ye, 2022) have a relatively large uncertainty especially at finer resolution. We tested if the addition to upstream slope of other variables improved the prediction of pCO_2 (Supplementary Table 2. 2). The MRL including elevation or forest cover in addition of upstream slope did not substantially improve the prediction of pCO_2 compared to the linear regression using upstream slope alone (Supplementary Table 2. 2).

The k cannot be measured directly but can be calculated from simultaneous measurements of the air-water gradient of gas concentration and the gas flux. The gas flux in streams can be measured with eddy-covariance, mass balance of deliberate tracers, or floating

chambers. Eddy-covariance is the most challenging technically, has been very seldom applied in rivers, and only in large systems (Van Dam et al., 2019; Lorke et al., 2015). Eddy-covariance measurements require long deployments (weeks-months) due to large data rejection, and are not adapted for "grab-sampling" during spatial surveys of short-duration, as in the present study. The mass balance of deliberate tracers such as argon, propane, SF6, krypton-85 and tritium allow to derive k values at short time intervals and small scales in a non-intrusive way (Raymond et al., 2012; Ulseth et al., 2019). Floating chamber flux measurements are easy to set-up and inexpensive, however, they might not be adapted for fast flowing small streams as those sampled in the present study. In fast flowing streams, it is required to anchor the floating chamber, leading to an over-estimations of flux estimates, due to enhanced turbulence under the chamber (Belanger and Korzun, 1991; Vingiani et al., 2021). Changes in pressure and temperature inside the chamber additionally affect the flux measurements and k estimates (Campeau et al., 2014). Chamber measurements can advantageously be used to measure gas ebullition which is important for CH_4 but not CO_2 and N_2O, in addition to gas diffusive flux. The k parametrization of Raymond et al.47 we used in the present study is based on 576 measurements of deliberate gas tracer injections, and has been used in global estimates of CO_2 emission from streams and rivers (Lauerwald et al., 2015; Liu et al., 2022; Raymond et al., 2013). The k values computed with this parameterization have been shown to satisfactorily compare to those derived from chamber measurements by several independent studies in contrasted rivers and streams (Lim et al., 2022; Rasilo et al., 2017; Schneider et al., 2020; Wallin et al., 2018; Willgoose, 1994).

To scale FCO_2 and FCH4, we used the spatial data, including SSA, from RiverATLAS68 that provides a standardized compilation of descriptive hydro-environmental information for all river basins of the world at high spatial resolution. The total SSA given by RiverATLAS (Linke et al., 2019)globally is 363,000 km^2, which is lower than the value of 624,000 km^2 given by Raymond et al.2013 and of 773,000 km^2 given by the Global River Widths from Landsat (GRWL) data-set (Anderson et al., 2018). At the scale of the Amazon basin, the SSA given by RiverATLAS(Linke et al., 2019) is also lower than other independent estimates, although the wide range of values reflects their uncertainty (Supplementary Table 2. 3). The SSA of the lowland Amazon basin (<500 m altitude) given by RiverATLAS (Linke et al., 2019) (37,972 km^2) is between 1.6 and 2.2 times lower than the one reported by Melack; 2016 (60,500-83,000 km2), but 1.4 times lower than the one reported by Liu et al. 2022 (52,640 km2) based on the GRWL data-set (Anderson et al., 2018) (Supplementary Table 2. 3). We acknowledge that the integrated fluvial emissions of CO2, CH_4 and N2O we computed for the Amazon basin should be considered as conservative, given the lower SSA given by RiverATLAS(Linke et al., 2019) compared to other estimates (Supplementary Table 2. 3). Yet, the general spatial patterns should be correct and the under-estimation of SSA given by RiverATLAS should not invalidate our major finding regarding the relative importance of the contribution of mountainous and piedmont regions to CO_2 and CH_4 emissions from the Amazon River basin (Figure 2.5).

Conclusions

We provide to the best of our knowledge the first large scale survey of CO_2, CH_4 and N_2O exchange between Andean mountainous streams of the Amazon River basin and the atmosphere. We showed that these mountainous headwater and piedmont streams were hotspots of CO_2 and CH_4 emissions from the whole Amazon River basin, accounting for a very significant fraction of total emissions (35 and 72% for CO_2 and CH_4 respectively). The present study also provides a baseline evaluation of CO2, CH_4 and N2O emissions from headwater mountainous and piedmont streams that could change in response to human alterations and activities on the catchments. In these areas, there are high rates of deforestation and conversion to croplands(McClain and Naiman, 2008). There have been concerns about the N2O emissions from soils to the atmosphere related to oil palm plantations (Skiba et al., 2020), and here we suggest that part of the N_2O emissions related to oil palm plantations indirectly occur through

streams. The oil palm plantations seemed to lead to a strong over-saturation of N_2O (~150%) in streams downstream compared to streams are similar elevations that were characterized by N_2O levels closer to saturation (~110%). Additionally, there has been a boom in hydropower development in the headwaters of the Amazon with potential consequences on aquatic biodiversity(Laraque et al., 2004). Hydropower development could also change sediment transport by rivers to and deposition in piedmont rivers, possibly affecting future CH_4 emissions that were shown here to be particularly high.

Data availability

The timestamped and georeferenced data-set is available at https://doi.org/10.5281/zenodo.6527837

Acknowledgements

We thank three anonymous reviewers for constructive comments on the initial manuscript. This research was funded by the *Académie de recherche et d'enseignement supérieur* (ARES). AVB is a research director at the *Fonds National de la Recherche Scientifique*.

Author contributions

AVB designed the research and analyzed the data. GC collected and analyzed the samples. AVB and GC equally contributed to drafting the manuscript.

Supplementary Material

SUPPLEMENTARY FIGURE 2.1 Location of stations in main-stem. Location of stations in main-stem (blue circles) and tributaries (green squares) and sampling dates. Stations in the main-stem are shown by blue circles and in the tributaries by green squares.

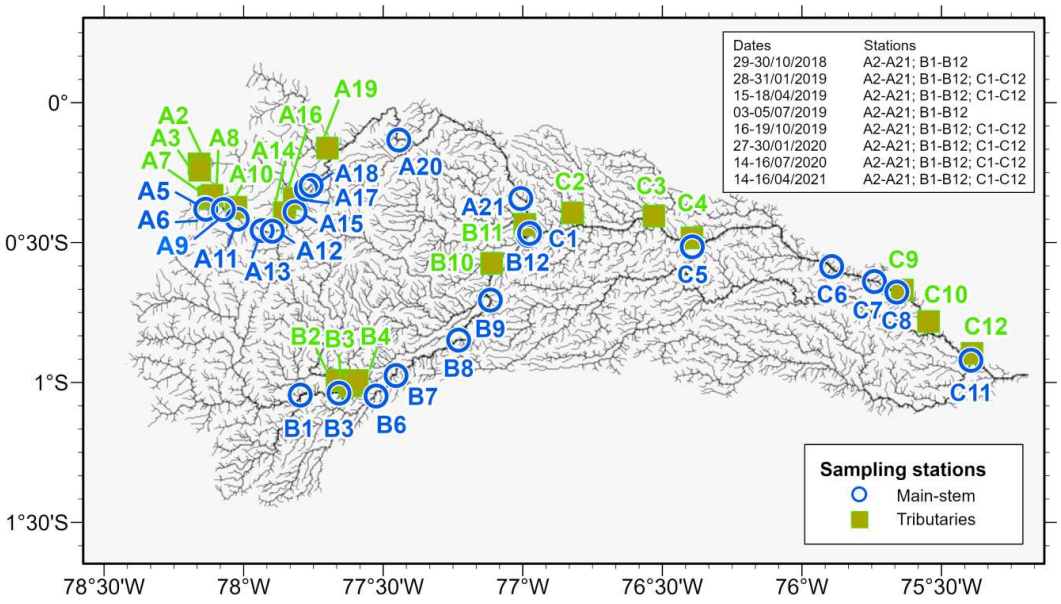

SUPPLEMENTARY FIGURE 2.2 Strong elevation gradients of water temperature and gas transfer velocity in the Andean headwater and piedmont streams. Variations of measured water temperature (a) and the gas transfer velocity normalized to Schmidt number of 600 (k_{600}) modelled from freshwater discharge and stream gradient from RiverATLAS (Linke et al., 2019) (b) in the Napo streams as a function of elevation. Symbols show the median and error bars the interquartile range, stations in the main-stem are shown by blue circles and in the tributaries by green squares, and solid lines show fits to the data (Supplementary Table 2. 4).

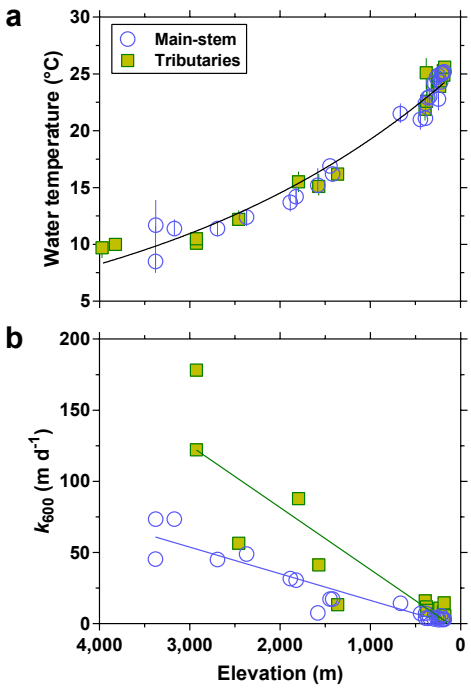

SUPPLEMENTARY FIGURE 2.3 Strong elevation gradients of land cover in the catchment of Andean headwater and piedmont streams. Variations of grassland cover (a), forest cover (b) and inundation extent (c) in the Napo streams as a function of elevation, from Global Land Cover 2000 and Global Inundation Extent from Multi-Satellites (GIEMS-D15) extracted from RiverATLAS(linke et al.,2019). Grassland and forest cover are given over the total catchment upstream the sampled stream; inundation extent is given at the reach level. Stations in the main-stem are shown by blue circles and in the tributaries by green squares, and solid lines show fits to the data (Supplementary Table 2. 4).

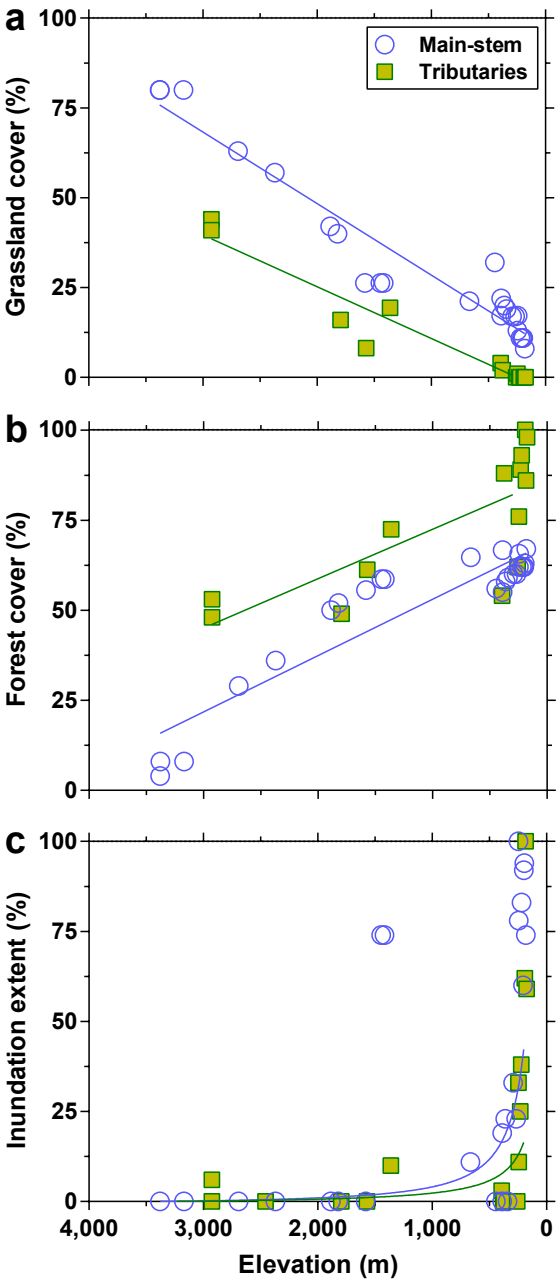

SUPPLEMENTARY FIGURE 2.4 Grassland cover and inundation extent affect pCO_2, CH_4 and $\%N_2O$ in the Andean headwater and piedmont streams. Variations of the partial pressure of CO_2 (pCO_2), CH_4 dissolved concentration, N_2O saturation level ($\%N_2O$), and oxygen saturation level ($\%O_2$) in the Napo streams as a function of grassland cover (a,c,e,g) and inundation extent (b,d,f,h) in the Napo streams, from Global Land Cover 2000 [115] and Global Inundation Extent from Multi-Satellites (GIEMS-D15)[18] extracted from RiverATLAS[68]. Symbols show the median and error bars the interquartile range, stations in the main-stem are shown by blue circles and in the tributaries by green squares, and solid lines show fits to the data (Supplementary Table 2. 4).

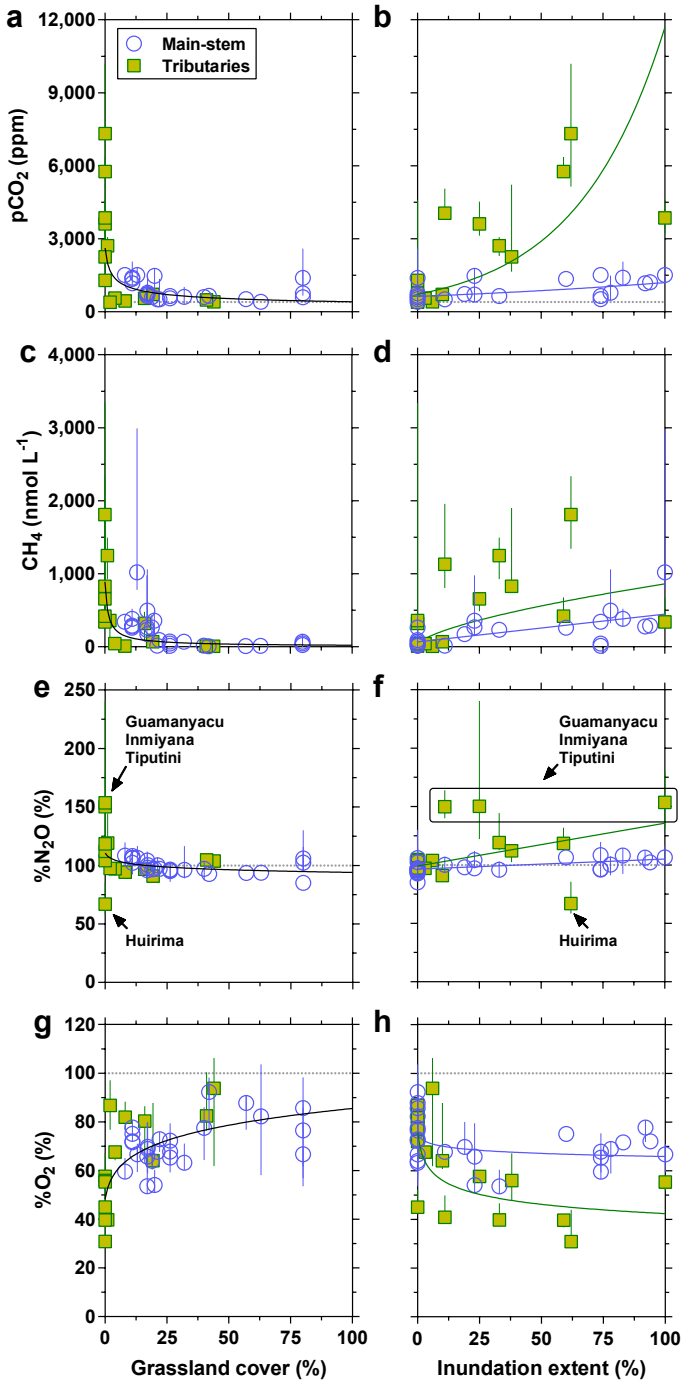

SUPPLEMENTARY FIGURE 2.5 Elevation gradients of dissolved inorganic nitrogen in the Andean headwater and piedmont streams. Nitrate (NO_3^-), ammonia (NH_4^+) and dissolved inorganic nitrogen (DIN) concentration as a function of elevation in the Napo streams. Symbols show the median and error bars the interquartile range, stations in the main-stem are shown by blue circles and in the tributaries by green squares, and solid lines show fits to the data (Supplementary Table 2. 4).

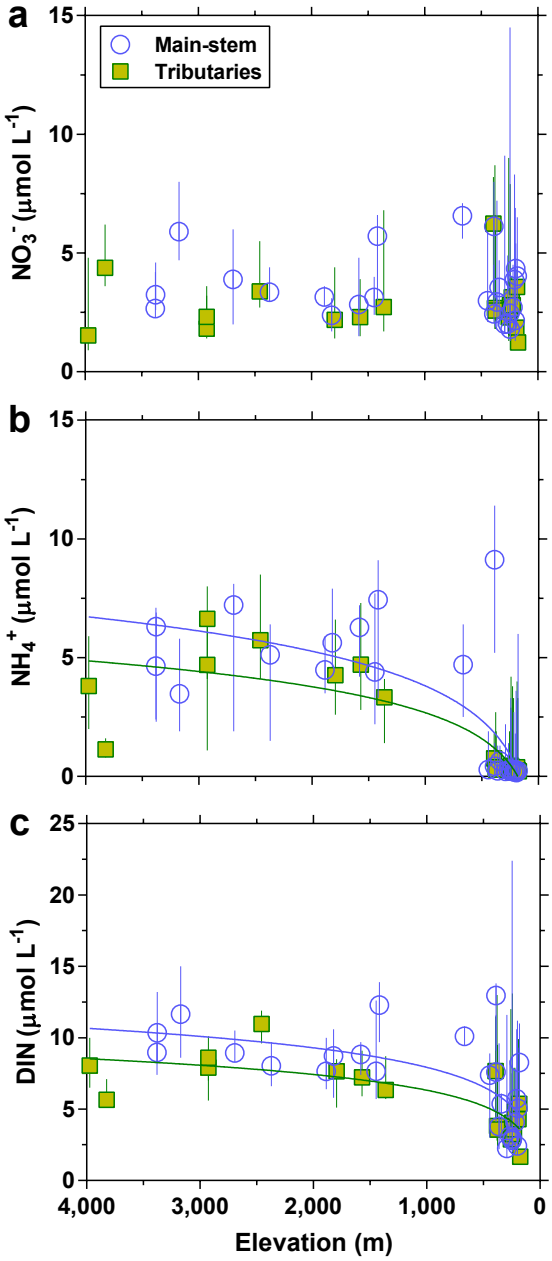

SUPPLEMENTARY FIGURE 2.6 Huirima stream showing meandering river course and presence of small lakes indicative of lateral inundation related to flat relief (low catchment slope). Landsat image was extracted from https://earthexplorer.usgs.gov/ and is in the U.S. Public Domain.

SUPPLEMENTARY FIGURE 2.7 High N_2O levels are related to the presence of oil palm plantations in the Andean piedmont streams. Distribution of "natural" vegetation (merging forest and grassland) and agriculturally impacted land (pastures and oil palm plantations) in the Napo streams, for the whole catchment upstream of the most downstream station (**a**), and for individual catchments for N_2O saturation levels ≤ 119% (**b**) and ≥ 150% (**c**). Land covered by forest and grassland was merged into a single class (natural vegetation) by opposition to land cover strongly impacted by human activity (pastures and oil palm plantations). Stations in the main-stem are shown by blue circles and in the tributaries by green squares.

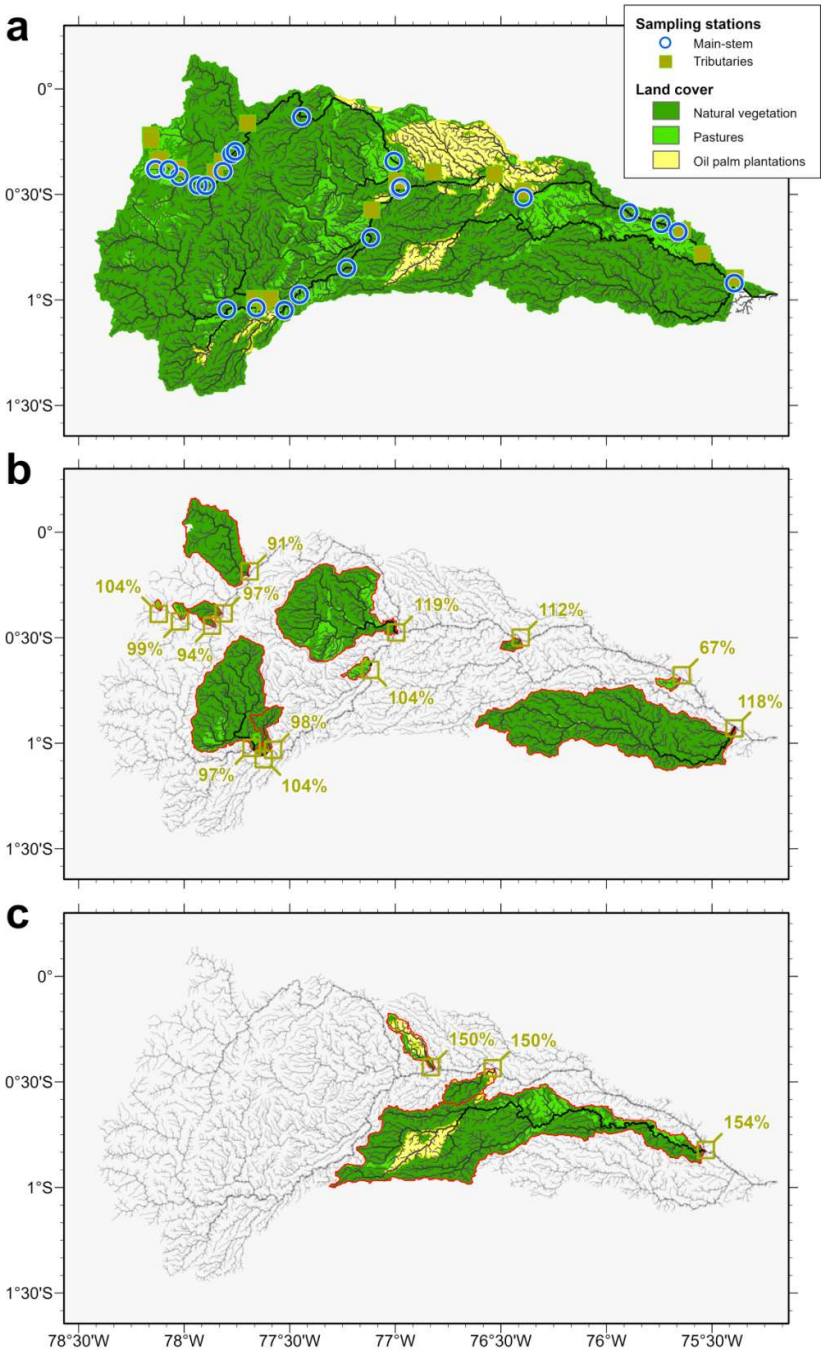

SUPPLEMENTARY FIGURE 2.8 Low variations of pCO_2, CH_4 and $\%N_2O$ in the Andean headwater and piedmont streams as function of stream size. Variations of the partial pressure of CO_2 (pCO_2), CH_4 dissolved concentration, N_2O saturation level ($\%N_2O$), and oxygen saturation level ($\%O_2$) in the Napo streams as a function of Strahler order irrespective of elevation (a,b,c,d), for elevation > 500 m (e,f,g,h) and < 500 m (i,j,k,l). Due to low number of samples in low order streams, orders 2 and 3 were binned. Symbols show the median and error bars the interquartile range. nd = no data.

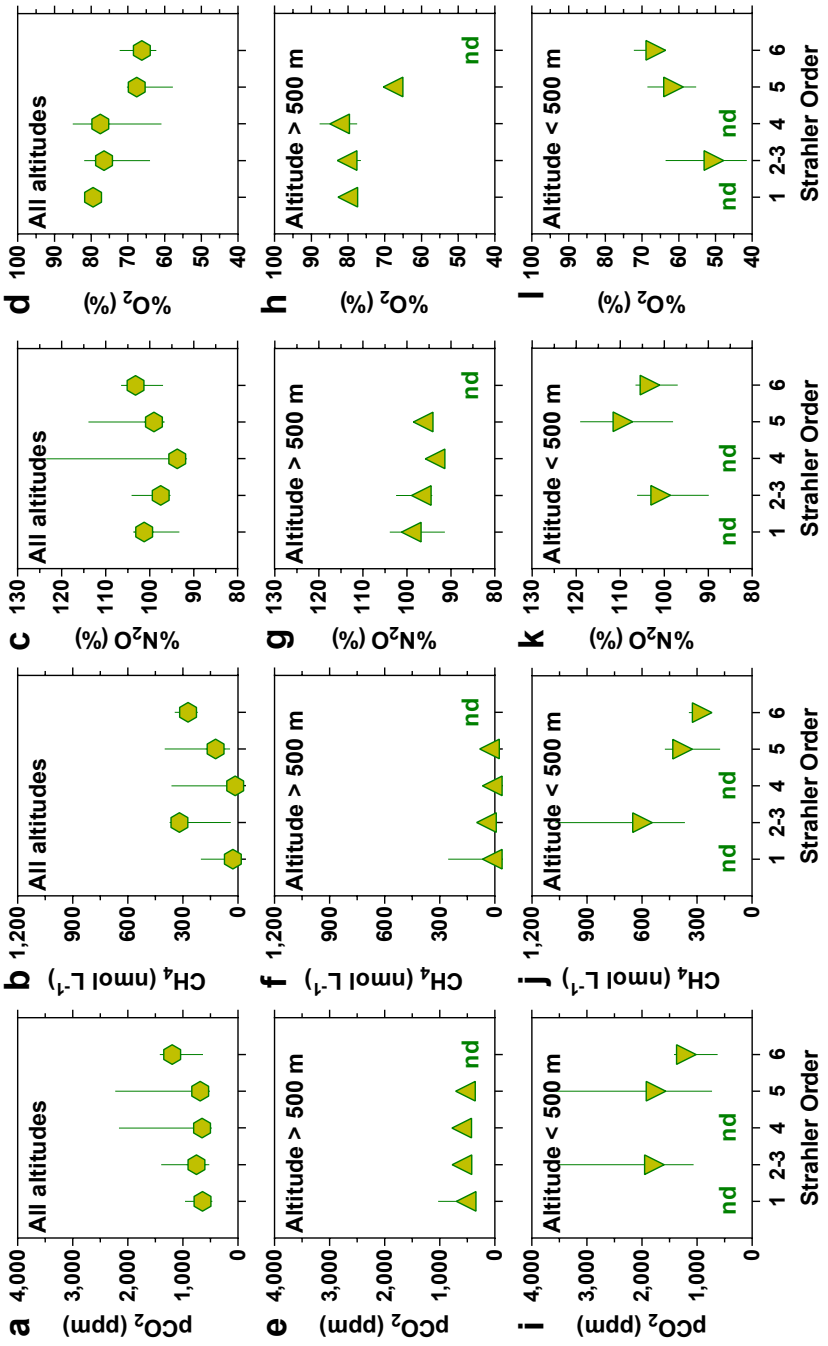

SUPPLEMENTARY FIGURE 2.9 Strong elevation gradients of CO_2, CH_4 and N_2O emissions in the Andean headwater and piedmont streams. Air-water flux of CO_2 (FCO_2) (a,b,c,d), of CH_4 (FCH_4) (e,f,g,h) and of N_2O (FN_2O) (i,j,k,l) as a function of elevation (a,e,i), upstream terrain slope (b,f,j), gas transfer velocity normalized to Schmidt number of 600 (k_{600}) (c,g,k), and respective dissolved gas content: partial pressure of CO_2 (pCO_2) (d), CH_4 dissolved concentration (h), N_2O saturation level ($\%N_2O$) (l). Symbols show the median and error bars the interquartile range, stations in the main-stem are shown by blue circles and in the tributaries by green squares, and solid lines show fits to the data (Supplementary Table 2. 4). Asterisk indicates streams with high CO_2 and CH_4 concentrations and high k_{600} values (refer to Figure 2. S10).

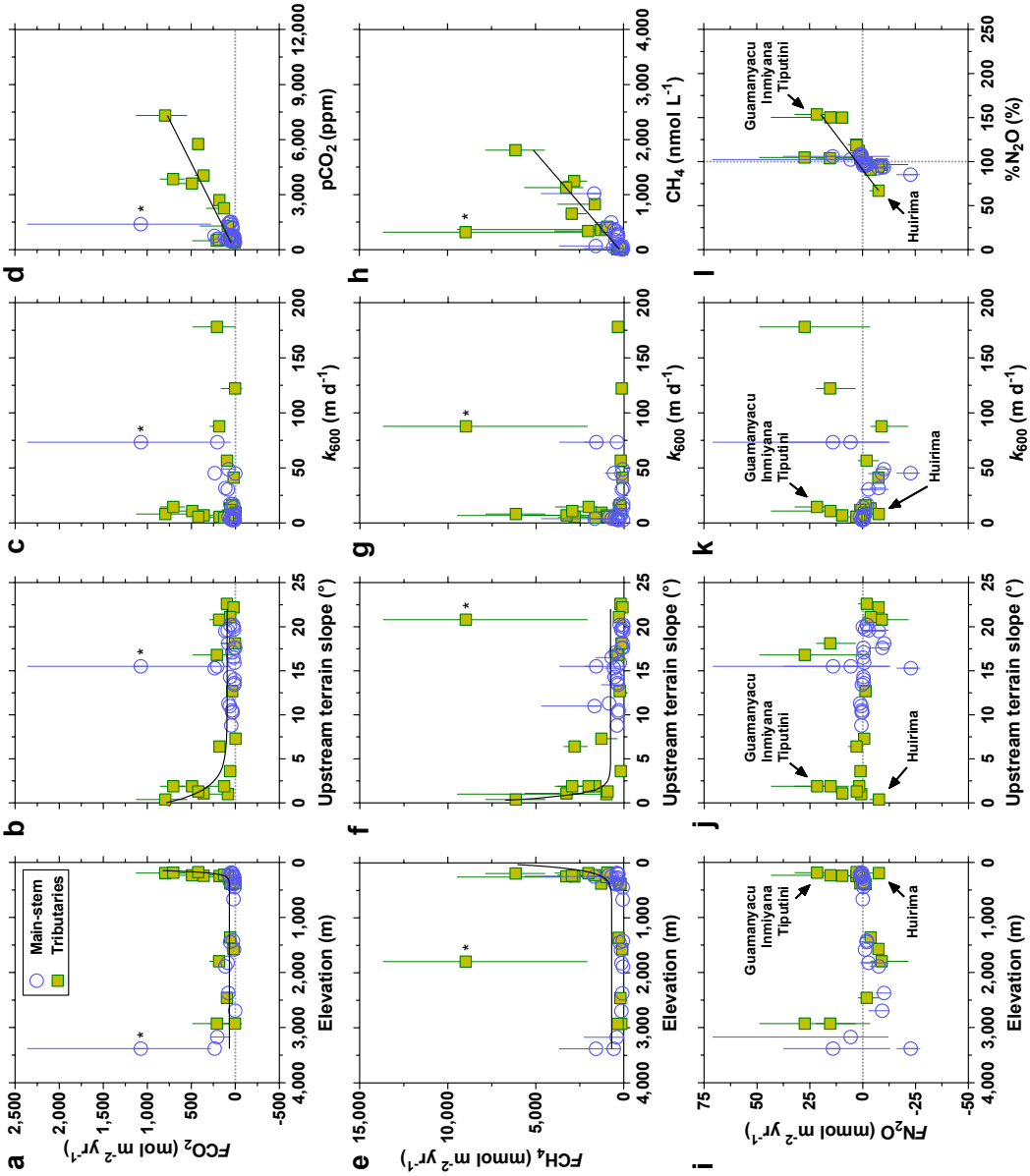

SUPPLEMENTARY FIGURE 2.10 Transport-limitation or supply-limitation of the gaseous exchange with the atmosphere in the Andean headwater and piedmont streams. Partial pressure of CO_2 (pCO_2) (a), CH_4 dissolved concentration (b), and N_2O saturation level ($\%N_2O$) (c) as a function of the gas transfer velocity normalized to Schmidt number of 600 (k_{600}). Symbols show the median and error bars the interquartile range, stations in the main-stem are shown by blue circles and in the tributaries by green squares, and solid lines show fits to the data (Supplementary Table 2. 4). Asterisk indicates streams with high CO_2 and CH_4 concentrations and high k_{600} values leading to comparatively higher emissions (refer to Figure 2. S9).

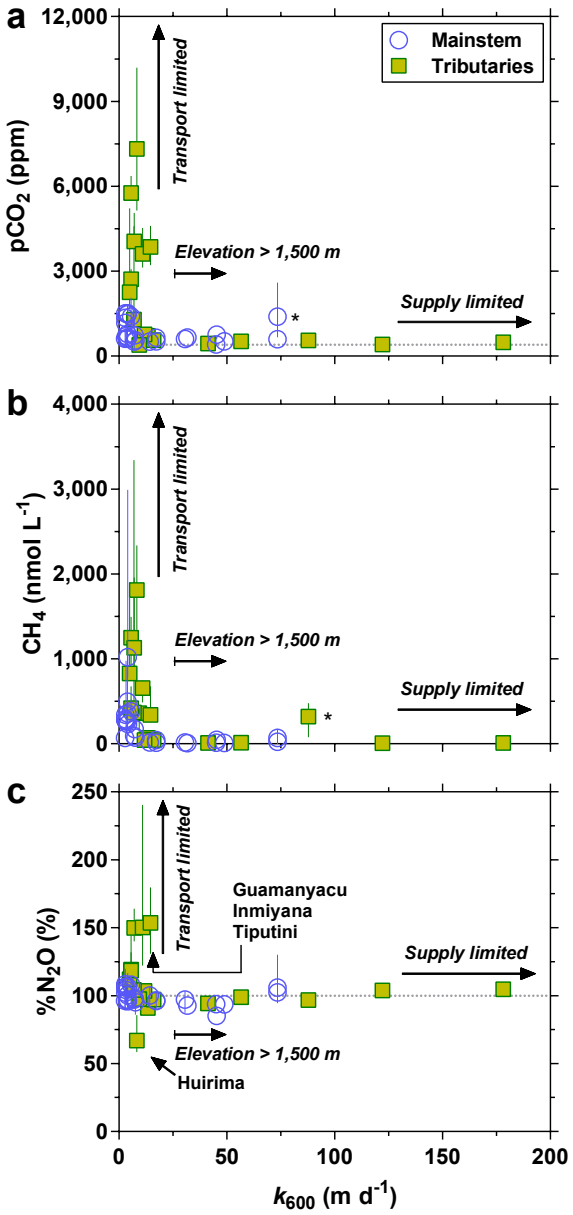

SUPPLEMENTARY FIGURE 2.11 Strong elevation gradients of CO_2, CH_4 and N_2O in streams and rivers across the whole Amazon basin. Variations of CH_4 dissolved concentration (a) and N_2O saturation level (%N_2O) (b) as a function of the partial pressure of CO_2 (pCO_2). Data in the lowland rivers and streams was compiled extracted from plots of Richey *et al.*1988 with Plot Digitizer (http://plotdigitizer.sourceforge.net). Small symbols show individual measurements, large symbols indicate the median, the blue triangles show the data in the mountainous headwater streams, green triangles show the data in piedmont streams, and the grey circles show the data in the lowland streams and rivers.

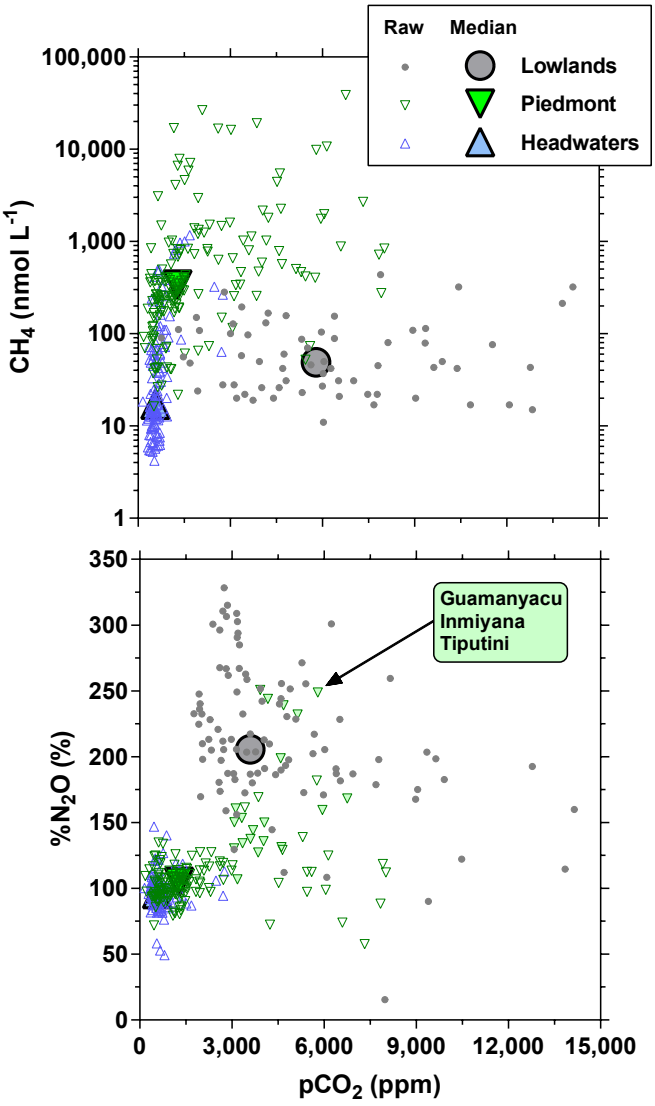

SUPPLEMENTARY TABLE 2.1 Comparison of air-water fluxes of CO_2 (FCO_2) and CH_4 (FCH_4) in the Amazon rivers and streams from this study and reported in (Liu et al., 2022 ; Borges, Abril, et al., 2015; Melack J.M., 2016 ; Melack et al., 2004 ; Barbosa et al., 2016). Only the diffusive component of FCH_4 is reported.

		FCO_2 mol m^{-2} yr^{-1}	FCH_4 mmol m^{-2} yr^{-1}
River channels < 150 m	**This study**	**161±11**	
	(Melack J.M., 2016)	156	
	(Liu et al., 2022)	157	
River channels ≥ 150 m	**This study**	**91±6**	
	(Melack J.M., 2016)	71	
	(Liu et al., 2022)	135	
Solimões/Amazon mainstem	**This study**		**66±29**
	(Melack et al., 2004)		75
River channels ≥ 200 m	**This study**		**199±55**
	(Borges, Abril, et al., 2015)		274±41
River channels (whole lowland basin)	**This study**		**564±141**
	(Barbosa et al., 2016)		370

SUPPLEMENTARY TABLE 2.2 Goodness of the linear regression of modelled partial pressure of CO_2 (pCO_2) based on three models versus observed pCO_2 from the Andean headwater and piedmont streams. The models were a linear regression (LR) as function of upstream slope, a multiple linear regression (MLR) as function of upstream slope and elevation, and a MLR as function of upstream slope and forest cover.

	Modelled pCO_2 versus initial pCO_2	r^2	S*y.x*
Upstream slope LR	y = 1.284±(0.072) + 0.594(±0.023)*x	0.59	0.202
Upstream slope + Elevation MLR	y = 1.199(±0.071) + 0.620(±0.022)*x	0.62	0.200
Upstream slope + Forest cover MLR	y = 1.221(±0.071) + 0.613(±0.022)*x	0.61	0.200

SUPPLEMENTARY TABLE 2.3 Comparison of stream surface area in the Amazon basin used in this study (extracted from RiverATLAS68) and reported in literature (Liu et al., 2022 ; Borges, Abril, et al., 2015; Melack J.M., 2016 ; Melack et al., 2004 ; Barbosa et al., 2016). The surface area for large lowland rivers used by (Sawakuchi et al. 2014) is two to three times higher than the range of values reported by (Melack J.M.,. 2016) for an equivalent river size class.

		Stream surface area km^2
River channels < 150 m	**This study**	**16,304 (*)**
	(Melack J.M., 2016)	31,000 (**)
	(Liu et al., 2022)	27,120 (***)
River channels ≥ 150 m	**This study**	**21,668 (*)**
	(Melack J.M., 2016)	29,500 (**) to 52,000 (****)
	(Liu et al., 2022)	25,500
Solimões/Amazon mainstem	**This study**	**4,994 (*)**
	(Melack et al., 2004)	8,856
River channels ≥ 200 m	**This study**	**19,828 (*)**
	(Borges, Abril, et al., 2015)	91,212 (*****)
River channels (whole lowland basin)	**This study**	**40,375 (*)**
	(Barbosa et al., 2016)	52,380 (******)

* Reference (Linke et al. 2019)
** Reference (Beighley et al., 2011)
*** Reference (Anderson et al., 2018)
**** from Shuttle Radar Topography Mission
***** Reference (Brown et al., 2003)
****** Unspecified data source

SUPPLEMENTARY TABLE 2. 4 Equations and statistics at 0.05 level of curve fits of data shown in this Chapter Figures 2…

Figure	Function	Equation	Average Residual	r^2	*p*	*n*
2 a	pCO_2 *versus* Elevation	$y = 7.730E+04*EXP(-1.768E-02*x)+6.623E+02$	6.20E+02			44
2 b	pCO_2 *versus* Upstream terrain slope	$y = 7.085E+03*EXP(-6.395E-01*x)+8.108E+02$	5.14E+02			42
2 c	pCO_2 *versus* Forest cover	$y = 2.773E-02*EXP(1.229E-01*x)+9.977E+02$	5.56E+02			42
2 d	pCO_2 *versus* Water temperature	$y = 6.775E-09*EXP(1.061E+00*x)+3.882E+02$	7.14E+02			42
2 e	CH_4 *versus* Elevation	$y = 1.695E+03*EXP(-5.725E-03*x)+9.183E+01$	2.19E+02			44
2 f	CH_4 *versus* Upstream terrain slope	$y = 1.202E+03*EXP(-6.150E-02*x)-3.034E+02$	1.71E+02			42
2 g	CH_4 *versus* Forest cover	$y = 1.804E+01*EXP(4.134E-02*x)-2.591E+00$	1.83E+02			42
2 h	CH_4 *versus* Water temperature	$y = 3.404E-02*EXP(3.844E-01*x)+9.299E+01$	2.29E+02			42
2 i	$\%N_2O$ *versus* Elevation	$y = 7.940E+01*EXP(-9.046E-03*x)+9.615E+01$	4.05E+00			40*
2 j	$\%N_2O$ *versus* Upstream terrain slope	$y = -0.8165*x + 112.3$		0.47	<0.0001	38*
2 k	$\%N_2O$ *versus* Forest cover	$y = 0.1619*x + 91.4$		0.20	0.006	38*
2 l	$\%N_2O$ *versus* Water temperature	$y = 9.648E-07*EXP(6.536E-01*x)+9.610E+01$	3.62E+00			38*
2 m	$\%O_2$ *versus* log(Elevation)	$y = 18.953*x + 15.0$		0.40	<0.0001	44
2 n	$\%O_2$ *versus* Upstream terrain slope	$y = 1.3564*x + 50.1$		0.40	<0.0001	42
2 o	$\%O_2$ *versus* Forest cover	$y = -0.3749*x + 90.4$		0.31	0.0002	42
2 p	$\%O_2$ *versus* Water temperature	$y = -1.5737*x + 98.8$		0.40	<0.0001	44
3 a	pCO_2 *versus* $\%O_2$	$y = 5.909E+04*EXP(-7.016E-02*x)+4.755E+02$	4.97E+02			44
3 b	pCO_2 *versus* CH_4	$y = 0.2022*x + 39$		0.55	<0.0001	44
3 c	CH_4 *versus* $\%O_2$	$y = 1.863E+04*EXP(-7.885E-02*x)+1.335E+02$	4.97E+02			44
3 d	$\%N_2O$ *versus* pCO_2	$y = 0.0053*x + 94.8$		0.46	<0.0001	40*
3 e	$\%N_2O$ *versus* $\%O_2$	$y = -0.2846*x + 120.2$		0.26	0.0009	40*
3 f	$\%N_2O$ *versus* DIN	$y = -0.9479*x + 106.5$		0.15	0.0126	40*
4 a	$\log(pCO_2)$ *versus* log(Elevation)	$y = -0.308*x + 3.8443$		0.50	<0.0001	403
4 b	$\log(pCO_2)$ *versus* log(Upstream terrain slope)	$y = -0.6519*x + 3.656$		0.57	<0.0001	403
4 c	$\log(CH_4)$ *versus* log(Elevation)	$y = -0.1799*x^3 + 0.6348*x^2 - 0.1668*x + 1.7272$		0.40	<0.0001	471
4 d	$\log(CH_4)$ *versus* Upstream terrain slope (for Elevation > 180 m)	$y = -0.0757*x + 3.0622$		0.42	<0.0001	297
4 d	$\log(CH_4)$ *versus* Upstream terrain slope (for Elevation < 180 m)	$y = -0.1775*x + 2.5974$		0.21	<0.0001	174
4 e	$\log(CH_4{:}CO_2)$ *versus* log(Elevation)	$y = -0.2342*x^3 + 0.9761*x^2 - 0.5717*x - 3.1345$		0.44		369
4 f	$\log(CH_4{:}CO_2)$ *versus* Upstream terrain slope (for Elevation > 180 m)	$y = -0.0489*x - 1.8328$		0.22	<0.0001	305
4 f	$\log(CH_4{:}CO_2)$ *versus* Upstream terrain slope (for Elevation < 180 m)	$y = -0.1094*x - 2.74$		0.08	0.0239	64
S2 a	Water temperature *versus* log(Elevation)	$y = -0.0001222*x + 1.406$		0.96	<0.0001	44
S2 b	k_{600} *versus* Elevation (for Main-stem)	$y = 0.01869*x - 2.266$		0.89	<0.0001	25
S2 b	k_{600} *versus* Elevation (for Tributaries)	$y = 0.0436*x - 5.528$		0.80	<0.0001	17
S3 a	Grassland cover *versus* Elevation (for Main-stem)	$y = 0.01994*x + 8.586$		0.93	<0.0001	25
S3 a	Grassland cover *versus* Elevation (for Tributaries)	$y = 0.01444*x - 3.572$		0.93	<0.0001	17
S3 b	Forest cover *versus* Elevation (for Main-stem)	$y = -0.01556*x + 68.6$		0.85	<0.0001	25
S3 b	Forest cover *versus* Elevation (for Tributaries)	$y = -0.01371*x + 86.13$		0.55	0.0025	17
S3 c	log(Inundation extent + 1) *versus* log(Elevation) (for Main-stem)	$y = -1.333*x + 4.702$		0.49	0.0001	25
S3 c	log(Inundation extent + 1) *versus* log(Elevation) (for Tributaries)	$y = -1.027*x + 3.604$		0.39	0.0078	17
S4 a	$\log(pCO_2)$ *versus* log(Grassland cover +1)	$y = -0.4003*x + 3.418$		0.53	<0.0001	39
S4 b	Inundation extent *versus* $\log(pCO_2)$ (for Main-stem)	$y = 0.002844*x + 2.799$		0.35	0.0017	25
S4 b	Inundation extent *versus* $\log(pCO_2)$ (for Tributaries)	$y = 0.01206*x + 2.858$		0.61	0.0002	17
S4 c	$\log(CH_4)$ *versus* log(Grassland cover +1)	$y = -0.8078*x + 2.95$		0.47	<0.0001	39
S4 d	$\log(CH_4)$ *versus* Inundation extent (for Main-stem)	$y = 0.009493*x + 1.635$		0.34	0.0024	25
S4 d	$\log(CH_4)$ *versus* Inundation extent (for Tributaries)	$y = 0.01461*x + 1.879$		0.27	0.0324	17
S4 e	$\log(\%N_2O)$ *versus* log(Grassland cover +1)	$y = -0.03509*x + 2.044$		0.35	0.0002	36*
S4 f	$\%N_2O$ *versus* Inundation extent (for Main-stem)	$y = 0.08749*x + 96.35$		0.34	0.0022	25*
S4 f	$\%N_2O$ *versus* Inundation extent (for Tributaries)	$y = 0.3674*x + 98.98$		0.64	0.001	13*
S4 g	$\log(\%O_2)$ *versus* log(Grassland cover +1)	$y = 0.123*x + 1.685$		0.49	<0.0001	39
S4 h	$\log(\%O_2)$ *versus* log(Inundation extent+1) (for Main-stem)	$y = -0.02816*x + 1.875$		0.19	0.0309	25
S4 h	$\log(\%O_2)$ *versus* log(Inundation extent+1) (for Tributaries)	$y = -0.1262*x + 1.88$		0.46	0.0027	17
S5 b	NH_4^+ cover *versus* Elevation (for Main-stem)	$y = 2.104*x - 10.73$		0.57	<0.0001	25
S5 b	NH_4^+ cover *versus* Elevation (for Tributaries)	$y = 1.58*x - 8.237$		0.71	<0.0001	17
S5 c	DIN cover *versus* Elevation (for Main-stem)	$y = 1.989*x - 5.851$		0.45	0.0004	25
S5 c	DIN cover *versus* Elevation (for Tributaries)	$y = 1.593*x - 4.679$		0.62	<0.0001	17
S9 a	FCO_2+2 *versus* Elevation	$y = 3.858E+04*EXP(-2.674E-02*x)+7.031E+01$	1.05E+02			42
S9 b	FCO_2+2 *versus* Upstream terrain slope	$y = 6.936E+02*EXP(-6.181E-01*x)+9.523E+01$	1.10E+02			42
S9 d	FCO_2 *versus* pCO2	$y = 0.1045*x + 6.451$		0.45	<0.0001	42
S9 e	FCH_4 *versus* Elevation	$y = 7.324E+03*EXP(-1.036E-02*x)+6.882E+02$	9.56E+02			42
S9 f	FCH_4 *versus* Upstream terrain slope	$y = 9.751E+03*EXP(-1.635E+00*x)+7.622E+02$	8.02E+02			42
S9 h	FCH_4 *versus* CH_4	$y = 2.711*x + 217$		0.38	<0.0001	42
S9 i	FN_2O *versus* N_2O	$y = 0.316*x - 28.72$		0.13	0.0206	42

* Excluding Guamanyacu, Inmiyana, Tiputini, and Huirima Rivers

CHAPTER 3.

DISTRIBUTION OF SUSPENDED MATTER AND ORGANIC CARBON POOLS IN THE MOUNTAINOUS AND PIEDMONT STREAMS OF THE NAPO RIVER BASIN (ECUADOR)

Rain falling in the Napo River, Community of Piñacocha (Piranha`s Lake)

Distribution of suspended matter and organic carbon pools in the mountainous and piedmont streams of the Napo River basin (Ecuador)

This chapter is a draft of a manuscript in early stages of preparation, presenting a description of the patterns of organic pools in the streams of the Napo River basin that complements the analysis of greenhouse gases given in Chapter 2

Introduction

Rivers play an important role in the global carbon cycle, as conduits of organic and inorganic carbon from land to the ocean, although materials are processed during transport, leading to the production and emission to the atmosphere of greenhouse gases (GHGs) such as carbon dioxide (CO_2) (Liu et al. 2022), methane (CH_4) (Rosentreter et al. 2021) and nitrous oxide (N_2O) (Maavara et al. 2018). Tropical rivers deliver ~60% of freshwater and an equivalent fraction of organic carbon to the oceans (Ludwig et al. 1996), and they sustain the majority of global riverine GHG emissions, ~60-80% for CO_2 (Raymond et al. 2013; Lauerwald et al. 2015; Sawakuchi et al. 2017; Liu et al. 2022), ~70% for CH_4 (Sawakuchi et al. 2014), and ~79% for N_2O (Hu et al. 2016).

The Amazon River is globally the largest river in terms of drainage area (5.9 10^6 km^2) and freshwater discharge (206,000 m^3 s^{-1}) and drains the largest tropical rain forest on Earth. The Amazon River contributes 16-18% of continental freshwater discharge (Dai and Trenberth 2002), 7% of dissolved inorganic elements (Moquet al. 2016) and ~10% of organic carbon (36 TgC yr^{-1}, Richey et al. 1990) fluvial fluxes to the ocean globally (380 TgC yr^{-1} Ludwig et al. 1996), of which 62% is in dissolved form. The flowing waters of the Central Amazon basin (river channels and floodplains) are important sources of CO_2 and CH_4 to the atmosphere (Richey et al. 2002; Melack et al. 2004; Abril et al. 2014; Sawakuchi et al. 2014; 2017; Barbosa et al. 2016). We recently showed that Andean mountainous headwater and piedmont streams and rivers represented 35% CO_2 and 72% CH_4 of basin scale integrated fluvial diffusive emissions from the Amazon River network (Chapter 2).

Rivers draining the Andes are part of Madeira River basin (Mamoré, Beni, Madre de Dios) and of the Solimões River (Ucayali, Huallaga, Marañón and Napo). They are characterized by high dissolved and particulate elemental concentrations and are typified as “white waters” (Sioli 1964). The rivers draining the Andes contribute to nearly 100% of the particulate (Meade et al. 1985) and 64% of inorganic solute (Gaillardet et al. 1997; Moquet el al. 2011; 2016) annual fluxes from the Amazon River to the Atlantic Ocean. Andean headwater streams largely control the distribution and composition of organic matter in the Amazon River (Richey et al. 1990; Quay et al. 1992; Hedges et al. 1994; 2000), although they remain largely unstudied (Townsend-Small et al. 2005; Aufdenkampe et al. 2007). There are differences in source, composition, and age of dissolved (DOM) and particulate (POM) organic matter in the Amazon rivers and streams, and in general DOM is richer in carbon, more degraded, and more recent than POM (Hedges et al. 1986; 1994; Richey et al. 1990; Quay et al. 1992; Mayorga et al. 2005).

Here, we report specific conductivity, total alkalinity (TA), CO_2, CH_4 and N_2O dissolved concentrations, dissolved inorganic carbon stable isotope ratios (δ^{13}C-DIC), TSM, POC and DOC organic carbon concentrations and stable isotope ratios (δ^{13}C-POC and δ^{13}C-DOC), and three optical proxies of colored dissolved organic matter (CDOM) collected in the streams and rivers of the Napo basin along an elevational transect from 3990 and 175 m above sea level, covering the transition from headwaters in the Andes Cordillera to the western Amazonian lowland plains.

Results and discussion

Specific conductivity showed a downstream decrease from 368 to 19 µS cm^{-1} in the mainstem (Fig. 3.1). In the tributaries, specific conductivity varied within a narrower range from 19 to 122 µS cm^{-1}, showing lower values at an elevation < 1000 m than > 1000 m. Specific conductivity was positively related to stream gradient, and negatively related to annual discharge and catchment area, but, was unrelated to upstream catchment slope (Fig. 3.1).

FIGURE 3.1 Specific conductivity (µS cm^{-1}), total alkalinity (µmol L^{-1}), dissolved inorganic carbon (DIC in µmol L^{-1}), CO_2 dissolved concentration (µmol L^{-1}), and carbon stable isotope ratios of DIC (δ^{13}C-DIC in ‰) versus elevation (m), upstream catchment slope (°), stream gradient (cm km^{-1}), annual freshwater discharge (m^3 s^{-1}) and catchment area (km^2) from RiverATLAS (Linke et al. 2019) in the Napo streams.

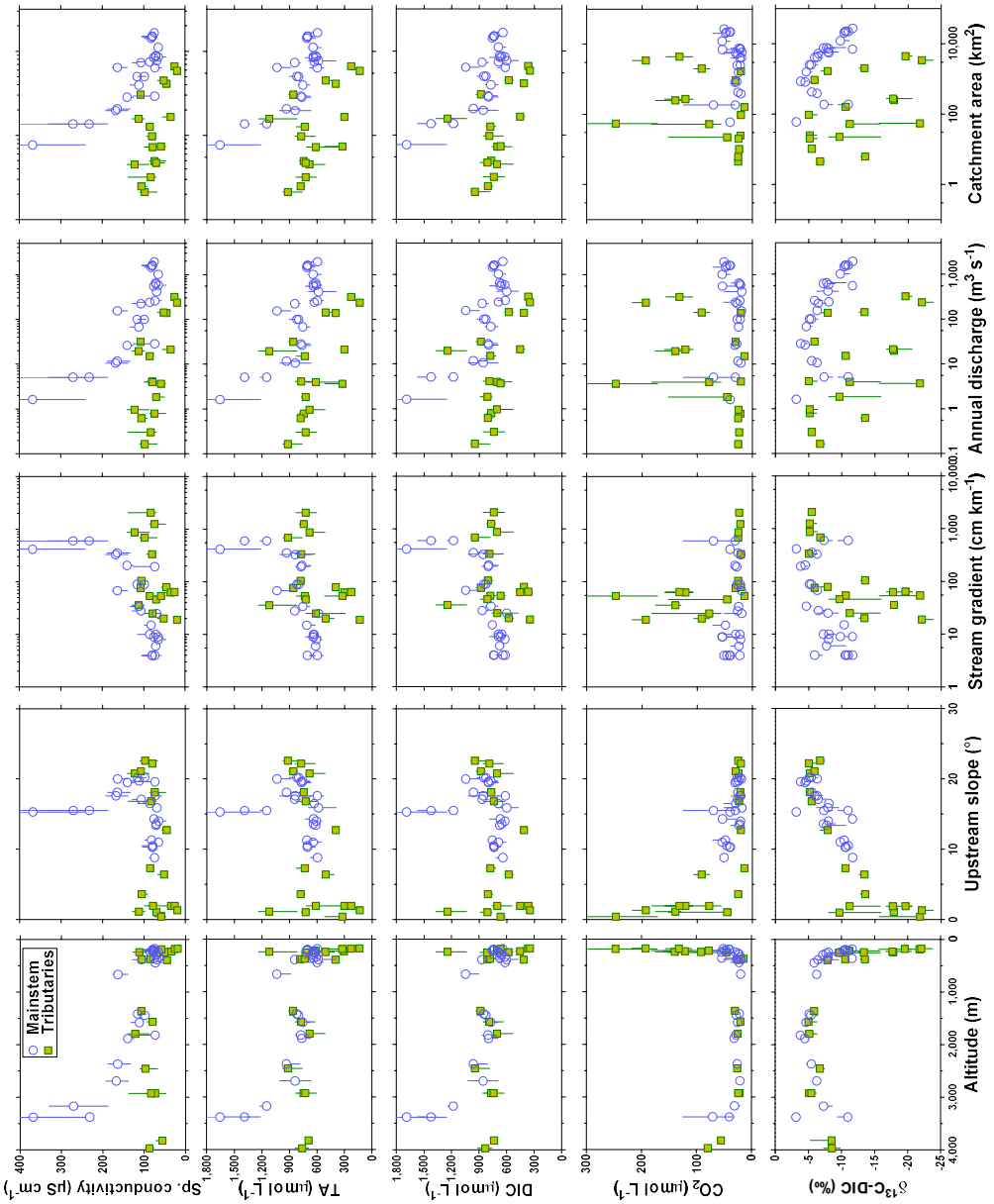

TA ranged between 135 and 1,656 µmol L^{-1} and exhibited patterns that paralleled very closely those of specific conductivity (Fig. 3.1). The elevational patterns of specific conductivity and TA resulted from intense rock weathering in the high elevation areas of the Andes cordillera (Gaillardet et al. 1997; Moquet el al. 2011; 2016) followed by dilution in the lower reaches with the increase of stream size, as indicated by negative correlations with catchment area and discharge. DIC ranged between 348 and 1,689 µmol L^{-1} and exhibited patterns that paralleled very closely those of TA as a result of the important contribution of HCO_3^- and CO_3^{2-} to DIC and TA (Fig. 3.1). The dissolved CO_2 concentrations ranged between 14 and 247 µmol L^{-1} and showed very different patterns from those of DIC, increasing exponentially downstream and decreasing with upstream catchment slope, with no clear patterns as a function of stream gradient, freshwater discharge, and catchment area (Fig. 3.1). The drivers of the variations of dissolved CO_2 concentrations were investigated in detail in Chapter 2, where the elevational gradient of the partial pressure of CO_2 (pCO_2) was attributed to variations in gas transfer velocity, forest cover, inundation extent, and water temperature, that scaled with upstream slope gradient. Upstream catchment slope determines to a large extent broad patterns in the variation of soil organic carbon content (Thompson and Kolka 2005; de Brogniez et al. 2015 ; Connolly et al. 2018), ground water discharge (Leach et al. 2017), stream water residence time (McGuire et al. 2005), and wetland abundance (Merot et al. 1999; Rodhe and Seibert 1999), that, combined, have a major impact on fluvial carbon cycling, including CO_2 dynamics, and as such was found to be an integrative metric for processes that affect dissolved CO_2 in the streams of the Napo basin, and also at larger scale for the whole Amazon basin (Chapter 2).

The δ^{13}C-DIC values ranged between -22.1 and +3.1 ‰ and showed a downstream decrease, generally mirroring the variations of dissolved CO_2 concentration (Fig. 3.1). δ^{13}C-DIC was positively related to upstream catchment slope. When taking separately the tributaries and the main-stem, the δ^{13}C-DIC was positively related to stream gradient and negatively related to catchment area and freshwater discharge, in line with the patterns of HCO_3^- as given by TA.The variations of δ^{13}C-DIC can provide information on the origin of CO_2, although the signal depends on the combination of several factors such as the biological processes that remove or add CO_2 to the water column (respiration and photosynthesis), rock weathering that adds HCO_3^-, and outgassing to the atmosphere which removes dissolved CO_2 that is ^{13}C-depleted relative to HCO_3^- and CO_3^{2-}. Spatial and temporal changes of δ^{13}C are related to the change of the relative abundance of HCO_3^- and CO_3^{2-} over CO_2. In the Tana River network, the downstream increase of δ^{13}C-DIC was attributed to a downstream accumulation of HCO_3^- due to rock weathering combined to CO_2 degassing (Bouillon et al. 2009; Tamooh et al. 2003). In contrast, the downstream decrease of δ^{13}C-DIC observed in the Napo basin (Fig. 3.1), as well as the negative relation between δ^{13}C-DIC and CO_2 concentration (and pCO_2) (Fig. 3.2) suggest in the lowland streams the combination of addition of CO_2 depleted in ^{12}C from heterotrophic process and dilution of HCO_3-. There was a general increase of δ^{13}C-DIC from (HCO_3^-+CO_3^{2-}):DIC~0.4 (60% the DIC is in the form of CO_2) towards (HCO_3^-+CO_3^{2-}):DIC~1 (nearly all of the DIC is in the form of HCO_3^- and CO_3^{2-}) (Fig. 3.2). This pattern reflected the mixing of two distinct types of rivers and streams: the mountainous systems draining the highland regions of the Andes with high rock weathering (high HCO_3^-) and low CO_2 due high degassing to the atmosphere owing to high gas transfer velocity values in these steep streams (Chapter 2), leading to (HCO_3^-+CO_3^{2-}):DIC close to 1 with high δ^{13}C-DIC, and the lowland streams in the Amazonian plains with a high input of CO_2 from respiration in forest soils and wetlands and a dilution of HCO_3^-, leading to (HCO_3^-+CO_3^{2-}):DIC~0.4 with low δ^{13}C-DIC.

TSM, fluvial C:N, POC and DOC concentrations showed clear elevational patterns (Fig. 3.3).TSM showed a consistent downstream increase from 3 to 480 mg L^{-1}. TSM values were lower than 12 mg L^{-1} at elevations above 1000 m, suggesting that the higher particulate matter content transported by lowland rivers originated from low elevation areas (<1000 m) rather than from headwater regions. The stream size increased downstream, so hydraulic variables (upstream catchment slope, stream gradient, catchment area, and freshwater discharge) increased with decreasing elevation (Fig. 3.4). Consequently, TSM was negatively related to upstream

catchment slope and stream gradient, and positively related to freshwater discharge and catchment area. These patterns of TSM reflected the accumulation of particles originated from erosion with the downstream increase of stream size. The relation between TSM and upstream catchment slope was different for tributaries and main-stem, because the relation between elevation and hydraulic variables, including upstream catchment slope, was different for tributarieFs and main-stem (Fig. 3.4).

FIGURE 3.2: Ratio of the sum of HCO_3^- and CO_3^{2-} and dissolved inorganic carbon (DIC), CO_2 dissolved concentration (µmol L^{-1}), and partial pressure of CO_2 (pCO_2 in ppm) versus carbon stable isotope ratios of DIC (δ^{13}C-DIC in ‰) in the Napo streams.

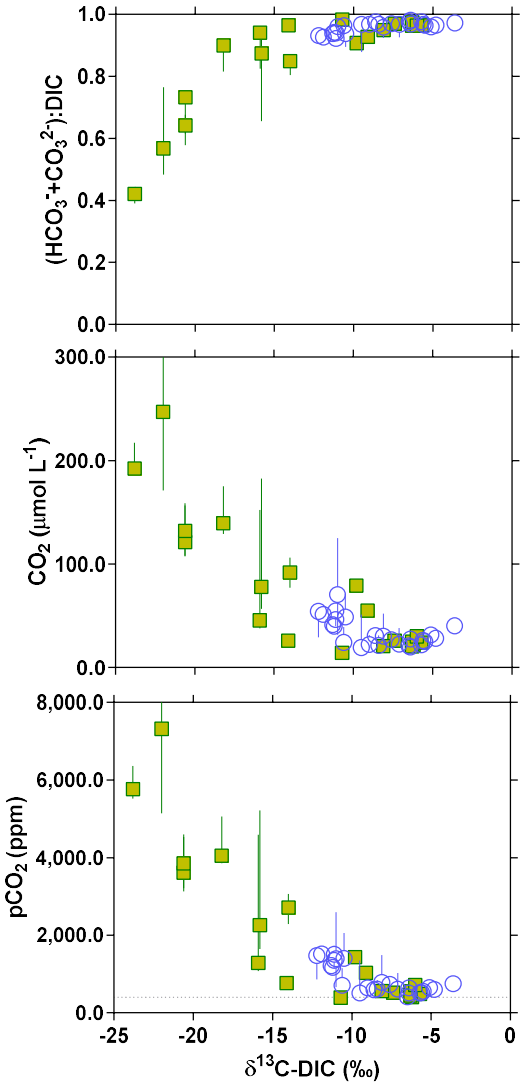

POC concentration ranged between 0.4 and 2.7 mg L^{-1} and was positively related to TSM (Fig. 3.5). The relative contribution of POC to TSM (%POC) ranged from 0.2 and 21.8% and was negatively related to TSM (Fig. 3.5). At a comparable elevation range (>1000;<4800m) the range %POC (3 to 22%) we observed in the Napo streams falls within the range (2 to 60%) reported by in the Peruvian headwaters of the Amazon (Townsend-Small et al. 2005). POC followed the same patterns as TSM, increasing downstream, with freshwater discharge and catchment area, and decreasing with stream gradient and upstream catchment slope. %POC showed the opposed

patterns of TSM, decreasing downstream, with freshwater discharge and catchment area, and increasing with stream gradient and upstream catchment slope. These patterns in %POC probably reflected a better preservation of organic matter fraction in colder high elevation region, the in-stream loss by microbial respiration of organic carbon and the dilution of POC by mineral particles during downstream transport.

Figure 3.3: Total suspended matter (TSM in mg L^{-1}), fraction of particulate organic carbon (POC) in TSM (%POC in %), POC (mg L^{-1}), dissolved organic carbon (DOC in mg L^{-1}), and DOC:POC ratio *versus* elevation (m), upstream catchment slope (°), stream gradient (cm km^{-1}), annual freshwater discharge (m^3 s^{-1}) and catchment area (km^2) from RiverATLAS (Linke et al. 2019) in the Napo streams.

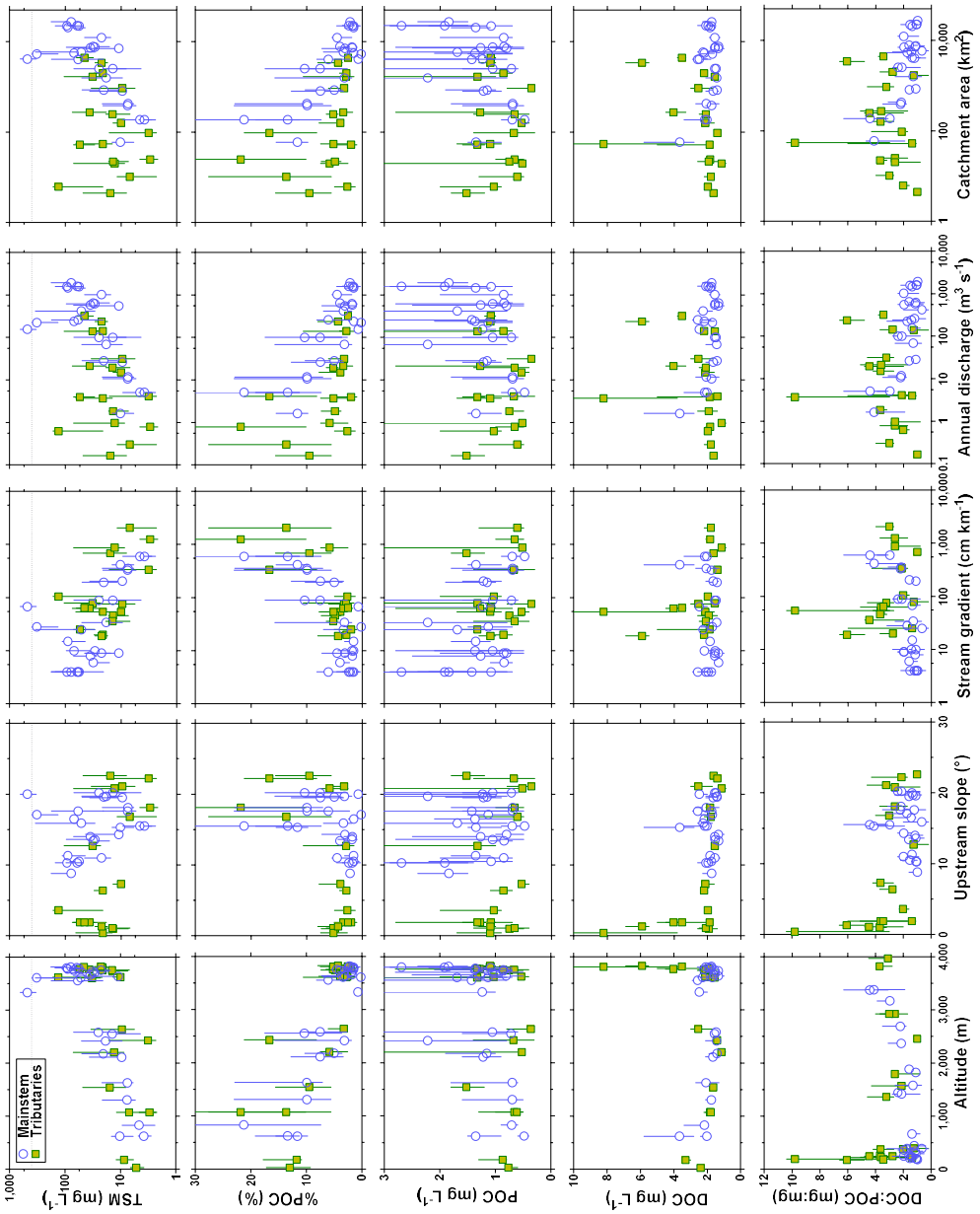

The C:N ratio of fluvial particulate organic matter (POM) ranged between 7 and 11 and decreased downstream (Fig. 3.6). The values C:N of fluvial POM we report in the Napo basin

were consistent with those reported by Townsend-Small et al. (2005) in Andean streams in Peru along an elevational gradient from 720 to 4,043 m (with the majority of C:N values ranging between 5 and 15 in the POM fraction <60 µm). The downstream decrease of the C:N ratio of fluvial POM is consistent with the decrease from highlands to lowlands of soil C:N ratio reported by Townsend-Small et al. (2005) in the Peruvian Andes that was attributed to a higher microbial source (with low C:N) in low-elevation soils compared to high-elevation soils with a higher contribution of plant source (with high C:N), due to elevational gradients of temperature.

Figure 3.4: Upstream catchment slope (°), stream gradient (cm km^{-1}), annual freshwater discharge (m^3 s^{-1}), catchment area (km^2), grassland cover on the upstream catchment (%), forest cover on the upstream catchment (%), and inundation extent at reach level from RiverATLAS (Linke et al. 2019) *versus* elevation (m), in the Napo streams.

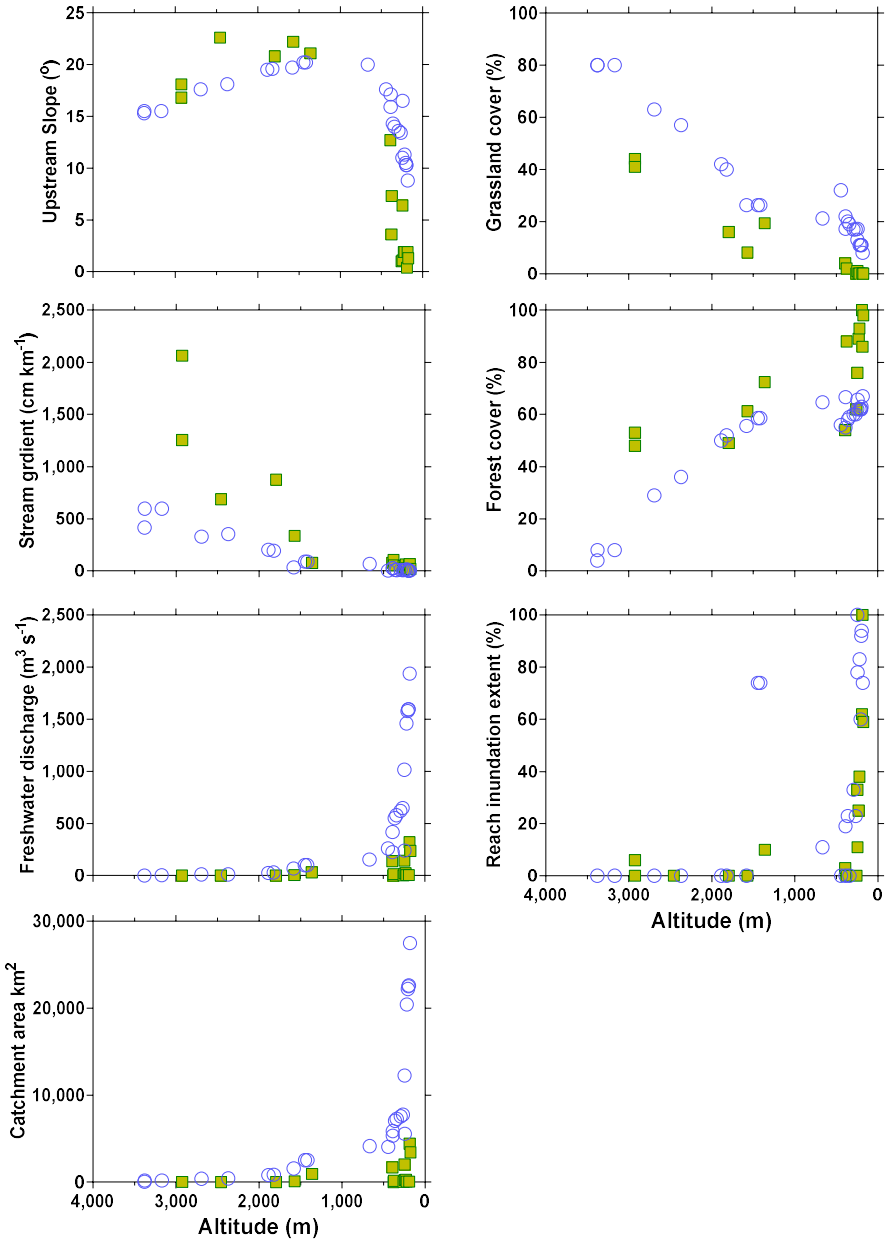

Figure 3.5: Particulate organic carbon (POC in mg L^{-1}), fraction of POC in TSM (%POC in %), dissolved organic carbon (DOC in mg L^{-1}) to POC ratio *versus* total suspended matter (TSM in mg L^{-1}) in the Napo streams.

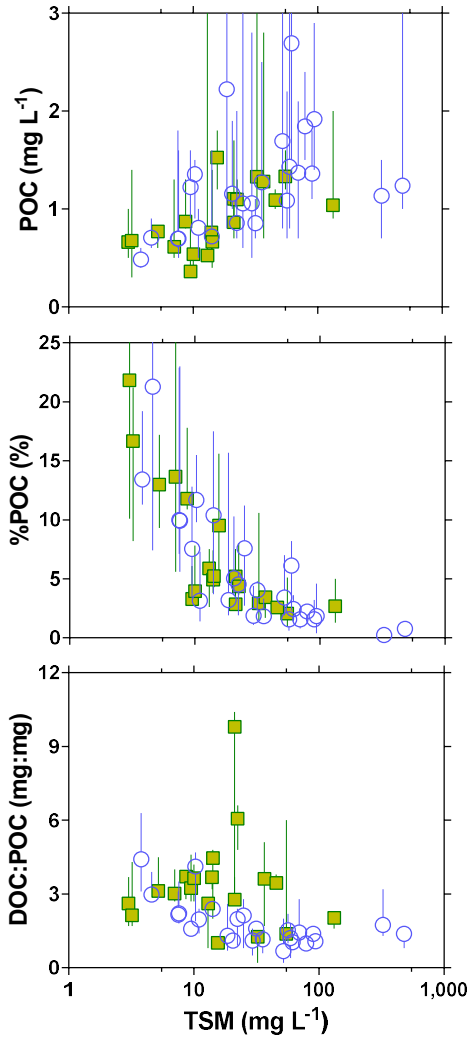

DOC concentrations ranged between 1.2 and 8.2 mg L^{-1} (Fig. 3.3), and at a comparable elevation range (>1000;<4800m) the range DOC (1.2 to 3.3 mg L^{-1}) we observed in the Napo streams falls within the range (0.8 to 10.7 mg L^{-1}) reported by in the Peruvian headwaters of the Amazon (Townsend-Small et al. 2005; Audfdenkampe et al. 2007). DOC ranged within a narrow range (1.2-3.7 mg L^{-1}) with a downstream decreasing pattern in the region between 4,000 and 1,350m, reflecting the increase of the soil organic carbon content with elevation because of the decrease of temperature that leads to a decrease of organic matter mineralization in soils enhancing organic matter accumulation in soils (Poulenard et al. 2003). At elevations < 1000 m, DOC values > 3 mg L^{-1} were observed in four streams. DOC decreased with upstream catchment slope but was unrelated to the other three hydraulic variables (stream gradient, freshwater discharge, and catchment area). This would suggest that elevational change of stream size was not the primary control of fluvial DOC that might be alternatively controlled by soil organic carbon inputs, as thus vary with elevational gradients in vegetation cover on the catchment. DOC was positively related to forest cover (Fig. 3.7) suggesting that leaching of DOC from forest soils strongly enhanced fluvial DOC content.

Note that the relation between DOC and upstream catchment slope (Fig. 3.3) in fact also reflected indirectly the dependency of DOC on forest cover, as forest cover was negatively related to upstream catchment slope (Fig. 3.8). Fluvial DOC did not show a clear pattern with inundation extent at reach level (Fig. 3.3). When analyzing the data separately for tributaries and main-stem, there was a weak positive relation between fluvial DOC and inundation extent for tributaries (excluding the data point with the highest freshwater discharge) but no relation for the main-stem. The DOC to POC (DOC:POC) ratio ranged between 0.7 and 9.8, and exhibited variations that generally followed those of DOC, with a general downstream decreasing weak pattern in the region between 4,000 and 1,500m, and a strong increase in the lowland forested regions (Fig. 3.3). The DOC:POC ratio decreased with upstream catchment slope but was unrelated to the other three hydraulic variables (stream gradient, catchment area and freshwater discharge), reflecting the dependency of forest cover on upstream catchment slope (Fig. 3.8), as the DOC:POC ratio was positively related to forest cover (Fig. 3.7), and negatively related to TSM (Fig. 3.5).The relations between TSM, POC, and %POC with vegetation cover (Fig. 3.7) might be spurious and reflect indirectly the relation between vegetation cover and elevation (Fig. 3.4) or upstream catchment slope (Fig. 3.8). Indeed, the patterns of TSM that imposed those of POC and %POC reflected elevational gradients of erosion and downstream accumulation of particles with stream size.

CDOM was characterized with three optical proxies: the absorption coefficient at 350 nm (a_{350}) that quantifies the content of CDOM, the slope ratio (S_R) that is inversely related to the molecular weight distribution of DOM, with values less than 1 indicative of enrichment in high-molecular-weight compounds (Helms et al. 2008), and the specific ultraviolet absorbance at 254 nm ($SUVA_{254}$) that is positively related to the degree of DOM aromaticity, with high values (>3.5 L mg^{-1} m^{-1}) indicative of the presence of more complex aromatic moieties and low values (<3.0 L mg^{-1} m^{-1}) indicative of the presence of more aliphatic compounds (Weishaar et al. 2003).

The a_{350} values varied from 2.4 to 31.6 m^{-1} and generally followed an exponential increase from high- to low-lands (Fig. 3.9). The a_{350} values in the two streams at the highest elevation (>3,500 m) were higher than the other mountainous streams at elevations > 1000 m, reflecting the high organic carbon content in the páramos combined to small stream size. The $SUVA_{254}$ values ranged between 2.1 and 6.1 L mg^{-1} m^{-1}, was highest in the in the two streams at the highest elevation (>3,500 m), then remains relatively stable (2.1-3.9 L mg^{-1} m^{-1}) between 3,400 and 1,361 m elevation, and finally increase in the lowlands. The a_{350} and $SUVA_{254}$ values were negatively correlated to upstream catchment slope but not S_R. Like DOC, the three DOM optical proxies were unrelated to other hydraulic variables (stream gradient, freshwater discharge, and catchment area). Like DOC, the a_{350} values were positively correlated to forest cover (Fig. 3.10), and the correlation with upstream catchment slope probably also reflects indirectly the relation with forest cover (Fig. 3.8). The a_{350} values were well correlated to DOC, the slope of the linear regression was higher for streams with >50% forest cover in the catchment than streams with <50% forest cover (Fig. 3.11). Lower a_{350} values at similar DOC levels in environments with a low forest cover indicates that DOM released from high-latitude grassland dominated soils is less optically active (that is, less absorptive) compared to DOM released from forest soils. Diverging patterns of a_{350} versus DOC were shown previously in Africa for streams draining catchments dominated by savannah *versus* forest (Lambert et al. 2006). The $SUVA_{254}$ values were positively correlated to forest cover and negatively correlated to grassland cover on the catchment (Fig. 3.10). This is indicative that a higher forest cover in the lowlands led to a higher quantity in streams of highly aromatic DOM. The S_R values ranged between 0.6 and 1.0 and increased downstream, indicating a stronger enrichment of high-molecular-weight DOM compounds in highlands (Fig. 3.9), although, the S_R values did not show clear patterns as a function of land cover.

Figure 3.6: Particulate organic carbon (POC) to particulate nitrogen (N) ratio (C:N molar), carbon stable isotope ratios of POC (δ^{13}C-POC in ‰), carbon stable isotope ratios of dissolved organic carbon (δ^{13}C-DOC in ‰) *versus* elevation (m), upstream catchment slope (°), stream gradient (cm km^{-1}), annual freshwater discharge (m^3 s^{-1}) and catchment area (km^2) from RiverATLAS (Linke et al. 2019) in the Napo streams.

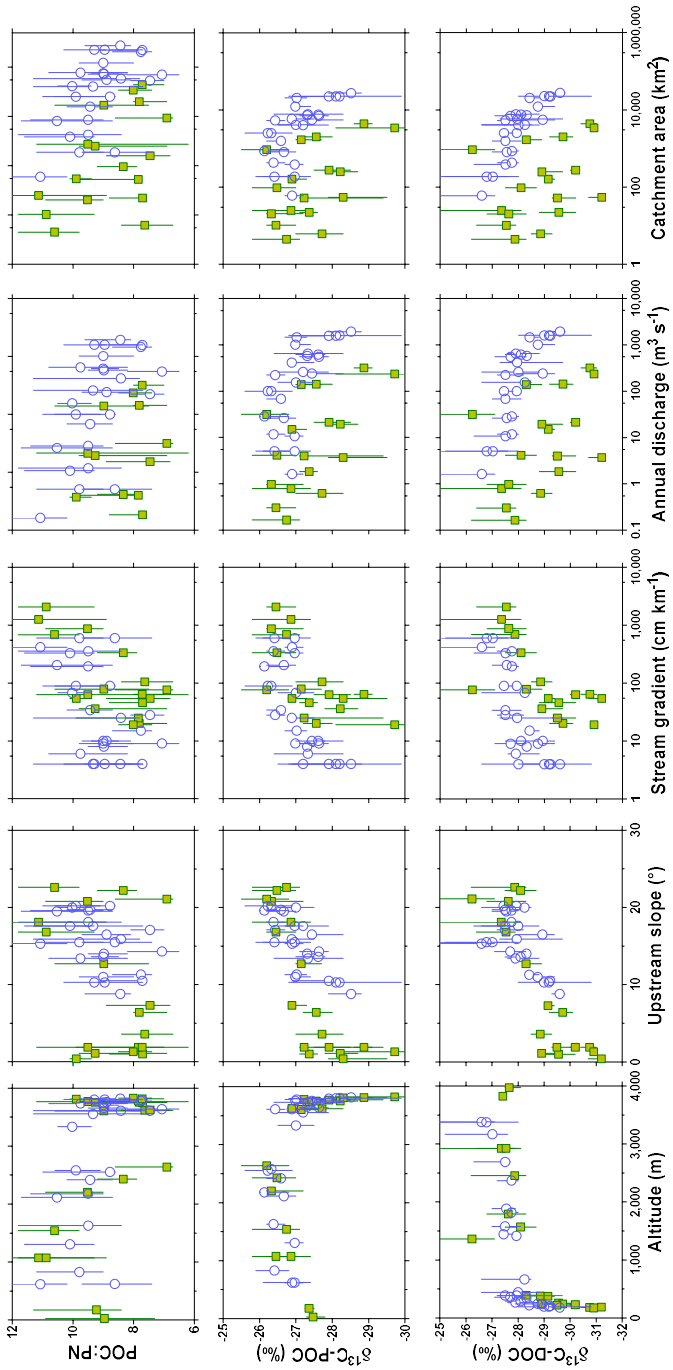

Figure 3.7: Total suspended matter (TSM in mg L^{-1}), fraction of particulate organic carbon (POC) in TSM (%POC in %), POC (mg L^{-1}), dissolved organic carbon (DOC in mg L^{-1}), and DOC:POC ratio *versus* forest cover on the upstream catchment (%) grassland cover on the upstream catchment (%), and inundation extent at reach level from RiverATLAS (Linke et al. 2019) in the Napo streams.

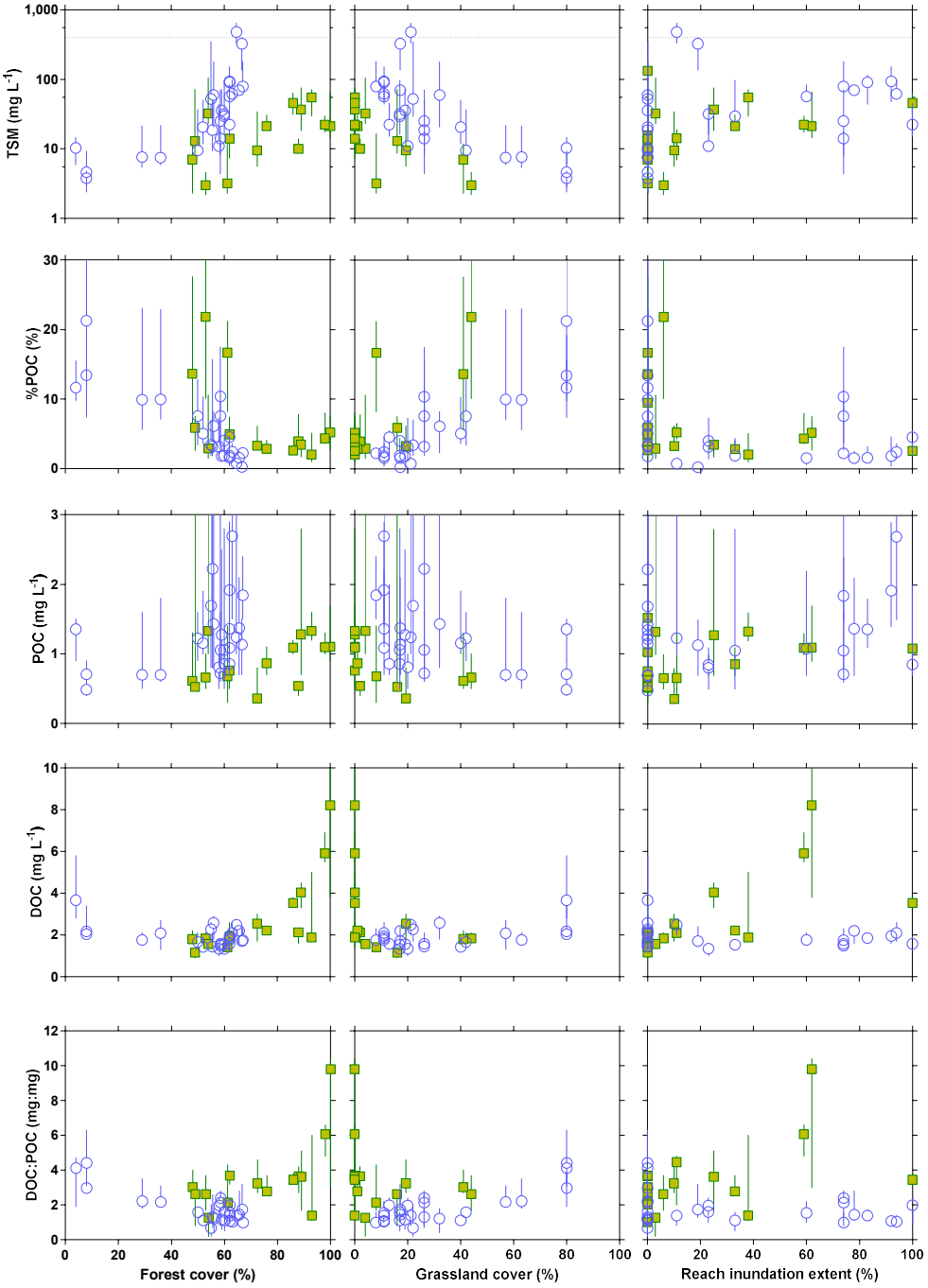

There was a general positive relation between pCO_2 and DOC (Fig. 3.12) that has been used to infer the role of terrestrial organic matter inputs on sustaining net heterotrophy and CO_2 production in inland waters (Lapierre and del Giorgio 2012). However, a pCO_2 and DOC relation can also be interpreted as an indication of simultaneous inputs from the catchment of both DOC and CO_2 derived from soils and/or wetlands.

Figure 3.8: Forest cover on the upstream catchment (%) *versus* upstream catchment slope (°) from RiverATLAS (Linke et al. 2019) in the Napo streams.

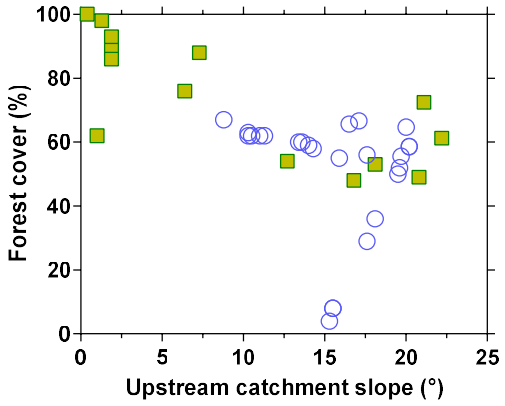

In African streams and rivers, pCO_2 strongly correlated with DOC, although, pelagic respiration was insufficient to sustain CO_2 emissions to the atmosphere, implying a strong lateral input of CO_2 from soils and wetlands (Borges et al. 2015; 2019). There was no relation between the other two GHGs (CH_4 and N_2O) and DOC (Fig. 3.12), although a relation between CH_4 and DOC emerged from a global analysis in rivers and streams (Stanley et al. 2016). In the Napo basin, the strong increase of CH_4 concentrations in the piedmont streams is attributed to an increase of organic matter supply to streams from forests, but also in relation to deposition of sediments as reported in the Mamoré river (Vauchel et al. 2017), while the lower CH_4 concentrations in the mountainous streams seem to be related to intense degassing to the atmosphere related high gas transfer velocities (Chapter 2). The lack of relation between CH_4 and DOC could be explained by multiple drivers acting simultaneously on CH_4 dynamics in the streams of the Napo in addition to organic matter delivery to streams, that might become the main explaining variable in an analysis at global scale (Stanley et al. 2016).

There was no relation between any of the three GHGs and POC (Fig. 3.12). pCO_2 correlated positively with a_{350} (Fig. 3.13) in line with the correlation between pCO_2 and DOC (Fig. 3.12), since a_{350} and DOC are tightly correlated. Yet, this relation is in line with the idea that inland waters with a higher CDOM content have higher CO_2 levels as shown for African (Borges et al. 2022) and boreal lakes (Sobek et al. 2003). This is also in line with the idea that CO_2 content increased in African rivers with presence of wetlands on the catchment (Borges et al. 2015) that in turn also increased the DOC and CDOM content (Lambert et al. 2016a;). However, pCO_2 did not correlate S_R and $SUVA_{254}$ which showed that other processes (lateral inputs and gas exchange) (Chapter 2) had an effect on pCO_2 that overshadowed the effect of modest changes in the specific composition of DOM. There was no relation between $\%N_2O$ and CH_4 and CDOM optical proxies (not shown), although there was on report of a potential contribution of CDOM to CH_4 production in eutrophic Lake Taihu (Zou et al. 2018).

Figure 3.9: Absorption coefficient at 350 nm (a_{350} in m^{-1}), slope ratio (S_R unitless), and the specific ultraviolet absorbance at 254 nm ($SUVA_{254}$ in L mg^{-1} m^{-1}) of colored dissolved organic matter *versus* elevation (m), upstream catchment slope (°), stream gradient (cm km^{-1}), annual freshwater discharge (m^3 s^{-1}) and catchment area (km^2) from RiverATLAS (Linke et al. 2019) in the Napo streams.

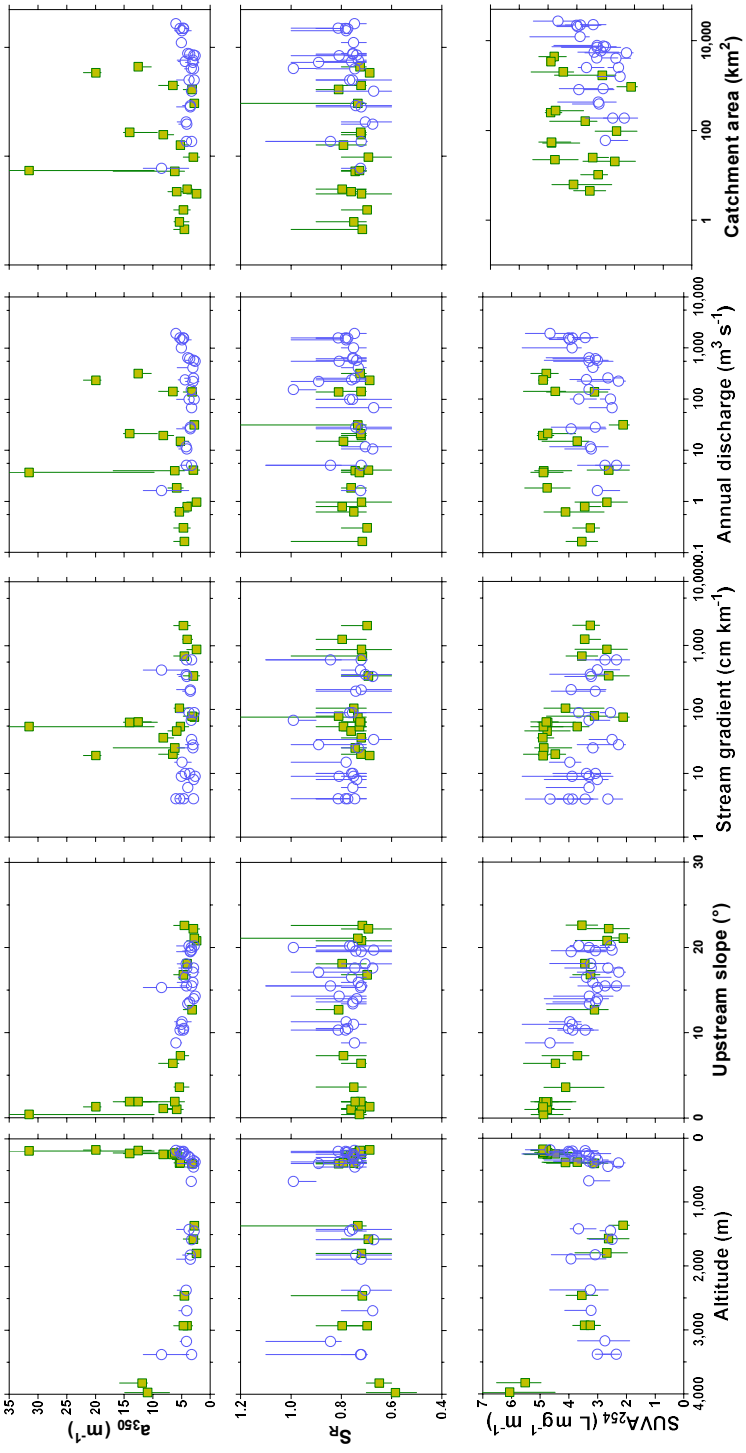

Figure 3.10: Absorption coefficient at 350 nm (a_{350} in m^{-1}), slope ratio (S_R unitless), and the specific ultraviolet absorbance at 254 nm ($SUVA_{254}$ in L mg^{-1} m^{-1}) of colored dissolved organic matter *versus* forest cover on the upstream catchment (%) grassland cover on the upstream catchment (%), and inundation extent at reach level from RiverATLAS (Linke et al. 2019) in the Napo streams.

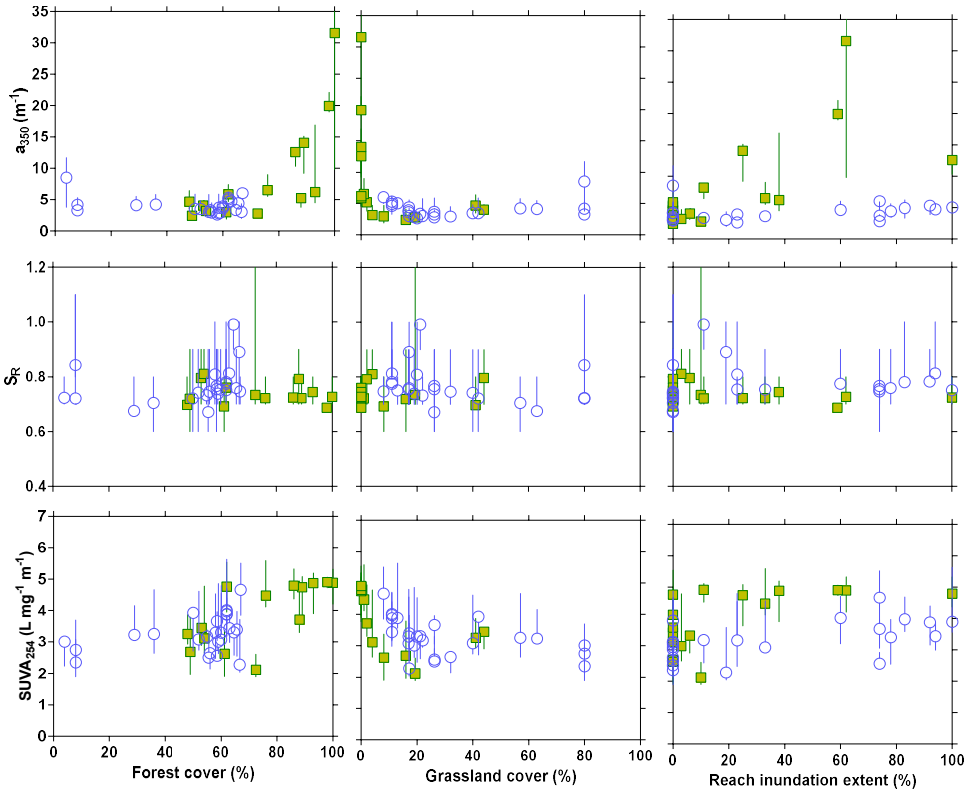

The fluvial δ^{13}C-DOC values ranged between -31.2 and -26.2 ‰ and δ^{13}C-POC values ranged between -29.7 and -26.1 ‰, and they decreased exponentially with elevation (Fig. 3.6). This range of δ^{13}C in organic matter is much broader than the one typical reported in the lowland streams and rivers -29.8 to -26.5‰ (Quay et al. 1992; Hedges et al. 1994; Mayorga et al. 2005) and is consistent with the range reported by Audfdenkampe et al. (2007) in the Peruvian headwaters of the Amazon (-29.6 to -21.8‰). The δ^{13}C-DOC was correlated to δ^{13}C-POC, although the bulk concentrations of DOC was unrelated to POC (Fig. 3.14). The fluvial δ^{13}C-DOC and δ^{13}C-POC values followed the elevational gradient of δ^{13}C of organic carbon from terrestrial vegetation (Fig. 3.15). The change δ^{13}C of organic carbon from terrestrial vegetation reflected the shift from C4 dominated grasslands in highlands to C3 dominated forests in lowlands (Bird and Pousai 1997), consistent with the negative relations between fluvial δ^{13}C-DOC and δ^{13}C-POC with forest cover, and conversely the positive relations between fluvial δ^{13}C-DOC and δ^{13}C-POC with grassland cover (Fig. 3.16). Fluvial δ^{13}C-DOC and δ^{13}C-POC values were also negatively (albeit weakly) related to inundation extent which would suggest that riparian wetlands are dominated by flooded forest (C3 vegetation) rather than macrophytes (C4 vegetation). In addition to shifts in C3 and C4 plants, the change δ^{13}C of organic carbon from terrestrial vegetation might also be related to a lower isotopic fractionation of carbon during photosynthesis due the decrease of atmospheric partial pressure of both CO_2 and O_2, and decreasing air temperature with increasing elevation (Körner et al. 1988; 1991). The δ^{13}C-DOC and δ^{13}C-POC values increased with upstream catchment slope and stream gradient, and decreased with freshwater discharge and catchment area, following the gradients of these hydraulic variables with elevation, but with

distinct relations for main-stem and tributaries. Indeed, these hydraulic variables showed distinct relations for main-stem and tributaries as a function of elevation, due to stream order effect. Additionally, the forest cover correlated with upstream catchment slope (Fig. 3.8). Although linearly correlated, the $\delta^{13}C$ values were lower in DOC than POC by about 1‰ (Fig. 3.14), probably reflecting the more refractory nature of riverine DOC compared to POC, the latter being removed faster during downstream transport, being gradually replaced by POC a higher $\delta^{13}C$ value from the forest vegetation.

Figure 3.11: Absorption coefficient at 350 nm (a_{350} in m^{-1}) versus dissolved organic carbon (DOC in mg L^{-1}) separated into main-stem and tributaries (top panel) and into streams with a forest cover on the upstream catchment > and < 50% (bottom panel).

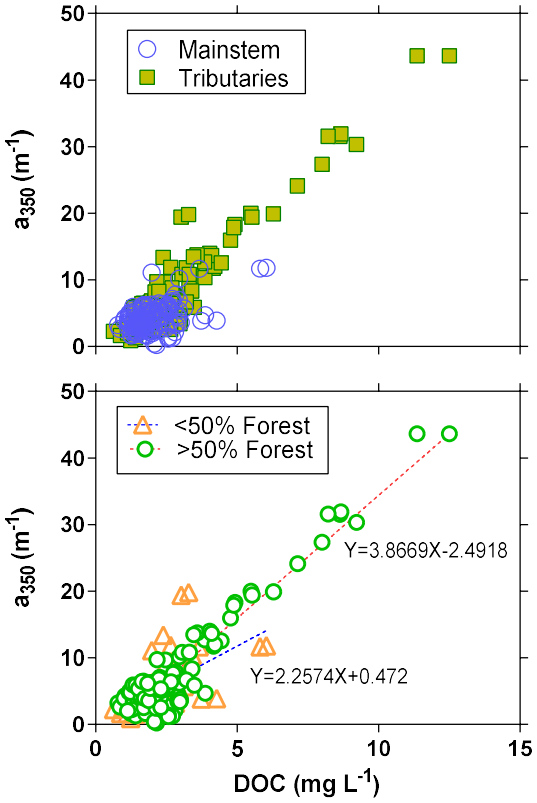

Since the transition between highland grasslands to lowland forest along the elevational gradient controlled both the carbon stable isotope ratios of DOC (Fig. 3.16) and the optical proprieties of DOM (Fig. 3.10), a_{350} and $SUVA_{254}$ were negatively related to $\delta^{13}C$-DOC (Fig. 3.17). However, there was no relation between $\delta^{13}C$-DOC and S_R which might be indicative of a more uniform distribution of molecular weight of fluvial DOM despite different plant sources, compared to strong gradients in

Figure 3.12: Partial pressure of CO_2 (pCO_2 in ppm), dissolved CH_4 concentration (nmol L^{-1}), and N_2O saturation level ($\%N_2O$ in %) *versus* dissolved (DOC) and particulated (POC) organic carbon (mg L^{-1}) in the Napo streams.

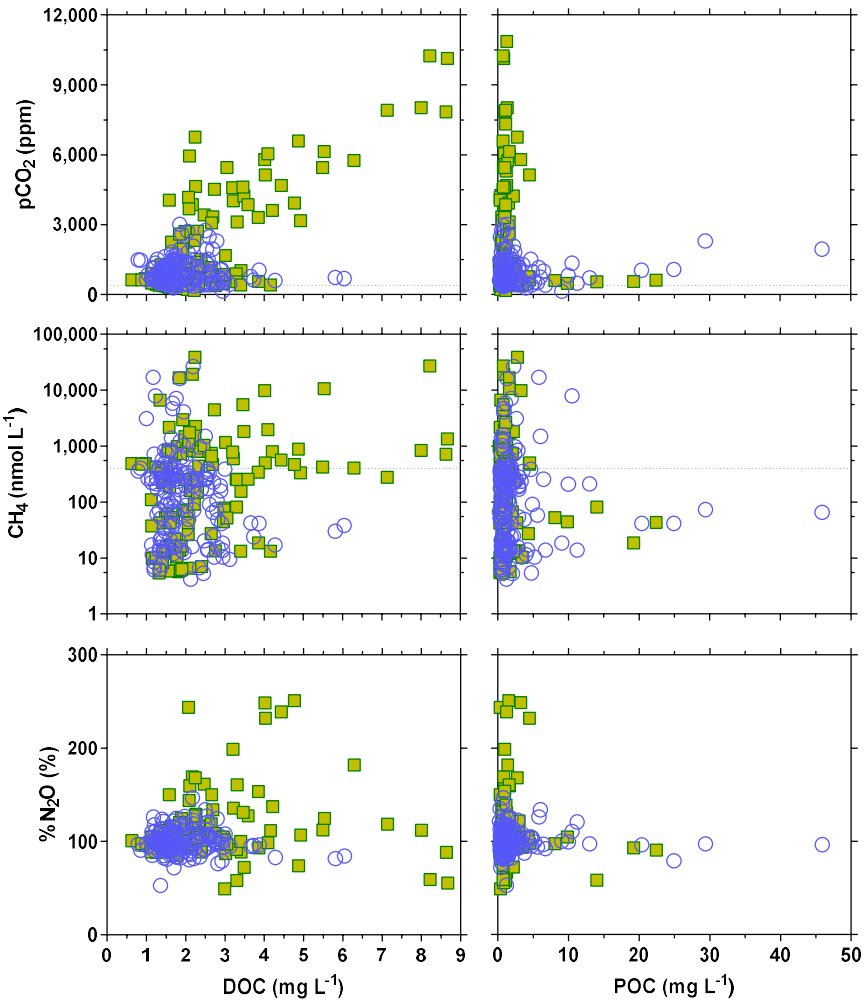

Figure 3.13: Partial pressure of CO_2 (pCO_2 in ppm) *versus* absorption coefficient at 350 nm (a_{350} in m^{-1}), slope ratio (S_R unitless), and the specific ultraviolet absorbance at 254 nm ($SUVA_{254}$ in L mg^{-1} m^{-1}) of colored dissolved organic matter in the Napo streams.

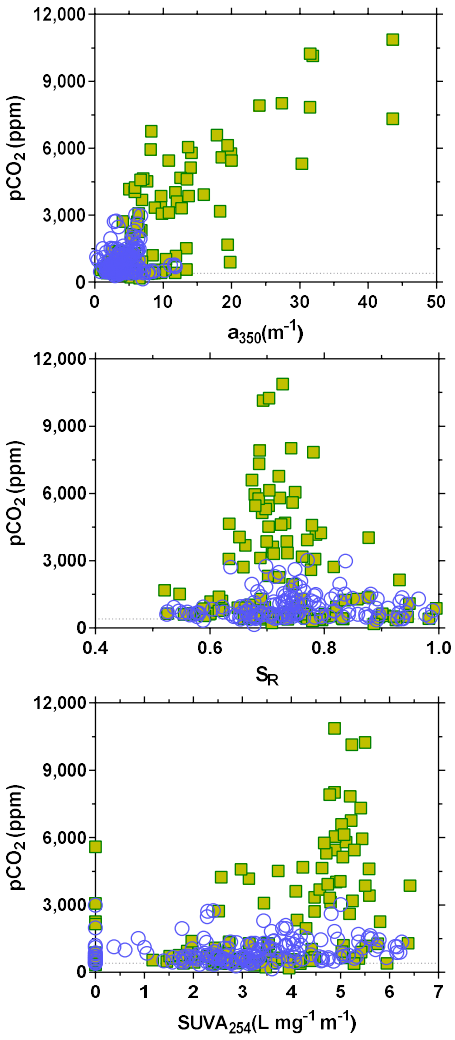

Figure 3.14: Carbon stable isotope ratios of dissolved organic carbon (DOC) (δ^{13}C-DOC in ‰) *versus* carbon stable isotoped ratios of particulate organic carbon (POC) (δ^{13}C-POC in ‰), and DOC *versus* POC in the Napo streams.

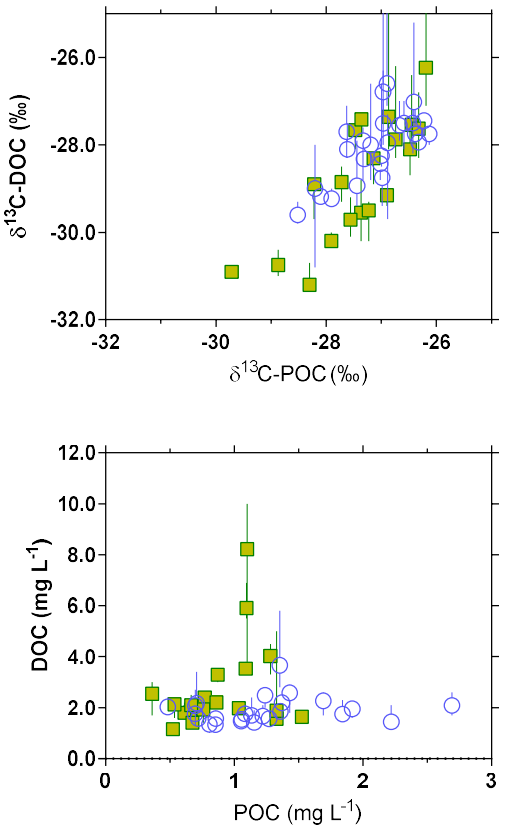

Figure 3.15: Carbon stable isotope ratios of plant material (δ^{13}C-plant in ‰) *versus* elevation (m) from vegetation collected along the Napo streams.

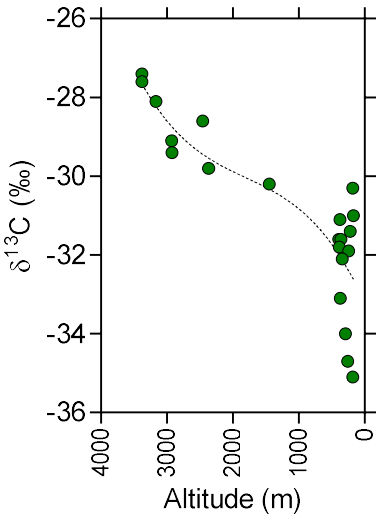

Figure 3.16: Particulate organic carbon (POC) to particulate nitrogen (N) ratio (C:N molar), carbon stable isotope ratios of POC (δ^{13}C-POC in ‰), carbon stable isotope ratios of dissolved organic carbon (δ^{13}C-DOC in ‰) *versus* forest cover on the upstream catchment (%) grassland cover on the upstream catchment (%), and inundation extent at reach level from RiverATLAS (Linke et al. 2019) in the Napo streams.

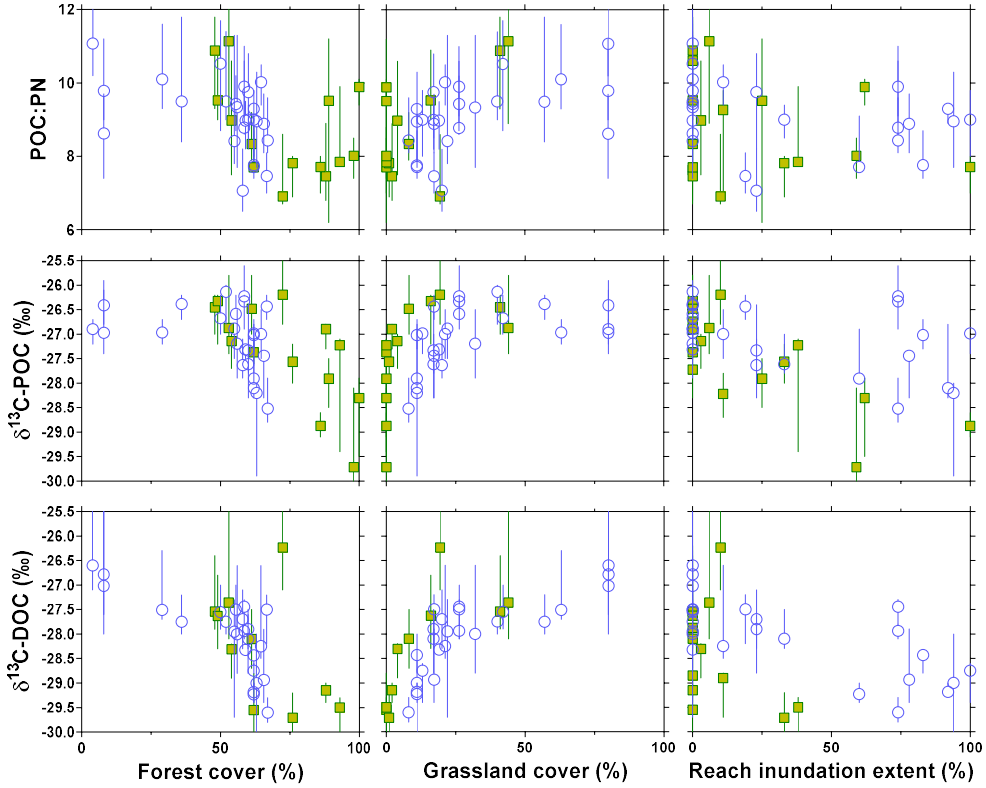

Figure 3.17: Absorption coefficient at 350 nm (a_{350} in m^{-1}), slope ratio (S_R unitless), and the specific ultraviolet absorbance at 254 nm ($SUVA_{254}$ in L mg^{-1} m^{-1}) of colored dissolved organic matter *versus* carbon stable isotope ratios of dissolved organic carbon (δ^{13}C-DOC in ‰) in the Napo streams.

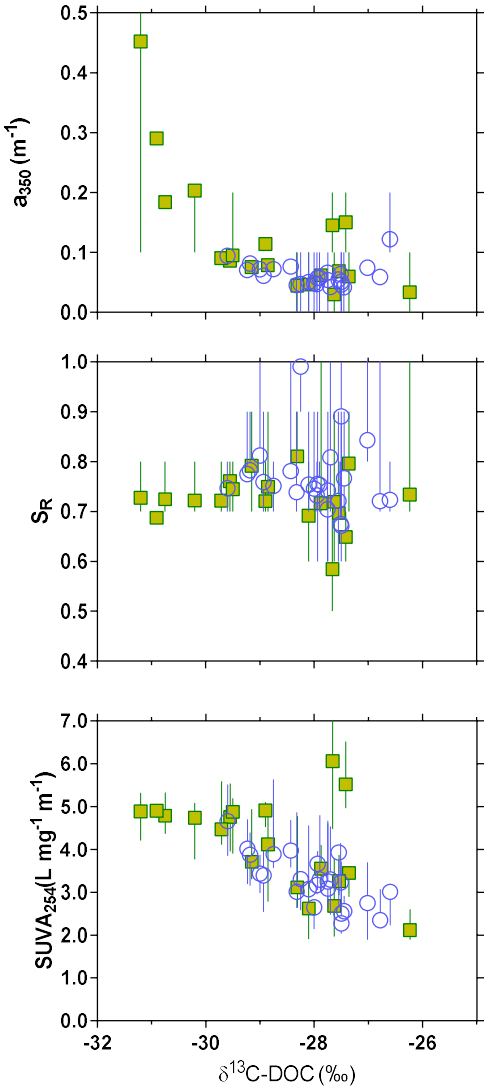

CHAPTER 4

DISSOLVED GREENHOUSE GAS (CO_2, CH_4, N_2O) EMISSIONS FROM HIGHLAND LAKES OF THE ANDES CORDILLERA IN NORTHERN ECUADOR

Loreto Lake in Salve Faccha Moorland

Dissolved greenhouse gas (CO_2, CH_4, N_2O) emissions from highland lakes of the Andes cordillera in Northern Ecuador.

This chapter is a submitted manuscript to the Journal Science of the Total Environment, which is in the peer-review stage, presenting a description of the emissions from highland lakes of the Andes cordillera in Northern Ecuador

Gonzalo Chiriboga[1,2], Steven Bouillon[3], Alberto V. Borges[1,*]

[1] Chemical Oceanography Unit, University of Liège, Liège, Belgium
[2] Facultad de Ingeniería Química, Universidad Central del Ecuador; Ritter s/n y Bolivia, Quito, Ecuador
[3] Department of Earth and Environmental Sciences, KU Leuven, 3001 Leuven, Belgium
* alberto.borges@uliege.be

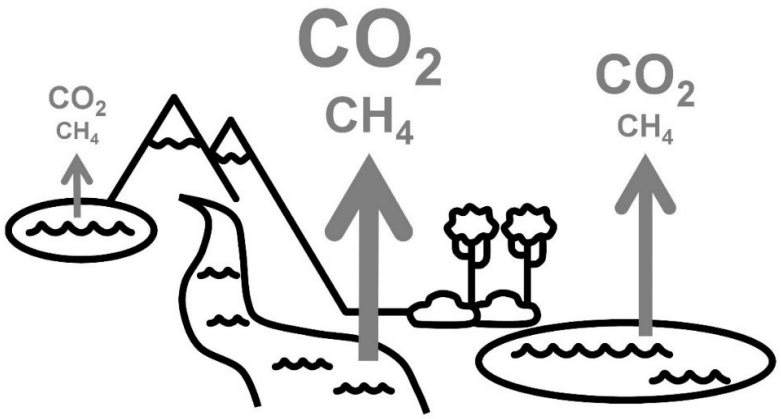

- CO_2, CH_4, N_2O measurements in 15 highland lakes in Andes cordillera (northern Ecuador)
- CO_2, CH_4, and N_2O correlated with lake surface area
- Three volcanic influenced lakes had much higher CO_2 values
- CO_2 in sampled highland lakes was lower than the values usually attributed to tropical lakes
- CH_4 in highland lakes was higher than in lowland lakes of the Amazon basin
- CO_2 in highland lakes was lower than in lowland lakes of the Amazon basin

Abstract

We report dissolved concentrations of CO_2, CH_4 and N_2O in 15 lakes located in the páramos of Salve Faccha and Antisana y Mojanda (northern region of Ecuadorian Andes), along an elevational gradient from 2,213 to 4,361 m above sea level, as well as a gradient of lake surface area (0.003 to 6.1 km^2) and depth (0.9 to 74 m). Most lakes were characterized by lower values of the partial pressure of CO_2 (pCO_2) (644-2,152 ppm) than usually attributed to tropical lakes (~1,900 ppm). Three lakes influenced by volcanic inputs were characterized by high pCO_2 values (3,269-10,069 ppm), while two lakes bordered by large cities were characterized by the lowest pCO_2 values (208-254 ppm). Dissolved CH_4 concentrations ranged between 170 and 24,908 nmol L^{-1} and were negatively correlated to lake area and depth. N_2O saturation levels ranged between 64% and 101%. The surface waters were under-saturated in N_2O with respect to atmospheric equilibrium, probably due to inputs soil-water with low N_2O levels owing to denitrification in soils. The data obtained in the sampled highland lakes was combined with published data from lowland lakes to derive relations between CO_2 and CH_4 and lake surface area allowing to compute CO_2 and CH_4 lacustrine emissions at the scale of the Amazon basin using the HydroLAKES spatial data-set. The CO_2 and CH_4 emissions from highland lakes (elevation > 500 m) only represented 0.4% and 5.2% of the total lacustrine emissions at the scale of the Amazon basin, respectively. Total CO_2 and CH_4 emissions from lakes represented a small fraction (8%) of total lentic and lotic CO_2 and CH_4 emissions at the scale of the Amazon basin.

Introduction

Inland waters (streams, rivers, lakes, and reservoirs) occupy a very small fraction of the Earth's surface but are quantitatively important global sources of CO_2 and CH_4 to atmosphere (Cole et al., 2007; Bastviken et al. 2011; Raymond et al., 2013; Rosentreter et al. 2021). Riverine CO_2 emissions from the tropics are disproportionately intense compared to their higher latitude counterparts (Raymond et al. 2013; Lauerwald et al. 2015; Borges et al. 2015a; 2015b; Liu et al. 2022; Battin et al. 2023). In contrast, the CO_2 emissions from tropical lakes might be lower than their counterparts at higher latitudes, and have been substantially over-estimated in past literature (Borges et al. 2022). The CH_4 emissions from tropical lakes and rivers are disproportionately intense compared to their higher latitude counterparts (Bastviken et al. 2011; Borges et al. 2015a; 2022; Rosentreter et al. 2020). Relatively higher riverine CO_2 and CH_4 emissions in tropical zones than at higher latitude are related to higher temperature and terrestrial biomass (Lauerwald et al. 2015) as well as a strong connectivity with floodplains (Abril et al. 2014; Borges et al. 2015a; 2015b; 2019). Relatively lower lacustrine CO_2 but higher lacustrine CH_4 emissions in tropical climates than at higher latitude are partly related to high phytoplankton production in non-humic lakes that leads to the uptake of dissolved CO_2 but at the same time high CH_4 production in sediments (Borges et al. 2022) due to the deposition of fresh phytoplankton detritus (Grasset et al. 2018).

Estimates of N_2O emissions from inland waters have been revised downwards by a factor of 70 (Hu et al. 2016) from early estimates (Kroeze et al. 2010). Emissions of N_2O from tropical lakes are lower compared to their boreal counterparts (Borges et al. 2022; 2023). Riverine N_2O emissions modelled from emission factors and nitrogen deposition rates are higher in tropical rivers than rivers at higher latitudes (Hu et al. 2016; Maavara et al. 2019). However, field measurements of riverine N_2O concentrations in tropical rivers are generally low and frequently below saturation (Teodoru et al. 2015; Borges et al. 2015a; 2019), except in areas impacted by urban effluents (Marwick et al. 2014). The riverine N_2O concentrations are much lower in large tropical rivers such as the Congo and Zambezi than in agriculturally impacted large European rivers such as the Meuse (Borges et al. 2018). This difference between modelled and *in situ* measured N_2O riverine fluxes probably reflects the uncertainty of emission factors (Clough et al. 2006) and the fact that the models do not represent the full reduction of N_2O to N_2 by denitrification and cannot compute an uptake of N_2O from inland waters (Borges et al. 2022).

Existing studies on CO_2 and CH_4 emission from tropical flowing waters have mainly focused on lowland areas, overlooking the contribution of mountainous areas. A vast amount of headwaters can be found in the Andes which contribute with the 82% of sediments and solutes to Amazon basin (McClain and Naiman 2008). Páramos are Andean mountain ecosystems which are located discontinuously in the Neotropics, at elevations between 3,000 up to 4,300 m mainly from Venezuela to northern Peru. The páramos occupy more than 30,000 km² in South America. Ecuador is the country with the highest proportion of its territory covered by páramos, with 7%. Páramo lakes constitute a primary source of drinking water for large populations in Ecuador, Colombia, and Venezuela. In Ecuador, the air temperature is relatively constant, the average annual rainfall is 1,345 mm and it occurs throughout most of the year only ~12 % of the days are dry. These conditions have favored the formation of peat and a large number of wetlands and lakes. The páramo usually presents deep and organic rich soils (30 % by volume) and its vegetation is dominated by grasslands (Zapata et al. 2021).

Here, we report the dissolved concentrations of CO_2, CH_4 and N_2O in 15 lakes located in the northern region of Ecuadorian Andes along an elevational gradient from 2,213 to 4,361 m above sea level, as well as a gradient of lake surface area (0.003 to 6.1 km^2) and depth (0.9 to 74 m) (Fig 4. 1). Most lakes were located in the páramos of Salve Faccha and Antisana y Mojanda.

Material and methods

Sampling and laboratory analysis

Sampling was carried out over a period from April 2019 to March 2022, with an inflatable boat approximately in the center of the lake, during day-time only (early morning to late afternoon). Water temperature, specific conductivity, pH, and $\%O_2$ were measured in surface water with a YSI multi-parameter probe (ProPlus). Water for CH_4 and N_2O samples was collected with a sampling devise consisting of a 2L polyethylene bottle with the bottom cut and fitted with a silicone tubing at the stopper (Abril et al. 2007). Two borosilicate serum bottles (Weathon) with a volume of 40 ml were filled with the silicone tubing, poisoned with 100 µl of a saturated solution of $HgCl_2$ and sealed with a butyl stopper and crimped with an aluminium cap. Measurements were made, after over-night equilibration, on an headspace (Weiss 1981) (created by injecting 15 ml of high-purity N_2 into the 40 ml sample bottles), with a gas chromatograph (SRI 8610C) with a flame ionisation detector for CH_4 and electron capture detector for N_2O calibrated with CH_4:N_2O:N_2 gas mixtures (Air Liquide Belgium) with mixing ratios of 1, 10 and 30 ppm for CH_4, and 0.2, 2.0 and 6.0 ppm for N_2O. The precision of measurement based on duplicate samples was ±10.9% for CH_4 and ±5.8% for N_2O.

The partial pressure of CO_2 (pCO_2) was measured in the field with a Li-Cor Li-820 infra-red gas analyser based on the headspace technique with four 60 ml polypropylene syringes that were filled directly with surface water. The pCO_2 in the atmosphere was measured by injecting ambient air sampled with an additional polypropylene syringe. The Li-Cor Li-820 was calibrated with pure N_2 and CO_2:N_2 gas mixtures (Air Liquide Belgium) of 388, 804, 3,707 and 8,146 ppm. The final pCO_2 value was computed taking into account the partitioning of CO_2 between water and the headspace, as well as equilibrium with HCO_3^- (Dickson et al. 2007) using water temperature measured in-situ and after equilibration, and total alkalinity (TA). The precision of pCO_2 measurement was ±5.2%.

The CO_2 concentration is expressed as partial pressure in parts per million (ppm) and as dissolved concentration for CH_4 (nmol L^{-1}), in accordance with convention in existing topical literature. Variations of N_2O were modest and concentrations fluctuated around atmospheric equilibrium, so data are presented as percent of saturation level ($\%N_2O$, where atmospheric equilibrium corresponds to 100%), computed from the global mean N_2O air mixing ratios given by the Global Monitoring Division (GMD) of the Earth System Research Laboratory (ESRL) of the National Oceanic and Atmospheric Administration (NOAA) (https://www.esrl.noaa.gov/gmd/hats/combined/N2O.html), using the Henry's constant (Weiss and Price 1980).

Samples for the stable isotope composition of DIC (δ^{13}C-DIC) were collected in 12 ml Exetainer vials (Labco) and poisoned with 50 µL of a saturated solution of $HgCl_2$. Prior to the analysis of δ^{13}C-DIC, a 2 ml helium headspace was created and 100 µL of phosphoric acid (H_3PO_4, 99%) was added in the vial in order to convert CO_3^{2-} and HCO_3^- to CO_2. After overnight equilibration, up to 1 mL of the headspace was injected with a gastight syringe into a coupled elemental analyser - IRMS (EA-IRMS, Thermo FlashHT or Carlo Erba EA1110 with DeltaV Advantage). The obtained data were corrected for isotopic equilibration between dissolved and gaseous CO_2 as described by Gillikin and Bouillon (2007). Calibration was performed with certified standards (NBS-19 or IAEA-CO^{-1}, and LSVEC). Reproducibility of measurement based on duplicate injections of samples was typically better than ±0.2 ‰.

Water was collected in surface water with a 2L polyethylene bottle. The water filtered through 47 mm diameter GF/F Whatman glass fibber filters was collected and further filtered through polyethersulfone syringe encapsulated filters (0.2 µm porosity) for nitrate (NO_3^-), nitrite (NO_2^-), ammonium (NH_4^+), TA, major elements (Na^+, Mg^{2+}, Ca^{2+}, K^+), as well as dissolved silicate (DSi) and Fe, stable isotope composition of O and H of H_2O ($\delta^{18}O$-H_2O and δ^2H-H_2O) and dissolved organic carbon (DOC). An additional water filtration was made on 25 mm diameter GF/F Whatman glass fibber filters for particulate organic carbon (POC) analysis.

Samples for NO_3^-, NO_2^-, and NH_4^+ were stored frozen (-20°C) in 50 ml polypropylene vials. NO_3^- and NO_2^- were determined with the sulfanilamide colorimetric with the vanadium reduction method (American Public Health Association, 1998), and NH_4^+ with the dichloroisocyanurate-salicylate-nitroprussiate colorimetric method (Standing committee of Analysts, 1981). Detection limits were 0.3, 0.01, and 0.15 µmol L^{-1} for NH_4^+, NO_2^- and NO_3^-, respectively. Precisions were ±0.02 µmol L^{-1}, ±0.02 µmol L^{-1}, and ±0.1 µmol L^{-1} for NH_4^+, NO_2^- and NO_3^-, respectively.

Samples for TA were stored at ambient temperature in polyethylene 55 ml vials and measurements were carried out by open-cell titration with HCl 0.1 mol L^{-1} according to Gran (1952), and data quality checked with certified reference material obtained from Andrew Dickson (Scripps Institution of Oceanography, University of California, San Diego, USA), with a typical reproducibility better than ±3 µmol kg^{-1}. DIC was computed from TA and pCO_2 measurements using the carbonic acid dissociation constants for freshwater of Millero (1979) using the CO_2sys package.

Samples for $\delta^{18}O$-H_2O and were δ^2H-H_2O stored at ambient temperature in polypropylene 8 ml vials. δ^2H-H_2O was measured on H_2 gas derived from a high-temperature (1,030°C) Cr-based reactor by automated injections of water using a TriPlus autosampler on an elemental analyzer (Thermo Flash HT/EA; Thermo Finnigan) coupled to a continuous-flow isotope-ratio mass spectrometer (Delta V Advantage; Thermo Finnigan). $\delta^{18}O$-H_2O values were measured on a Thermo GasBench II coupled to a Thermo Delta XP IRMS after equilibration with CO_2. The long-term uncertainty for standard $\delta^{18}O$ values was ±0.1‰.

Samples for major elements were stored at ambient temperature in 20 ml scintillation vials and preserved with 50 µl of HNO_3 (65%). Major elements were measured with inductively coupled plasma MS (ICP-MS; Agilent 7700x) calibrated with the following standards: SRM1640a from National Institute of Standards and Technology, TM-27.3 (lot 0412) and TMRain-04 (lot 0913) from Environment Canada, and SPS-SW2 Batch 130 from Spectrapure Standard. Limit of quantification was 0.5 µmol L^{-1} for Na^+, Mg^{2+} and Ca^{2+}, 1.0 µmol L^{-1} for K^+ and 8 µmol L^{-1} for DSi.

Samples to determine DOC were stored at ambient temperature and in the dark in 40 ml brown borosilicate vials with polytetrafluoroethylene (PTFE) coated septa and poisoned with 50 µL of H_3PO_4 (85%), and DOC concentration was determined with a wet oxidation total organic carbon analyzer (IO Analytical Aurora 1030W), with a typical reproducibility better than ±5%.

Filters for POC analysis were decarbonated with HCl fumes for 4h and dried before encapsulation into silver cups; POC concentration was analysed on an EA-IRMS (Thermo FlashHT with DeltaV Advantage), with a reproducibility better than ±5%. Data were calibrated with certified (IAEA-600: caffeine) and in-house standards (leucine, tuna muscle tissue) that were previously calibrated versus certified standards.

Flux computations and upscaling

The dissolved concentrations of CO_2 and CH_4 were derived from statistical relations as function of lake surface area for each of the lakes (*n*=12,549) in HydroLAKES (Messager et al. 2016). We excluded from the analysis reservoirs that represent 0.06% of lake counts (n=8) and 11% of total lacustrine surface area (2,773 km^2) in the HydroLAKES data-set. The statistical relations were derived from our own data in Ecuadorian highland lakes and data available from literature in the floodplain lakes of the Central Amazon (Abril et al. 2013; Amaral et al. 2020; Barbosa et al. 2016; Mitchell et al. 2018).

The pCO_2 (in ppm) was computed from two linear regressions as a function of lake surface area (LSA in km^2) according to:

$\log(pCO_2) = -0.1293(\pm 0.0346) \times LSA + 3.063(\pm 0.073)$

(r^2=0.58; *p*=0.0039; n=12)

for an elevation > 500 m (highlands) excluding three lakes (Cuicocha, Loreto and Papallacta)

and

$\log(pCO_2) = -0.0003745(\pm 0.0001642) \times LSA + 3.508(\pm 0.061)$
(r^2=0.26; p=0.0376; n=17)
for an elevation < 500 m (lowlands)

The CH_4 (in nmol L^{-1}) was computed from a linear regression as function of LSA (in km^2) according to:

$\log(CH_4) = -0.3753(\pm 0.0426) \times \log(LSA) + 2.545(\pm 0.066)$
(r^2=0.71; p<0.0001; n=34)
for both highland and lowland lakes

The water temperature (WT in °C) was computed from the air temperature (AT in x10°C) from HydroLAKES, according to:

$\log(WT) = 0.002192(\pm 0.000069) \times AT + 0.8905(\pm 0.0151)$
(r2=0.98; p<0.0001; n=23)

The flux of CO_2 (FCO_2) and CH4 (FCH_4) between surface waters and the atmosphere was computed according to:

$F = k \times \Delta G$

where k is the gas transfer velocity and ΔG is the air-water gradient of a given gas.
The k normalized to a Schmidt number (Sc) of 600 (k600 in cm h^{-1}) was derived from the parameterisation as a function wind speed (Cole and Caraco 1998):

$k_{600} = 2.07 + 0.215 \times u^{1.7}$

where u is wind speed (m s^{-1}) that was extracted from WorldClim (Fick and Hijmans 2017) for each lake in HydroLAKES.

k_{600} was converted to k for the Sc at *in-situ* temperature (Wanninkhof 1992) according to:

$k = k_{600} \times (Sc/600)^{-0.5}$

A Monte-Carlo error analysis was made by propagating errors (10,000 iterations) on the slope and constant of the equations to the gas concentrations and WT (refer to above equations) and an error of ±30% for k_{600} based on the reported variability across different lakes of k at low wind speeds (Cole and Caraco 1998).

Results and discussion

We sampled 15 lakes in Ecuador along an elevational gradient (2,213-4,361 m) (Fig 4. 1). The surface area of the sampled lakes ranged between 0.003 to 6.1 km^2, and lakes at higher elevation tended to be smaller (Fig 4. 2). Lakes were generally shallow, with depths ranging between 0.9 and 72 m, with a tendency towards shallower lakes at higher elevation (Fig 4. 2). Lakes Cuicocha, Loreto and Papallacta are crater lakes (hereafter referred to as “volcanic”) and the others are of glacial origin. Among the latter, San Pablo and Yaguarcocha are surrounded by the cities of Otavalo and Ibarra, respectively (hereafter referred to as “urban”).

Figure 4.1: Fifteen sampled highland lakes in Northern Ecuador

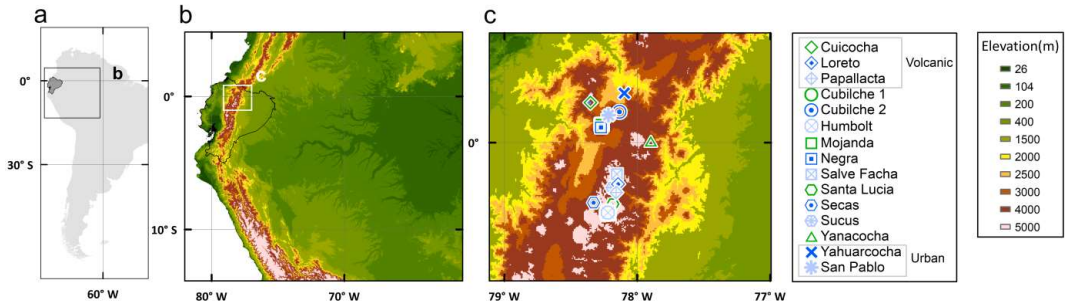

Figure 4.2: Lake area (km^2), lake depth (m), water temperature (°C), stable.isotope composition of O of H_2O ($\delta^{18}O$-H_2O in ‰), specific (Sp.) conductivity (µS cm^{-1}) and total alkalinity (TA in mmol L^{-1}) in surface waters *versus* elevation (m). Solid grey lines show fits to the data (Table 4.S2). Dotted blue line indicates the $\delta^{18}O$-H_2O elevation gradient for Ecuador based on the global rainwater iso-scape given by Inguaggiato et al. (2010).

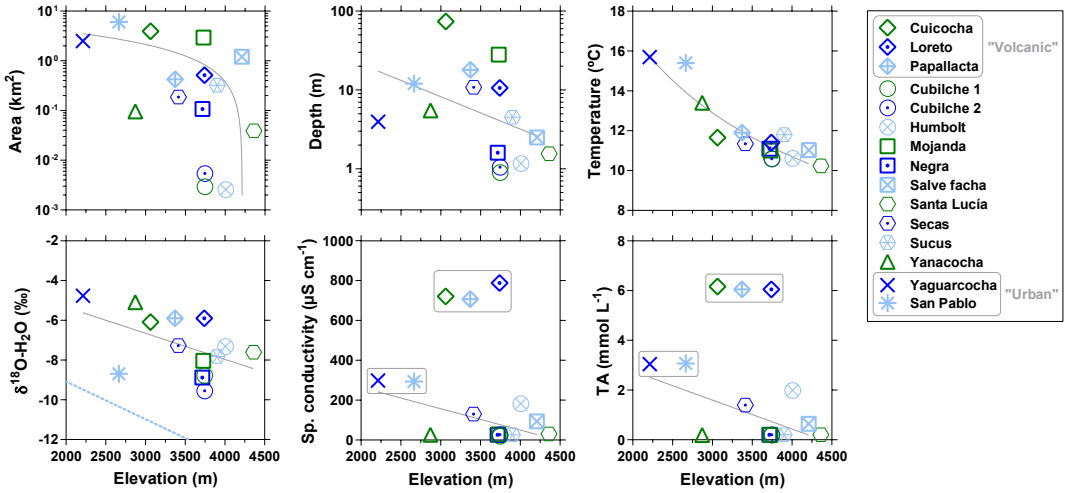

Water temperature ranged between 10.2 and 15.7°C and followed a clear elevational gradient (Fig 4. 2). The specific conductivity in the sampled lakes was generally low (20-183 µS cm^{-1}), except for the two "urban" lakes (San Pablo and Yaguarcocha) (294-298 µS cm^{-1}) and the three "volcanic" lakes (Cuicocha, Loreto and Papallacta) (708-722 µS cm^{-1}) (Fig 4. 2). The conductivity of the three "volcanic" lakes was lower than in crater lakes in active volcanic systems in Ecuador characterized by conductivity values >10,000 µS cm^{-1} (Inguaggiato et al. 2010; Melián et al. 2021). Conductivity was negatively related to elevation for the non-"volcanic" lakes possibly reflecting the combination of decreasing lake size and increasing soil organic matter content with elevation. In the Andean páramo, the soil organic carbon increases with elevation because of the decrease of temperature that leads to a decrease of organic matter mineralization in soils enhancing organic matter accumulation in soils (Poulenard et al. 2003). The high organic matter content of soils and lower temperature are not favorable to rock weathering leading to soil water with low mineral content (low conductivity). Additionally, high elevation páramo areas are characterized by high precipitation leading to dilution of solutes in surface waters which should additionally contribute to decrease conductivity. TA showed very similar patterns to those of conductivity, with the three "volcanic" lakes characterized by higher TA values (6.05-6.16 mmol L^{-1}), followed by the two "urban" lakes (3.04-3.07 mmol L^{-1}), and the remaining lakes with the lowest TA values (0.19-1.99 mmol L^{-1}). The cation sequence was dominated by Ca^{2+} or Na^{+} followed by Mg^{2+} and K^{+} (Table 4.S1). The lakes with a high total cation content (21-147 mg L^{-1}

and 1,035-7,916 µeq L^{-1}) were dominated by Na^+ (Na^+>Ca^{2+}>Mg^{2+}>K^+) characteristic of sodium bicarbonate lakes. Lakes with a lower total cation content (~5 mg L^{-1} and ~235 µeq L^{-1}) were dominated by Ca^{2+} (Ca^{2+}>Na^+>Mg^{2+}>K^+) (Table 4.S1). This might indicate that the cation content of the sample lakes was related to the weathering of primarily volcanic rocks that dominate in the area (rhyolite, andesite, dacite, and diorite) (Mosquera et al. 2022). The three "volcanic" lakes (Cuicocha, Loreto and Papallacta) were characterized by higher total cation content (144-147 mg L^{-1} 7,778-7,916 µeq L^{-1}) than the other 12 lakes (Table 4.S1). The composition of the three "volcanic" lakes in divalent ions (Ca^{2+} and Mg^{2+}) relative to Na^+ was consistent with the other 12 lakes (Fig 4. S1). However, the three "volcanic" lakes had lower K^+, DSi and TA relative to the other 12 lakes (Fig 4. S1), which might indicate different weathering mechanism in the three "volcanic" lakes compared to the other 12 lakes: either a non-congruent dissolution of aluminosilicate minerals or alternatively the weathering of a higher portion of sodium rich volcanic rocks in the three "volcanic" lakes compared to the other 12 lakes (Mosquera et al. 2022). The Fe content was negatively related to Na^+, and the three "volcanic" lakes had lower Fe relative to Na^+ compared to the other 12 lakes. This pattern might be related to the chelation of Fe to dissolved organic matter, as Fe was correlated to DOC (Fig 4. S2).

Table 4.1: Emissions to the atmosphere of CO_2 (FCO_2) and CH_4 (FCH_4) from the lakes and rivers of the Amazon basin. The FCO_2 and FCH_4 in lakes was modelled from relations of CO_2 and CH_4 dissolved concentration as a function of lake surface area based on our own data in Ecuadorian highland lakes and data from literature for lowland floodplain lakes (Fig 4.7), using the HydroLAKES spatial data-set (Messager et al. 2016), and the gas transfer velocity (k_{600}) derived from a parameterization as a function of wind speed (Cole and Caraco 1998) and wind speed from the WorldClime spatial data-set (Fick and Hijmans 2017). The FCO_2 and FCH_4 in rivers was modelled from of CO_2 and CH_4 dissolved concentration as a function of catchment slope, k_{600} derived from a parameterization as a function of stream slope and flow (Raymond et al. 2012) and the RiverATLAS spatial data-set (Linke et al. 2019) as detailed by Chiriboga and Borges (2023).

	Elevation	
	<500 m	>500 m
Lakes		
FCH_4 (TgC yr^{-1})	0.0130 ± 0.0036	0.0007 ± 0.0002
FCH_4 (gC m^{-2} yr^{-1})	0.58 ± 0.16	0.75 ± 0.21
Surface area weighted average CH_4 (nmol L^{-1})	179	265
FCO_2 (TgC yr^{-1})	5.7 ± 1.2	0.022 ± 0.005
FCO_2 (gC m^{-2} yr^{-1})	255 ± 55	23 ± 5
Surface area weighted average pCO_2 (ppm)	2,909	530
Wind speed (m s^{-1})	1.4 ± 0.6	3.0 ± 0.6
k_{600} (cm h^{-1})	2.5 ± 0.3	3.5 ± 0.5
Total lake surface area (km^2)	22,282	952
Number of lakes	12,549	1,116
Average lake surface area (km^2)	1.78 ± 15.54	0.85 ± 5.54
Rivers		
FCH_4 (TgC yr^{-1})	0.273 ± 0.084	0.030 ± 0.007
FCH_4 (gC m^{-2} yr^{-1})	6.77 ± 2.08	12.93 ± 2.88
Average CH_4 (nmol L^{-1})	427	157
FCO_2 (TgC yr^{-1})	58.9 ± 4.1	5.5 ± 1.0
FCO_2 (gC m^{-2} yr^{-1})	1,459 ± 103	2,364 ± 418
Average pCO_2 (ppm)	2,702	1,033
k_{600} (cm h^{-1})	15.8 ± 0.4	148.8 ± 3.2
Total stream surface area (km^2)	40,375	2,338

The $\delta^{18}O$-H_2O values were negatively related to elevation and paralleled elevational *gradient based on the global rain water iso-scape (*Inguaggiato et al. 2010) (Fig 4. 2). This indicates that the sampled lakes were mainly recharged by local precipitation (meteoric recharge). The offset between observed $\delta^{18}O$-H_2O values in the sampled lakes and the precipitation elevational gradient most probably resulted from fractionation during evaporation. The observed

δ^2H and $\delta^{18}O$-H_2O values in the sampled lakes deviated from local meteoric water line (LMWL) (Inguaggiato et al. 2010), confirming substantial fractionation during evaporation (Fig 4. S3).

The DOC concentrations ranged between 1.2 and 12.8 mg L^{-1}, and DOC data points were grouped in clusters as a function of several variables such as elevation, lake area, lake depth, conductivity, and water temperature (Fig 4. 3). The three "volcanic" lakes (Cuicocha, Loreto and Papallacta) were characterized by the lowest DOC concentrations (1.2 to 2.3 mg L^{-1}), the two "urban" lakes (San Pablo and Yaguarcocha) were characterized by intermediate DOC concentrations (4.7 to 5.4 mg L^{-1}), and the remaining 10 lakes were characterized by the highest DOC concentrations (8.3 to 12.8 mg L^{-1}). DOC was positively correlated to elevation and negatively related to temperature (excluding the three "volcanic" lakes). This might reflect the higher inputs of soil DOC in lakes more strongly influenced by inputs from the páramos. The negative relation between DOC and conductivity is consistent with the idea that soils richer in organic matter tend to lead to less mineralized water. Low inputs of soil DOC in the three "volcanic" lakes are related to a low ratio of catchment area to lake surface area which reduces the inputs from soils to the lake. Additionally, the DOC content could be partly modulated by lake size, as indicated by the negative relation between DOC concentration and lake area (Fig 4. 3).

Small lakes have a greater connectivity and potential exchange of organic carbon with the riparian wetlands and surrounding terrestrial landscape along its periphery relative to lake surface area than larger lakes (Staehr et al. 2012). The two above explanations of DOC patterns are compatible as lake size decreases with elevation and the smaller lakes were, thus, located in the páramos with organic carbon rich soils. The POC concentrations ranged between 0.4 and 5.7 mg L^{-1}, and the POC data points were less clearly clustered than DOC data points and did not correlate with elevation, lake area, lake depth, or water temperature, but did show a relationship with conductivity (Fig 4. 3). One of the two "urban" lakes (San Pablo) was characterized by the highest POC value (5.7 mg L^{-1}), while the three "volcanic" lakes were characterized by some the lowest POC values (0.4 to 0.6 mg L^{-1}). The correlation of POC with conductivity (excluding the three "volcanic" lakes) might reflect a general dilution pattern by meteoric water of solutes and POC. Variations of DIN were modest (3.6 to 11.0 µmol L^{-1}) and DIN did not significantly correlate with elevation, lake area, lake depth, conductivity and water temperature. DIN was dominated by NH_4^+ (70-98%) that ranged between 3.4 and 9.2 µmol L^{-1}. NH_4^+ did not significantly correlate with elevation, lake area, lake depth, conductivity, and water temperature. NO_3^- ranged between 0.1 and 1.9 µmol L^{-1} and did not significantly correlate with elevation and temperature but correlated positively to lake area, lake depth and conductivity. These correlations might reflect a stronger impact in smaller and shallower water bodies of soil-water inputs with a low NO_3^- content related to denitrification in highland soils (Pineda et al. 2021).

The pCO_2 values ranged between 208 and 10,069 ppm (Fig 4. 4). The pCO_2 data points were distinctly grouped into the same three clusters observed for DOC (Fig 4. 4). The three "volcanic" lakes (Cuicocha, Loreto and Papallacta) were characterized by higher pCO_2 values (3,269-10,069 ppm), the two "urban" lakes (San Pablo and Yaguarcocha) by the lowest pCO_2 values (208-254 ppm), and the other páramo lakes by intermediary pCO_2 values (644-2,152 ppm). All lakes had pCO_2 values above atmospheric equilibrium (400 ppm) and thus acted as sources of CO_2 to the atmosphere, except for the two "urban" lakes that acted as sinks of atmospheric CO_2. The highest pCO_2 values in the three "volcanic" lakes seemed to be in part related to geogenic CO_2 inputs, reflecting the influence of post-volcanic activities, such as emission of volcanic gases and input of hydrothermal water.

Figure 4.3: Particulate (POC in mg L^{-1}) and dissolved (DOC in mg L^{-1}) organic carbon, dissolved inorganic nitrogen (DIN in µmol L^{-1}), NO_3^- (µmol L^{-1}) and NH_4^+ (µmol L^{-1}) in surface waters *versus* elevation (m), lake surface area (km^2), lake depth (m), specific conductivity (µS cm^{-1}) and water temperature (°C). Solid grey lines show fits to the data (Table 4.S2).

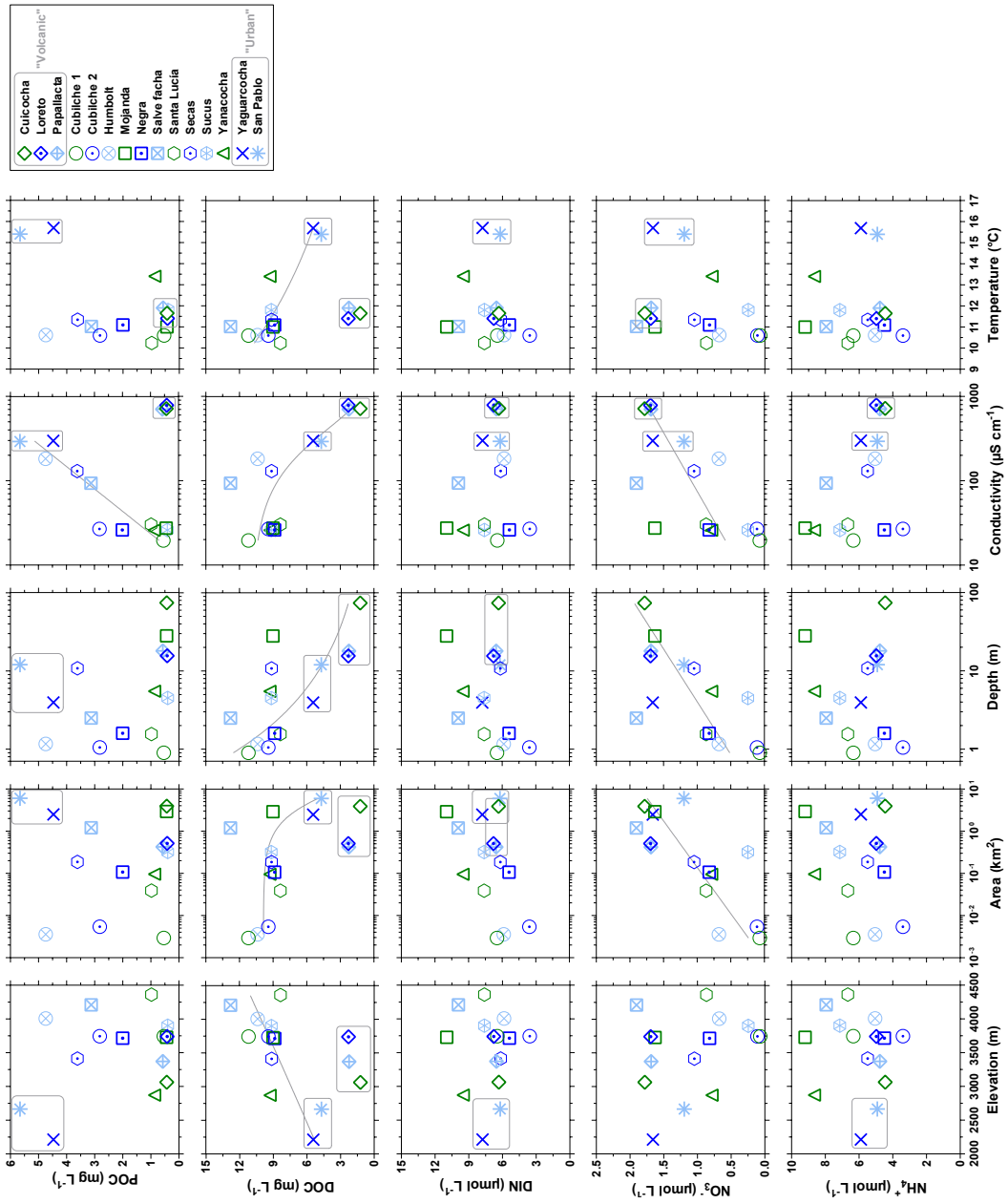

The δ^{13}C-DIC values in surface waters of the "volcanic" lakes were extremely high (~3.5 ‰) (Fig 4. S4), and magmatic inputs likely provide the dominant imprint on δ^{13}C-DIC signatures as also reported in Lakes Kivu (~1.0 ‰) and Sonachi (~9.0 ‰) (also a crater lake) (Borges et al. 2012). The δ^{13}C values of volcanic CO_2 in gas bubbles in Ecuadorian crater lakes range between -2 and -6 ‰ (Inguaggiato et al. 2010; Melián et al. 2021). Consequently, the positive δ^{13}C-DIC values observed in the three "volcanic" lakes also reflect the uptake of ^{12}C by primary production and enrichment in ^{13}C in the residual DIC. This effect might be enhanced by long water residence time typical of small crater lakes devoid of outlets. The two "urban" lakes were also characterized

by enriched δ^{13}C-DIC signatures also indicative of uptake of ^{12}C by primary production consistent with the low pCO_2 values (and high POC values).

Figure 4.4: Partial pressure of CO_2 (pCO_2 in ppm), dissolved CH_4 concentration (nmol L^{-1}), N_2O saturation level (%N_2O in %), O_2 saturation level (%O_2 in %) in surface waters *versus* elevation (m), lake surface area (km^2), lake depth (m), specific conductivity (µS cm^{-1}) and water temperature (°C). Dotted horizontal lines indicate equilibrium of respective gases with the atmosphere and solid grey lines show fits to the data (Table 4.S2).

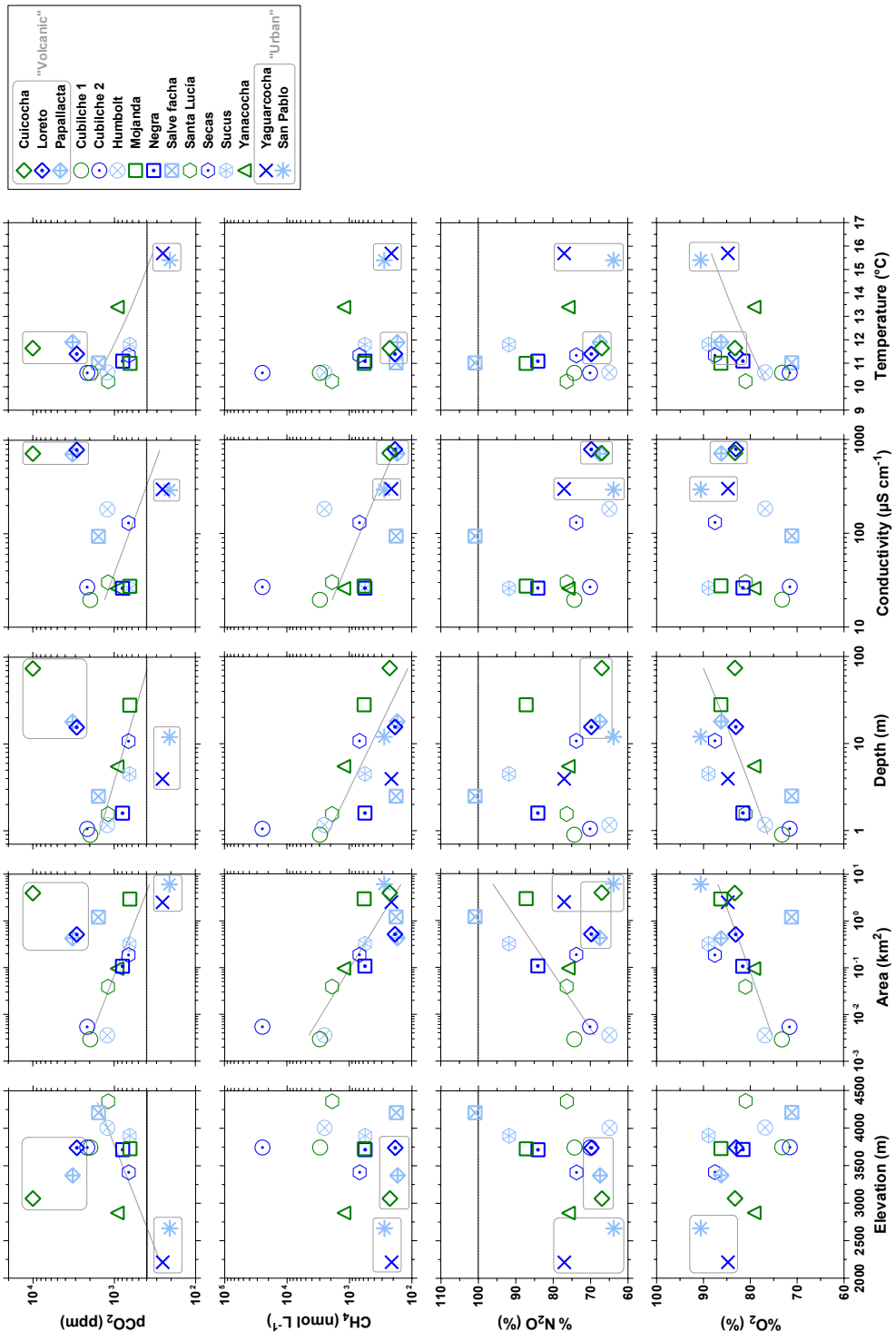

A general increase of δ^{13}C-DIC was observed from (HCO_3^- + CO_3^{2-}):DIC=0.5 (half of the DIC is in the form of CO_2) towards (HCO_3^- + CO_3^{2-}):DIC=1 (all of the DIC is in the form of HCO_3^- + CO_3^{2-}). This pattern reflects a gradient of lakes from systems with low rock weathering due to dominance of deep organic soils (low HCO_3^-) and high CO_2 from respiration leading to (HCO_3^- + CO_3^{2-}):DIC close to 0.5 with low δ^{13}C-DIC, and lakes with higher rock weathering leading to (HCO_3^- + CO_3^{2-}):DIC closer to 1 with high δ^{13}C-DIC.

Figure 4.5: Partial pressure of CO_2 (pCO_2 in ppm) and dissolved CH_4 concentration (nmol L^{-1}) *versus* particulate (POC in mg L^{-1}) and dissolved (DOC in mg L^{-1}) organic carbon and O_2 saturation level (%O_2 in %) in surface. Dotted horizontal lines indicate equilibrium with the atmosphere and solid grey lines show fits to the data (Table 4.S2).

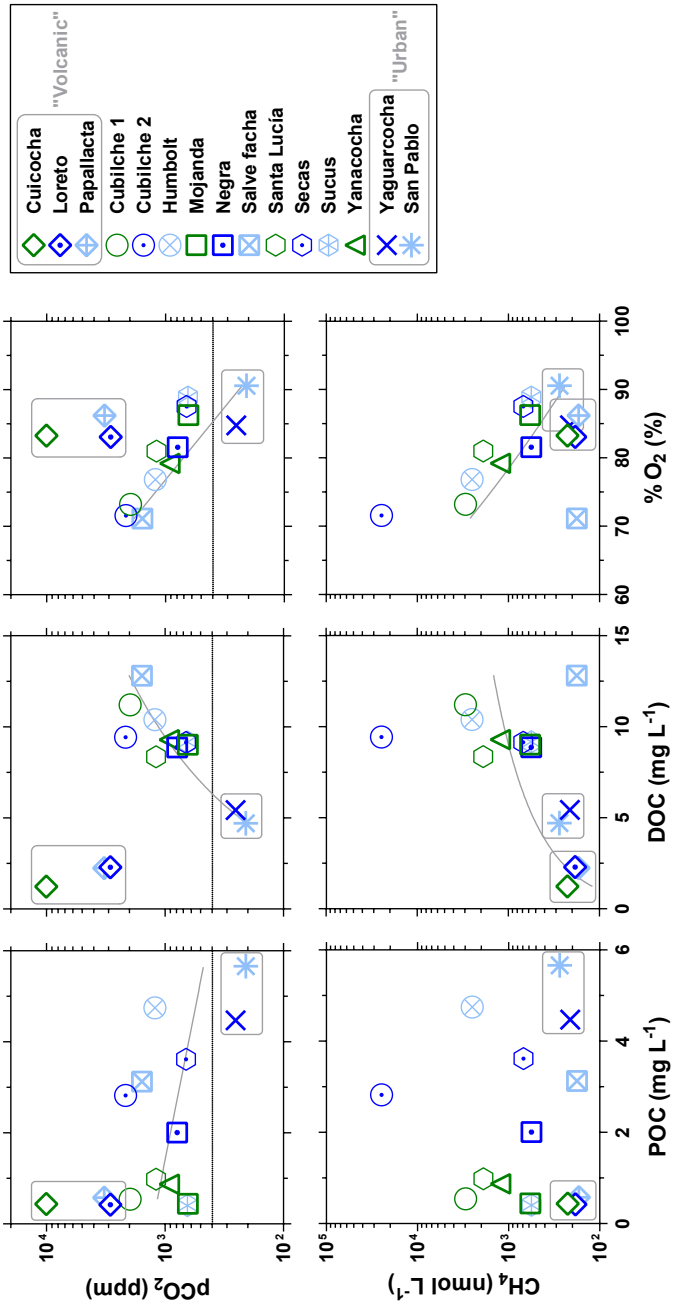

Figure 4.6: N_2O saturation level (%N_2O in %) *versus* NH_4^+ (µmol L^{-1}), dissolved inorganic nitrogen (DIN in µmol L^{-1}), NO_3^- (µmol L^{-1}), NO_2^- (µmol L^{-1}) and O_2 saturation level (%O_2 in %) in surface waters. Dotted horizontal lines indicate equilibrium with the atmosphere and solid grey lines show fits to the data (Table 4.S2).

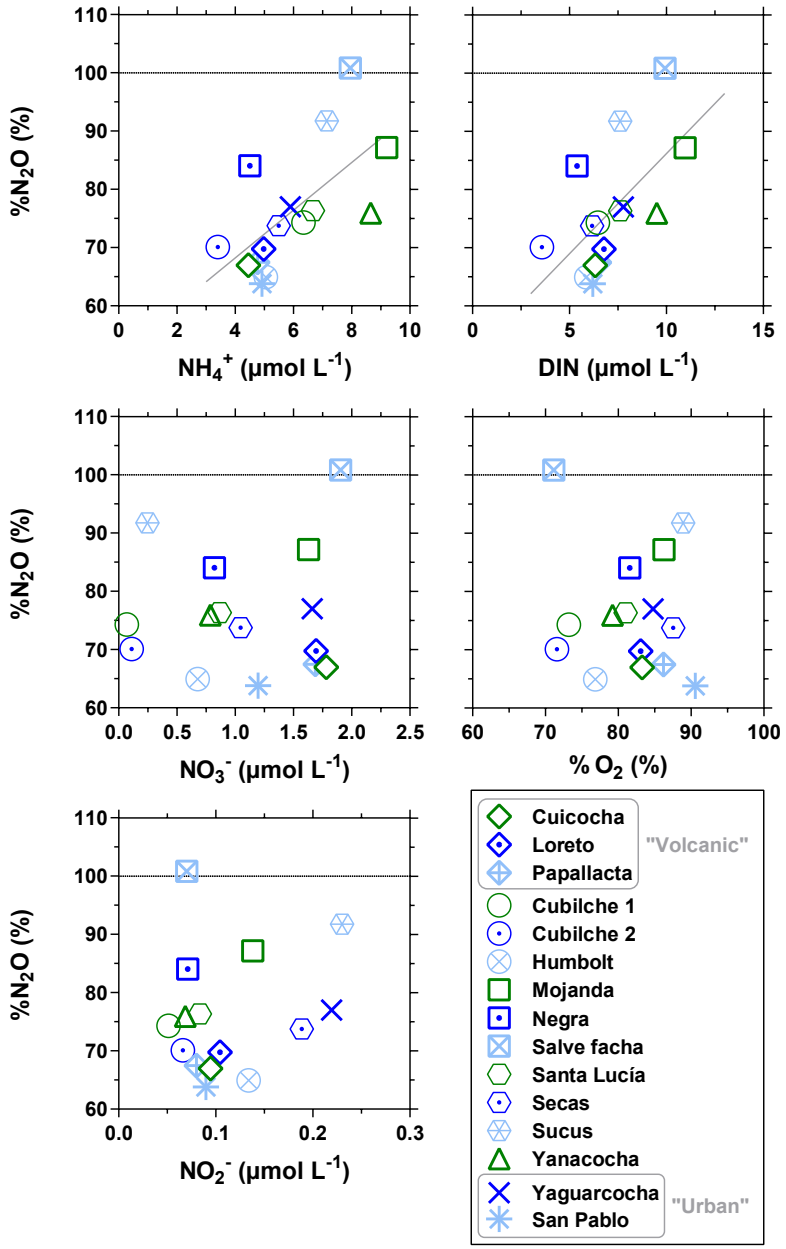

The pCO_2 values in the páramo lakes were positively correlated to elevation and negatively correlated to lake area, lake depth, temperature and conductivity (excluding the three "volcanic" lakes - Cuicocha, Loreto and Papallacta). This is indicative of higher lacustrine pCO_2 values in páramo lakes bordered by soils with a higher organic carbon content, as shown above for DOC (Fig 4. 3). Indeed, pCO_2 was positively correlated to DOC, negatively to %O_2 and POC (Fig 4. 5). This indicates a gradient of inputs of soil water with a low O_2 and conductivity and high DOC and pCO_2 among the páramo lakes that were more important at high elevations owing to

soils with a higher organic matter content. Conversely, in lakes with lower inputs of soil DOC (the "urban" lakes at lower elevation), lower DOC allowed the development of phytoplankton (lesser light limitation) contributing to the decreasing pattern of pCO_2 with decreasing DOC and increasing POC. Additionally, the lakes at higher elevation tended to be shallower and smaller (Fig 4. 2). As mentioned above to explain the pattern of DOC and lake size, smaller lakes have a greater connectivity and potential exchange of CO_2 from soils along its periphery relative to lake surface area (Staehr et al. 2012). Also, there is a stronger fetch limitation of *k* in smaller lakes (Wanninkhof 1992) that can contribute to the accumulation of CO_2 in lake surface water of smaller lakes, while higher *k* in larger lakes promotes gazing and brings CO_2 levels closer to atmospheric equilibrium. These processes combined contribute to explain the negative relation between pCO_2 with lake surface area as well as with lake depth (Fig 4. 4). Since the CO_2 dynamics were related to organic matter degradation (in soils or in-lake), $\%O_2$ correlated to pCO_2 (Fig 4. 5) and $\%O_2$ patterns mirrored those of pCO_2: $\%O_2$ was positively related to lake area, lake depth and water temperature but was not significantly correlated to conductivity and elevation (Fig 4. 4).

Dissolved CH_4 concentrations ranged between 170 and 24,908 nmol L^{-1} in the sampled lakes (Fig 4. 4). Dissolved CH_4 concentrations were not significantly correlated to elevation, water temperature, and POC but were negatively correlated to lake area, lake depth, conductivity, DOC and $\%O_2$ (Figs. 4,5). The patterns of CH_4 paralleled those of pCO_2. The smaller lakes bordered by soils with a higher organic carbon content were likely characterized by a higher CH_4 production in lake sediments or in surrounding soils.

$\%N_2O$ ranged between 63.8 and 100.8%. All the sampled lakes were sinks of atmospheric N_2O except Salve Fecha that was close to saturation (100.8%). This implies a removal of N_2O by denitrification due to the complete reduction of N_2O to N_2. $\%N_2O$ did not significantly correlate to elevation, lake depth, conductivity and temperature, but correlated to lake area (Fig 4. 4). NO_3^- also correlated with lake area (Fig 4. 3). Similar patterns of $\%N_2O$ and NO_3^- as function of lake area might reflect a stronger impact in smaller water bodies of soil-water inputs with low content in N_2O and NO_3^- related to denitrification in highland páramo soils (Pineda et al. 2021). Yet, paradoxically, $\%N_2O$ did not significantly correlate with NO_3^- but correlated with NH_4^+ (and thus also with DIN) (Fig 4. 6), although NH_4^+ did not correlate with lake area (Fig 4. 3). $\%N_2O$ did not also significantly correlate to NO_2^- and $\%O_2$. The general lack of correlation of $\%N_2O$ with other variables might reflect that there was a low internal cycling of N_2O within the lakes, and that the N_2O levels in lakes were primarily controlled by the inputs of soil-water in a low N_2O level related to soil denitrification. Additionally, N_2O was driven closer to equilibrium with the atmosphere in larger lakes where *k* increases with fetch (Wanninkhof 1992). Combined, these two processes led to a relation between $\%N_2O$ and lake surface area.

Comparison with floodplain lakes in central Amazon

The páramo lakes were generally smaller (1.1±1.9 km^2, average ± standard deviation) with higher DOC concentration (9.0±2.2 mg L^{-1}) than the lowland floodplain lakes compiled from literature (183±311 km^2; 5.3±1.1 mg L^{-1}) (Fig 4. 7). Yet, the pCO_2 values in lowland floodplain lakes were higher (3,115±1,605 ppm) than in the páramo lakes (1,037±615 ppm) even for overlapping values of depth, lake surface area and DOC concentrations (Fig 4. 7). This pattern probably resulted from inputs of fluvial CO_2 in the floodplain lakes that led to higher pCO_2 values than in the páramo lakes.

The CH_4 values in the sampled highland lakes were higher (3,564±7,186 nmol L^{-1}) than in the floodplain lakes in the Central Amazon basin (170±215 nmol L^{-1}) compiled from literature (Fig 4. 7). Yet, CH_4 concentration was correlated with depth, lake surface area, and DOC across the full data-set including both highland and lowland lakes. A tighter relation between CH_4 and lake morphology (depth and surface area) would suggest a dominant effect of lake size on the internal production and external inputs from soils of CH_4 despite different settings across the elevational gradient in the whole Amazon basin. Such an effect seems to override the difference in water temperature between highland (12.4±1.9°C) and lowland lakes (30.7±1.4°C), despite the fact that methanogenesis shows a strong temperature dependence (Yvon-Durocher et al. 2014).

This differed from pCO_2 for which there seemed to be a stronger dependency on external local drivers, in particular the connectivity with the river channel in the floodplain lakes. Consequently, a simple "unifying" correlation between pCO_2 and other variables (DOC, lake size) did not emerge for both highland and lowland lakes from our data-set. Since CH_4 was higher and CO_2 lower in highland lakes compared to lowland lakes, the CH_4:CO_2 ratio was markedly higher and also correlated with lake surface area, depth and DOC (Fig 4. 7).

The pCO_2 was not correlated with DOC across the whole basin suggesting that pCO_2-DOC relationship was regionally specific, as also suggested in boreal landscapes (Roehm et al. 2009; Lapierre and del Giorgio 2012). This would suggest that the relation of pCO_2 and DOC results from multiple processes and do not provide consistent and reproducible patterns across large regions as noted in boreal landscapes. This is possibly related to regional patterns in DOC composition and/or in landscape morphology and lake position in the landscape that dictate the amount and relative proportions of DOC and CO_2 exports from soils to lakes (Roehm et al. 2009; Lapierre & del Giorgio 2012). This is also in line with a recent analysis of pCO_2 in African lakes showing diverging pCO_2-DOC relations in different type of lakes, in particular in humic and non-humic lakes (Borges et al. 2022). In our particular case, the difference between highland and lowland pCO_2-DOC patterns is most likely related to the strong influence of riverine inputs in lowland floodplain lakes. It is unclear if the correlation between CH_4 and DOC is spurious or reflects a causal relation. This relation could be spurious because shallower lakes tend to have higher CH_4 concentrations due to lower effect of the removal of CH_4 by MOX and stronger effect of CH_4 inputs from sediments or soils (Borges et al. 2011; Holgerson and Raymond 2016). Shallower lakes tended to be smaller in our data-set, and smaller water bodies tend to have higher DOC concentrations because small lakes have a greater connectivity and potential exchange of organic carbon with the riparian wetlands and surrounding terrestrial landscape along its periphery relative to lake surface area than larger lakes (Staehr et al. 2012).

Emissions of CO_2 and CH_4 from lakes and streams of the Amazon basin.

We use relationships as a function of lake surface area (Fig 4. 7) to scale pCO_2 and dissolved CH_4 concentration to the all the lakes in the Amazon basin (n=12,549) given by the HydroLAKES data-set (Messager et al. 2016). For CH_4, there was a robust relation with lake surface area across the whole Amazon basin. For consistency, we also used a relation as function of lake surface area to scale pCO_2 but two separate relations were needed for highland and lowland lakes. Such an approach is applicable because the distribution of lake numbers and surface areas given by HydroLAKES follows a bimodal distribution with the majority located in lowlands (elevation < 500 m) followed by highlands (elevation > 2,500 m) with very few lakes located at elevations between 500 and 2,500 m (Fig 4. S5).

The CH_4 emission (0.0007 TgC yr^{-1}) from highland lakes (elevation >500m) was 18 times lower than from lowland lakes (elevation <500m) (0.0130 TgC yr^{-1}) (Table 4.1). This was due to the fact that lakes in lowlands were 11 times more numerous (12,549 *versus* 1,116) and covered a surface area 23 times larger (22,282 *versus* 952 km^2) than in highlands (Fig 4. S5, Table 4.1). The average areal FCH_4 (per m^2) was in fact 1.3 times higher in highland lakes (0.75 gC m^{-2} yr^{-1}) than in lowland lakes (0.58 gC m^{-2} yr^{-1}) owing to the combination of higher dissolved CH_4 concentration (265 nmol L^{-1} *versus* 179 nmol L^{-1}) and higher k values (3.5 cm h^{-1} vs 2.5 cm h^{-1}). The average dissolved CH_4 concentration was higher in highland lakes because they were on average smaller (0.85 km^2) than lowland lakes (1.78 km^2). The k values were on average higher in highland lakes because of higher average wind speed (3.0 m s^{-1}) than lowland lakes (1.4 m s^{-1}) (Table 4.1).

The CO_2 emission (0.022 TgC yr^{-1}) from highland lakes was 257 times lower than from lowland lakes (5.7 TgC yr^{-1}) (Table 4.1). The average areal FCO_2 was also 11 times lower in highlands (23 gC m^{-2} yr^{-1}) than in lowlands (255 gC m^{-2} yr^{-1}) owing to the lower pCO_2 values (530 ppm *versus* 2,909 ppm) despite higher k values (3.5 cm h^{-1} *versus* 2.5 cm h^{-1}).

The total lacustrine emissions of CH_4 (0.01 TgC yr^{-1}) and of CO_2 (5.71 TgC yr^{-1}) were, respectively, 22 and 11 times lower than the fluvial emissions of CH_4 (0.31 TgC yr^{-1}) and CO_2

(64.42 TgC yr^{-1}) at the scale of the Amazon basin (Table 4.1). The relative contribution of the lacustrine FCH_4 to total carbon emissions (CO_2+CH_4) was low, yet more important in highland lakes (3.1%) that in lowland lakes (0.2%). The relative contribution of FCH_4 to total carbon emissions (CO_2+CH_4) for the whole Amazon basin (both high- and low-lands) was similarly low in lakes (0.2%) and rivers (0.5%).

Figure 4.7: Partial pressure of CO_2 (pCO_2 in ppm), dissolved CH_4 concentration (nmol L^{-1}) and CH_4:CO_2 ratio (µmol:µmol) *versus* lake surface area (km^2), lake depth (m) and dissolved organic carbon (DOC in mg L^{-1}). Samples in highland lakes in Northern Ecuador (excluding lakes Cuicocha, Loreto and Papallacta influenced by volcanic inputs) and in lowland floodplain lakes of the Amazon basin gathered from literature (Abril et al. 2013; Albéric et al. 2018; Amaral et al. 2020; Barbosa et al. 2016; Mitchell et al. 2018). For pCO_2 only data directly measured by equilibration were compiled, data computed from pH and total alkalinity were excluded as they can be prone too large errors (Abril et al. 2015). Dotted horizontal lines indicate equilibrium with the atmosphere and solid lines show fits to the data (Table 4.S2) (blue solid lines = highland lakes; black solid lines =lowland lakes; grey dotted lines = high- and low-land lakes).

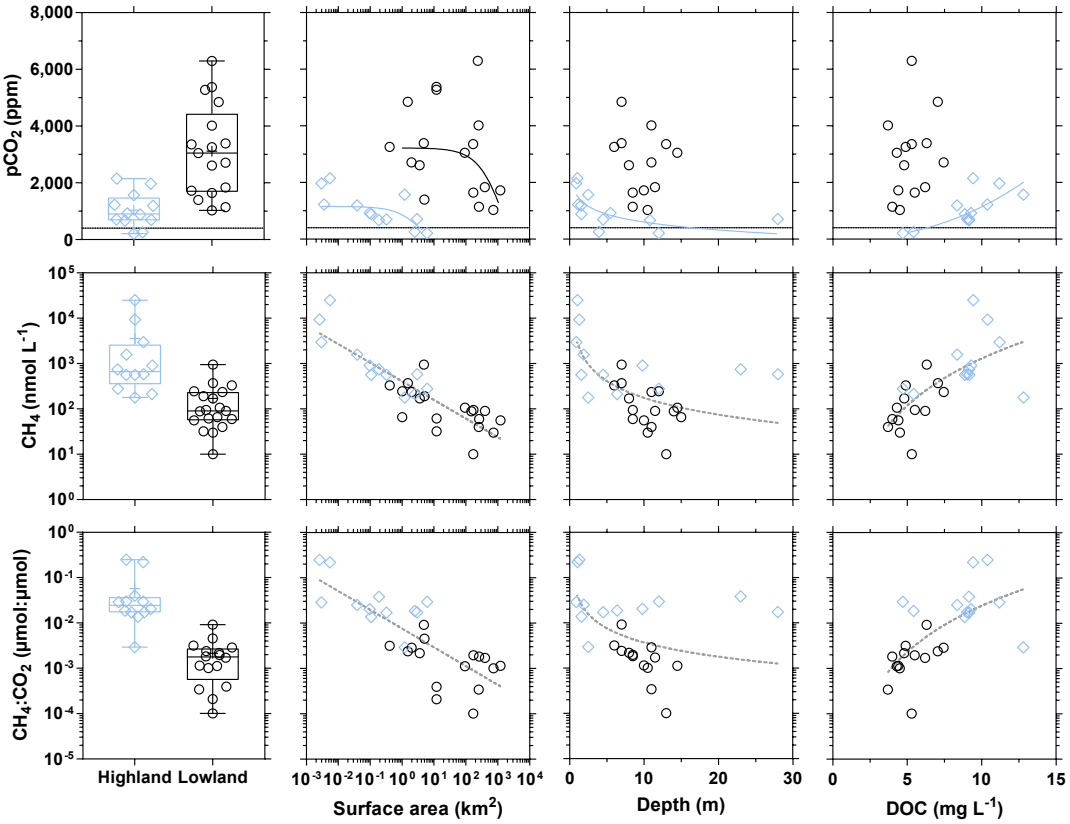

Conclusions

Global estimates of CO_2, CH_4 and N_2O emissions from lakes and rivers are uncertain because available data-sets do not capture the inherent large variability, and are insufficient to derive robust statistical functions to scale fluxes with confidence, despite the recent emergence of detailed spatial data-sets of location and surface area for rivers (Allen and Pavelsky 2018; Linke et al. 2019) and lakes (Messager et al. 2016) that can be used to scale fluxes. Tropical lakes are under-sampled with regards to GHG emissions compared to higher latitude systems, and this is particularly true for mountainous lakes. The surface-area averaged pCO_2 of 465 ppm we reported for 12 Andean mountainous lakes at elevations between ~2,200 and ~4,350 m (excluding three lakes influenced by volcanic activity) was lower than the values usually attributed

to tropical lakes of ~1,900 ppm (Aufdenkampe et al. 2011; Raymond et al. 2013; Marotta et al. 2009). The average pCO_2 in the sampled 12 Andean mountainous lakes was also lower than in the floodplain lakes of the Central Amazon with a surface averaged pCO_2 of 2,020 ppm. The surface-area averaged CH_4 in the 12 Andean mountainous lakes of 322 nmol L^{-1} was higher than in the floodplain lakes of the Central Amazon with a surface-area averaged CH_4 of 58 nmol L^{-1}. The CO_2 and CH_4 emissions from highland lakes only represented 0.4% and 5.2% of the total lacustrine emissions at the scale of the Amazon basin. Total CO_2 and CH_4 emissions from lakes (5.7 TgC yr^{-1}) represented a small fraction (8%) of total lentic and lotic CO_2 and CH_4 emissions at the scale of the Amazon basin (70.5 TgC yr^{-1}).

Acknowledgments

We thank Yannick Stroobandt for analytical assistance with stable isotope and POC and DOC concentration measurements, and Gwenaël Abril for providing CH_4 data in Central Amazonian lakes. This research was funded by the *Académie de recherche et d'enseignement supérieur* (ARES). AVB is a research director at the *Fonds National de la Recherche Scientifique*.

Supplementary material

TABLE 4S.1: Major cations (Na^+, K^+, Mg^{2+}, Ca^{2+}) (in mg L^{-1} and µequivalents L^{-1}) in surface waters.

	Na^+ mg L^{-1}	K^+ mg L^{-1}	Mg^{2+} mg L^{-1}	Ca^{2+} mg L^{-1}	Na^+ µeq L^{-1}	K^+ µeq L^{-1}	Mg^{2+} µeq L^{-1}	Ca^{2+} µeq L^{-1}	Cation sequence
Cubilche 1	1.6	1.2	0.6	1.7	69	30	48	84	$Ca^{2+}>Na^+>Mg^{2+}>K^+$
Cubilche 2	1.6	1.4	0.6	1.8	70	35	51	88	$Ca^{2+}>Na^+>Mg^{2+}>K^+$
Cuicocha	62.3	5.7	34.6	44.4	2,709	145	2,845	2,216	$Na^+>Ca^{2+}>Mg^{2+}>K^+$
Humbolt	16.4	5.0	9.2	9.7	711	128	760	485	$Na^+>Ca^{2+}>Mg^{2+}>K^+$
Loreto	60.6	5.8	34.2	43.7	2,637	149	2,814	2,179	$Na^+>Ca^{2+}>Mg^{2+}>K^+$
Mojanda	1.7	1.2	0.6	1.6	73	30	48	78	$Ca^{2+}>Na^+>Mg^{2+}>K^+$
Negra	1.8	1.3	0.6	1.6	78	33	50	81	$Ca^{2+}>Na^+>Mg^{2+}>K^+$
Papallacta	60.6	5.7	34.4	43.7	2,637	145	2,828	2,182	$Na^+>Ca^{2+}>Mg^{2+}>K^+$
Salve Faccha	10.2	1.5	2.2	7.4	445	38	184	369	$Na^+>Ca^{2+}>Mg^{2+}>K^+$
San Pablo	23.7	4.0	12.7	16.9	1,032	104	1,046	845	$Na^+>Ca^{2+}>Mg^{2+}>K^+$
Santa lucía	1.6	1.2	0.6	1.8	71	31	52	88	$Ca^{2+}>Na^+>Mg^{2+}>K^+$
Secas	10.6	3.3	5.8	6.9	459	83	475	343	$Na^+>Ca^{2+}>Mg^{2+}>K^+$
Sucus	1.64	1.18	0.58	1.60	71	30	48	80	$Ca^{2+}>Na^+>Mg^{2+}>K^+$
Yaguarcocha	24.0	4.2	12.7	17.0	1,045	107	1,046	848	$Na^+>Ca^{2+}>Mg^{2+}>K^+$
Yanacocha	1.57	1.19	0.58	1.58	68	30	48	79	$Ca^{2+}>Na^+>Mg^{2+}>K^+$

TABLE 4S.2: Equations and statistics at 0.05 level of curve fits of data shown in **Figures 4...**

Fig.	Function	Equation	r^2	*p*	*n*
2	surface area *versus* elevation	Y = -0.001756*X + 7.4	0.32	0.0272	15
2	log(depth) *versus* elevation	Y = -0.0004121*X + 2.151	0.18	0.1150	15
2	log(water temperature) *versus* log(elevation)	Y = -0.6515*X + 3.376	0.84	<0.0001	15
2	$\delta^{18}O$-H_2O *versus* elevation	Y = -0.001312*X - 2.713	0.26	0.0636	15
2	conductivity *versus* elevation	Y = -0.1072*X + 479	0.43	0.0204	12 *
2	TA *versus* elevation	Y = -0.001162*X + 5.084	0.44	0.0189	12 *
3	POC *versus* log(conductivity)	Y = 3.767*X - 4.175	0.85	<0.0001	12 *
3	log(DOC) *versus* log(elevation)	Y = 1.074*X - 2.865	0.61	0.0029	12 *
3	log(DOC) *versus* log(surface area)	Y = -0.04877*X + 0.9942	0.56	0.0052	12 *
3	log(DOC) *versus* log(depth)	Y = -0.3862*X + 1.081	0.55	0.0016	15
3	log(DOC) *versus* conductivity	Y = -0.001015*X + 1.035	0.89	<0.0001	15
3	log(DOC) *versus* temperature	Y = -0.05368*X + 1.578	0.69	0.0008	12 *
3	NO_3^- *versus* log(surface area)	Y = 0.4539*X + 1.388	0.62	0.0005	15
3	NO_3^- *versus* log(depth)	Y = 0.7412*X + 0.5505	0.47	0.0049	15
3	NO_3^- *versus* log(conductivity)	Y = 0.7178*X - 0.3462	0.48	0.0041	15
4	log(pCO_2) *versus* elevation	Y = 0.0003642*X + 1.626	0.56	0.0054	12 *
4	log(pCO_2) *versus* log(surface area)	Y = -0.2228*X + 2.74	0.60	0.0033	12 *
4	log(pCO_2) *versus* log(depth)	Y = -0.3118*X + 3.176	0.59	0.0092	10 **
4	log(pCO_2) *versus* log(conductivity)	Y = -0.4246*X + 3.668	0.38	0.0338	12 *
4	log(pCO_2) *versus* log(temperature)	Y = -3.824*X + 7.105	0.72	0.0005	12 *
4	log(CH_4) *versus* log(surface area)	Y = -0.4573*X + 2.53	0.69	0.0001	15
4	log(CH_4) *versus* log(depth)	Y = -0.6757*X + 3.323	0.42	0.0085	15
4	log(CH_4) *versus* log(conductivity)	Y = -0.6283*X + 4.089	0.40	0.0111	15
4	%N_2O *versus* log(surface area)	Y = 8.459*X + 89.49	0.65	0.0048	10 **
4	log(%O_2) *versus* log(surface area)	Y = 0.01921*X + 1.924	0.39	0.0122	15
4	log(%O_2) *versus* log(depth)	Y = 0.03767*X + 1.884	0.43	0.0082	15
4	log(%O_2) *versus* log(temperature)	Y = 0.3271*X + 1.555	0.38	0.0139	15
5	log(pCO_2) *versus* POC	Y = -0.07622*X + 3.107	0.20	0.1421	12 *
5	log(pCO_2) *versus* log(DOC)	Y = 2.287*X + 0.7695	0.77	0.0002	12 *
5	pCO_2 *versus* %O_2	Y = -83.21*X + 7766	0.82	<0.0001	12 *
5	log(CH_4) *versus* log(DOC)	Y = 1.068*X + 1.981	0.29	0.0393	15
5	log(CH_4) *versus* log(%O_2)	Y = -9.975*X + 21.9	0.31	0.0320	15
6	%N_2O *versus* NH_4^+	Y = 4.101*X + 51.83	0.42	0.0088	15
6	%N_2O *versus* DIN	Y = 3.441*X + 51.79	0.38	0.0150	15
7	log(pCO_2) *versus* surface area (highland)	Y = -0.1293*X + 3.063	0.58	0.0039	12 *
7	log(pCO_2) *versus* surface area (lowland)	Y = -0.0003745*X + 3.508	0.26	0.0376	17
7	pCO_2 *versus* log(depth) (highland)	Y = -927.4*X + 1531	0.52	0.0083	12 *
7	log(pCO_2) *versus* log(DOC) (highland)	Y = 2.287*X + 0.7695	0.77	0.0002	12 *
7	log(CH_4) *versus* log (surface area) (highland+lowland)	Y = -0.3753*X + 2.545	0.71	<0.0001	34 *
7	log(CH_4) *versus* log (depth) (highland+lowland)	Y = -1.232*X + 3.477	0.44	0.0001	28 *
7	log(CH_4) *versus* log (DOC) (highland+lowland)	Y = 3.442*X - 0.33	0.50	<0.0001	25 *
7	log(CH_4:CO_2) *versus* log (surface area) (highland+lowland)	Y = -0.4136*X - 2.118	0.63	<0.0001	28 *
7	log(CH_4:CO_2) *versus* log (DOC) (highland+lowland)	Y = 3.391*X - 5.006	0.43	0.0004	25 *
7	log(CH_4:CO_2) *versus* log (depth) (highland+lowland)	Y = -1.042*X - 1.39	0.27	0.0074	25 *
S1	Ca^{2+} *versus* Na^+	Y = 0.6659*X + 0.4364	0.99	<0.0001	12 *
S1	Mg^{2+} *versus* Na^+	Y = 0.5443*X - 0.4691	0.96	<0.0001	12 *
S1	TA *versus* Na^+	Y = 0.1261*X - 0.05166	0.97	<0.0001	12 *
S1	K^+ *versus* Na^+	Y = 0.1487*X + 1.022	0.81	<0.0001	12 *
S1	DSi^+ *versus* Na^+	Y = 0.8402*X - 0.7169	0.94	<0.0001	12 *
S1	Fe *versus* Na^+	Y = -2.512*X + 97.74	0.89	<0.0001	12 *
S2	log(Fe) versus DOC	Y = 0.06804*X + 1.284	0.87	<0.0001	15
S3	δD *versus* $\delta^{18}O$-H_2O	Y = 5.131*X - 19.57	0.91	<0.0001	15
S4	log(pCO_2) *versus* $\delta^{13}C$-DIC	Y = -0.06483*X + 2.258	0.44	0.0196	12 *
S4	$\delta^{13}C$-DIC versus (HCO_3^- + CO_3^{2-}):DIC	Y = 0.02482*X + 1.092	0.53	0.0069	12 *

* Excluding "volcanic" lakes (Cuicocha, Loreto and Papallacta)

** Excluding "volcanic" lakes (Cuicocha, Loreto and Papallacta) and "urban" lakes (Yaguarcocha and San Pablo)

FIGURE 4S.1: Major cations (K^+, Mg^{2+}, Ca^{2+} in mg L^{-1}), dissolved silica (DSi) (mg L^{-1}), total alkalinity (TA in mmol L^{-1}) and Fe (µg L^{-1}) versus Na^+ in surface waters of fifteen highland lakes in Northern Ecuador (Fig 4. 1). Solid grey lines show fits to the data (Table 4.S2).

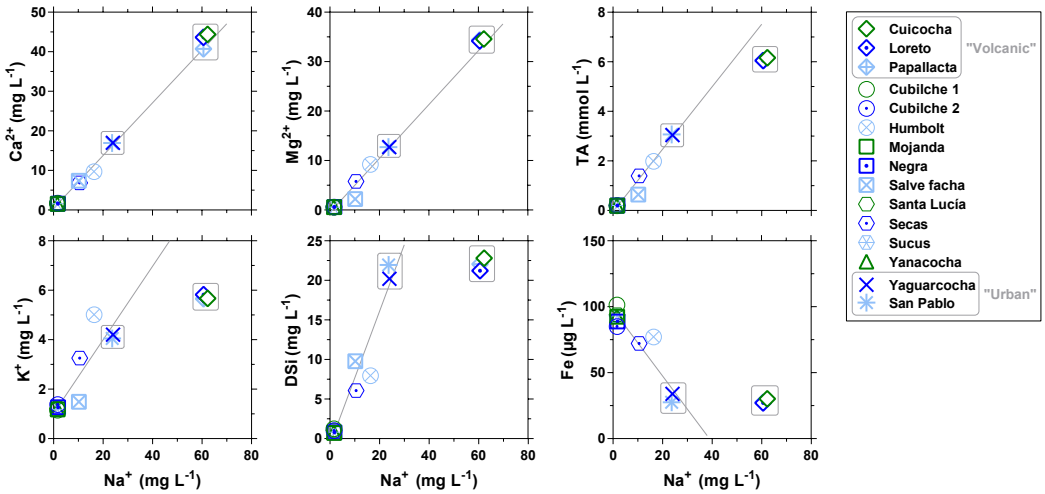

FIGURE 4S.2: Fe (µg L^{-1}) *versus* dissolved organic carbon (DOC in mg L^{-1}) in surface waters of fifteen highland lakes in Northern Ecuador (Fig 4. 1). Solid grey line shows fit to the data (Table 4.S2).

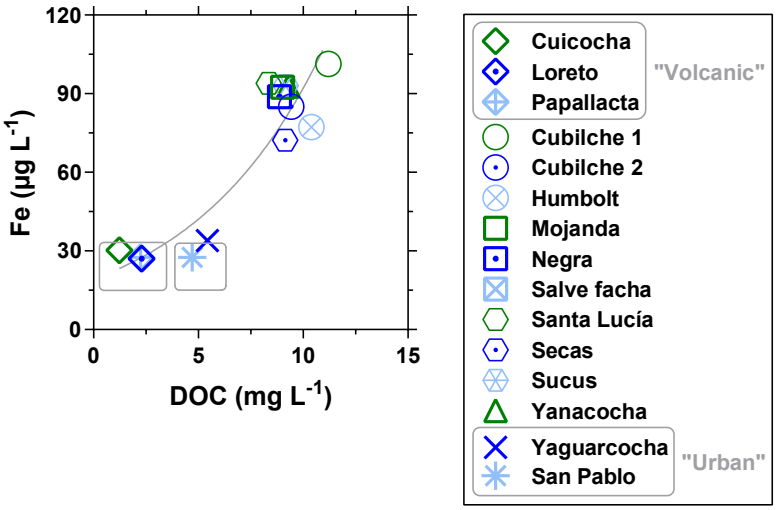

FIGURE 4S.3: Stable.isotope composition of H and O of H_2O ($\delta^{18}O$-H_2O and δD-H_2O in ‰) in surface waters of fifteen highland lakes in Northern Ecuador (Fig 4. 1). Solid grey line shows fit to the data (Table 4.S2) and gives the local evaporative line (LEL). Dotted line is the local meteoric water line (LMWL) (Inguaggiato et al. 2010).

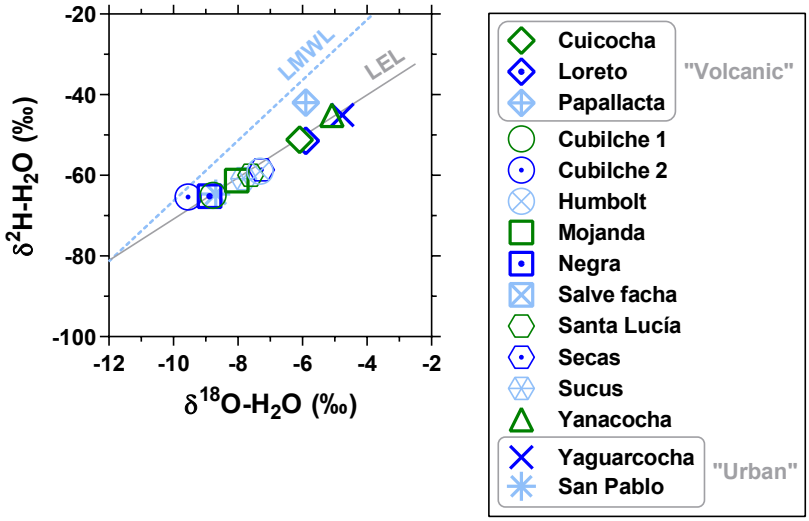

FIGURE 4S.4: Partial pressure of CO_2 (pCO_2 in ppm) and the ratio of HCO_3^-+CO_3^{2-} to dissolved inorganic carbon (DIC) (mol:mol) *versus* the stable.isotope composition of DIC ($\delta^{13}C$-DIC in ‰) in surface waters of fifteen highland lakes in Northern Ecuador (Fig 4. 1). Solid grey lines show fits to the data (Table 4.S2).

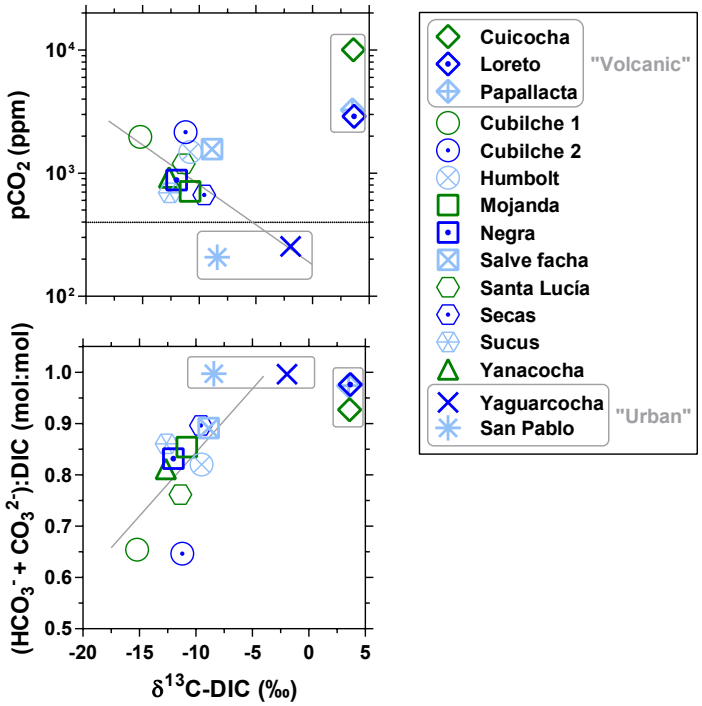

FIGURE 4S.5: Lake counts and cumulated lake surface area (km^2) as function of elevation (in m by bins of 500 m) in the Amazon basin from the HydroLAKES spatial data-set (Messager et al. 2016).

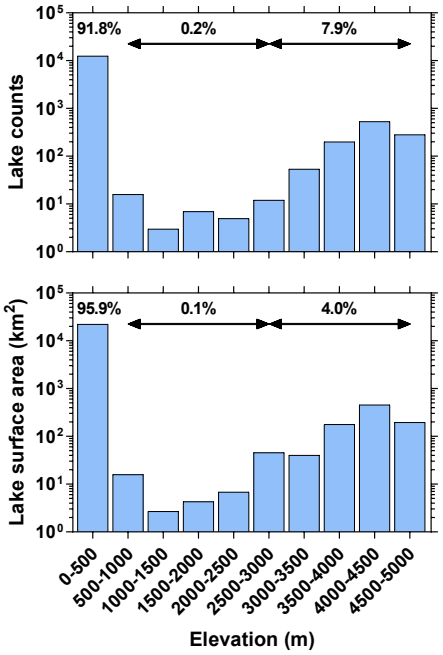

CONCLUSIONS

This study provides 1) the first large-scale survey across an altitudinal gradient of CO_2, CH_4, and N_2O exchange between Andean mountainous streams of the Amazon River basin and the atmosphere 2) the C dynamics within the Basin based on properties such as TSM, DOC, POC, specific conductivity, total alkalinity, stable isotope ratios, and three optical proxies of CDOM and 3) the dissolved concentrations of CO_2, CH_4, and N_2O in 15 lakes located in the northern region of Ecuadorian Andes along an elevational gradient from 2,213 to 4,361 m above sea level.

Reveling the significance of the project.

Understanding the functioning of the natural drivers of the C and N cycles is crucial to face climate change. Inland waters are the primary natural source of greenhouse gases for CO_2 (~21%) and CH_4 (~41%), and the third one for N_2O (~2%). In this sense, estimates of CO_2 emissions from inland waters could range from 0.7 to 2.9 PgC yr^{-1}, being the most probable value of 2.1 PgC yr^{-1}(Borges et al., 2015c; Raymond et al., 2013), This number is significant considering global anthropogenic CO2 emissions total 10.0 PgC yr^{-1}. Compared with the primary natural C sinks, these emissions are similar to the uptake capacity of all oceans (2.0 PgC yr^{-1}) and slightly lower than the total land sink (3.1 PgC yr^{-1}). Collectively, aquatic ecosystems contribute 41% of total global CH_4 emissions from anthropogenic sources (359 $TgCH_4$ yr^{-1}) (Saunois et al., 2020), which is equivalent to the enteric fermentation and manure management (111 TgCH4 yr^{-1}) and rice paddies (30 $TgCH_4$ yr^{-1}) together. Estimates of N_2O emissions from rivers have been dramatically revised downwards to 0.4 Tg N yr^{-1}, which represents ~1.7% of the natural and anthropogenic sources (Tian et al., 2020); nevertheless, N_2O has a GWP 273 times that of CO_2 for a 100-year timescale. Despite these data, GHGs from inland waters have not been fully incorporated into national GHG inventories due to the uncertainties in estimations, the paucity of in situ direct measures, the spatial skewing in sampling, and the immense heterogeneity between ecosystems and driving factors. With about 44% of the global inland waters surface (Raymond et al., 2013), the tropics can produce ~60-80% of CO_2, ~70% of CH_4, and ~79% of N_2O of the global inland water emissions. Favorable conditions in the tropics are adequate for GHG formation within the water body and surrounding ecosystems. For instance, temperature, light availability, hydrological inputs, plenty of labile organic C, bacterial degradation, biogeochemical processing, and connectivity between riparian zones and the watershed (Borges et al., 2015a; Stanley et al., 2015). Therefore, several studies encompassing the most significant number of drivers and territories in the tropics are required to comprehensively understand biogeochemical cycles.

The interest in CO_2 evasion fluxes has centered mainly on rivers draining low-altitude catchments, mostly in boreal regions. Nevertheless, mountains account for 25% of the Earth's land surface, and their streams contribute more than a third to the global runoff (Meybeck et al., 2001). Higher CO_2, CH_4, and N_2O emissions from low-order streams in the mountains are characterized by high gas transfer velocity (k) (Ulseth et al., 2019). This massive degassing results in concentrations of CO_2 and CH_4 close to equilibrium with the atmosphere (Crawford et al., 2015). This gap has increased uncertainty in global GHG estimates since models employ spatial extrapolations without considering particular evasion rates from rivers of Strahler order 1 or 2 (width < 200m). Consequently, the studies should incorporate specific information on ecosystems scarcely sampled, such as the Andean zone of South America.

As important as measuring GHGs is understanding the C dynamics that produce them. For instance, it is known that Andes are a crucial source of sediments and dissolved matter to the Amazon River, the largest single source of fresh water and OC to the oceans (Gibbs, 1967). In

the Amazon basin, the average export of DOC and POC are 21.6 and 14.4 Tg yr^{-1} (Richey et al., 1990). Of these, between 30 and 50% of the POC could have Andean origin in large tributaries such as the Óbidos River (Hedges et al., 2000; Quay et al., 1992). Unlike POC, DOC appears to derive mainly from lowland sources. So, the study includes a report of the C dynamics within the Basin. Like rivers, lacustrine systems have also been under-sampled in the tropics; nonetheless, the CH_4 emissions from lakes are disproportionately more intense than their higher latitude counterparts (Bastviken et al., 2011; Rosentreter et al., 2021), possibly, due to the higher phytoplankton production in non-humic lakes and the high CH_4 methanogenesis rates, driven by light availability and temperatures in tropics, respectively. A particular ecosystem of the tropics is the páramo located between 3,000 to 4,300 m. with intensive peat formation and many wetlands and lakes. However, the low temperature significantly limits the development of biochemical processes.
Ecuador is the smallest of the 17 megadiverse countries in the world and harbors an astounding number of ecosystems (Cuesta et al., 2017), which offered the conditions to study in a relatively small space, the GHGs evasions of the Napo, as well as a diverse lacustrine system. First, the fluvial system includes 44 stations along the Napo and Coca Rivers basin (25 main rivers and 19 tributary rivers). The campaigns included the Andean páramos (>3,000 m), the highlands (3,000 – 1,500 m), the foothills (1,500 – 500), and the lowlands of the Napo basin (<500 m). Second, a lacustrine system composed of 15 lakes located in the Andean páramos and the highlands (4,361 -2,213 m) with different characteristics of size (0.003 to 6.1 km^2), depth (0.9 to 74 m) and type (moorland, urban, and volcanic lakes). Together, the two stages focus on areas whose ecosystems are analogous to more than 13% of the Amazon basin and for which there are few emissions records.

GHGs dynamics in the Napo River Basin

We sampled 25 stations in the mainstem Napo and Coca rivers and 19 stations in the tributaries along an elevation gradient from 3990 m to 175 m on eight occasions from 2018 to 2021. The sampled streams were over-saturated in CO_2 and CH_4; consequently, the flux was unidirectional from the water to the atmosphere (emission). In contrast, N_2O oscillated between under and over-saturation, corresponding to a sink or source of N_2O in the atmosphere.

The pCO_2 and dissolved CH_4 concentration values in streams at elevations > 500 m (median 560 ppm and 17 nmol L^{-1}, respectively) were distinctly lower than at elevations < 500 m (median 1,280 ppm and 370 nmol L^{-1}) and increased exponentially from highlands to lowlands. By including O_2 in the analysis, we observed that the $\%O_2$ decreased exponentially from highlands to lowlands. For instance, values in streams at elevations > 500 m (median 74.4 %) were higher than at elevations < 500 m (median 63.2 %). This trend suggests that the same input and output processes controlled pCO_2 and dissolved CH_4 concentration. For instance, at highlands, CO_2 and CH_4 degasification (high k values), primary production (clear waters that enables photosynthesis), and water aeration (turbulence and velocity). Conversely, lowlands intensive respiration (O2 consumption), organic matter mineralization (wetlands presence), low light penetration (black and white waters), low oxygen availability (methanogenesis), and low degassing rates (low k values).

Temperature varies markedly with altitude and controls the rates of respiration and methanogenesis in soils and riverine sediments. The outcomes suggest the warmer conditions in the lowland rivers contributed to higher pCO_2 and dissolved CH_4 concentration values since pCO_2 and dissolved CH_4 concentration values increased exponentially with water temperature. The variability of land cover changed considerably with elevation. A clear transition from the dominance of grasslands in uplands (páramos) to evergreen forests in lowlands was observed.

Stream pCO_2 and dissolved CH_4 concentration values increased exponentially with forest cover and were generally higher where grassland cover was low to zero. Also, pCO_2 and dissolved CH_4 concentration values were found to be negatively related to the catchment slope due to massive evasions but directly related with$\%O_2$. Both phenomena imply the same result of oxygenation of the water.

The N_2O saturation levels ($\%N_2O$) in streams at an altitude > 500 m (median 95.4 %) were lower than at elevations < 500 m (median 105.0 %). The $\%N_2O$ increased exponentially with decreasing elevation, although lower than for the other GHGs. Lower N_2O in high-elevation streams was consistent with reported elevation gradients of N_2O soil-air fluxes in the Ecuadorian Andes, with a soil N_2O sink at high elevation (2,200-3,010 m) and an N_2O source from soils to the atmosphere at lower elevation (400-1,100 m). The removal of N_2O in soils was due to complete denitrification (reduction of N_2O to N_2) in highlands related to low soil dissolved inorganic N (DIN) content. The combination of higher stream DIN and low $\%N_2O$ in highland streams and the opposite pattern in lowland streams led to a negative relation between $\%N_2O$ and DIN. Such a negative relation is unique compared to previously reported patterns, as N_2O content in rivers is generally positively related to DIN.

The air-water diffusive flux of CO_2 (FCO_2) ranged between -1 and 1,074 mol m^{-2} yr^{-1} and was higher in tributaries (median 128 mol m^{-2} yr^{-1}) than in the main stem (median 34 mol m^{-2} yr^{-1}). The air-water diffusive flux of CH_4 (FCH_4) ranged between 45 and 8,985 mmol m^{-2} yr^{-1} and was also higher in tributaries (median 999 mmol m^{-2} yr^{-1}) than in the main stem (332 mmol m^{-2} yr^{-1}). Both FCO_2 and FCH_4 were inversely correlated to elevation and upstream terrain slope. The air-water diffusive flux of N_2O (FN_2O) ranged between -23 and 27 mmol m^{-2} yr^{-1} and did not show a marked difference between tributaries and the main stem. There was a general tendency towards a sink of N_2O at an elevation > 1,000m, with 12 sites showing negative FN_2O values and only 4 showing positive FN_2O values. At an elevation < 1,000m, the FN_2O values were close to zero ($^{-1}$.3 to 3 mmol m^{-2} yr^{-1}), except for the Guamanyacu, Inmiyana, and Tiputini streams that showed distinctly positive FN_2O values (9.7 to 21.6 mmol m^{-2} yr^{-1}) and the Huirima that showed a distinctly negative FN_2O value (-7.6 mmol m^{-2} yr^{-1}). The underlying idea is that in highly turbulent systems (high k values), degassing brings gases to equilibrium with the atmosphere, and emissions are near zero. Consequently, the gaseous emission is assumed to be limited by gas availability.

Lowland rivers dominate the integrated FCO_2 (64±5 TgC yr^{-1}) (65%). However, FCO_2 per m^2 in highland and piedmont rivers (197±35 and 143±3 mol m^{-2} yr^{-1}) were 1.7 and 1.2 times higher than in lowland rivers (115±8 mol m^{-2} yr^{-1}), respectively, due to higher k values. The deposition of sediments and the presence of forests in the piedmont region are favorable to high in-stream CH_4 production. In larger lowland river channels that are relatively disconnected from floodplains, the deep water column and strong currents do not promote the accumulation of dissolved CH_4 in the water column but promote the removal of dissolved CH_4 either by emission of CH_4 to the atmosphere or by microbial oxidation (Borges et al., 2015). The piedmont streams accounted for 62% of the total integrated diffusive FCH_4 (0.4±0.1 TgCH_4 yr^{-1}), higher than the contribution from lowland rivers (28%). In comparison, highland streams accounted for only 10% due to much higher k values (148.8±3.2 versus 14.5±0.4 cm h^{-1}). Interestingly, the diffusive FCH_4 per m^2 in piedmont streams (1,573±350 mmol m^{-2} yr^{-1}) was 6.6 times higher than in lowland rivers (137±79 mmol m^{-2} yr^{-1}) because of much higher dissolved CH4 concentrations (797±174 versus 307±100 nmol L^{-1}), while k was relatively closer (20.0±0.5 versus 14.5±0.4 cm h^{-1}). The integrated FN_2O (25±4 GgN_2O-N yr^{-1}) was dominated by lowland rivers and streams (99% of total), while piedmont streams were a minimal source of N_2O, and highland streams were a tiny sink of N_2O. The computation of integrated FN_2O value for the Amazon River basin resulted in 9±4 GgN_2O-N yr^{-1}, close to the range of N_2O emissions for the Amazon River basin of 11 to 16 GgN_2O-N yr^{-1} modeled from N deposition and emission factors (Maavara et al., 2019).

We concluded that mountainous headwater and piedmont streams were hotspots of CO_2 and CH_4 emissions from the Amazon River basin, accounting for a significant fraction of total emissions (35 and 72% for CO_2 and CH_4, respectively). Although the present study constitutes a baseline for the integration of the systems that make up the Amazon Basin, such as the Andes, Piedmont, and Amazonia, it is necessary to expand the sampling area and analyze the factors that drive the degassing rate (k values) a significant parameter assumed to the obtained results.

Suspended matter and organic carbon pools.

We report specific conductivity, TA, stable isotope ratios (δ13C-DIC, δ13C-POC δ13C-DOC), TSM, total organic matter (POC and DOC) and three optical proxies of CDOM. Specific conductivity showed a downstream decrease from 368 to 19 μS cm^{-1} in the main-stem. Conversely, in the tributaries, specific conductivity varied within a narrower range from 19 to 122 μS cm^{-1}. Specific conductivity was positively related to stream gradient. TA ranged between 135 and 1,656 μmol L^{-1} and mimicked of specific conductivity. The elevational patterns of specific conductivity and TA resulted from intense rock weathering in the high elevation areas followed by dilution in the lower reaches with the increase of stream size, as indicated by negative correlations with catchment area and discharge. The δ^{13}C-DIC values ranged between -22.1 and +3.1 ‰, and by differentiating between the tributaries and the main-stem, δ^{13}C-DIC is in line with the patterns of HCO_3^-. A negative relation between δ^{13}C-DIC and CO_2 concentration suggests the addition of CO_2 depleted in ^{13}C from heterotrophic process and the gradual dilution of HCO_3- in lowlands waters.

TSM showed a consistent downstream increase from 3 to 480 mg L^{-1}. Nevertheless, the indicates that the higher particulate matter content transported by lowland rivers originated from moderate elevation areas (<1000 m) rather than from headwater regions. TSM was negatively related to upstream catchment slope and stream gradient, and positively related to freshwater discharge and catchment area, implying an accumulation of particles when the river size increases and reaches lowlands. TSM and POC are positively correlated, Conversely, TSM and %POC, ranged from 0.2 and 21.8%, were negatively correlated, this trend probably reflected a better preservation of organic matter fraction in colder high elevation region, the in-stream loss by microbial respiration of organic carbon and the dilution of POC by mineral particles during downstream transport. The downstream decrease of the C:N ratio of fluvial POM is consistent with the decrease from highlands to lowlands of soil C:N ratio reported by Townsend-Small et al. (2005) in the Peruvian Andes that was attributed to a higher microbial source (with low C:N) in low-elevation soils compared to high-elevation soils with a higher contribution of plant source (with high C:N), due to elevational gradients of temperature.

DOC ranged from 1.2 to 8.2 mg L^{-1}, which is consistent with (Townsend-Small et al. 2005; Audfdenkampe et al. 2007) for comparable elevations (>1000;<4800m). Between 4,000 and 1,350m, DOC showed a decreasing pattern from 13.7 to 1.2 mg L^{-1}; the decrease of temperature at paramos leads to a decrease of organic matter mineralization and enhancing organic matter accumulation in soils (Poulenard et al. 2003). Hydraulic variables were not the primary driver controlling DOC, at contrary it was controlled by soil organic carbon inputs. For example, leaching forest soils strongly enhanced fluvial DOC content.

CDOM was characterized with three optical proxies. The a_{350} and the $SUVA_{254}$ values in the two streams at the highest elevation (>3,500 m) were higher than the other mountainous streams at elevations > 1000 m, reflecting the high organic carbon content in the páramos combined to small stream size. The a_{350} and $SUVA_{254}$ values were negatively correlated to upstream catchment slope but not S_R. Like DOC, the three DOM optical proxies were unrelated to other hydraulic

variables, but related with forest cover. Lower a_{350} values at similar DOC levels in environments with a low forest cover indicates that DOM released from high-latitude grassland dominated soils is less optically active compared to DOM released from forest soils. High values of $SUVA_{254}$ at lowlands suggest that a higher forest cover in the lowlands led to a higher quantity in streams of highly aromatic DOM. Conversely, The S_R values ranged between 0.6 and 1.0 and increased downstream, indicating a stronger enrichment of high-molecular-weight DOM compounds in highlands.

Positive relation between pCO_2 and DOC was observed, which suggests heterotrophy CO_2 production and simultaneous inputs from the catchment of both DOC and CO_2 derived from soils. Conversely, the lack of relation between CH_4 and DOC could be explained by multiple drivers acting simultaneously on CH_4, in addition to organic matter delivery to streams, that might become the main explaining variable in an analysis at global scale. The fluvial $\delta^{13}C$-DOC values ranged between -31.2 and -26.2 ‰ and $\delta^{13}C$-POC values ranged between -29.7 and -26.1 ‰ and followed the elevational gradient of $\delta^{13}C$ of organic carbon from terrestrial vegetation, which reflected the shift from C4 dominated grasslands in highlands to C3 dominated forests in lowlands.

We collected 21 representative plant samples from each area to complement the analysis, maintaining an altitudinal variation between 181 and 3,300 m. A proportional relationship between the $\delta^{13}C$ content and the altitude was observed. This trend follows the pattern between the $\delta^{13}C$ POC and the altitude presented previously. Significant differences between average values of $\delta^{13}C$ in lowland (-28.78 ‰) and Andean-draining rivers (-32.28 ‰) confirm the influence of sources of plant material on the $\delta^{13}C$ POC signature. The trend could also suggest high dilution of the $\delta^{13}C$ POC downstream in the main river and depleted POC input to replace the POC that respired in the river. C dynamics reinforced the conclusions reached in Chapter 2 regarding GHG emissions. Clearly, DOC supports CO2 generation. Although, more research is needed to interpret the relationships with the other GHGs.

GHGs dynamics in the lacustrine system

Lakes at high altitudes have a particular dynamic concerning GHGs due to the influence of organic matter stored in the soil. However, low temperatures could counteract this effect. In the frame of the present thesis, we reported the dissolved concentrations of CO_2, CH_4, and N_2O in 15 lakes located in the northern region of the Ecuadorian Andes along an elevational gradient from 2,213 to 4,361 m of altitude, as well as a gradient of lake surface area (0.003 to 6.1 km^2) and depth (0.9 to 74 m). Lakes were grouped in clusters as a function of several variables, such as elevation, the lake area, lake depth, conductivity, and water temperature. Lakes Cuicocha, Loreto, and Papallacta are "volcanic lakes" with high conductivity and TA. Yaguarcocha and San Pablo "urban lakes" are surrounded by the cities of Otavalo and Ibarra and present medium values of TA and the highest surface area. The rest, "páramo" lakes, are of glacial origin, shallows, and located in the Andean paramo above 3000 m altitude.

Water temperature ranged between 10.2 and 15.7°C and followed the elevational pattern. Conductivity was negatively related to elevation for the non-“volcanic” lakes, possibly reflecting the combination of decreasing lake size and increasing soil organic matter content with elevation. In the Andean páramo, the soil organic carbon increases with elevation because of the decrease in temperature that leads to a decrease of organic matter mineralization in soils, enhancing organic matter accumulation in soils.

The DOC ranged between 1.2 and 12.8 mg L^{-1}. The three “volcanic” lakes showed the lowest DOC concentrations (1.2 to 2.3 mg L^{-1}), the two “urban” lakes (San Pablo and Yaguarcocha) showed intermediate DOC concentrations (4.7 to 5.4 mg L^{-1}). The remaining ten lakes were

characterized by the highest DOC content (8.3 to 12.8 mg L^{-1}). DOC was positively correlated to elevation and negatively related to temperature (excluding the three "volcanic" lakes). This might reflect the higher inputs of soil DOC in lakes from the páramos. The negative relation between DOC and conductivity is consistent with the idea that soils richer in organic matter tend to lead to less mineralized water. Low inputs of soil DOC in the three "volcanic" lakes are related to a low ratio of catchment area to lake surface area, which reduces the inputs from soils to the lake.
The POC values ranged between 0.4 and 5.7 mg L^{-1}, and the POC data points were less clearly clustered than DOC. POC only correlated positively with conductivity, possibly due to a general dilution pattern by meteoric water of solutes and POC. One of the two "urban" lakes (San Pablo) was characterized by the highest POC value (5.7 mg L^{-1}), while the three "volcanic" lakes were characterized by among the lowest POC values (0.4 to 0.6 mg L^{-1}).
The pCO_2 values ranged between 208 and 10,069 ppm. The three "volcanic" lakes were characterized by higher pCO_2 values (3,269-10,069 ppm), the two "urban" lakes (San Pablo and Yaguarcocha) by the lowest pCO_2 values (208-254 ppm) and the other páramo lakes by intermediary pCO_2 values (644-2,152 ppm). Dissolved CH_4 concentrations ranged between 170 and 24,908 nmol L^{-1}. Higher methane production is characterized by the smaller lakes bordered by soils with higher organic carbon content in lake sediments or surrounding soils CH_4 follows the patterns of pCO_2. and was not significantly correlated to elevation, water temperature, and POC but was negatively correlated to the lake area, lake depth, conductivity, DOC, and $\%O_2$.
Variations of DIN ranged from 3.6 to 11.0 µmol L^{-1}. DIN was dominated by NH_4^+ (70-98%) that ranged between 3.4 and 9.2 µmol L^{-1}. NH_4^+ did not significantly correlate with elevation, the lake area, depth, conductivity, and water temperature. NO_3^- ranged between 0.1 and 1.9 µmol L^{-1} and did not significantly correlate with elevation and temperature but positively correlated to the lake area, depth, and conductivity. $\%N_2O$ ranged between 63.8 and 100.8%. All the sampled lakes were sinks of atmospheric N_2O except Salve Faccha, which was close to saturation (100.8%). This implies the removal of N_2O by denitrification due to the complete reduction of N_2O to N_2. $\%N_2O$ did not significantly correlate to elevation, lake depth, conductivity, and temperature but correlated to the lake area.
Considering the global estimations of the whole basin, the CH_4 emission (0.0007 TgC yr^{-1}) from highland lakes (elevation >500m) was 18 times lower than from lowland lakes (elevation <500m) (0.0130 TgC yr^{-1}). The average areal FCH_4 (per m^2) was, in fact, 1.3 times higher in highland lakes (0.75 gC m^{-2} yr^{-1}) than in lowland lakes (0.58 gC m^{-2} yr^{-1}) owing to the combination of higher dissolved CH_4 concentration (265 nmol L^{-1} versus 179 nmol L^{-1}) and higher k values (3.5 cm h^{-1} vs. 2.5 cm h^{-1}). As a result, the CO_2 emission (0.022 TgC yr^{-1}) from highland lakes was 257 times lower than from lowland lakes (5.7 TgC yr^{-1}). The average areal FCO_2 was also 11 times lower in highlands (23 gC m^{-2} yr^{-1}) than in lowlands (255 gC m^{-2} yr^{-1}) owing to the lower pCO_2 values (530 ppm versus 2,909 ppm) despite higher k values (3.5 cm h^{-1} versus 2.5 cm h^{-1}).

REFERENCES

Abril, G. & Borges, (2019). Ideas and perspectives: Carbon leaks from flooded land: do we need to replumb the inland water active pipe? Biogeosciences, 16(3), 769–784. https://doi.org/10.5194/bg-16-769-2019

Abril, G. et al. Amazon River carbon dioxide outgassing fuelled by wetlands. Nature 505, 395-398 (2014).

Abril, G. et al. Technical Note: Large overestimation of calculated pCO2 in acidic, organic-rich freshwaters. Biogeosciences 12, 67–78 (2015).

Abril, G., Bouillon, S., Darchambeau, F., Teodoru, C.R., Marwick, T.R., Tamooh, F., Omengo, F.O., Geeraert, N., Deirmendjian, L., Polsenaere, P., Borges, A.V., 2015. Technical note: Large overestimation of pCO2 calculated from pH and alkalinity in acidic, organic-rich freshwaters. Biogeosciences 12, 67-78. https://doi.org/10.5194/bg-12-67-2015

Abril, G., Commarieu, M.-V., Guérin, F., 2007. Enhanced methane oxidation in an estuarine turbidity maximum. Limnol. Oceanogr. 52, 470-475. https://doi.org/10.4319/lo.2007.52.1.0470

Abril, G., Martinez, J.-M., Artigas, L. F., Moreira-Turcq, P., Benedetti, M. F., Vidal, L., Meziane, T., Kim, J.-H., Bernardes, M. C., Savoye, N., Deborde, J., Souza, E. L., Albéric, P., Landim de Souza, M. F. & Roland, F. (2014). Amazon River carbon dioxide outgassing fuelled by wetlands. Nature, 505(7483), 395–398. https://doi.org/10.1038/nature12797

Akshit, S. (2020). Nitrous oxide human emissions increased 30% in 36 yrs. Nitrous Oxide Human Emissions Increased 30% in 36 Yrs. https://www.downtoearth.org.in/news/climate-change/nitrous-oxide-human-emissions-increased-30-in-36-yrs-report-73741

Albéric, P., Pérez, M.A.P., Moreira-Turcq, P., Benedetti, M.F., Bouillon, S., Abril, G., 2018. Variation of the isotopic composition of dissolved organic carbon during the runoff cycle in the Amazon River and the floodplains, C.R. Geoscience 350 65-75. https://doi.org/10.1016/j.crte.2017.11.001

Alin, S. R., Rasera, M. de F. F. L., Salimon, C. I., Richey, J. E., Holtgrieve, G. W., Krusche, & Snidvongs, A. (2011). Physical controls on carbon dioxide transfer velocity and flux in low-gradient river systems and implications for regional carbon budgets. Journal of Geophysical Research, 116(G1), G01009. https://doi.org/10.1029/2010JG001398

Allan, J. D., Flecker, A. S. & Kling, G. W. (2006). Limnology of Andean piedmont rivers of Venezuela. North American Benthological Society, 25(1), 66–81.

Allen, G.H., Pavelsky, T.M., 2018. Global extent of rivers and streams. Science 361, 585-588. https://doi.org/10.1126/science.aat0636

Amaral, J.H.F., Melack, J.M., Barbosa, P.M., MacIntyre, S., Kasper, D., Cortés, A., Freire Silva, T.S., Nunes de Sousa, R., Forsberg, B.R., 2020. Carbon dioxide fluxes to the atmosphere from waters within flooded forests in the Amazon basin. J. Geophys. Res. Biogeosci. 125, e2019JG005293, https://doi.org/10.1029/2019JG005293

Amazon Waters. (2022). Sediments. The Alluvial Gift of the Andes Sediment Transport Is Highly Dynamic in the Amazon River. https://amazonwaters.org/waters/flow-floods/sediments

American Chemical Society. (2022). Energy Balance and Planetary Temperatures. https://www.acs.org/climatescience/energybalance.html#:~:text=The temperature at the surface,vast variety of complex life.

American Public Health Association. Standard methods for the examination of water and wastewater, (APHA, 1998).

Anderson, E. P., Jenkins, C. N., Heilpern, S., Maldonado-Ocampo, J. A., Carvajal-Vallejos, F. M., Encalada, A. C., Rivadeneira, J. F., Hidalgo, M., Cañas, C. M., Ortega, H., Salcedo, N., Maldonado, M. & Tedesco, P. A. (2018). Fragmentation of Andes-to-Amazon connectivity by hydropower dams. Science Advances, 4(1). https://doi.org/10.1126/sciadv.aao1642

Armijos, E., Laraque, A., Barba, S., Bourrel, L., Ceron, C., Lagane, C., Magat, P., Moquet, J. S., Pombosa, R., Sondag, F., Vauchel, P., Vera, A. & Guyot, J. L. (2013). Yields of suspended sediment and dissolved solids from the Andean basins of Ecuador. Hydrological Sciences Journal, 58(7), 1478–1494. https://doi.org/10.1080/02626667.2013.826359

Arrhenius, S. (1896). XXXI. On the influence of carbonic acid in the air upon the temperature of the ground. The London, Edinburgh, and Dublin Philosophical Magazine and Journal of Science, 41(251), 237–276. https://doi.org/10.1080/14786449608620846

Aufdenkampe AK, E Mayorga, JI Hedges , C Llerena, PD Quay, J Gudeman, AV Krusche, JE Richey, Organic matter in the Peruvian headwaters of the Amazon: Compositional evolution from the Andes to the lowland Amazon mainstem, Organic Geochemistry 38 (2007) 337–364

Aufdenkampe, A. K., Mayorga, E., Raymond, P. A., Melack, J. M., Doney, S. C., Alin, S. R., Aalto, R. E. & Yoo, K. (2011). Riverine coupling of biogeochemical cycles between land, oceans, and atmosphere. Frontiers in Ecology and the Environment, 9(1), 53–60. https://doi.org/10.1890/100014

Baede, A., Aholondou, E. & Dchimel, D. (2016). The Climate System : an Overview. In Introduction to the Climate System. An Overview (Second, pp. 1–98). IPCC. https://www.ipcc.ch/site/assets/uploads/2018/03/TAR-01.pdf

Bartholome, E., & Belward, A. S. (2005). GLC2000: a new approach to global land cover mapping from Earth observation data. *International Journal of Remote Sensing*, *26*(9), 1959-1977.

Barbosa P.M., Melack, J.M., Farjalla, V.F., Amaral, J.H.F., Scofield, V., Forsberg, B.R., 2016. Diffusive methane fluxes from Negro, Solimões and Madeira rivers and fringing lakes in the Amazon basin. Limnol. Oceanogr. 61(S1) S221-S237. https://doi.org/10.1002/lno.10358

Barbosa, P.M. et al. Diffusive methane fluxes from Negro, Solimões and Madeira rivers and fringing lakes in the Amazon basin. Limnol. Oceanogr. 61, S221-S237 (2016).

Barnett, T. P., Hasselmann, K., Chelliah, M., Delworth, T., Hegerl, G., Jones, P., Rasmusson, E., Roeckner, E., Ropelewski, C., Santer, B. & Tett, S. (1999). Detection and attribution of recent climate change: A status report. Bulletin of the American Meteorological Society, 80(12), 2631–2659. https://doi.org/10.1175/1520-0477(1999)080<2631:DAAORC>2.0.CO;2

Basso, L. S., Marani, L., Gatti, L. V., Miller, J. B., Gloor, M., Melack, J., Cassol, H. L. G., Tejada, G., Domingues, L. G., Arai, E., Sanchez, A. H., Corrêa, S. M., Anderson, L., Aragão, L. E. O. C., Correia, C. S. C., Crispim, S. P. & Neves, R. A. L. (2021). Amazon methane budget derived from multi-year airborne observations highlights regional variations in emissions. Communications Earth & Environment, 2(1), 246. https://doi.org/10.1038/s43247-021-00314-4

Bastviken, D. (2022). Methane. In K. T. Thomas Mehner (Ed.), Encyclopedia of Inland Waters (Second edi, pp. 136–154). Elsevier. https://doi.org/10.1016/B978-0-12-819166-8.00147-X

Bastviken, D., Tranvik, L. J., Downing, J. A., Crill, P. M. & Enrich-Prast, A. (2011). Freshwater Methane Emissions Offset the Continental Carbon Sink. Science, 331(6013), 50–50. https://doi.org/10.1126/science.1196808

Battin, T. J., Kaplan, L. A., Findlay, S., Hopkinson, C. S., Marti, E., Packman, A. I., Newbold, J. D. & Sabater, F. (2009). Erratum: Biophysical controls on organic carbon fluxes in fluvial networks. Nature Geoscience, 2(8), 595–595. https://doi.org/10.1038/ngeo602

Battin, T. J., Luyssaert, S., Kaplan, L. A., Aufdenkampe, A. K., Richter, A. & Tranvik, L. J. (2009). The boundless carbon cycle. Nature Geoscience, 2(9), 598–600. https://doi.org/10.1038/ngeo618

Battin, T.J., Lauerwald, R., Bernhardt, E.S., Bertuzzo, E., Gómez Gener, L., Hall Jr, R.O., Hotchkiss, E.R., Maavara, T., Pavelsky, T.M., Ran, L., Raymond, P., Rosentreter, J.A., Regnier, P., 2023. River ecosystem metabolism and carbon biogeochemistry in a changing world, Nature, 613, 449-459, https://doi.org/10.1038/s41586-022-05500-8

Becker, J. C., Rodibaugh, K. J., Labay, B. J., Bonner, T. H., Zhang, Y. & Nowlin, W. H. (2014). Physiographic gradients determine nutrient concentrations more than land use in a Gulf Slope (USA) river system. Freshwater Science, 33(3), 731–744. https://doi.org/10.1086/676635

Beighley, R. E. & Gummadi, V. (2011). Developing channel and floodplain dimensions with limited data: A case study in the Amazon Basin. Earth Surface Processes and Landforms, 36(8), 1059–1071. https://doi.org/10.1002/esp.2132

Belanger, T. V. & Korzun, E. A. (1991). Critique of Floating-Dome Technique for Estimating Reaeration Rates. Journal of Environmental Engineering, 117(1), 144–150. https://doi.org/10.1061/(ASCE)0733-9372(1991)117:1(144)

Berger, A. & Tricot, Ch. (1992). The greenhouse effect. Surveys in Geophysics, 13(6), 523–549. https://doi.org/10.1007/BF01904998

Bird, M. I., and Pousai, P.: Variations of δ13C in the surface soil organic carbon pool. Global Biogeoch. Cycles, 11, 313-322, doi: 10.1029/97GB01197, 1997.

Borges, A. V., Abril, G., Darchambeau, F., Teodoru, C. R., Deborde, J., Vidal, L. O., Lambert, T. & Bouillon, S. (2015). Divergent biophysical controls of aquatic CO2 and CH4 in the World's two largest rivers. Scientific Reports, 5, 1–10. https://doi.org/10.1038/srep15614

Borges, A. V., Darchambeau, F., Lambert, T., Bouillon, S., Morana, C., Brouyère, S., Hakoun, V., Jurado, A., Tseng, H.-C., Descy, J.-P. & Roland, F. A. E. (2018). Effects of agricultural land use on fluvial carbon dioxide, methane and nitrous oxide concentrations in a large European river, the Meuse (Belgium). Science of The Total Environment, 610–611, 342–355. https://doi.org/10.1016/j.scitotenv.2017.08.047

Borges, A. V., Darchambeau, F., Lambert, T., Morana, C., Allen, G. H., Tambwe, E., Toengaho Sembaito, A., Mambo, T., Wabakhangazi, J. N., Descy, J. P., Teodoru, C. R. & Bouillon, S. (2019). Variations in dissolved greenhouse gases (CO2, CH4, N2O) in the Congo River network overwhelmingly driven by fluvial-wetland connectivity. Biogeosciences, 16(19), 3801–3834. https://doi.org/10.5194/bg-16-3801-2019

Borges, A. V., Darchambeau, F., Teodoru, C. R., Marwick, T. R., Tamooh, F., Geeraert, N., Omengo, F. O., Guérin, F., Lambert, T., Morana, C., Okuku, E. & Bouillon, S. (2015). Globally significant greenhouse-gas emissions from African inland waters. Nature Geoscience, 8(8), 637–642. https://doi.org/10.1038/ngeo2486

Borges, A. V., Deirmendjian, L., Bouillon, S., Okello, W., Lambert, T., Roland, F. A. E., Razanamahandry, V. F., Voarintsoa, N. R. G., Darchambeau, F., Kimirei, I. A., Descy, J. P., Allen,

G. H. & Morana, C. (2022). Greenhouse gas emissions from African lakes are no longer a blind spot. Science Advances, 8(25), 17. https://doi.org/10.1126/sciadv.abi8716

Borges, A.V., Abril, G., Delille, B., Descy, J.-P., Darchambeau, F., 2011. Diffusive methane emissions to the atmosphere from Lake Kivu (Eastern Africa), J. Geophys. Res. Biogeosc. 116, G03032, https://doi.org/10.1029/2011JG001673

Borges, A.V., Bouillon, S., Abril, G., Delille, B., Poirier, D., Commarieu, M.-V., Lepoint, G., Morana, C., Champenois, W., Servais, P., Descy, J.-P., Darchambeau, F., 2012. Variability of carbon dioxide and methane in the epilimnion of Lake Kivu, In Lake Kivu: Limnology and biogeochemistry of a tropical great lake (J.-P. Descy, F. Darchambeau, M. Schmid, Eds), pp 47-66, Aquatic Ecology Series, Springer, https://doi.org/10.1007/978-94-007-4243-7_4

Borges, A.V., Okello, W., Bouillon, S., Deirmendjian, L., Nankabirwa, A., Nabafu, E., Lambert, T., Descy, J.-P., Morana, C., 2023. Spatial and temporal variations of dissolved CO2, CH4 and N2O in Lakes Edward and George (East Africa). J. Great Lakes Res. 49, 229-245, https://doi.org/10.1016/j.jglr.2022.11.010

Bouchez, J., Galy, V., Hilton, R. G., Gaillardet, J., Moreira-Turcq, P., Pérez, M. A., France-Lanord, C. & Maurice, L. (2014). Source, transport and fluxes of Amazon River particulate organic carbon: Insights from river sediment depth-profiles. Geochimica et Cosmochimica Acta, 133, 280–298. https://doi.org/10.1016/j.gca.2014.02.032

Bouillon, S., Abril, G., Borges, A. V., Dehairs, F., Govers, G., Hughes, H. J., Merckx, R., Meysman, F. J. R., Nyunja, J., Osburn, C., and Middelburg, J. J.: Distribution, origin and cycling of carbon in the Tana River (Kenya): a dry season basin-scale survey from headwaters to the delta, Biogeosciences, 6, 2475–2493, doi:10.5194/bg-6-2475-2009, 2009.

Broecker, W. S., Takahashi, T., Simpson, H. J. & Peng, T.-H. (1979). Fate of Fossil Fuel Carbon Dioxide and the Global Carbon Budget. Science, 206(4417), 409–418. https://doi.org/10.1126/science.206.4417.409

Brookshire, E. N. J., Gerber, S., Menge, D. N. L. & Hedin, L. O. (2012). Large losses of inorganic nitrogen from tropical rainforests suggest a lack of nitrogen limitation. Ecology Letters, 15(1), 9–16. https://doi.org/10.1111/j.1461-0248.2011.01701.x

Brookshire, E. N. Jack, Hedin, L. O., Newbold, J. D., Sigman, D. M. & Jackson, J. K. (2012). Sustained losses of bioavailable nitrogen from montane tropical forests. Nature Geoscience, 5(2), 123–126. https://doi.org/10.1038/ngeo1372

Brown, J., Loveland, T., Ohlen, D. & Zhu, Z. LBA Regional Land Cover from AVHRR, 1-km, Version 1.2 (IGBP). Oak Ridge National Laboratory Distributed Active Archive Center, Oak Ridge, Tennessee, USA. https://doi.org/10.3334/ORNLDAAC/679 (2003).

Burton, M. R., Sawyer, G. M. & Granieri, D. (2013). Deep Carbon Emissions from Volcanoes. Reviews in Mineralogy and Geochemistry, 75(1), 323–354. https://doi.org/10.2138/rmg.2013.75.11

Butman, D. & Raymond, P. A. (2011). Significant efflux of carbon dioxide from streams and rivers in the United States. Nature Geoscience, 4(12), 839–842. https://doi.org/10.1038/ngeo1294

Butterbach-Bahl, K., Baggs, E. M., Dannenmann, M., Kiese, R. & Zechmeister-Boltenstern, S. (2013). Nitrous oxide emissions from soils: how well do we understand the processes and their controls? Philosophical Transactions of the Royal Society B: Biological Sciences, 368(1621), 20130122. https://doi.org/10.1098/rstb.2013.0122

Call, M., Sanders, C. J., Enrich-Prast, A., Sanders, L., Marotta, H., Santos, I. R. & Maher, D. T. (2018). Radon-traced pore-water as a potential source of CO2 and CH4 to receding black and

clear water environments in the Amazon Basin. Limnology and Oceanography Letters, 3(5), 375–383. https://doi.org/10.1002/lol2.10089

Callendar, G. S. (1938). The artificial production of carbon dioxide and its influence on temperature. Quarterly Journal of the Royal Meteorological Society, 64(275), 223–240. https://doi.org/10.1002/qj.49706427503

Campeau, A., Lapierre, J.-F., Vachon, D. & del Giorgio, P. A. (2014). Regional contribution of CO 2 and CH 4 fluxes from the fluvial network in a lowland boreal landscape of Québec. Global Biogeochemical Cycles, 28(1), 57–69. https://doi.org/10.1002/2013GB004685

Canadell, J. G., Mooney, H. A., Baldocchi, D. D., Berry, J. A., Ehleringer, J. R., Field, C. B., Gower, S. T., Hollinger, D. Y., Hunt, J. E., Jackson, R. B., Running, S. W., Shaver, G. R., Steffen, W., Trumbore, S. E., Valentini, R. & Bond, B. Y. (2000). Carbon metabolism of the terrestrial biosphere: A multitechnique approach for improved understanding. Ecosystems, 3(2), 115–130. https://doi.org/10.1007/s100210000014

Canning, A., Wehrli, B. & Körtzinger, A. (2021). Methane in the Danube Delta: the importance of spatial patterns and diel cycles for atmospheric emission estimates. Biogeosciences, 159, 3961–3979. https://doi.org/10.5194/bg-18-3961-2021

Cardoso, S. J., Enrich-Prast, A., Pace, M. L. & Roland, F. (2014). Do models of organic carbon mineralization extrapolate to warmer tropical sediments? Limnology and Oceanography, 59(1), 48–54. https://doi.org/10.4319/lo.2014.59.1.0048

Chiriboga, G., Borges, A.V. 2023, Andean headwater and piedmont streams are hot spots of carbon dioxide and methane emissions in the Amazon basin, Commun. Earth Environ. submitted.

Ciais, P., Borges, A. V., Abril, G., Meybeck, M., Folberth, G., Hauglustaine, D. & Janssens, I. A. (2008). The impact of lateral carbon fluxes on the European carbon balance. Biogeosciences, 5(5), 1259–1271. https://doi.org/10.5194/bg-5-1259-2008

Clark, K. E., Hilton, R. G., West, A. J., Malhi, Y., Gröcke, D. R., Bryant, C. L., Ascough, P. L., Robles Caceres, A. & New, M. (2013). New views on “old” carbon in the Amazon River: Insight from the source of organic carbon eroded from the Peruvian Andes. Geochemistry, Geophysics, Geosystems, 14(5), 1644–1659. https://doi.org/10.1002/ggge.20122

Clough, T. J., Bertam, J. E., Sherlock, R. R., Leonard, R. L. & Nowiki, B. L. (2006). Comparison of measured and EF5-r-derived N2O fluxes from a spring-fed river. Global Change Biology, 12(2), 352–363. https://doi.org/10.1111/j.1365-2486.2005.01089.x

Cole, J. J., Prairie, Y. T., Caraco, N. F., McDowell, W. H., Tranvik, L. J., Striegl, R. G., Duarte, C. M., Kortelainen, P., Downing, J. A., Middelburg, J. J. & Melack, J. (2007). Plumbing the Global Carbon Cycle: Integrating Inland Waters into the Terrestrial Carbon Budget. Ecosystems, 10(1), 172–185. https://doi.org/10.1007/s10021-006-9013-8

Cole, J.J., Caraco, N.F., 2018. Atmospheric exchange of carbon dioxide in a low-wind oligotrophic lake measured by the addition of SF6. Limnol. Oceanogr. 43, 647-656. https://doi.org/10.4319/lo.1998.43.4.0647

Cole, Jonathan J. (2013). Freshwater ecosystems and the carbon cycle. In Colin S. Reynolds (Ed.), Excellence in Ecology (Vol. 18). International Ecology Institute. https://doi.org/10.5860/choice.51-6732

Cole, Jonathan J., Pace, M. L., Carpenter, S. R. & Kitchell, J. F. (2000). Persistence of net heterotrophy in lakes during nutrient addition and food web manipulations. Limnology and Oceanography, 45(8), 1718–1730. https://doi.org/10.4319/lo.2000.45.8.1718

Connolly, C. T., Khosh, M. S., Burkart, G. A., Douglas, T. A., Holmes, R. M., Jacobson, A. D., Tank, S. E. & McClelland, J. W. (2018). Watershed slope as a predictor of fluvial dissolved organic matter and nitrate concentrations across geographical space and catchment size in the Arctic. Environmental Research Letters, 13(10), 104015. https://doi.org/10.1088/1748-9326/aae35d

Connolly, C.T. et al. Watershed slope as a predictor of fluvial dissolved organic matter and nitrate concentrations across geographical space and catchment size in the Arctic. Environ. Res. Lett. 13,104015, 1-9 (2018).

Crawford, J. T., Dornblaser, M. M., Stanley, E. H., Clow, D. W. & Striegl, R. G. (2015). Source limitation of carbon gas emissions in high-elevation mountain streams and lakes. Journal of Geophysical Research: Biogeosciences, 120(5), 952–964. https://doi.org/10.1002/2014JG002861

Dai, A., and K. E. Trenberth (2002), Estimates of Freshwater Discharge from Continents: Latitudinal and Seasonal Variations, Journal of hydrometeorology, 3, 660–687.

de Brogniez, D. et al. A map of the topsoil organic carbon content of Europe generated by a generalized additive model. Eur. J. Soil Sci. 66, 121-134 (2015).

de Brogniez, D., Ballabio, C., Stevens, A., Jones, R. J. A., Montanarella, L. & van Wesemael, B. (2015). A map of the topsoil organic carbon content of Europe generated by a generalized additive model. European Journal of Soil Science, 66(1), 121–134. https://doi.org/10.1111/ejss.12193

de Fátima F. L. Rasera, M., Ballester, M. V. R., Krusche, A. V., Salimon, C., Montebelo, L. A., Alin, S. R., Victoria, R. L. & Richey, J. E. (2008). Estimating the Surface Area of Small Rivers in the Southwestern Amazon and Their Role in CO2 Outgassing. Earth Interactions, 12(6), 1–16. https://doi.org/10.1175/2008EI257.1

De Paiva, R. C. D., Buarque, D. C., Collischonn, W., Bonnet, M. P., Frappart, F., Calmant, S. & Bulhões Mendes, C. A. (2013). Large-scale hydrologic and hydrodynamic modeling of the Amazon River basin. Water Resources Research, 49(3), 1226–1243. https://doi.org/10.1002/wrcr.20067

DelSontro, T., Beaulieu, J. J. & Downing, J. A. (2018). Greenhouse gas emissions from lakes and impoundments: Upscaling in the face of global change. Limnology And Oceanography Letters, 3(3), 64–75. https://doi.org/10.1002/lol2.10073

Descy, J.-P., Darchambeau, F., Lambert, T., Stoyneva-Gaertner, M. P., Bouillon, S. & Borges, (2017). Phytoplankton dynamics in the Congo River. Freshwater Biology, 62(1), 87–101. https://doi.org/10.1111/fwb.12851

Devol, A. H. & Hedges, J. I. (2001). Organic Matter and Nutrients in the Mainstem Amazon River. In The Biogeochemistry of the Amazon Basin (p. 256). Oxford University Press. https://doi.org/10.1093/oso/9780195114317.003.0018

Dickson, A. G., Sabine, C. L. & Christian, J. R. (2007). Guide to Best Practices for Ocean CO2 Measurements (Issue 8). North Pacific Marine Science Organization.

Downing, J. A., Cole, J. J., Middelburg, J. J., Striegl, R. G., Duarte, C. M., Kortelainen, P., Prairie, Y. T. & Laube, K. A. (2008). Sediment organic carbon burial in agriculturally eutrophic impoundments over the last century. Global Biogeochemical Cycles, 22(1), 1–10. https://doi.org/10.1029/2006GB002854

Downing, John A. (2010). Emerging global role of small lakes and ponds: little things mean a lot. Limnetica, 29(1), 9–24. https://doi.org/10.23818/limn.29.02

Duffie, J. A. & Beckman, W. A. (2013). Solar Engineering of Thermal Processes. In American Journal of Physics (Vol. 53, Issue 4). John Wiley & Sons, Inc. https://doi.org/10.1119/1.14178

Duvert, C., Butman, D. E., Marx, A., Ribolzi, O. & Hutley, L. B. (2018). CO2 evasion along streams driven by groundwater inputs and geomorphic controls. Nature Geoscience, 11(11), 813–818. https://doi.org/10.1038/s41561-018-0245-y

EPA. (2020). Overview of Greenhouse Gases. Total U.S. Emissions in 2020 = 5,981 Million Metric Tons of CO2 Equivalent (Excludes Land Sector). https://www.epa.gov/ghgemissions/overview-greenhouse-gases

European Commission. (2020). Causes of climate change. The Consequences of Climate Change Are Extremely Serious, and Affect Many Aspects of Our Lives. https://climate.ec.europa.eu/climate-change/causes-climate-change_en

Farfan Portilla, F. (2018). Agroclimatologia del Ecuador (1, Ed.). Universidad Politécnica Salesiana.

Farquhar, G. D., Fasham, M. J. R., Goulden, M. L., Heimann, M., Jaramillo, V. J., Kheshgi, H. S., Le Quéré, C., Scholes, R. J. & Wallace, D. W. R. (2001). The carbon cycle and atmospheric carbon dioxide. In Climate Change 2001: The Scientific Basis IPCC (pp. 183–237). Farquhar, G. D., Fasham, M. J. R., Goulden, M. L., Heimann, M., Jaramillo, V. J., Kheshgi, H. S., … Wallace, D. W. R. (2001). The carbon cycle and atmospheric carbon dioxide. In Climate Change 2001: The Scientific Basis IPCC (pp. 183–237). Geneva. Retriev.

Ferrio, J. P., Voltas, J. & Araus, J. L. (2003). Use of carbon isotope composition in monitoring environmental changes. Management of Environmental Quality: An International Journal, 14(1), 82–98. https://doi.org/10.1108/14777830310460405

Fick, S.E., Hijmans, R.J., 2017. WorldClim 2: new 1km spatial resolution climate surfaces for global land areas. Int. J. Climatol. 37, 4302-4315. https://doi.org/10.1002/joc.5086

Flint, J. J. (1974). Stream gradient as a function of order, magnitude, and discharge. Water Resources Research, 10(5), 969–973. https://doi.org/10.1029/WR010i005p00969

Fluet-Chouinard, E., Lehner, B., Rebelo, L.-M., Papa, F. & Hamilton, S. K. (2015). Development of a global inundation map at high spatial resolution from topographic downscaling of coarse-scale remote sensing data. Remote Sensing of Environment, 158, 348–361. https://doi.org/10.1016/j.rse.2014.10.015

Friedlingstein, P., Jones, M. W., O'Sullivan, M., Andrew, R. M., Bakker, D. C. E., Hauck, J., Le Quéré, C., Peters, G. P., Peters, W., Pongratz, J., Sitch, S., Canadell, J. G., Ciais, P., Jackson, R. B., Alin, S. R., Anthoni, P., Bates, N. R., Becker, M., Bellouin, N., … Zeng, J. (2022). Global Carbon Budget 2021. Earth System Science Data, 14(4), 1917–2005. https://doi.org/10.5194/essd-14-1917-2022

FU, B.-J., LIU, S.-L., CHEN, L.-D., LÜ, Y.-H. & QIU, J. (2004). Soil quality regime in relation to land cover and slope position across a highly modified slope landscape. Ecological Research, 19(1), 111–118. https://doi.org/10.1111/j.1440-1703.2003.00614.x

Gaillardet, J., B. Dupré, C.-J. Allègre, and P. Négrel (1997), Chemical and physical denudation in the Amazon River Basin, Chemical Geology, 142, 141–173.

Gao, H., Jia, G. S. & Fu, Y. (2020). Identifying and quantifying pixel-level uncertainty among major satellite derived global land cover product. Meteor, 34(4), 806–821. https://doi.org/0.1007/s13351-020-9183-x

Gao, Y., Wang, Z., Ding, D., Li, W., Ma, Y., Hao, Y. & Zhang, H. (2019). Novel Methods to Harness Solar Radiation for Advanced Energy Applications. ES Energy & Environment, 5, 1–7. https://doi.org/10.30919/esee8c328

Ghil, M. & Lucarini, V. (2020). The physics of climate variability and climate change. Reviews of Modern Physics, 92(3), 1–86. https://doi.org/10.1103/RevModPhys.92.035002

Ghil, M. (2019). A Century of Nonlinearity in the Geosciences. Earth and Space Science, 6(7), 1007–1042. https://doi.org/10.1029/2019EA000599

Gibbs, R. J. (1967). The Geochemistry of the Amazon River System. Geological Society of America, 72(2), 202–213. https://doi.org/10.1130/0016-7606(1967)78[1203:TGOTAR]2.0.CO;2

Gillikin, D.P., Bouillon, S., 2007. Determination of δ18O of water and δ13C of dissolved inorganic carbon using a simple modification of an elemental analyzer – isotope ratio mass spectrometer (EA-IRMS): an evaluation, Rapid Comm. Mass Spectrom. 21, 1475-1478, https://doi.org/10.1002/rcm.2968

Gómez-Gener, L., Rocher-Ros, G., Battin, T., Cohen, M. J., Dalmagro, H. J., Dinsmore, K. J., Drake, T. W., Duvert, C., Enrich-Prast, A., Horgby, Å., Johnson, M. S., Kirk, L., Machado-Silva, F., Marzolf, N. S., McDowell, M. J., McDowell, W. H., Miettinen, H., Ojala, A. K., Peter, H., … Sponseller, R. A. (2021). Global carbon dioxide efflux from rivers enhanced by high nocturnal emissions. Nature Geoscience, 14(5), 289–294. https://doi.org/10.1038/s41561-021-00722-3

Gran, G., 1952. Determination of the equivalence point in potentiometric titrations Part II, The Analyst, 77, 661-671, https://doi.org/10.1039/AN9527700661.

Grasset, C., Mendonça, R., Villamor Saucedo, G., Bastviken, D., Roland, F., Sobek, S., 2018. Large but variable methane production in anoxic freshwater sediment upon addition of allochthonous and autochthonous organic matter. Limnol. Oceanogr., 63: 1488-1501, https://doi.org/10.1002/lno.10786

Guilhen, J., Al Bitar, A., Sauvage, S., Parrens, M., Martinez, J. M., Abril, G., Moreira-Turcq, P. & Sanchez-Perez, J. M. (2020). Denitrification and associated nitrous oxide and carbon dioxide emissions from the Amazonian wetlands. Biogeosciences, 17(16), 4297–4311. https://doi.org/10.5194/bg-17-4297-2020

Guyot, J. L., Jouanneau, J. M. & Wasson, J. G. (1999). Characterisation of river bed and suspended sediments in the Rio Madeira drainage basin (Bolivian Amazonia). Journal of South American Earth Sciences, 12(4), 401–410. https://doi.org/10.1016/S0895-9811(99)00030-9

Hall, R. O., Tank, J. L., Baker, M. A., Rosi-Marshall, E. J. & Hotchkiss, E. R. (2016). Metabolism, Gas Exchange, and Carbon Spiraling in Rivers. Ecosystems, 19(1), 73–86. https://doi.org/10.1007/s10021-015-9918-1

Harms, T. K., Edmonds, J. W., Genet, H., Creed, I. F., Aldred, D., Balser, A. & Jones, J. B. (2016). Catchment influence on nitrate and dissolved organic matter in Alaskan streams across a latitudinal gradient. Journal of Geophysical Research: Biogeosciences, 121(2), 350–369. https://doi.org/10.1002/2015JG003201

Harrison, E. L., Veron, F., Ho, D. T., Reid, M. C., Orton, P. & McGillis, W. R. (2012). Nonlinear interaction between rain- and wind-induced air-water gas exchange. Journal of Geophysical Research: Oceans, 117(C3), 1–16. https://doi.org/10.1029/2011JC007693

Hedges, G. L. Cowie, J. E. Richey, P. D. Quay, R. Benner, M. Strom, B.R. Forsberg. 1994. Origins and processing of organic matter in the Amazon River as indicated by carbohydrates and amino acids. Limnol. Oceanogr. 39: 743–761.

Hedges, G. L., et al. 2000. Organic matter in Bolivian tributaries of the Amazon River: A comparison to the lower mainstream. Limnol. Oceanogr. 45: 1449–1466.

Hedges, J. I., W. A. Clark, P. D. Quay, J. E. Richey, A. Devol, and U. Santos (1986), Composition and fluxes of particulate organic material in the Amazon River, Limnol. Oceanogr., 31, 717–738.

Hegerl, G. C. (2022). Climate change is physics. Communications Earth & Environment, 3(1), 14. https://doi.org/10.1038/s43247-022-00342-8

Helms, J. R., Stubbins, A., Ritchie, J. D., Minor, E. C., Kieber, D. J., and Mopper, K.: Absorption spectral slopes and slope ratios as indicators of molecular weight, source, and photobleaching of chromophoric dissolved organic matter, Limnol. Oceanogr., 53, 955–969, 2008.

Herreid, A. M., Wymore, A. S., Varner, R. K., Potter, J. D. & McDowell, W. H. (2021). Divergent Controls on Stream Greenhouse Gas Concentrations Across a Land-Use Gradient. Ecosystems, 24(6), 1299–1316. https://doi.org/10.1007/s10021-020-00584-7

Holgerson M.A., Raymond, P.A., 2016. Large contribution to inland water CO2 and CH4 emissions from very small ponds, Nat. Geosci. 9, 222–226, https://doi.org/10.1038/ngeo2654

Hong, C., Burney, J. A., Pongratz, J., Nabel, J. E. M. S., Mueller, N. D., Jackson, R. B. & Davis, S. J. (2021). Global and regional drivers of land-use emissions in 1961 – 2017. Nature, 589(January). https://doi.org/10.1038/s41586-020-03138-y

Horgby, Å., Segatto, P. L., Bertuzzo, E., Lauerwald, R., Lehner, B., Ulseth, A. J., Vennemann, T. W. & Battin, T. J. (2019). Unexpected large evasion fluxes of carbon dioxide from turbulent streams draining the world's mountains. Nature Communications, 10(1). https://doi.org/10.1038/s41467-019-12905-z

House, J. I., Colin Prentice, I. & Le Querré, C. (2002). Maximum impacts of future reforestation or deforestation on atmospheric CO2. Global Change Biology, 8(11), 1047–1052. https://doi.org/10.1046/j.1365-2486.2002.00536.x

Hu, M., Chen, D. & Dahlgren, R. A. (2016). Modeling nitrous oxide emission from rivers: a global assessment. Global Change Biology, 22(11), 3566–3582. https://doi.org/10.1111/gcb.13351

Hu, M., Chen, D. & Dahlgren, R. A. Modeling nitrous oxide emission from rivers: a global assessment. Glob. Change Biol. 22, 3566-3582 (2016).

Hu, M., Chen, D., Dahlgren, R. A., 2016. Modeling nitrous oxide emission from rivers: a global assessment. Glob. Change Biol. 22, 3566-3582, https://doi.org/10.1111/gcb.13351

Hua, T., Zhao, W., Liu, Y., Wang, S. & Yang, S. (2018). Spatial Consistency Assessments for Global Land-Cover Datasets: A Comparison among GLC2000, CCI LC, MCD12, GLOBCOVER and GLCNMO. Remote Sensing, 10(11), 1846. https://doi.org/10.3390/rs10111846

Huff, W. D. & Owen, L. A. (2015). Volcanic Landforms and Hazards. In Treatise on Geomorphology. Academic Press (Ed.), Tectonic Geomorphology (pp. 1–48). Elsevier Inc. https://doi.org/10.1016/B978-0-12-409548-9.09512-9

Huotari, J., Haapanala, S., Pumpanen, J., Vesala, T. & Ojala, A. (2013). Efficient gas exchange between a boreal river and the atmosphere. Geophysical Research Letters, 40(21), 5683–5686. https://doi.org/10.1002/2013GL057705

Inglezakis, V. J. (2016). Extraterrestrial Environment. In Environment and Development (pp. 453–498). Elsevier. https://doi.org/10.1016/B978-0-444-62733-9.00007-1

Inguaggiato, S., Hidalgo, S., Beate, B., Bourquin, J., 2010. Geochemical and isotopic characterization of volcanic and geothermal fluids discharged from the Ecuadorian volcanic arc. Geofluids 10, 525-541, https://doi.org/10.1111/j.1468-8123.2010.00315.x

IPCC. (2021). Climate change widespread, rapid, and intensifying. Climate Change Widespread, Rapid, and Intensifying – IPCC. https://www.ipcc.ch/2021/08/09/ar6-wg1-20210809-pr/#:~:text=Faster warming&text=The report shows that emissions,1.5°C of warming.

IPCC. (2022). Climate Change 2022, Mitigation of Climate Change. In Summary for Policymakers (SPM) (Issue 1). Cambridge University Press.

Jiang, X. & Green, C. (2017). The Impact on Global Greenhouse Gas Emissions of Geographic Shifts in Global Supply Chains. Ecological Economics, 139, 102–114. https://doi.org/10.1016/j.ecolecon.2017.04.027

Johnson, M. S., Lehmann, J., Riha, S. J., Krusche, A. V., Richey, J. E., Ometto, J. P. H. B. & Couto, E. G. (2008). CO2 efflux from Amazonian headwater streams represents a significant fate for deep soil respiration. Geophysical Research Letters, 35(17), 1–5. https://doi.org/10.1029/2008GL034619

Junk, W. J., Piedade, M. T. F., Schöngart, J., Cohn-Haft, M., Adeney, J. M. & Wittmann, F. (2011). A Classification of Major Naturally-Occurring Amazonian Lowland Wetlands. Wetlands, 31(4), 623–640. https://doi.org/10.1007/s13157-011-0190-7

Keller, D. P., Lenton, A., Littleton, E. W., Oschlies, A., Scott, V. & Vaughan, N. E. (2018). The Effects of Carbon Dioxide Removal on the Carbon Cycle. Current Climate Change Reports, 4(3), 250–265. https://doi.org/10.1007/s40641-018-0104-3

Kempe, S. (1984). Sinks of the anthropogenically enhanced carbon cycle in surface fresh waters. Journal of Geophysical Research, 89(D3), 4657. https://doi.org/10.1029/JD089iD03p04657

Kirschbaum, M. U. F. (1995). The temperature dependence of soil organic matter decomposition, and the effect of global warming on soil organic C storage. Soil Biology and Biochemistry, 27(6), 753–760. https://doi.org/10.1016/0038-0717(94)00242-S

Körner C., G.D. Farquhar, S.C. Wong, 1991, Carbon isotopic discrimination by plants follows latitudinal and elevational trends, Oecologia, 88, 30-40

Körner C., G.D. Farquhar, Z. Roksandic 1988, A global survey of carbon isotopic discrimination in plants from high elevation, Oecologia, 74, 623-632.

Koven, C. D., Ringeval, B., Friedlingstein, P., Ciais, P., Cadule, P., Khvorostyanov, D., Krinner, G. & Tarnocai, C. (2011). Permafrost carbon-climate feedbacks accelerate global warming. Proceedings of the National Academy of Sciences, 108(36), 14769–14774. https://doi.org/10.1073/pnas.1103910108

Kroeze, C., Dumont, E. & Seitzinger, S. (2010). Future trends in emissions of N 2 O from rivers and estuaries. Journal of Integrative Environmental Sciences, 7(sup1), 71–78. https://doi.org/10.1080/1943815X.2010.496789

Kweku, D., Bismark, O., Maxwell, A., Desmond, K., Danso, K., Oti-Mensah, E., Quachie, A. & Adormaa, B. (2018). Greenhouse Effect: Greenhouse Gases and Their Impact on Global Warming. Journal of Scientific Research and Reports, 17(6), 1–9. https://doi.org/10.9734/JSRR/2017/39630

Lambert, T., Bouillon, S., Darchambeau, F., Massicotte, P., and Borges, A. V.: Shifts in the chemical composition of dissolved organic matter in the Congo River network, Biogeosciences, 13, 5405-5420, doi:10.5194/bg-13-5405-2016, 2016b.

Lambert, T., Teodoru, C. R., Nyoni, F., Bouillon, S., Darchambeau, F., Massicotte, P., and Borges, A. V.: Along-stream transport and transformation of dissolved organic matter in a large tropical river, Biogeosciences, 13, 2727-2741, doi:10.5194/bg-13-2727-2016, 2016a.

Langeveld, J., Bouwman, A. F., van Hoek, W. J., Vilmin, L., Beusen, A. H. W., Mogollón, J. M. & Middelburg, J. J. (2020). Estimating dissolved carbon concentrations in global soils: a global database and model. SN Applied Sciences, 2(10), 1626. https://doi.org/10.1007/s42452-020-03290-0

Lapierre, J.-F., and P. A. del Giorgio (2012), Geographical and environmental drivers of regional differences in the lake pCO2 versus DOC relationship across northern landscapes, J. Geophys. Res., 117, G03015, doi:10.1029/2012JG001945

Laraque, A., Ceron, C., Armijos, E., Pombosa, R., Magat, P. & Guyot, J. L. (2004). Sediment yields and erosion rates in the Napo River basin: An Ecuadorian Andean Amazon tributary. IAHS-AISH Publication, 288, 220–225.

LaRowe, D. E., Arndt, S., Bradley, J. A., Estes, E. R., Hoarfrost, A., Lang, S. Q., Lloyd, K. G., Mahmoudi, N., Orsi, W. D., Shah Walter, S. R., Steen, A. D. & Zhao, R. (2020). The fate of organic carbon in marine sediments - New insights from recent data and analysis. Earth-Science Reviews, 204(February), 26. https://doi.org/10.1016/j.earscirev.2020.103146

Lauerwald, R. et al. Spatial patterns in CO2 evasion from the global river network. Global Biogeochem. Cycles 29, 534-554 (2015).

Lauerwald, R., Hartmann, J., Moosdorf, N., Kempe, S. & Raymond, P. A. (2013). What controls the spatial patterns of the riverine carbonate system? — A case study for North America. Chemical Geology, 337–338, 114–127. https://doi.org/10.1016/j.chemgeo.2012.11.011

Lauerwald, R., Laruelle, G. G., Hartmann, J., Ciais, P. & Regnier, P. A. G. (2015). Spatial patterns in CO 2 evasion from the global river network. Global Biogeochemical Cycles, 29(5), 534–554. https://doi.org/10.1002/2014GB004941

Leach, J. A., Lidberg, W., Kuglerová, L., Peralta-Tapia, A., Ågren, A. & Laudon, H. (2017). Evaluating topography-based predictions of shallow lateral groundwater discharge zones for a boreal lake-stream system. Water Resources Research, 53(7), 5420–5437. https://doi.org/10.1002/2016WR019804

Lim, A. G., Krickov, I. V., Vorobyev, S. N., Korets, M. A., Kopysov, S., Shirokova, L. S., Karlsson, J. & Pokrovsky, O. S. (2022). Carbon emission and export from the Ket River, western Siberia. Biogeosciences, 19(24), 5859–5877. https://doi.org/10.5194/bg-19-5859-2022

Linke, S., Lehner, B., Ouellet Dallaire, C., Ariwi, J., Grill, G., Anand, M., Beames, P., Burchard-Levine, V., Maxwell, S., Moidu, H., Tan, F. & Thieme, M. (2019). Global hydro-environmental sub-basin and river reach characteristics at high spatial resolution. Scientific Data, 6(1), 283. https://doi.org/10.1038/s41597-019-0300-6

Liu, B., Tian, M., Shih, K., Chan, C. N., Yang, X. & Ran, L. (2021). Spatial and temporal variability of pCO2 and CO2 emissions from the Dong River in south China. Biogeosciences, 18(18), 5231–5245. https://doi.org/10.5194/bg-18-5231-2021

Liu, S., Kuhn, C., Amatulli, G., Aho, K., Butman, D. E., Allen, G. H., Lin, P., Pan, M., Yamazaki, D., Brinkerhoff, C., Gleason, C., Xia, X. & Raymond, P. A. (2022). The importance of hydrology in routing terrestrial carbon to the atmosphere via global streams and rivers. Proceedings of the National Academy of Sciences of the United States of America, 119(11), 1–9. https://doi.org/10.1073/pnas.2106322119

Liu, Y., Xiao, J., Ju, W., Zhu, G., Wu, X., Fan, W., Li, D. & Zhou, Y. (2018). Satellite-derived LAI products exhibit large discrepancies and can lead to substantial uncertainty in simulated carbon and water fluxes. Remote Sensing of Environment, 206, 174–188. https://doi.org/10.1016/j.rse.2017.12.024

Lorke, A., Bodmer, P., Noss, C., Alshboul, Z., Koschorreck, M., Somlai-Haase, C., Bastviken, D., Flury, S., McGinnis, D. F., Maeck, A., Müller, D. & Premke, K. (2015). Technical note: drifting versus anchored flux chambers for measuring greenhouse gas emissions from running waters. Biogeosciences, 12(23), 7013–7024. https://doi.org/10.5194/bg-12-7013-2015

Lucarini, V., Blender, R., Herbert, C., Ragone, F., Pascale, S. & Wouters, J. (2014). Mathematical and physical ideas for climate science. Reviews of Geophysics, 52, 809–859. https://doi.org/10.1002/2013RG000446.Received

Ludwig, W., J. L. Probst, and S. Kempe. 1996a. Predicting the oceanic input of organic carbon by continental erosion. Global Biogeochemical Cycles 10: 23-41.

Maavara, T., Lauerwald, R., Laruelle, G. G., Akbarzadeh, Z., Bouskill, N. J., Van Cappellen, P. & Regnier, P. (2019). Nitrous oxide emissions from inland waters: Are IPCC estimates too high? Global Change Biology, 25(2), 473–488. https://doi.org/10.1111/gcb.14504

MacIntyre, S., Jonsson, A., Jansson, M., Aberg, J., Turney, D. E. & Miller, S. D. (2010). Buoyancy flux, turbulence, and the gas transfer coefficient in a stratified lake. Geophysical Research Letters, 37(24), n/a-n/a. https://doi.org/10.1029/2010GL044164

Marotta, H., Duarte, C.M., Sobek, S., Enrich-Prast, A., 2009. Large CO2 disequilibria in tropical lakes. Global Biogeochem. Cycles 23: GB4022, https://doi.org/10.1029/2008GB003434

Marwick, T.R., Tamooh, F., Ogwoka, B., Teodoru, C., Borges, A.V., Darchambeau, F., Bouillon, S., 2014. Dynamic seasonal nitrogen cycling in response to anthropogenic N loading in a tropical catchment, Athi–Galana–Sabaki River, Kenya, Biogeosciences, 11, 443-460, https://doi.org/10.5194/bg-11-443-2014

Marx, A., Dusek, J., Jankovec, J., Sanda, M., Vogel, T., van Geldern, R., Hartmann, J. & Barth, J. A. C. (2017a). A review of CO2 and associated carbon dynamics in headwater streams: A global perspective. Reviews of Geophysics, 55(2), 560–585. https://doi.org/10.1002/2016RG000547

Maslin, M. (2016). Forty years of linking orbits to ice ages. Nature, 540(7632), 208–209. https://doi.org/10.1038/540208a

Massetti, E. (2011). Carbon tax scenarios for China and India: exploring politically feasible mitigation goals. International Environmental Agreements: Politics, Law and Economics, 11(3), 209–227. https://doi.org/10.1007/s10784-011-9157-7

Mayorga, E., A. K. Aufdenkampe, C. A. Masiello, Krushe, J. I. Hedges, P. D. Quay, J. E. Richey, and T. A. Brown (2005), Young organic matter as a source of carbon dioxide outgassing from Amazonian rivers, Nature, 436, 538–541.

Mccartney, K., Huffman, A. R. & Tredoux, M. (1990). A paradigm for endogenous causation of mass extinctions. Geological Society of America, 247, 125–138. https://doi.org/10.1130/SPE247-p125

McClain, M. E., Richey, J. E. & Victoria, R. L. (1995). Andean contributions to the biogeochemistry of the Amazon River system. Bulletin - Institut Francais d'Etudes Andines, 24(3), 425–437. https://doi.org/10.3406/bifea.1995.1193

McClain, Michael E. & Naiman, R. J. (2008). Andean influences on the biogeochemistry and ecology of the Amazon River. BioScience, 58(4), 325–338. https://doi.org/10.1641/B580408

McClain, Michael E., Richey, J. E., Brandes, J. A. & Pimentel, T. P. (1997). Dissolved organic matter and terrestrial-lotic linkages in the Central Amazon Basin of Brazil. Global Biogeochemical Cycles, 11(3), 295–311. https://doi.org/10.1029/97GB01056

McDonald, C. P., Stets, E. G., Striegl, R. G. & Butman, D. (2013). Inorganic carbon loading as a primary driver of dissolved carbon dioxide concentrations in the lakes and reservoirs of the contiguous United States. Global Biogeochemical Cycles, 27(2), 285–295. https://doi.org/10.1002/gbc.20032

McGuire, K.J. et al. The role of topography on catchment-scale water residence time. Water Resour. Res. 41, W05002, doi:10.1029/2004WR003657 (2005).

McKinley, G. A., Fay, A. R., Lovenduski, N. S. & Pilcher, D. J. (2017). Natural Variability and Anthropogenic Trends in the Ocean Carbon Sink. Annual Review of Marine Science, 9(1), 125–150. https://doi.org/10.1146/annurev-marine-010816-060529

Meade, R. H. (1994). Suspended sediments of the modern Amazon and Orinoco rivers. Quaternary International, 21, 29–39. https://doi.org/10.1016/1040-6182(94)90019-1

Meade, R. H., T. Dunne, J. E. Richey, U. de M. Santos, E. Salati. 1985. Storage and remineralization of suspended sediment in the lower Amazon River of Brazil. Science 228: 488–490.

Melack, J. (2017). Interactions Between Biosphere, Atmosphere and Human Land Use in the Amazon Basin. In L. Nagy, B. R. Forsberg & P. Artaxo (Eds.), Ecological Studies (Vol. 227, Issue 0). Springer Berlin Heidelberg. https://doi.org/10.1007/978-3-662-49902-3

Melack, (2016) J.M. Aquatic ecosystems. In: Nagy, L., Forsberg, B.R., Artaxo, P. (Eds.), Interactions between Biosphere, Atmosphere and Human Land Use in the Amazon Basin. Springer Berlin Heidelberg, Berlin, Heidelberg, pp. 119–148

Melack, J. M. & Hess, L. L. (2010). Remote Sensing of the Distribution and Extent of Wetlands in the Amazon Basin. In Amazonian Floodplain Forests (pp. 43–59). Springer Science. https://doi.org/10.1007/978-90-481-8725-6_3

Melack, J. M., Basso, L. S., Fleischmann, A. S., Botía, S., Guo, M., Zhou, W., Barbosa, P. M., Amaral, J. H. F. & MacIntyre, S. (2022). Challenges Regionalizing Methane Emissions Using Aquatic Environments in the Amazon Basin as Examples. Frontiers in Environmental Science, 10(May), 1–26. https://doi.org/10.3389/fenvs.2022.866082

Melack, J. M., Hess, L. L., Gastil, M., Forsberg, B. R., Hamilton, S. K., Lima, I. B. T. & Novo, E. M. L. M. (2004). Regionalization of methane emissions in the Amazon Basin with microwave remote sensing. Global Change Biology, 10(5), 530–544. https://doi.org/10.1111/j.1365-2486.2004.00763.x

Melián, G.V., Toulkeridis, T., Pérez, N.M., Hernández, P.A., Somoza, L., Padrón, E., Amonte, C., Alonso, M., Asensio-Ramos, M., Cordero, M., 2021. Geochemistry of water and gas emissions from Cuicocha and Quilotoa volcanic lakes, Ecuador. Front. Earth Sci. 9:741528. https://doi.org/10.3389/feart.2021.741528

Merot, Ph., Squividant, H., Aurousseau, P., Hefting, M., Burt, T., Maitre, V., Kruk, M., Butturini, A., Thenail, C. & Viaud, V. (2003). Testing a climato-topographic index for predicting wetlands distribution along an European climate gradient. Ecological Modelling, 163(1–2), 51–71. https://doi.org/10.1016/S0304-3800(02)00387-3

Messager, M.L., Lehner, B., Grill, G., Nedeva, I., Schmitt, O., 2016. Estimating the volume and age of water stored in global lakes using a geo-statistical approach. Nat. Commun. 13603, https://doi.org/10.1038/ncomms13603.

Millero, F.J., 1979. The thermodynamics of the carbonate system in seawater. Geochem. Cosmochem. Acta, 43, 1651-1661, https://doi.org/10.1016/0016-7037(79)90184-4

Mitchell, C., Sanders, C.J., Enrich-Prast, A., Sanders, L., Marotta, H., Santos, I.R., Maher, D.T., 2018. Radon-traced pore-water as a potential source of CO2 and CH4 to receding black and clear water environments in the Amazon Basin, Limnol. Oceanogr. Lett. 3, 375-383, https://doi.org/10.1002/lol2.10089.

Mitchell, J. F. B. (1989). The “Greenhouse” effect and climate change. Reviews of Geophysics, 27(1), 115. https://doi.org/10.1029/RG027i001p00115

Mitchell, J. F. B. (2009). The Greenhouse Effect and Climate Change. In The Environment (Issue 89, pp. 409–436). CRC Press. https://doi.org/10.1201/9781420007336-26

Moore, I. D., Grayson, R. B. & Ladson, A. R. (1991). Digital terrain modelling: A review of hydrological, geomorphological, and biological applications. Hydrological Processes, 5(1), 3–30. https://doi.org/10.1002/hyp.3360050103

Moquet, J. S. et al. (2016), Dissolved Amazon River dissolved load: temporal dynamic and annual budget from the Andes to the ocean, Environmental Science and Pollution Research, 23(12), 11405–11429, doi:10.1007/s11356-015-5503-6.

Moquet, J.-S. et al. (2011), Chemical weathering and atmospheric/soil CO2 uptake in the Andean and Foreland Amazon basins, Chemical Geology, 287(1–2), 1–26.

Mortatti, J. & Probst, J. (2003). Silicate rock weathering and atmospheric/soil CO2 uptake in the Amazon basin estimated from river water geochemistry: seasonal and spatial variations. Chemical Geology, 197(1–4), 177–196. https://doi.org/10.1016/S0009-2541(02)00349-2

Mosquera, P.V., Hampel, H., Vázquez, R.F. and Catalan, J., 2022. Water chemistry variation in tropical high-mountain lakes on old volcanic bedrocks. Limnol Oceanogr, 67: 1522-1536. https://doi.org/10.1002/lno.12099

Mulholland, P. J. (2007). Dissolved organic matter concentration and flux in streams. Journal of the North American Benthological Society, 16, 131–144.

Nahlik, A. M. & Fennessy, M. S. (2016). Carbon storage in US wetlands. Nature Communications, 7, 1–9. https://doi.org/10.1038/ncomms13835

National Institute of Meteorology and Hydrology. (2021). Estaciones Hidrologicas Ecuador. http://186.42.174.236/InamhiEmas/#

Neu, V., Neill, C. & Krusche, (2011). Gaseous and fluvial carbon export from an Amazon forest watershed. Biogeochemistry, 105(1), 133–147. https://doi.org/10.1007/S10533-01

North Caroline Climate Office. (2016). Earth’s Energy Balance. https://legacy.climate.ncsu.edu/edu/EnergyBalance

Pan, Y., Birdsey, R. A., Fang, J., Houghton, R., Kauppi, P. E., Kurz, W. A., Phillips, O. L., Shvidenko, A., Lewis, S. L., Canadell, J. G., Ciais, P., Jackson, R. B., Pacala, S. W., McGuire, A. D., Piao, S., Rautiainen, A., Sitch, S. & Hayes, D. (2011). A Large and Persistent Carbon Sink in the World’s Forests. Science, 333(6045), 988–993. https://doi.org/10.1126/science.1201609

Pangala, S. R., Enrich-Prast, A., Basso, L. S., Peixoto, R. B., Bastviken, D., Hornibrook, E. R. C., Gatti, L. V., Marotta, H., Calazans, L. S. B., Sakuragui, C. M., Bastos, W. R., Malm, O., Gloor, E.,

Miller, J. B. & Gauci, V. (2017). Large emissions from floodplain trees close the Amazon methane budget. Nature, 552(7684), 230–234. https://doi.org/10.1038/nature24639

Pidwirny, M. (2006). The Nature of Radiation. http://www.physicalgeography.net/fundamentals/6f.html#:~:text=According to the above equation,Kelvins) is approximately 10.0 micrometers.

Pineda Lampreda, A. P., Bauters, M., Verbeeck, H., Baez, S., Barthel, M. & Bodé, S. (2021). Ideas and perspectives : patterns of soil CO2 , CH4 , and N2O fluxes along an altitudinal gradient – a pilot study from an Ecuadorian neotropical montane forest. Biogeosciences, 18, 413–421. https://doi.org/10.5194/bg-18-413-2021

Pittock, A. B. (2013). What climate changes are likely? In Climate Change (Second, pp. 430–435). Taylor & Francis. https://doi.org/10.4324/9781315870359

PLASS, G. N. (1956). The Carbon Dioxide Theory of Climatic Change. Tellus, 8(2), 140–154. https://doi.org/10.1111/j.2153-3490.1956.tb01206.x

Pongratz, J. & Caldeira, K. (2012). Attribution of atmospheric CO2 and temperature increases to regions: Importance of preindustrial land use change. Environmental Research Letters, 7(3), 8. https://doi.org/10.1088/1748-9326/7/3/034001

Poulenard, J., Podwojewski, P., Herbillon, A.J., 2003. Characteristics of non-allophanic Andisols with hydric properties from the Ecuadorian páramos, Geoderma, 117, 267-281, https://doi.org/10.1016/S0016-7061(03)00128-9

Pradeep Ram, A. S., Nair, S. & Chandramohan, D. (2007). Bacterial growth efficiency in a tropical estuary: Seasonal variability subsidized by allochthonous carbon. Microbial Ecology, 53(4), 591–599. https://doi.org/10.1007/s00248-006-9124-y

Puy, A., Beneventano, P., Levin, S. A., Lo Piano, S., Portaluri, T. & Saltelli, A. (2022). Models with higher effective dimensions tend to produce more uncertain estimates. Science Advances, 8(42). https://doi.org/10.1126/sciadv.abn9450

Quay, P., Wilbur, D. O., Richey, J. E., Hedges, J. I., Devol, A. H. & Reynaldo, V. (1992). Carbon cycling in the Amazon River : Implications from the 13C compositions of particles and solutes. Limnology and Oceanography, 37(4), 854–871. https://doi.org/10.4319/o.1992.37.4.0857

Ran, L., Li, L., Tian, M., Yang, X., Yu, R., Zhao, J., Wang, L. & Lu, X. X. (2017). Riverine CO 2 emissions in the Wuding River catchment on the Loess Plateau: Environmental controls and dam impoundment impact. Journal of Geophysical Research: Biogeosciences, 122(6), 1439–1455. https://doi.org/10.1002/2016JG003713

Rasilo, T., Hutchins, R. H. S., Ruiz-González, C. & del Giorgio, P. A. (2017). Transport and transformation of soil-derived CO2, CH4 and DOC sustain CO2 supersaturation in small boreal streams. Science of The Total Environment, 579, 902–912. https://doi.org/10.1016/j.scitotenv.2016.10.187

Raymond, Hartmann, L. et al. (2013). Global carbon dioxide emissions from inland waters. Nature, 503(7476), 355–359.

Raymond, P. A., Caraco, N. F. & Cole, J. J. (1997). Carbon Dioxide Concentration and Atmospheric Flux in the Hudson River. Estuaries, 20(2), 381. https://doi.org/10.2307/1352351

Raymond, P. A., Hartmann, J., Lauerwald, R., Sobek, S., McDonald, C., Hoover, M., Butman, D., Striegl, R., Mayorga, E., Humborg, C., Kortelainen, P., Dürr, H., Meybeck, M., Ciais, P. & Guth, P. (2013). Global carbon dioxide emissions from inland waters. Nature, 503(7476), 355–359. https://doi.org/10.1038/nature12760

Raymond, P. A., Zappa, C. J., Butman, D., Bott, T. L., Potter, J., Mulholland, P., Laursen, A. E., McDowell, W. H. & Newbold, D. (2012). Scaling the gas transfer velocity and hydraulic geometry in streams and small rivers. Limnology and Oceanography: Fluids and Environments, 2(1), 41–53. https://doi.org/10.1215/21573689-1597669

Reynolds, C. S. (1994). The long, the short and the stalled: on the attributes of phytoplankton selected by physical mixing in lakes and rivers. Hydrobiologia, 289(1–3), 9–21. https://doi.org/10.1007/BF00007405

Ribeiro-Kumara, C., Koster, E., Aaltonen, H. & Kajar, K. (2020). How do forest fires affect soil greenhouse gas emissions in upland boreal forests ? A review. Environmental Research, 184(February), 1–10. https://doi.org/10.1038/ncomms13835

Richey, J. E., Hedges, J. I., Devol, A. H., Quay, P. D., Victoria, R., Martinelli, L. & Forsberg, B. R. (1990). Biogeochemistry of carbon in the Amazon River. Limnology and Oceanography, 35(2), 352–371. https://doi.org/10.4319/lo.1990.35.2.0352

Richey, J. E., Melack, J. M., Aufdenkampe, A. K., Ballester, V. M. & Hess, L. L. (2002). Outgassing from Amazonian rivers and wetlands as a large tropical source of atmospheric CO2. Nature, 416(6881), 617–620. https://doi.org/10.1038/416617a

Richey, J. R., J. I. Hedges, A. H. Devol, P. D. Quay, R. Victoria, L. A. Martinelli, and B. R. Forsberg (1990), Biogeochemistry of carbon in the Amazon River, Limnol. Oceanogr., 35, 352–371.

Rocher-Ros, G., Sponseller, R. A., Lidberg, W., Mörth, C. & Giesler, R. (2019). Landscape process domains drive patterns of CO 2 evasion from river networks. Limnology and Oceanography Letters, 4(4), 87–95. https://doi.org/10.1002/lol2.10108

Rodhe, A. & Seibert, J. (1999). Wetland occurrence in relation to topography: a test of topographic indices as moisture indicators. Agricultural and Forest Meteorology, 98–99, 325–340. https://doi.org/10.1016/S0168-1923(99)00104-5

Rodhe, A. & Seibert, J. Wetland occurrence in relation to topography: a test of topographic indices as moisture indicators. Agric. For. Meteorol. 98-99, 325-340 (1999).

Roehm, C.L., Prairie, Y.T., del Giorgio, P.A., 2009. The pCO2 dynamics in lakes in the boreal region of northern Québec, Canada. Global Biogeochem. Cycles, 23, GB3013, https://doi.org/10.1029/2008GB003297

Roland, F. & Cole, J. J. (1999). Regulation of bacterial growth efficiency in a large turbid estuary. Aquatic Microbial Ecology, 20(1), 31–38. https://doi.org/10.3354/ame020031

Rosamond, M. S., Thuss, S. J. & Schiff, S. L. (2012). Dependence of riverine nitrous oxide emissions on dissolved oxygen levels. Nature Geoscience, 5(10), 715–718. https://doi.org/10.1038/ngeo1556

Rosentreter, J. A., Borges, A. V., Deemer, B. R., Holgerson, M. A., Liu, S., Song, C., Melack, J., Raymond, P. A., Duarte, C. M., Allen, G. H., Olefeldt, D., Poulter, B., Battin, T. I. & Eyre, B. D. (2021). Half of global methane emissions come from highly variable aquatic ecosystem sources. Nature Geoscience, 14(4), 225–230. https://doi.org/10.1038/s41561-021-00715-2

Saito, T., Fang, X., Stohl, A., Yokouchi, Y., Zeng, J., Fukuyama, Y. & Mukai, H. (2015). Extraordinary halocarbon emissions initiated by the 2011 Tohoku earthquake. Geophysical Research Letters, 42(7), 2500–2507. https://doi.org/10.1002/2014GL062814

Santander, A. (2015). Los páramos en el filo de la navaja. https://web.archive.org/web/20090214211824/http://www.biodiversityreporting.org/article.sub?docId=694&c=Colombia&cRef=Colombia&year=2003&date=February 2003

Sarmiento, J. L. & Gruber, N. (2002). Sinks for Anthropogenic Carbon. Physics Today, 55(8), 30–36. https://doi.org/10.1063/1.1510279

Saunois, M., Stavert, A. R., Poulter, B., Bousquet, P., Canadell, J. G., Jackson, R. B., Raymond, P. A., Dlugokencky, E. J., Houweling, S., Patra, P. K., Ciais, P., Arora, V. K., Bastviken, D., Bergamaschi, P., Blake, D. R., Brailsford, G., Bruhwiler, L., Carlson, K. M., Carrol, M., … Zhuang, Q. (2020). The Global Methane Budget 2000–2017. Earth System Science Data, 12(3), 1561–1623. https://doi.org/10.5194/essd-12-1561-2020

Sawakuchi, H. O., Bastviken, D., Sawakuchi, A. O., Krusche, A. V., Ballester, M. V. R. & Richey, J. E. (2014). Methane emissions from Amazonian Rivers and their contribution to the global methane budget. Global Change Biology, 20(9), 2829–2840. https://doi.org/10.1111/gcb.12646

Sawakuchi, H. O., Neu, V., Ward, N. D., Barros, M. de L. C., Valerio, A. M., Gagne-Maynard, W., Cunha, A. C., Less, D. F. S., Diniz, J. E. M., Brito, D. C., Krusche, & Richey, J. E. (2017). Carbon Dioxide Emissions along the Lower Amazon River. Frontiers in Marine Science, 4. https://doi.org/10.3389/fmars.2017.00076

Schimel, D. S., Braswell, B. H. & Parton, W. J. (1997). Equilibration of the Terrestrial Water, Nitrogen, and Carbon Cycle. Proceedings of the National Academy of Sciences of the United States of America, 94(16), 8280–8283. https://doi.org/10.1073/pnas.94.16.8280

Schlesinger, W. H. & Melack, J. M. (1981). Transport of organic carbon in the world's rivers. Tellus, 33(2), 172–187. https://doi.org/10.3402/tellusa.v33i2.10706

Schneider, C. L., Herrera, M., Raisle, M. L., Murray, A. R., Whitmore, K. M., Encalada, A. C., Suárez, E. & Riveros-Iregui, D. A. (2020). Carbon Dioxide (CO2) Fluxes From Terrestrial and Aquatic Environments in a High-Altitude Tropical Catchment. Journal of Geophysical Research: Biogeosciences, 125(8). https://doi.org/10.1029/2020JG005844

Scofield, V., Melack, J. M., Barbosa, P. M., Amaral, J. H. F., Forsberg, B. R. & Farjalla, V. F. (2016). Carbon dioxide outgassing from Amazonian aquatic ecosystems in the Negro River basin. Biogeochemistry, 129(1–2), 77–91. https://doi.org/10.1007/s10533-016-0220-x

Shi, G., Luo, Y., Zhang, X., Yu, G., Zhang, R., Gao, X. & Dong, W. (2016). The Attribution of Climate Change and Its Uncertainty. In Climate and Environmental Change in China (pp. 47–67). Springer Netherlands. https://doi.org/10.1007/978-3-662-48482-1_3

Siegenthaler, U. & Sarmiento, J. L. (1993). Atmospheric carbon dioxide and the ocean. Nature, 365(6442), 119–125. https://doi.org/10.1038/365119a0

Sioli, H. (1964), General features of the limnology of Amazonia, Verh.Internat.Verein.Limnol., 15, 1053–1058.

Skiba, U., Hergoualc'h, K., Drewer, J., Meijide, A. & Knohl, A. (2020). Oil palm plantations are large sources of nitrous oxide, but where are the data to quantify the impact on global warming? Current Opinion in Environmental Sustainability, 47, 81–88. https://doi.org/10.1016/j.cosust.2020.08.019

Smirnov, B. M. (2016). Greenhouse effect in the atmosphere. The Frontiers of Physics, 114(2). https://doi.org/10.1209/0295-5075/114/24005

Sobek S., G. Algesten, A.-K. Bergström, M. Jansson, L. Tranvik, The catchement and climate regulation of pCO2 in boreal lakes. Global Change Biol. 9, 630-641 (2003).

Soued, C., Del Giorgio, P. A. & Maranger, R. (2016). Nitrous oxide sinks and emissions in boreal aquatic networks in Quebec. Nature Geoscience, 9(2), 116–120. https://doi.org/10.1038/ngeo2611

Spencer, W. (2022). The Discovery of Global Warming. The Discovery of Global Warming. https://history.aip.org/climate/index.htm#contents

Staddon, P. L. (2004). Carbon isotopes in functional soil ecology. Trends in Ecology and Evolution, 19(3), 148–154. https://doi.org/10.1016/j.tree.2003.12.003

Staehr, P.A., Baastrup-Spohr, L., Sand-Jensen, K., Stedmon, C., 2012. Lake metabolism scales with lake morphometry and catchment conditions, Aquat. Sci. 74, 155-169. https://doi.org/10.1007/s00027-011-0207-6

Standing committee of Analysts (1981). Ammonia in waters. Methods for the examination of waters and associated materials. 16 pp (HMSO, 1981).

Stanley, E. H., Casson, N. J., Christel, S. T., Crawford, J. T., Loken, L. C. & Oliver, S. K. (2015). The ecology of methane in streams and rivers: patterns, controls, and global significance. Ecological Monographs, 86(2), 15-1027.1. https://doi.org/10.1890/15-1027.1

Stocker, T. F., Qin, D., Plattner, G. K., Tignor, M. M. M., K., B. A. S., Boschung, J. & Midgley, P. M. (2013). Contribution of working group I to the fifth assessment report of the intergovernmental panel on climate change. In Climate Change 2013: The Physical Science Basis (p. 256). Cambridge University Press.

Sulzman, E. W. (2000). The Carbon Cycle Surface Sediment Immediate & Deep Ocean. University Corporation for Atmospheric Research.

Tamooh, F., Borges, A. V., Meysman, F. J. R., Van Den Meersche, K., Dehairs, F., Merckx, R., and Bouillon, S.:Dynamics of dissolved inorganic carbon and aquatic metabolism in the Tana River basin, Kenya, Biogeosciences, 10, 6911–6928, doi:10.5194/bg-10-6911-2013, 2013

Tamooh, F., Van Den Meersche, K., Meysman, F., Marwick, T. R., Borges, A. V., Merckx, R., Dehairs, F., Schmidt, S., Nyunja, J. & Bouillon, S. (2012). Distribution and origin of suspended matter and organic carbon pools in the Tana River Basin, Kenya. Biogeosciences, 9(8), 2905–2920. https://doi.org/10.5194/bg-9-2905-2012

Tarnocai, C., Canadell, J. G., Schuur, E. A. G., Kuhry, P., Mazhitova, G. & Zimov, S. (2009). Soil organic carbon pools in the northern circumpolar permafrost region. Global Biogeochemical Cycles, 23(2), n/a-n/a. https://doi.org/10.1029/2008GB003327

Technical Secretary of Planning. (2021). Sistema de Información Geográfica. Cobertura Vegetal. https://sni.gob.ec/mapa-cobertura-uso

Templer, P. H., Mack, M. C., III, F. S. C., Christenson, L. M., Compton, J. E., Crook, H. D., Currie, W. S., Curtis, C. J., Dail, D. B., D'Antonio, C. M., Emmett, B. A., Epstein, H. E., Goodale, C. L., Gundersen, P., Hobbie, S. E., Holland, K., Hooper, D. U., Hungate, B. A., Lamontagne, S., … Zak, D. R. (2012). Sinks for nitrogen inputs in terrestrial ecosystems: a meta-analysis of 15 N tracer field studies. Ecology, 93(8), 1816–1829. https://doi.org/10.1890/11-1146.1

Teodoru, C. R., Nyoni, F. C., Borges, A. V., Darchambeau, F., Nyambe, I. & Bouillon, S. (2015). Dynamics of greenhouse gases (CO2, CH4, N2O) along the Zambezi River and major tributaries, and their importance in the riverine carbon budget. Biogeosciences, 12(8), 2431–2453. https://doi.org/10.5194/bg-12-2431-2015

Thompson, J. A. & Kolka, R. K. (2005). Soil Carbon Storage Estimation in a Forested Watershed using Quantitative Soil-Landscape Modeling. Soil Science Society of America Journal, 69(4), 1086–1093. https://doi.org/10.2136/sssaj2004.0322

Tian, H., Xu, R., Canadell, J. G., Thompson, R. L., Winiwarter, W., Suntharalingam, P., Davidson, E. A., Ciais, P., Jackson, R. B., Janssens-Maenhout, G., Prather, M. J., Regnier, P., Pan, N., Pan,

S., Peters, G. P., Shi, H., Tubiello, F. N., Zaehle, S., Zhou, F., … Yao, Y. (2020). A comprehensive quantification of global nitrous oxide sources and sinks. Nature, 586(7828), 248–256. https://doi.org/10.1038/s41586-020-2780-0

Torres, B., Vasseur, L., López, R., Lozano, P., García, Y., Arteaga, Y., Bravo, C., Barba, C. & García, A. (2020). Structure and above ground biomass along an elevation small-scale gradient: case study in an Evergreen Andean Amazon forest, Ecuador. Agroforestry Systems, 94(4), 1235–1245. https://doi.org/10.1007/s10457-018-00342-8

Townsend-Small, A., McClain, M. E., and Brandes, J. A.: Contributions of carbon and nitrogen from the Andes Mountains to the Amazon River: evidence from an elevational gradient of soils, plants, and river material. Limnol. Oceanogr., 50, 672-685, 2005.

Townsend-Small, A., Noguera, J. L., McClain, M. E. & Brandes, J. A. (2007). Radiocarbon and stable isotope geochemistry of organic matter in the Amazon headwaters, Peruvian Andes. Global Biogeochemical Cycles, 21(2), 1–9. https://doi.org/10.1029/2006GB002835

Tranvik, L. J., Downing, J. A., Cotner, J. B., Loiselle, S. A., Striegl, R. G., Ballatore, T. J., Dillon, P., Finlay, K., Fortino, K., Knoll, L. B., Kortelainen, P. L., Kutser, T., Larsen, S., Laurion, I., Leech, D. M., McCallister, S. L., McKnight, D. M., Melack, J. M., Overholt, E., … Weyhenmeyer, G. A. (2009). Lakes and reservoirs as regulators of carbon cycling and climate. Limnology and Oceanography, 54(6part2), 2298–2314. https://doi.org/10.4319/lo.2009.54.6_part_2.2298

Tyndall, J. (1861). XXIII. On the absorption and radiation of heat by gases and vapours, and on the physical connexion of radiation, absorption, and conduction.—The bakerian lecture. The London, Edinburgh, and Dublin Philosophical Magazine and Journal of Science, 22(146), 169–194. https://doi.org/10.1080/14786446108643138

Ulseth, A. J., Hall, R. O., Boix Canadell, M., Madinger, H. L., Niayifar, A. & Battin, T. J. (2019). Distinct air–water gas exchange regimes in low- and high-energy streams. Nature Geoscience, 12(4), 259–263. https://doi.org/10.1038/s41561-019-0324-8

US National Weather Service. (2019). The Earth-Atmosphere Energy Balance. US National Weather Service. https://www.weather.gov/jetstream/energy

Van Amstel, A. (2012). Methane. A review. Journal of Integrative Environmental Sciences, 9(sup1), 5–30. https://doi.org/10.1080/1943815X.2012.694892

Van Dam, B. R., Edson, J. B. & Tobias, C. (2019). Parameterizing Air-Water Gas Exchange in the Shallow, Microtidal New River Estuary. Journal of Geophysical Research: Biogeosciences, 124(7), 2351–2363. https://doi.org/10.1029/2018JG004908

van der Werf, G. R., Morton, D. C., DeFries, R. S., Olivier, J. G. J., Kasibhatla, P. S., Jackson, R. B., Collatz, G. J. & Randerson, J. T. (2009). CO2 emissions from forest loss. Nature Geoscience, 2(11), 737–738. https://doi.org/10.1038/ngeo671

van der Werf, G. R., Randerson, J. T., Giglio, L., Collatz, G. J., Mu, M., Kasibhatla, P. S., Morton, D. C., DeFries, R. S., Jin, Y. & van Leeuwen, T. T. (2010). Global fire emissions and the contribution of deforestation, savanna, forest, agricultural, and peat fires (1997–2009). Atmospheric Chemistry and Physics, 10(23), 11707–11735. https://doi.org/10.5194/acp-10-11707-2010

Vauchel, P., Santini, W., Guyot, J. L., Moquet, J. S., Martinez, J. M., Espinoza, J. C., Baby, P., Fuertes, O., Noriega, L., Puita, O., Sondag, F., Fraizy, P., Armijos, E., Cochonneau, G., Timouk, F., de Oliveira, E., Filizola, N., Molina, J. & Ronchail, J. (2017). A reassessment of the suspended sediment load in the Madeira River basin from the Andes of Peru and Bolivia to the Amazon River

in Brazil, based on 10 years of data from the HYBAM monitoring programme. Journal of Hydrology, 553, 35–48. https://doi.org/10.1016/j.jhydrol.2017.07.018

Vingiani, F., Durighetto, N., Klaus, M., Schelker, J., Labasque, T. & Botter, G. (2021). Evaluating stream CO2 outgassing via drifting and anchored flux chambers in a controlled flume experiment. Biogeosciences, 18(3), 1223–1240. https://doi.org/10.5194/bg-18-1223-2021

Wainwright, J., Parsons, A. J., Cooper, J. R., Gao, P., Gillies, J. A., Mao, L., Orford, J. D. & Knight, P. G. (2015). The concept of transport capacity in geomorphology. Reviews of Geophysics, 53(4), 1155–1202. https://doi.org/10.1002/2014RG000474

Wallace, A. R. (1853). Narrative of travels on the Amazon and Rio Negro. Reeve & Co. https://doi.org/10.5962/bhl.title.122472

Wallin, M. B., Campeau, A., Audet, J., Bastviken, D., Bishop, K., Kokic, J., Laudon, H., Lundin, E., Löfgren, S., Natchimuthu, S., Sobek, S., Teutschbein, C., Weyhenmeyer, G. A. & Grabs, T. (2018). Carbon dioxide and methane emissions of Swedish low-order streams—a national estimate and lessons learnt from more than a decade of observations. Limnology and Oceanography Letters, 3(3), 156–167. https://doi.org/10.1002/lol2.10061

Wanninkhof, R., 1992. Relationship between wind speed and gas exchange over the ocean. J. Geophys. Res. 97, 7373-7382. https://doi.org/10.1029/92JC00188

Webb, J. R., Clough, T. J. & Quayle, W. C. (2021). A review of indirect N 2 O emission factors from artificial agricultural waters. Environmental Research Letters, 16(4), 043005. https://doi.org/10.1088/1748-9326/abed00

Wei, P. S., Hsieh, Y. C., Chiu, H. H., Yen, D. L., Lee, C., Tsai, Y. C. & Ting, T. C. (2018). Absorption coefficient of carbon dioxide across atmospheric troposphere layer. Heliyon, 4(10), e00785. https://doi.org/10.1016/j.heliyon.2018.e00785

Weishaar, J. L., Aiken, G. R., Bergamaschi, B. A., Fram, M. S., Fujii, R., and Mopper, K.: Evaluation of specific ultraviolet absorbance as an indicator of the chemical composition and reactivity of dissolved organic carbon, Environ. Sci. Technol., 37, 4702–4708, doi: 10.1021/es030360x, 2003.

Weiss, R.F., 1981. Determinations of carbon dioxide and methane by dual catalyst flame ionization chromatography and nitrous oxide by electron capture chromatography. J. Chromatogr. Sci. 19, 611-616. https://doi.org/10.1093/chromsci/19.12.611

Weiss, R.F., Price, B.A., 1980. Nitrous oxide solubility in water and seawater. Mar. Chem. 8, 347-359. https://doi.org/10.1016/0304-4203(80)90024-9

Widén, J. & Munkhammar, J. (2019). Solar Radiation Theory. In Solar Radiation Theory. Joakim Widén and Joakim Munkhammar. https://doi.org/10.33063/diva-381852

Willgoose, G. (1994). A physical explanation for an observed area-slope-elevation relationship for catchments with declining relief. Water Resources Research, 30(2), 151–159. https://doi.org/10.1029/93WR01810

Wunch, D., Wennberg, P. O., Toon, G. C., Keppel-Aleks, G. & Yavin, Y. G. (2009). Emissions of greenhouse gases from a North American megacity. Geophysical Research Letters, 36(15), 5. https://doi.org/10.1029/2009GL039825

YUE, X.-L. & GAO, Q.-X. (2018). Contributions of natural systems and human activity to greenhouse gas emissions. Advances in Climate Change Research, 9(4), 243–252. https://doi.org/10.1016/j.accre.2018.12.003

Yvon-Durocher, G., Allen, A. P., Bastviken, D., Conrad, R., Gudasz, C., St-Pierre, A., Thanh-Duc, N. & Del Giorgio, P. A. (2014). Methane fluxes show consistent temperature dependence across microbial to ecosystem scales. Nature, 507(7493), 488–491. https://doi.org/10.1038/nature13164

Zaehle, S. & Dalmonech, D. (2011). Carbon–nitrogen interactions on land at global scales: current understanding in modelling climate biosphere feedbacks. Current Opinion in Environmental Sustainability, 3(5), 311–320. https://doi.org/10.1016/j.cosust.2011.08.008

Zapata, A., Rivera-Rondón, C. A., Valoyes, D., Muñoz-López, C. L., Mejía-Rocha, M. & Catalan, J. (2021). Páramo Lakes of Colombia: An Overview of Their Geographical Distribution and Physicochemical Characteristics. Water, 13(16), 2175. https://doi.org/10.3390/w13162175

Zhang, L., Zhang, S., Xia, X., Battin, T. J., Liu, S., Wang, Q., Liu, R., Yang, Z., Ni, J. & Stanley, E. H. (2022). Unexpectedly minor nitrous oxide emissions from fluvial networks draining permafrost catchments of the East Qinghai-Tibet Plateau. Nature Communications, 13(1), 950. https://doi.org/10.1038/s41467-022-28651-8

Zhang, X., Peng, S., Ciais, P., Wang, Y., Silver, J. D., Piao, S. & Rayner, P. J. (2019). Greenhouse Gas Concentration and Volcanic Eruptions Controlled the Variability of Terrestrial Carbon Uptake Over the Last Millennium. Journal of Advances in Modeling Earth Systems, 11(6), 1715–1734. https://doi.org/10.1029/2018MS001566

Zhang, Y. & Ye, A. (2022). Uncertainty analysis of multiple terrestrial gross primary productivity products. Global Ecology and Biogeography, 31(11), 2204–2218. https://doi.org/10.1111/geb.13578

Zhang, Z., Zimmermann, N. E., Stenke, A., Li, X., Hodson, E. L., Zhu, G., Huang, C. & Poulter, B. (2017). Emerging role of wetland methane emissions in driving 21st century climate change. Proceedings of the National Academy of Sciences, 114(36), 9647–9652. https://doi.org/10.1073/pnas.1618765114

Zhou YQ, Xiao QT, Yao XL, Zhang YL, Zhang M, Shi K, Lee XH, Podgorski DC, Qin BQ, Spencer RGM, Jeppesen E. 2018. Accumulation of Terrestrial Dissolved Organic Matter Potentially Enhances Dissolved Methane Levels in Eutrophic Lake Taihu, China. Environ Sci Technol. 52(18):10297-10306.

ANNEXES

Highlights on the field.

FIGURE AN 1. SHOT TAKEN FROM THE PÁRAMO SALVE FACCHA DAM. THE SALVE FACCHA RESERVOIR IS A VITAL CATCHMENT POINT FOR THE DRINKING WATER SUPPLY OF THE BIGGEST CITY IN ECUADOR. IT IS AT 3,900 M ALTITUDE IN AN ANCIENT VOLCANIC CALDERA. IT PRESENTS HYDROTHERMAL SPRINGS THAT MAY INFLUENCE ITS CHEMISTRY. FIDEICOMISO FONDO PARA LA PROTECCIÓN DEL AGUA (FONAG) FACILITATED ADMISSION TO THE ZONE FOR SAMPLING.

FIGURE AN 2 PHOTOGRAPH TAKEN FROM THE BASE OF THE SALVE FACCHA RESERVOIR, THE TEMPERATURE IS 8°C AND RELATIVE HUMIDITY OF 90%. THE COVERTURE IS DOMINATED BY PAJONALES, THESE ECOSYSTEMS LOSE AROUND 51% LESS WATER TO THE ATMOSPHERE THAN OTHER VEGETATION COVER TYPES, WHICH IS CRUCIAL FOR CAPTURING AND CONSERVING WATER.

FIGURE AN 3 PAPALLACTA IS A STREAM BORN IN THE ANDEAN PÁRAMOS AND ENDS IN THE PROVINCE OF NAPO. IT IS LOCATED AT AN ALTITUDE OF 2,300 M ALTITUDE. ITS MOST IMPORTANT TRIBUTARIES ARE THE CHALPI AND THE CUYUJA. DOWNSTREAM IT TAKES THE NAME OF QUIJOS.

FIGURE AN 4. PHOTOS OF THE SAME POINT, ON THE RIGHT, THE VEGETATION OF QUIJOS AT 2000 M, HIGHER HEIGHT OF THE PLANTS IS OBSERVED DUE TO THE WARMER AVERAGE TEMPERATURE. SAMPLING IS FROM A BRIDGE ON THE LEFT DUE TO DIFFICULTY ACCESSING THE POINT.

FIGURE AN 5 CAPTURE OF SATELLITE IMAGERY. THE STATION EL SALADO, SAMPLED FROM THE BRIDGE AND THE STATION COCA CODO, SAMPLED IN THE RIVER AFTER THE HYDROPOWER DAM. MOREOVER, THE PICTURE SHOWS THE UNION OF EL SALADO AND COCA RIVER.

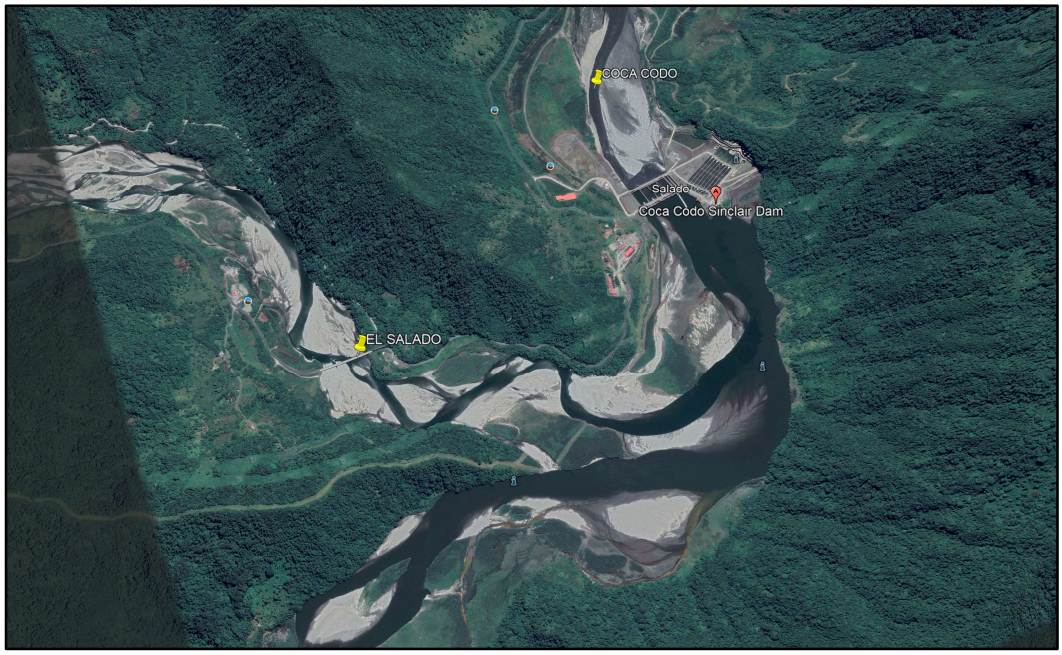

FIGURE AN 6 SAMPLING POINT IN COCA RIVER AT 600 M ALTITUDE.

FIGURE AN 7 AFTER BREAKING THE MOUNTAIN RANGE OF THE ECUADORIAN ANDES, IT ENTERS THE ENORMOUS AMAZONIAN PLAIN, PASSING SOMETHING TO THE SOUTH OF THE CITY OF TENA, THE CAPITAL OF THE NAPO PROVINCE, AT 500 M ALTITUDE. AT THE BACK OF THE PICTURE, THE PÁRAMOS AND EASTERN FOOTHILLS OF THE LLANGANATES NATIONAL PARK.

FIGURE AN 8 NAPO UPSTREAM OF THE CONFLUENCE WITH COCA. IN PUERTO MISAHUALLI, BOATS ARE THE PRIMARY MEANS OF TRANSPORTATION FOR THE COMMUNITIES SCATTERED ON THE BANKS OF THE RIVER.

FIGURE AN 9 SUNSET IN THE NAPO RIVER TAKEN FROM NUEVO ROCAFUERTE THE EASTERNMOST TOWN OF ECUADOR A FEW METERS FROM THE BORDER WITH PERU.

FIGURE AN 10 LAKE SAN PABLO, SURROUNDED BY THE COMMUNITY OF OTAVALO. AT THE BACK OF THE PICTURE, IT IS THE IMBABURA VOLCANO. IT PRESENTS AN IRREGULAR FIGURE OF 3.5 X 2.2 KM WITH A WATER MIRROR OF APPROXIMATELY 583 HECTARES WITH AN APPROXIMATE DEPTH OF 83 M.

FIGURE AN 11 WETLAND AT ANTISANA NATURAL RESERVE. THE WETLANDS AT PÁRAMOS ACT AS A SPONGE TO "CAPTURE" WATER. THEY ARE CRUCIAL FOR THE EXISTENCE OF ECOSYSTEMS SUCH AS FAUNA AND FLORA AND EVEN FOR HUMAN WELL-BEING SINCE CARBON CAPTURE IS LINKED TO THE CONSERVATION OF PÁRAMOS AND WETLANDS.

FIGURE AN 12. SECAS LAKE IN THE ANTISANA PARAMO, IT WAS FORMED WHEN THE ANTISANA VOLCANO ERUPTED MORE THAN 400 YEARS AGO.

FIGURE AN 13 THE TEAM, SEBASTÍAN PINTADO, BRYAN MOROCHO, JOHNNY CHÁVEZ AND GONZALO CHIRIBOGA SAILING FROM MISAHUALLÍ.

Greenhouse gas (CO_2, CH_4, N_2O) emissions from Ecuadorian mountainous streams and high elevation lakes

Rivers and streams contribute substantially to global emissions of carbon dioxide (CO_2) and methane (CH_4). Most riverine GHG emissions are from the tropics, ~60-80% for CO_2, ~70% for CH_4, and ~79% for nitrous oxide (N_2O). Nevertheless, the total stream surface area (SSA) in the tropics (24°N-24°S) corresponds to ~44% of the total SSA globally, implying that riverine areal emissions of GHGs (per m^2) are higher than in other climatic zones. Ecuador localizes on the tropics, and it is the smallest of the 17 megadiverse countries in the world harboring an astounding number of ecosystems, which offers the conditions to study in a relatively short space the GHG evasions of both, an important river tributary to the Amazon, as well as a diverse lacustrine system. The present thesis is divided into two sections. Firstly, we report for the first time the dissolved concentrations CO_2, CH_4, and N_2O in Andean headwater and piedmont streams in the Napo River basin in Ecuador, part of the Amazon River catchment. We found that concentrations increased exponentially with elevation decrease, i.e., between 3,990 and 175 m above sea level. Conversely, Andean mountainous headwater and piedmont streams are hotspots of CO_2 and CH_4 emissions; the respective areal fluxes are 1.7 and 4.5 higher in headwater streams and 1.2 and 6.6 higher in piedmont streams than in lowland streams.

Secondly, report the dissolved GHGs of 15 lakes along an elevational gradient ranging from 2,213 to 4,361 m. Lakes were grouped into three clusters as a function of their characteristics and obtained outcomes. Most lakes showed lower values of the partial pressure of CO_2 (pCO_2) (644-2,152 ppm) than usually attributed to tropical lakes (~1,900 ppm). Three lakes, influenced by volcanic inputs, denoted higher pCO_2 values (3,269-10,069 ppm), while two lakes bordered by large cities showed the lowest pCO_2 values (208-254 ppm), the remaining ten lakes had moderated pCO_2 and the highest dissolved organic carbon concentrations (8.3 to 12.8 mg L^{-1}) that is characteristic of páramo lakes (644-2,152 ppm). Dissolved CH4 concentrations ranged between 170 and 24,908 nmol L^{-1} and were negatively correlated to lake area and depth. N_2O saturation levels ranged between 64 % and 101 %. The surface waters were under-saturated in N_2O regarding atmospheric equilibrium, probably due to soil-water inputs with low N_2O levels due to soil denitrification. By upscaling to lakes in the whole Amazon basin, we found that the average areal FCH_4 (per m^2) was 1.3 times higher in highland lakes (0.75 gC m^{-2} yr^{-1}) than in lowland lakes (0.58 gC m^{-2} yr^{-1}) owing to the combination of higher dissolved CH_4 concentration (265 nmol L^{-1} versus 179 nmol L^{-1}) and higher gas transport velocity (k) values (3.5 cm h^{-1} versus 2.5 cm h^{-1}). Meanwhile, the average areal FCO_2 was 11 times lower in the highlands (23 gC m^{-2} yr^{-1}) than in the lowlands (255 gC m^{-2} yr^{-1}) owing to the lower pCO_2 values (530 ppm versus 2,909 ppm).